DOC.20080121.0002

QA: QA

ANL-NBS-HS-000057 REV 00

January 2008

Postclosure Analysis of the Range of Design Thermal Loadings

Prepared for:
U.S. Department of Energy
Office of Civilian Radioactive Waste Management
Office of Repository Development
1551 Hillshire Drive
Las Vegas, Nevada 89134-6321

Prepared by:
Sandia National Laboratories
OCRWM Lead Laboratory for Repository Systems
1180 Town Center Drive
Las Vegas, Nevada 89144

Under Contract Number
DE-AC04-94AL85000

DISCLAIMER

This report was prepared as an account of work sponsored by an agency of the United States Government. Neither the United States Government nor any agency thereof, nor any of their employees, nor any of their contractors, subcontractors or their employees, makes any warranty, express or implied, or assumes any legal liability or responsibility for the accuracy, completeness, or any third party's use or the results of such use of any information, apparatus, product, or process disclosed, or represents that its use would not infringe privately owned rights. Reference herein to any specific commercial product, process, or service by trade name, trademark, manufacturer, or otherwise, does not necessarily constitute or imply its endorsement, recommendation, or favoring by the United States Government or any agency thereof or its contractors or subcontractors. The views and opinions of authors expressed herein do not necessarily state or reflect those of the United States Government or any agency thereof.

QA: QA

Postclosure Analysis of the Range of Design Thermal Loadings

ANL-NBS-HS-000057 REV 00

January 2008

Scientific Analysis/Calculation Signature Page/Change History

Complete only applicable items.

1. Total Pages: 262

2. Document Title			
Postclosure Analysis of the Range of Design Thermal Loadings			
3. DI (including Rev. No.)			
ANL-NBS-HS-000057 REV 00			
	Printed Name	Signature	Date
4. Originator	Ernest Hardin		1/17/08
5. Checker	Charles Haukwa		01/17/2008
6. QCS	Robert E. Spencer		01/17/08
7. Responsible Manager/ Lead	Geoff Freeze		1/17/08
8. Responsible Manager	M. Kathryn Knowles		1/17/08
9. Remarks			

Change History

10. Revision No.	11. Description of Change
REV 00	Initial Issue.

INTENTIONALLY LEFT BLANK

ACKNOWLEDGEMENTS

The following individuals contributed to sections of this report: Charles Bryan (6.4.3), Tom Buscheck (6.4.2), John Case (6.1 and 6.5), Branko Damjanac (6.4.1), Junghun Leem (6.2), and Shane Schumacher (6.3).

INTENTIONALLY LEFT BLANK

CONTENTS

CONTENTS (Continued)

Page

CONTENTS (Continued)

Page

INTENTIONALLY LEFT BLANK

FIGURES

Page

FIGURES (Continued)

Page

FIGURES (Continued)

Page

FIGURES (Continued)

Page

TABLES

Page

TABLES (Continued)

Page

ACRONYMS AND ABBREVIATIONS

AC	acceptance criteria
BWR	boiling water reactor (in reference to a waste package type)
CDSP	codisposal
CR	Condition Report
CSNF	commercial spent nuclear fuel
DDT	discrete heat source, drift-scale, thermal conduction (MSTHM submodel)
DDTH	discrete heat source, drift-scale, thermal-hydrologic (MSTHM submodel)
DIRS	Document Input Reference System
DOE	U.S. Department of Energy
DQP	Data Qualification Plan
DSNF	defense spent nuclear fuel
DST	Drift Scale Test
DTN	data tracking number
EBS	Engineered Barrier System
ELWS	estimated limiting waste stream
FEP	features, events, and processes
HLW	high-level waste
LDTH	line-averaged-heat-source, drift-scale, thermal hydrologic (MSTHM submodel)
MSTHM	multiscale thermohydrologic model
NFC	near-field chemistry
PWR	pressurized water reactor (in reference to a waste package type)
QARD	*Quality Assurance Requirements and Description*
SAR	Safety Analysis Report
SDT	smeared heat source, drift-scale, thermal conduction (MSTHM submodel)
SNF	spent nuclear fuel
TAD	transportation, aging, and disposal (canister)
TH	thermal-hydrologic
THC	thermal-hydrologic-chemical
THM	thermal-hydrologic-mechanical
TSM	total system model
TSPA	total system performance assessment
TWP	technical work plan

ACRONYMS AND ABBREVIATIONS (Continued)

WPIMP	waste package index – mid-pillar
WPIDW	waste package index – drift wall
WRIP	water–rock interaction parameter
YMRP	*Yucca Mountain Review Plan, Final Report*
2-D	two-dimensional
3-D	three-dimensional

1. PURPOSE

This report presents a two-phased approach to develop and analyze a "thermal envelope" to represent the postclosure response of the repository to the anticipated range of repository design thermal loadings. In Phase 1 an estimated limiting waste stream (ELWS) is identified and analyzed to determine the extremes of average and local thermal loading conditions. The coldest thermal loading condition is represented by an emplacement drift loaded exclusively with high-level radioactive waste (HLW) and/or defense spent nuclear fuel (DSNF). The hottest thermal loading condition is a local average identified within a likely ELWS loading sequence. Phase 2 of this study analyzes the postclosure geomechanical, geochemical, and hydrogeologic responses of the repository host rock to these hottest and coldest thermal loading conditions.

The actual waste stream that will be encountered during operation of the repository is likely to differ from the ELWS used in this study. However, the ELWS is a plausible basis for identifying limiting thermal loading conditions that define a "thermal envelope" for analysis.

The results of this study (Section 7) show that the postclosure thermal reference case used for total system performance assessment (TSPA) (DTN: MO0702PASTREAM.001 [DIRS 179925]) is an upper bound on the ELWS, when both are expressed as average thermal line loads. This proves in principle that the ELWS can be controlled so as to meet the postclosure temperature limits for the mid-pillar, drift wall, and waste package surface. Previous work already demonstrated that these limits are met by the postclosure thermal reference case for TSPA (SNL 2007 [DIRS 181383], Tables 6.3-49[a] and 6.3-51[a]). This result also shows that far-field system responses are adequately represented by existing analyses and models, if the waste packages are emplaced to maintain the overall average thermal load over distances corresponding to the drift spacing. Far-field geomechanical, hydrogeologic, and geochemical behaviors respond to the average thermal load and are not sensitive to drift-scale variability of waste package heat output.

To represent the effect of drift-scale variability on in-drift temperatures, two ELWS emplacement sequences are analyzed (Section 6.1.3). From these sequences the hottest location is identified, and the corresponding limiting waste package heat output and arrangement are selected. This limiting case is slightly hotter than the postclosure thermal reference case for TSPA, but is shown to satisfy the postclosure temperature limits. The limiting case is analyzed to evaluate the responses of the geomechanical, hydrogeologic, and geochemical systems. The results show that system behavior is within the range of conditions evaluated for TSPA, and that the treatment of features, events and processes (FEPs) for TSPA is unchanged.

The information provided in this report directly addresses the Safety Analysis Report (SAR) content requirements of 10 CFR 63.21(c)(10) as discussed in Section 4.3. This study also directly addresses Condition Report (CR) 6343, which states that realistic descriptions of the waste stream are inconsistent with certain design assumptions and details, and with the postclosure thermal reference case. This study is intended to fulfill Corrective Actions 6343-006, -007, and -008.

Phase 1 of this study includes several deviations from the technical work plan (TWP) (BSC 2006 [DIRS 179791]):

- CR-9053 is not addressed in this report because the Corrective Action Program investigation was completed and found no error, and the CR is closed.

- CR-10832 is addressed in Section 6.3, which shows that re-calculated heat capacities produce peak postclosure waste package and drift wall temperatures that are approximately 10°C lower, when applied in ANSYS simulations. Note that the only usage of nonlinear heat capacity functions, which are the subject of this CR, has been in ANSYS calculations performed in *Repository Twelve Waste Package Segment Thermal Calculation* (BSC 2006 [DIRS 179686]), which is cited by this report; however, it is not critical to the postclosure performance assessment. This report uses the prior heat capacity functions, but only in a comparative sense to evaluate the impact of changes in rock properties and thermal loading.

  The nonlinear heat capacity functions were originally developed for use with ANSYS software. ANSYS can incorporate nonlinear material properties, but does not simulate flow and transport, or thermal hydrology. The nonlinear heat capacity concept is an approximation that accounts for short-term sensible heat loss in the rock due to dewatering but does not account for the fate of the water vapor, nor of the associated latent heat. Accordingly, application of ANSYS in this way is best suited for preclosure and early postclosure temperature predictions; at later times, thermal-hydrologic processes in the host rock become increasingly important.

  Because application of the nonlinear heat capacity concept (including associated assumptions) represents a rough approximation, it is not critical that previous calculations used the functions from *Heat Capacity Analysis Report* (BSC 2004 [DIRS 170003]), except that conservatively high temperatures were obtained. For perspective, these calculations also used mean values for host rock thermal properties, and those properties have uncertainty distributions. When lower (e.g., 10th percentile) values for host-rock thermal conductivity are used, higher peak temperatures (on the order of 10°C) are also obtained by this report.

- Decay curves for waste packages were obtained from the total system model (TSM) output and qualified for use (Appendices A and B) rather than developed in this study.

- The repository thermal integration activity was accomplished in this study by qualifying emplacement sequences from the TSM rather than by developing new ones. This is justified because they were also used for other purposes including demonstrating feasibility of repository operations. Thus, this study is integrated with design-supporting engineering studies.

- The emplacement sequences evaluated in this report are not optimized with respect to emplacement of the hottest waste packages at the drift ends, or in edge-drifts, as planned in the TWP. This step was not needed to achieve postclosure temperature limits, and omitting this step preserves flexibility of emplacement operations.

- Certain of the acceptance criteria (AC) from *Yucca Mountain Review Plan, Final Report* (YMRP) (NRC 2003 [DIRS 163274], Section 2.2.1.3.3.3) listed in the TWP were determined to be beyond the scope of this analysis and are not addressed:

  – AC 2(1) is not addressed because data used for model support are addressed in the model reports cited in Section 6.4.

  – AC 3(2) is not addressed because the parameter values, assumed ranges, probability distributions, and bounding assumptions used in the TSPA modeling basis are described in the model reports cited in Section 6.4.

  – AC 3(4) is not addressed because parameter development for conceptual models, process-level models, and alternative conceptual models is described in the model reports cited in Section 6.4.

  – AC 5(3) is not addressed because numerical and abstraction models are supported by objective comparisons, e.g., model validation, described in the model reports cited in Section 6.4.

Phase 2 of this study follows the second option identified in the TWP (BSC 2006 [DIRS 179791], Section 2.1.2.2), namely, "the ELWS involves significantly higher thermal loading within parts of the repository, and reevaluation of drift-scale coupled processes (thermal-hydrologic (TH), thermal-hydrologic-chemical (THC), and thermal-hydrologic-mechanical (THM) models) is warranted" with the following deviations:

- Thermomechanical analysis similar to that reported in *Drift Degradation Analysis* (BSC 2004 [DIRS 166107]) is used to describe the geomechanical response, in lieu of the THM model (BSC 2004 [DIRS 169864]) discussed in the TWP. The justification for this is that the drift degradation analysis is a more complete representation of uncertainty in host rock response, particularly the lithophysal units. Also, the THM model uses linear elasticity to describe host rock deformation, which is not suited for evaluating the potential for significantly increased rockfall or likelihood of drift collapse.

- The near-field chemistry (NFC) model (SNL 2007 [DIRS 177412]) is used in Section 6.4.3 to describe the response of the geochemical system, in lieu of the THC model (SNL 2007 [DIRS 177404]) discussed in the TWP. This is justified because the NFC model is used to represent the composition of seepage waters in TSPA.

- Finally, the TWP (BSC 2006 [DIRS 179791], Section 7) identifies a need for quality verification of the TSM-generated information used in this study. The information is qualified as data by technical assessment in accordance with SCI-PRO-001, *Qualification of Unqualified Data* (see Appendices A and B of this report). This approach provides adequate assurance that the information is qualified for use in this study.

Section 6.4 provides further discussion of the scope of Phase 2.

INTENTIONALLY LEFT BLANK

2. QUALITY ASSURANCE

The work described in this report was performed under SCI-PRO-005, *Scientific Analyses and Calculations*. The work is subject to the requirements of *Quality Assurance Requirements and Description* (QARD) (DOE 2007 [DIRS 182051]) because: (1) it characterizes the repository thermal environment, which affects engineered and natural barriers important to waste isolation as identified in *Q-List* (BSC 2005 [DIRS 175539]); and (2) it comprises scientific studies that support the applicability of TSPA. Applicability of the QARD is evaluated in the controlling TWP (BSC 2006 [DIRS 179791]).

The TWP describes a quality verification activity which is documented in Appendices A and B of this report. Data qualification in accordance with the procedure SCI-PRO-001 was determined be an appropriate approach for this verification, and the appendices contain the associated plan (Appendix A), and results of the assessment (Appendix B).

The methods used in this study for control of electronic management of information are specified in the TWP (BSC 2006 [DIRS 179791], Section 8.4). Password protection and backed-up network servers were used. Data transmission errors were minimized through review by originators of data sets submitted to the Technical Data Management System.

INTENTIONALLY LEFT BLANK

3. SOFTWARE

Table 3.1-1. Qualified Software Used in This Analysis

Software Name	Software Tracking Number	DIRS #	Description of Use	Operating Environment
UDEC v3.14	10173-3.14-00	[DIRS 172322]	Geomechanical simulation	Windows 2000
ANSYS v8.0	10364-8.0-00	[DIRS 170070]	Simulate postclosure drift wall temperature	HP-UX 11.0 HP-UX 11.22 SunOS 5.8
NUFT v3.0s	10088-3.0s-01	[DIRS 157280]	Thermal-hydrologic simulation	Sun OS 5.7
NUFT v4.0	11228-4.0-00	[DIRS 180382]	Thermal-hydrologic simulation	Solaris 5.8
mView v2.20	10072-2.20-00	[DIRS 155201]	Post-processing and plotting of NUFT output	Solaris 5.7
RADPRO v4.0	10204-4.0-00	[DIRS 164273]	Radiative coupling in NUFT	Sun OS 5.8
XTOOL v10.1	10208-10.1-00	[DIRS 148638]	Post-processing and plotting of NUFT output	Sun OS 5.6.1
EQ3/6 v8.0	10813-8.0-00	[DIRS 162228]	Geochemical simulation	Windows 2000
GetEQData v1.0.1	10809-1.0.1-00	[DIRS 173680]	Post-processing EQ3/6	Windows 2000

NOTE: DIRS = Document Input Reference System.

3.1 USE OF QUALIFIED SOFTWARE

The following sections describe the baselined, qualified software used for this study in more detail. The work described in this report did not use any software prior to its required qualification and baselining.

3.1.1 UDEC v3.14

UDEC v3.14 is baselined, qualified software per IM-PRO-003, *Software Management*. UDEC is a general purpose software application for numerical simulation of mechanical interaction of deformable polygonal blocks, which is used in this study to simulate mechanical response of the emplacement drifts to heating of the surrounding rock mass. UDEC is appropriate for this analysis because: (1) it is commonly used in the engineering community for analysis of deformation and damage of jointed rock mass, and (2) it was used and validated for the same application in *Drift Degradation Analysis* (BSC 2004 [DIRS 166107]). There are no imposed limitations on outputs in this application. Use of UDEC v3.14 for this study is within the documented validation range of the software.

3.1.2 ANSYS v8.0

ANSYS v8.0 is baselined, qualified software per IM-PRO-003. ANSYS is a general purpose finite element code that is used in this study (Section 6.3) to solve governing equations for thermal conduction, convection, and radiation, for sensitivity analysis of postclosure drift wall temperature. ANSYS is appropriate for this application because: (1) it is widely used in the engineering community, and (2) it was used for previous sensitivity analyses (BSC 2006 [DIRS 179686]), which are the starting point for analyses in this report. There are no imposed limitations on outputs in this application. Use of ANSYS v8.0 for this study is within the documented validation range of the software.

3.1.3 NUFT v3.0s and NUFT v4.0

NUFT v3.0s and NUFT v4.0 are baselined, qualified software per IM-PRO-003 and are used for thermal-hydrologic simulations. NUFT v3.0s and v4.0 solve the governing equations of the mathematical model used to represent thermal-hydrology for TSPA (SNL 2007 [DIRS 181383], Section 6.2), and are therefore appropriate for use in this study. There are no imposed limitations on outputs in this application. Use of NUFT v3.0s and v4.0 for this study is within the documented validation range of the software.

NUFT v3.0s and v4.0 are general-purpose codes for simulating mass and heat transport in fractured porous media, implementing conservation of mass and energy. These software codes are valid for any such calculation provided that mass- and heat-transport parameters (e.g., thermal conductivity, permeability) are used within ranges appropriate for the application. Further discussion of the applicability of NUFT v3.0s and v4.0) is provided in *Multiscale Thermohydrologic Model* (SNL 2007 [DIRS 181383], Sections 3.1.1 and 3.1.1.9[a]).

3.1.4 mView v2.20

mView v2.20 is baselined, qualified software per IM-PRO-003. mView v2.20 is used (Section 6.2) to extract specific time-history data of the output from NUFT time-history files (which are files with the suffix: *.ext). mView v2.20 was developed specifically for this task. Because this software is only used to extract data without any manipulation from the original output files, it is not applicable to identify validation ranges or limitations of use.

3.1.5 RADPRO v4.0

RADPRO v4.0 is baselined, qualified software per IM-PRO-003. RADPRO v4.0 was selected because it calculates the radiative heat transfer coefficients in the emplacement drift (SNL 2007 [DIRS 181383], Section 6.2.3.3, Equation 10) in a manner compatible with NUFT v3.0s. There are no limitations on its output. Its use in this study (Section 6.4.2) is consistent with its intended use and within the documented validation range of the software. Because this software is only used to conduct simple arithmetic functions, it is not applicable to identify validation ranges or limitations of use.

3.1.6 XTOOL v10.1

XTOOL v10.1 is baselined, qualified software per IM-PRO-003. XTOOL v10.1 is used in this report (Section 6.4.2) to generate graphical representations of the output from NUFT time-history files (which are files with the suffix: *.ext). XTOOL v10.1 was developed specifically for this task. Because this software is only used to generate graphical displays of data, it is not applicable to identify validation ranges or limitations of use.

3.1.7 EQ3/6 v8.0

EQ3/6 v8.0 was used for geochemical simulations, using a server running the Windows 2000 operating system. This software is best suited for implementing the geochemical calculations described in this report (Section 6.4.3), which are based on the near-field chemistry model (SNL 2007 [DIRS 177412]). There are no limitations of the software within the range of

application. This software is appropriate for the application and was used only within the range of model validation in accordance with IM-PRO-003. The EQ3/6 package includes EQ3NR and EQ6 (among other components), both of which are used in this analysis.

3.1.8 GetEQData v1.0.1

GetEQData v1.0.1 implements an Excel (97 or 2000) macro to post-process output from EQ3NR (**.3o*) or EQ6 (**.6o*). This software is used in this report (Section 6.4.3) to extract specified data from the EQ3/6 output files, as Excel spreadsheet files. The macro performs specific extraction of data as directed at run time. There are no limitations on its output. Its use in this study is consistent with its intended use and within the documented validation range of the software. Because this software is only used to parse files and sort data, it is not applicable to identify validation ranges or limitations of use.

3.2 USE OF EXEMPT SOFTWARE

Exempt software is used in this analysis for data compilation, plotting, and other activities meeting the criteria for exemption in Section 2 of IM-PRO-003. Exempt software includes Excel v97-SR2, Excel 2003, Mathcad v13, MATLAB v6.1.0.450 release 12.1, and TrueGrid v2.2.0.

Excel v97-SR2 and Microsoft Excel 2003, bundled with Microsoft Office, are commercial off-the-shelf software programs used in this report (throughout Section 6). Excel v97-SR2 and Microsoft Excel 2003 were installed on PCs equipped with the Windows 2000 Professional and Windows XP Version 2002 operating systems, respectively. This software is appropriate for this application as it offers the mathematical and graphical functionality necessary to perform and document the numerical manipulations used in this report. The Excel computations performed in this report use only standard built-in functions and are documented in sufficient detail to allow an independent technical reviewer to reproduce or verify the results by visual inspection or hand calculation without recourse to the originator. The Excel files are included in the output data tracking numbers (DTNs). The calculation results are not dependent upon the use of this particular software; therefore use of this software is not subject to the qualification requirements of IM-PRO-003.

Mathcad Version 13 and MATLAB v6.1.0.450 release 12.1 are commercial off-the-shelf software programs used in this report (Sections 6.1, 6.4, and 6.5.1). These programs were installed on a PC equipped with the Windows 2000 Professional operating system. The software is appropriate for this application as it offers the mathematical and graphical functionality necessary to perform and document the numerical manipulations used. The Mathcad and MATLAB computations performed in this report use only standard built-in functions and are documented in sufficient detail in the output DTNs to allow an independent technical reviewer to reproduce or verify the results by visual inspection or hand calculation without recourse to the originator. The Mathcad and MATLAB files are included in output DTNs. The calculation results are not dependent upon the use of these particular software; therefore use of this software is not subject to the qualification requirement of IM-PRO-003.

The gridding package TrueGrid v2.2.0 was used to modify the ANSYS finite-element grids developed in *Repository Twelve Waste Package Segment Thermal Calculation* (BSC 2006 [DIRS 179686]), to implement changes in waste package dimensions and Engineered Barrier System (EBS) geometry (Section 6.3). This software was determined to be Level 3 in accordance with procedure IM-PRO-003 and appears in the current *Level 3 Usage Controlled Software Report*. The software was run on the Unix-based workstation Milo (Tag Number: 151665). It was selected because it has been used extensively in support of previous ANSYS analyses. Because this software directly implements geometrical data provided as input, there are no limitations on its use.

4. INPUTS

4.1 DIRECT INPUTS

4.1.1 Inputs for Phase 1 Thermal Analysis

Phase 1 activities described in the TWP (BSC 2006 [DIRS 179791]) include adoption of an estimated limiting waste stream (ELWS), which is a forecast of the likely sequence of waste packages that will be received at the Yucca Mountain repository, for use in evaluating the range of thermal loading conditions. The ELWS data used as direct input in Sections 6.1.2 through 6.1.5 of this report are obtained from DTN: MO0707ELWSDNSL.000, [DIRS 183774], which contains a subset of data from unqualified DTN: MO0705WASTELIM.000 [DIRS 181570]. The qualification of DTN: MO0707ELWSDNSL.000 [DIRS 183774] is located in Appendix B of this report. The files include a spreadsheet entitled *WP_Decay_70K22kw_011707_DS.xls*, containing the list of waste packages received at Yucca Mountain with their lengths and thermal decay information (used in Sections 6.1.2 through 6.1.5), and one entitled *WP_Emplaced_ELWS_011707_23C_050107_DS.xls*, containing the as-emplaced sequences for the 85/4 and 96/2 cases described in Section 6.1.3. The other direct inputs used in Sections 6.1.2 through 6.1.5 are posted in Tables 4.1-1 through 4.1-3 below.

Table 4.1-1. Summary of Engineering Direct Inputs for the Phase 1 Thermal Analysis

Input	Value	Units	Source
Geometry of the Engineered System			
Pillar width	81	m	SNL 2007 [DIRS 179466], Table 4-1, Parameter 01-13
Drift diameter	5.5	m	SNL 2007 [DIRS 179354], Table 4-1, Parameter 01-10
End-to-end waste package spacing	0.1	m	SNL 2007 [DIRS 179354], Table 4-4, Parameter 05-02
Waste Package Dimensions			
21-PWR and 44-BWR (TAD) overall lengths	5.8501	m	SNL 2007 [DIRS 179394], Table 4-3; lengths based on "unloaded canister"
DHLW-SHORT overall length	3.6974	m	SNL 2007 [DIRS 179567], Table 4-8; lengths based on "unloaded canister", see also Assumption 5.3
DHLW-LONG overall length	5.3039	m	SNL 2007 [DIRS 179567], Table 4-9; lengths based on "unloaded canister", see Assumption 5.3
21-PWR and 44-BWR (TAD) diameters	1.882	m	SNL 2007 [DIRS 179394], Table 4-3; used "Outer Corrosion Barrier" diameter
DHLW-SHORT and DHLW-LONG diameters	2.045	m	SNL 2007 [DIRS 179567], Tables 4-8 and 4-9, used "Outer Corrosion Barrier" diameter
Waste Package Heat Generation			
Postclosure thermal reference case average line load thermal decay function	See DTN	N/A	SNL 2007 [DIRS 180472], Table 7-5[a]; also DTN: MO0702PASTREAM.001 [DIRS 179925], file: *DTN-Inventory-Rev00.xl*s, worksheet: "DECAY CURVES"

NOTE: BWR = boiling water reactor; TAD = transportation, aging, and disposal; PWR = pressurized water reactor.

Table 4.1-2. Thermal Conductivity for Host Rock Units

	tsw33 Tptpul	tsw34 Tptpmn	tsw35 Tptpll	tsw36 Tptpln
	Dry (W/m-K)	Dry (W/m-K)	Dry (W/m-K)	Dry (W/m-K)
10th	0.949	1.147	1.071	1.283
Global Mean	1.220	1.390	1.240	1.440
90th	1.369	1.626	1.414	1.609
	Wet (W/m-K)	Wet (W/m-K)	Wet (W/m-K)	Wet (W/m-K)
10th	1.55	1.827	1.690	1.944
Global Mean	1.780	2.060	1.870	2.110
90th	1.982	2.302	2.055	2.274

Source: DTNs: MO0612MEANTHER.000 [DIRS 180552] (mean wet and dry values) and MO0702PAGLOBAL.000 [DIRS 179343] (10th, 50th, and 90th percentile values).

NOTE: Mean used instead of 50th percentile; the values are statistically similar.

Sampling weights for host-rock thermal conductivity values were developed for the multiscale thermohydrologic model (MSTHM) (SNL 2007 [DIRS 181383]) and used in Section 6.1.3:

Table 4.1-3. Sampling Weights for Thermal Conductivity Uncertainty Used in the Phase 1 Thermal Analysis

	Sampling Weight
10th percentile	0.29
Global mean	0.37
90th percentile	0.34

Source: SNL 2007 [DIRS 181383], Table 6.3-47;
DTN: LL0703PA026MST.013 [DIRS 179981].

Mean thermal and physical properties of the host rock, and thermophysical properties of liquid water used for Phase 1 analyses, were taken from *Thermal Management Flexibility Analysis* (SNL 2007 [DIRS 179196]) for consistency with the previous work (Table 4.1-4). These values, and the thermal diffusivity parameter they are used to calculate, are discussed in Section 6.1.3.

Table 4.1-4. Lower Lithophysal (Tptpll) Host Rock and Water Properties Used for Phase 1 Analyses

Property	Value	Source and Rationale
Rock grain density	2,550 kg/m^2	SNL 2007 [DIRS 179196], Appendix A
Matrix porosity	0.1486	SN0404T0503102.011 [DIRS 169129], file: *ReadMe_Summery.doc*
Lithophysal porosity	0.0883	SN0404T0503102.011 [DIRS 169129], file: *ReadMe_Summery.doc*
Rock grain specific heat	930 J/kg-K	DTN: SN0307T0510902.003 [DIRS 164196], file: *rock_grain_heat_capacity (edited).xls*, worksheet: "Cp grain 25-325"
Water density (interpolated at 62°C)	982.3 kg/m^3	Incropera and DeWitt 2002 [DIRS 163337], Table A.6[a]
Water specific heat (interpolated at 62°C)	4,186 J/kg-K	Incropera and DeWitt 2002 [DIRS 163337], Table A.6[a]

[a] The interpolated values used from Incropera and DeWitt (2002 [DIRS 163337], Table A.6) are corroborated by *Perry's Chemical Engineers' Handbook* (Perry et. al. 1984 [DIRS 125806], Table 3-28 for density of water and Table 3-195 for specific heat of solutions containing no solute). The density of water interpolated from this handbook at 62°C is 982.160 kg/m^3, which is within 0.02% of the value given above. The specific heat interpolated at 62°C is 1.0063 cal/g °C, converted to 4,213.2 J/kg °C (conversion factors from Perry et al. 1984 [DIRS 125806], Table 1-6), which is within 1% of the value given above.

4.1.2 Inputs for Thermal-Hydrologic Margin Analysis

Section 6.1 describes various temperature calculations performed using conduction-only analytical solutions, to describe limits on thermal loading. Whereas the mid-pillar temperature analysis relies principally on the mean thermal conductivity of the Tptpll (lower lithophysal) host rock unit, the conductivity may be lower (e.g., 10th percentile; Table 4.1-2). A margin analysis (Section 6.2) was performed to determine whether the effects of hydrology on peak mid-pillar temperature represent a margin that offsets the temperature differences associated with use of the 10th percentile values of the host rock thermal conductivity.

The two-dimensional thermal-hydrologic analysis was performed using a line averaged-heat-source, drift-scale, thermal hydrologic (LDTH) submodel from the MSTHM (SNL 2007 [DIRS 181383], Section 6.2.6). The LDTH submodel is located approximately in the center of the repository footprint (SNL 2007 [DIRS 181383], Figure 6.3-1, location P2WR5C10). Details of the location are presented in Table 6.3-9 of *Multiscale Thermohydrologic Model* (SNL 2007 [DIRS 181383]). Input files of the LDTH submodel were obtained from DTN: LL030808623122.036 [DIRS 165790].

For the margin analysis, the LDTH submodel (Table 4.1-5) was modified with respect to: (1) thermal and hydrologic properties of the stratigraphic units; and (2) linear thermal heat loads.

Table 4.1-5. Source DTNs for Margin Analysis

Data Description	Source DTN	DIRS #
LDTH submodel inputs	LL030808623122.036	[DIRS 165790]
Thermal and hydrologic properties of repository layers and EBS[a]	LL0702PA014MST.069	[DIRS 179591]

[a] Preliminary data; impact analysis is presented in Section 6.2.2 and Figure 6.2-4.

The thermal and hydrologic properties of the repository stratigraphic units and the EBS materials were updated from DTN: LL030808623122.036 [DIRS 165790] to DTN: LL0702PA014MST.069 [DIRS 179591] (see details in SNL 2007 [DIRS 181383], Table 4.1-1). The margin analysis was conducted using preliminary 30th percentile hydrologic data for the repository stratigraphic units; there are slight differences between the 30th percentile hydrologic properties and the properties used in the margin analysis.

The linear thermal heat load used in the margin analysis was provided from a preliminary calculation. Updated heat load was provided later after the analysis. The updated data (Output DTN: MO0705SUPPCALC.000, folder: \YFF5_22 Envelope, file: *Unit Pulse Solution for the Calculation of Drift Wall Temperatures Rev01.xmcd*) is not significantly different from the heat load used in the analysis (Figure 6.2-3).

4.1.3 Inputs for Peak Drift Wall Temperature Analysis

The analysis described in Section 6.3 uses the methodology, software, and input data, including design information, for the base case (Case 1) previously developed in *Repository Twelve Waste Package Segment Thermal Calculation* (BSC 2006 [DIRS 179686]). The input files for the base case were obtained from the electronic Attachment IV to that report. Scenario 1 (Section 6.3.1.1) uses the base case input files, modified by changing the thermal conductivity values for the four host-rock units as shown in Table 4.1-6, based on the values in Table 4.1-2. Scenario 2 (Section 6.3.1.2) uses the same thermal conductivity inputs, and the same base case heat capacity data with changes as shown in Table 4.1-7, based on Appendix C.

For Scenarios 3 and 4 (Sections 6.3.1.3 and 6.3.1.4), the ANSYS grid is modified to incorporate the deeper invert (Table 4.1-8). Rock thermal property inputs for Scenarios 3 and 4 are the same as for Scenario 2. Scenarios 3 and 4 involve changes in the waste package dimensions, heat output, and preclosure ventilation time as discussed in Section 6.3.

Table 4.1-6. Dry Bulk Density and Thermal Conductivity of Rock Layers for ANSYS Analysis

Abbreviation	Geologic Framework Model Unit	Dry Bulk Density (kg/m^3)	Wet Bulk Thermal Conductivity ($T < 95°C$) (W/m·K)	Dry Bulk Thermal Conductivity ($T \geq 95°C$) (W/m·K)
QaBase[a]	Alluvium	2,190	1.81	1.30
Qa[a]		2,190	1.81	1.30
Tmr[b]	Crystal-Rich Tiva/Post-Tiva	2,190	1.81	1.30
Tpk[b]		2,190	1.81	1.30
Tpc_un	Tpcp	2,190	1.81	1.30
Tpcpv3	Tpcpv3	2,310	0.80	0.69
Tpcpv2	Tpcpv2	1,460	1.06	0.49
Tpcpv1	Tpcpv1	1,460	1.06	0.49
Tpbt4	Tpbt4	1,460	1.06	0.49
Tpy	Yucca	1,460	1.06	0.49
Tpbt3	Tpbt3_dc	1,460	1.06	0.49
Tpp	Pah	1,460	1.06	0.49
Tpbt2	Tpbt2	1,460	1.06	0.49
Tptrv3	Tptrv3	1,460	1.06	0.49
Tptrv2	Tptrv2	1,460	1.06	0.49
Tptrv1	Tptrv1	2,310	0.80	0.69
Tptrn	Tptrn	2,190	1.81	1.30
Tptrl	Tptrl	2,190	1.81	1.30
Tptf	Tptf	2,190	1.81	1.30
Tptpul	Tptpul	1,834	1.55	0.95
Tptpmn	Tptpmn	2,148	1.83	1.15
Tptpll	Tptpll	1,979	1.69	1.07
Tptpln	Tptpln	2,211	1.94	1.28
Tptpv3	Tptpv3	2,310	0.80	0.69
Tptpv2	Tptpv2	1,460	1.06	0.49
Tptpv1	Tptpv1	1,460	1.06	0.49
Tpbt1	Tpbt1	1,460	1.06	0.49
Tac	Calico	1,670	1.26	0.60
Tacbt	Calicobt	1,670	1.26	0.60
Tcpuv	Prowuv	1,790	1.13	0.57
Tcpuc	Prowuc	1,790	1.13	0.57
Tcpm	Prowmd	2,070	1.63	1.06
Tcplc	Prowlc	1,790	1.13	0.57
Tcplv	Prowlv	1,790	1.13	0.57
Tcpbt	Prowbt	1,790	1.13	0.57
Tcbuv	Bullfroguv	1,880	1.19	0.66
Tcbuc	Bullfroguc	1,880	1.19	0.66

Table 4.1-6. Dry Bulk Density and Thermal Conductivity of Rock Layers for ANSYS Analysis (Continued)

Abbreviation	Geologic Framework Model Unit	Dry Bulk Density (kg/m^3)	Wet Bulk Thermal Conductivity (T < 95°C) (W/m·K)	Dry Bulk Thermal Conductivity (T ≥ 95°C) (W/m·K)
Tcbm	Bullfrogmd	2,260	1.81	1.30
Tcblc	Bullfroglc	1,880	1.19	0.66
Tcblv	Bullfroglv	1,880	1.19	0.66
Tcbbt	Bullfrogbt	1,880	1.19	0.66
Tctuv	Tramuv	1,760	1.10	0.54
Tctuc	Tramuc	1,760	1.10	0.54
Tctm	Trammd	2,140	1.63	1.06
Tctlc	Tramlc	1,760	1.10	0.54
Tctlv	Tramlv	1,760	1.10	0.54
Tctbt	Trambt	1,760	1.10	0.54

Source: Non-shaded areas: DTN: SN0303T0503102.008 [DIRS 162401], file: *NonrepositoryThermalConductivityModel_031403.xls*

[a] See Assumption 5.4.
[b] These values were used in Scenarios 1 and 2 only; see Section 6.3.1.1 and 6.3.1.2.

NOTE: Areas shaded in gray contain values from Table 4.1-2, included here for comparison.

Table 4.1-7. Heat Capacity Values Revised for Drift Area Rock, for ANSYS Analysis

Abbreviation	Geologic Framework Model Unit	Specific Heat (J/kg·K)		
		T < 95°C	95°C ≤ T ≤ 114°C	T > 114°C
QaBase[a]	Alluvium	913	2,958	990
Qa[a]		913	2,958	990
Tmr[a]	Crystal-Rich Tiva/Post-Tiva	913	2,958	990
Tpk[a]		913	2,958	990
Tpc_un	Tpcp	913	2,958	990
Tpcpv3	Tpcpv3	1,245	8,393	1,000
Tpcpv2	Tpcpv2	1,245	8,393	1,000
Tpcpv1[b]	Tpcpv1	1,291	9,116	1,000
Tpbt4[b]	Tpbt4	1,291	9,116	1,000
Tpy[b]	Yucca	1,291	9,116	1,000
Tpbt3[b]	Tpbt3_dc	1,291	9,116	1,000
Tpp[b]	Pah	1,291	9,116	1,000
Tpbt2[b]	Tpbt2	1,291	9,116	1,000
Tptrv3[b]	Tptrv3	1,291	9,116	1,000
Tptrv2[b]	Tptrv2	1,291	9,116	1,000
Tptrv1	Tptrv1	894	1,815	990

Table 4.1-7. Heat Capacity Values Revised for Drift Area Rock, for ANSYS Analysis (Continued)

Abbreviation	Geologic Framework Model Unit	Specific Heat (J/kg·K)		
		T < 95°C	95°C ≤ T ≤ 114°C	T > 114°C
Tptrn	Tptrn	891	2,740	990
Tptrl	Tptrl	891	2,740	990
Tptf	Tptf	891	2,740	990
Tptpul[c]	Tptpul	938	3,566	990
Tptpmn[c]	Tptpmn	908	3,043	990
Tptpll[c]	Tptpll	926	3,343	990
Tptpln[c]	Tptpln	896	2,825	990
Tptpul[d]	Tptpul	1,107.8	8,110	930
Tptpmn[d]	Tptpmn	1,079.5	6,322	930
Tptpll[d]	Tptpll	1,107.8	7,840	930
Tptpln[d]	Tptpln	1,079.5[e]	6,340	930
Tptpv3[f]	Tptpv3	907	1,736	1,020
Tptpv2	Tptpv2	1,095	5,082	1,020
Tptpv1	Tptpv1	1,245	6,438	1,120
Tpbt1	Tpbt1	1,245	6,438	1,120
Tac[g]	Calico	1,403	9,804	1,120
Tacbt	Calicobt	1,247	7,622	1,070
Tcpuv	Prowuv	1,367	9,670	1,090
Tcpuc	Prowuc	1,043	5,423	990
Tcpm[h]	Prowmd	1,043	5,423	990
Tcplc	Prowlc	1,043	5,423	990
Tcplv	Prowlv	1,293	7,208	1,150
Tcpbt	Prowbt	1,293	7,208	1,150
Tcbuv	Bullfroguv	1,293	7,208	1,150
Tcbuc	Bullfroguc	946	3,703	990
Tcbm[h]	Bullfrogmd	946	3,703	990
Tcblc	Bullfroglc	946	3,703	990
Tcblv	Bullfroglv	1,234	7,059	1,100
Tcbbt	Bullfrogbt	1,234	7,059	1,100
Tctuv	Tramuv	1,234	7,059	1,100
Tctuc	Tramuc	1,328	10,830	990
Tctm[h]	Trammd	1,328	10,830	990
Tctlc	Tramlc	1,328	10,830	990

Table 4.1-7. Heat Capacity Values Revised for Drift Area Rock, for ANSYS Analysis (Continued)

Abbreviation	Geologic Framework Model Unit	Specific Heat (J/kg·K)		
		T < 95°C	95°C ≤ T ≤ 114°C	T > 114°C
Tctlv	Tramlv	1,190	8,151	990
Tctbt	Trambt	1,190	8,151	990

Source: Non-shaded area: DTN: SN0307T0510902.003 [DIRS 164196], file: *rock_mass_heat_capacity(edited).xls*. Also see BSC 2004 [DIRS 170003], Table 6-9. Gray shaded area: Values are developed in Appendix C of this report, and included here for comparison.

[a] See Assumption 5.4

[b] Following Table 6-9 of BSC 2004 [DIRS 170003], properties for the PTn unit are assigned to the Tpcpv1, Tpbt4, Tpy, Tpbt3, Tpp, Tpbt2, Tptrv3, and Tptrv2.

[c] These values were used in Scenario 1 (Section 6.3.1.1).

[d] These values were used in Scenarios 2 through 4 (Sections 6.3.1.2 through 6.3.1.4).

[e] The value for specific heat of the Tptpln unit, for T < 95°C, that was used in Scenarios 2, 3, and 4 (Section 6.3) is the same value shown above for the Tptpmn unit, due to a transcription error. The difference is insignificant, particularly when expressed in terms of volumetric heat capacitance (using the bulk density). The difference is much less than the corresponding differences in bulk density values used in Scenarios 1 through 4 (Table 4.1-6) compared to the values calculated in Appendix C and tabulated in Output DTN: MO0709REVTHERM.000.

[f] The values for the unit Tptpv3 were incorrectly transcribed into the input file matprops09.dat in Output DTNs: MO0709THERMAL2.000, MO0709THERMAL3.000 and MO0709THERMAL4.000. See Section 6.3.1 for further discussion.

[g] Average of Tac1, Tac2, Tac3, and Tac4 units as used in BSC 2006 [DIRS 179686], Table 9.

[h] The Tcpm, Tcbm, and Tctm units in this table (and Table 9 of BSC 2006 [DIRS 179686]) correspond respectively to the Tcpmd, Tcbmd, and Tctmd units from the source DTN indicated above.

NOTE: PTn = Tpcpv1, Tpbt4, Tpy, Tpbt3, Tpp, Tpbt2, Tptrv3, Tptrv2.

Table 4.1-8. Additional Design Information for the ANSYS Drift Wall Temperature Analysis

Input	Value	Units	Source
Invert height	1.321	m	SNL 2007 [DIRS 179354], Figure 4-1

4.1.4 Inputs for Phase 2 Response Analyses

The following subsections describe the inputs used for Sections 6.4.1 through 6.4.3, which respectively analyze the responses of the geomechancial, hydrogeologic, and geochemical systems to the anticipated range of thermal loading described in Section 6.1.

4.1.4.1 Inputs for Geomechanical Analysis

The geomechanical analysis described in Section 6.4.1 was performed following the methods established in *Drift Degradation Analysis* (BSC 2004 [DIRS 166107]) using inputs presented in Table 4.1-1, and Tables 4.1-9 through 4.1-11. Thermal loading conditions for these sensitivity analyses are the local-average thermal line loads corresponding to the 3-package and 7-package hottest segments, developed in Section 6.1 (Output DTN: MO0705SUPPCALC.000, folder: \Select Hot and Cold Cases, file: *Hottest and Coolest Discrete Values 1E6 yr (ventilation).xls*).

Table 4.1-9. Categories of Lithophysal Host Rock Mass Properties

Category	Base Case Properties				Bounding Unconfined Compressive Strength		Estimated Lithophysal Porosity (%)
	Unconfined Compressive Strength (MPa)	Young's Modulus, E (GPa)	Bulk Modulus, K (GPa)	Shear Modulus, G (GPa)	Lower Bound (MPa)	Upper Bound (MPa)	
1	10	1.9	1.07	0.80	10	11	35
2	15	6.4	3.54	2.65	10	23	28
3	20	10.8	6.01	4.51	10	32	21
4	25	15.3	8.48	6.36	13	40	13
5	30	19.7	10.95	8.21	16	47	7

Source: BSC 2004 [DIRS 166107], Table 6-41.

Table 4.1-10. Inputs from Calibrated Properties of the Bonded Fractures and Intact Blocks in the Model with 0.3 m Block Size

Category	Friction Angle (deg)	Residual Friction Angle (deg)	Cohesion (MPa)	Tension (MPa)	Normal Stiffness (GPa/m)	Shear Stiffness (GPa/m)	Block Bulk Modulus (GPa)	Block Shear Modulus (GPa)
1	35	15	3.83	1.53	9.34	4.67	9.03	6.80
2	35	15	5.85	2.34	31.48	15.72	30.44	22.88
3	35	15	7.94	3.18	53.08	26.57	51.37	38.60
4	35	15	10.09	4.03	74.90	37.60	72.80	54.70
5	35	15	12.30	4.92	97.00	48.40	93.60	70.50

Source: BSC 2004 [DIRS 166107], Table 6-43.

Table 4.1-11. Thermal Expansion Inputs for Various Thermal Mechanical Units

Thermal Mechanical Unit	Thermal Expansion Coefficient (per °C)			
	25°C < T ≤ 50°C	50°C < T ≤ 75°C	75°C < T ≤ 100°C	100°C < T ≤ 125°C
TCw	7.09×10^{-6}	7.62×10^{-6}	8.08×10^{-6}	10.34×10^{-6}
PTn	4.46×10^{-6}	4.28×10^{-6}	-1.45×10^{-6}	-30.42×10^{-6}
TSw1	6.56×10^{-6}	7.32×10^{-6}	6.83×10^{-6}	6.92×10^{-6}
TSw2	7.14×10^{-6}	7.47×10^{-6}	7.46×10^{-6}	9.07×10^{-6}

Source: Brodsky et al. 1997 [DIRS 100653], Table 4-4.

NOTE: T = temperature.

4.1.4.2 Inputs for Hydrogeologic Response Analysis

The hydrogeologic response analysis described in Section 6.4.2 was performed following the methods established in *Multiscale Thermohydrologic Model* (SNL 2007 [DIRS 181383]). The two-dimensional (2-D) and three-dimensional (3-D) submodels from the multiscale model were used to simulate the thermal-hydrologic responses to the selected hottest loading conditions. The source DTNs required for the inputs in Section 6.4.2 are presented in Table 4.1-12.

Table 4.1-12. Source DTNs for the Respective Models Used in Section 6.4.2

Model Type	Case Description	Percolation-Flux / Host-Rock Thermal Conductivity Case	Source DTN(s)
1-D SDT	3-point	NA	LL0702PA013MST.068 [DIRS 180553]
1-D SDT	7-point	NA	LL0702PA013MST.068 [DIRS 180553]
1-D SDT	ELWS	NA	LL0702PA013MST.068 [DIRS 180553]
2-D LDTH	base-case, nominal	P10	LL0702PA014MST.069 [DIRS 179591]
2-D LDTH	ELWS, nominal	P10	LL0702PA014MST.069 [DIRS 179591]
2-D LDTH	3-point, nominal	P10	LL0702PA014MST.069 [DIRS 179591]
2-D LDTH	3-point, nominal	P10L	LL0702PA022MST.077 [DIRS 179595]
2-D LDTH	3-point, nominal	P90	LL0702PA020MST.075 [DIRS 179594]
2-D LDTH	7-point, nominal	P10	LL0702PA014MST.069 [DIRS 179591]
2-D LDTH	7-point, nominal	P10L	LL0702PA022MST.077 [DIRS 179595]
2-D LDTH	7-point, nominal	P90	LL0702PA020MST.075 [DIRS 179594]
3-D DDTH	3-point, nominal	P10	LL0705PA032MST.028 [DIRS 182706]
3-D DDTH	3-point, nominal	P10L	LL0705PA032MST.028 [DIRS 182706] LL0702PA022MST.077 [DIRS 179595]
3-D DDTH	3-point, nominal	P90	LL0705PA032MST.028 [DIRS 182706] LL0702PA020MST.075 [DIRS 179594]
3-D DDTH	7-point, nominal	P10	LL0705PA032MST.028 [DIRS 182706] LL0702PA014MST.069 [DIRS 179591]
3-D DDTH	7-point, nominal	P10L	LL0705PA032MST.028 [DIRS 182706] LL0702PA022MST.077 [DIRS 179595]
3-D DDTH	7-point, nominal	P90	LL0705PA032MST.028 [DIRS 182706] LL0702PA020MST.075 [DIRS 179594]
3-D DDTH	base-case, nominal	P10	LL0705PA032MST.028 [DIRS 182706] LL0702PA014MST.069 [DIRS 179591]
3-D DDTH	base-case, nominal	P10L	LL0705PA032MST.028 [DIRS 182706] LL0702PA022MST.077 [DIRS 179595]
3-D DDTH	base-case, nominal	P90	LL0705PA032MST.028 [DIRS 182706] LL0702PA020MST.075 [DIRS 179594]
3-D DDTH	3-point, full drift collapse	P10L	LL0705PA032MST.028 [DIRS 182706] LL0702PA022MST.077 [DIRS 179595] LL0702PA027MST.082 [DIRS 179590]
3-D DDTH	7-point, full drift collapse	P10L	LL0705PA032MST.028 [DIRS 182706] LL0702PA022MST.077 [DIRS 179595] LL0702PA027MST.082 [DIRS 179590]

NOTES: DDTH = discrete heat source, drift-scale, thermal-hydrologic (MSTHM submodel); SDT = smeared heat source, drift-scale, thermal conduction (MSTHM submodel).

The 3- and 7-point 3-D DDTH models represent 13 discrete waste packages, while the base-case 3-D DDTH models represent 8 discrete waste packages. Base-case models are those using the base-case heat-generation tables.

Note that the source DTNs for the nominal cases (with no drift collapse) provide the cross-sectional dimensions of the numerical meshes. When necessary, the axial dimensions in the numerical meshes of the 3-D DDTH models are adjusted to correspond to the waste package sequencing to that case (e.g., 3-point waste package sequencing). The 3-D DDTH models for full drift collapse use the cross-sectional dimensions of the discrete heat source, drift-scale, thermal conduction (DDT) submodel used in DTN: LL0702PA027MST.082 [DIRS 179590].

The 3-D DDTH models for full drift collapse also use the rubble properties from DTN: LL0702PA027MST.082 [DIRS 179590].

4.1.4.3 Inputs for Geochemical Response Analysis

The effects of increased thermal loading on the chemistry of potential drift seepage water are evaluated in Section 6.4.3. The calculations are based on the near-field chemistry (NFC) model; inputs for these calculations are the original files used to generate the NFC model. Inputs to the base-case NFC model are documented in *Engineered Barrier System: Physical and Chemical Environment* (SNL 2007 [DIRS 177412], Section 6.3.2). Additional inputs for this analysis consist of the EQ3/6 output files used to generate potential seepage water compositions as functions of the NFC water–rock interaction parameter (WRIP) and drift wall temperature. The input parameters for the geochemical response analysis are summarized in Table 4.1-13.

Table 4.1-13. Direct Inputs for the Geochemical Response Analysis

DTN	Description of Input	Location
SN0703PAEBSPCE.006 [DIRS 181571]	Mathcad file implementing the NFC model calculation of the WRIP map for the mean thermal conductivity case	Folder: \WRIP calculations\Mathcad calculations of WRIP values\thermal-K, mean, file: *Model for water-rock interactions, mean.xmcd*
	Mathcad file implementing NFC model calculation for the evolution of the thermal field, mean thermal conductivity case, Drift choice 5	Folder: \WRIP calculations\Mathcad calculations of WRIP values\thermal-K, mean, file: *Model for thermal field, mean, Drift choice 5.xmcd*
SN0701PAEBSPCE.002 [DIRS 179425]	EQ6 output files for calculating the composition of potential Group 1 seepage water as a function of WRIP value and temperature	Folder: \EQ3_6 seepage\Gp1 Files: *10t96.6o*, *1bt96.6o*, *1ct96.6o*, *1dt96.6o*, *1et96.6o*, *1ft96.6o*, *1gt96.6o*, *1ht96.6o*, *1it96.6o*, *1jt96.6o*, *1lt96.6o*

4.1.4.4 Inputs for Revised Host Rock Heat Capacity Functions

Nonlinear heat capacitance (i.e., volumetric heat capacity) functions for each of the four host-rock units are derived in Appendix C for use as inputs to the ANSYS analysis described in Section 6.3. The approach follows that used in *Heat Capacity Analysis Report* (BSC 2004 [DIRS 170003], Section 6.7), with certain differences as explained in Appendix C.

Inputs include mean matrix porosity values for the Tptpmn and Tptpll units, and lithophysal porosity values for all four host-rock units, as shown in Table 4.1-14. Matrix porosity values for the Tptpmn and Tptpll units were selected for consistency and direct comparisons with earlier work (SNL 2007 [DIRS 179196], Table 4-4; BSC 2004 [DIRS 169854], Table 6-6). The Tptpul unit is represented using the porosity value for the Tptpll unit, and the Tptpln is represented using the Tptpmn value, following the same simplification made for hydrologic properties in the multiscale model (SNL 2007 [DIRS 181383], Section 6.2.16[a]). The values used for matrix porosity of the host rock units are thus similar, but not exactly the same as those used in the multiscale model (SNL 2007 [DIRS 181383]) or in Sections 6.2 and 6.4.2 of this report. The matrix porosity values in Table 4.1-14 are rounded down to two significant figures for use in

Appendix C, reflecting the variability and uncertainty (BSC 2004 [DIRS 169854], Table 6-6 for variability, and Figures 6-44 and 6-49 for uncertainty on the expected values).

Mean values for lithophysal porosity of the host rock units are obtained from *Thermal Conductivity of the Potential Repository Horizon* (BSC 2004 [DIRS 169854], Figures 6-34, 6-43, 6-48, and 6-53). The means of the uncertainty distributions on the expected values were selected as the representative estimates. There is considerable uncertainty and variability on lithophysal porosity as indicated by the range of values in Table 4.1-9. However, the heat capacity functions developed in Appendix C represent average, not extreme behavior. Also, the effect of lithophysal porosity on heat capacity is minor because porosity is subtracted from unity in the calculation.

The grain density value used (2,549.9 kg/m^3) is for all host rock units and is consistent with earlier work (SNL 2007 [DIRS 179196], Appendix A). This value is also very similar to the average of the values for the host rock units given in *Thermal Conductivity of the Potential Repository Horizon* (BSC 2004 [DIRS 169854], Table 5-4). The grain heat capacity (gravimetric; 930 J/kg-K) was also used in the previous work, and is the same value used for all four host-rock units in the multiscale model (value extracted from representative multiscale input DTN: LL0702PA014MST.069 [DIRS 179591], file: *DKM-afc-1Dds-vgm-P30-H34-H35-06-05*). From previously published ranges for these parameters (BSC 2004 [DIRS 170003], Table 6-8 for grain density; also Table 6-6 for overall average heat capacity), there is relatively little uncertainty, compared to the effect of dewatering on effective heat capacitance.

In situ matrix saturation of 90.5%, based on an assumption justified in *Thermal Management Flexibility Analysis* (SNL 2007 [DIRS 179196], Section 5.3), is used for all host-rock units (and rounded to 90% for heat capacitance derivation).

Physical properties of water (density, enthalpy of vaporization) were taken from Incropera and DeWitt (1996 [DIRS 108184], Table A.6). Values for these properties are further discussed in Appendix C.

The heat of vaporization is distributed over a temperature range from 94°C to 115°C, first ramping linearly from 94°C to a plateau that starts at 95°C, then uniformly from 95°C to 114°C, then ramping back to the dry rock heat capacitance at 115°C. These temperature limits were selected in *Heat Capacity Analysis Report* (BSC 2004 [DIRS 170003], Section 6.7) based on threshold dewatering behavior observed in the heated rock around the Drift Scale Test.

Table 4.1-14. Host Rock Properties Used in Heat Capacitance Analysis

Host-Rock Unit	Mean Matrix Porosity	Mean Lithophysal Porosity
Tptpul	Use Tptpll value for Tptpul as discussed in text	0.123
Tptpmn	0.12	0.025
Tptpll	0.14	0.088
Tptpln	Use Tptpll value for Tptpln as discussed in text	0.030

Source: Matrix porosity: DTN: LL0702PA014MST.069 [DIRS 179591], file: *DKM-afc-1Dds-vgm-P30-H34-H35-06-0* (values rounded down to 2 significant figures); lithophysal porosity: DTN: SN0404T0503102.011 [DIRS 169129] and BSC 2004 [DIRS 169854], Table 6-6 (values rounded to 3 significant figures).

4.1.4.5 Inputs for Drift Collapse Coincident with Peak Thermal Conditions

The probabilistic analysis in Section 6.5.1 shows that the probability of waste package temperature exceeding 300°C during the first few decades after repository closure is low, and there is low risk associated with seismically induced drift collapse immediately after repository closure. This analysis is based on *Seismic Consequence Abstraction* (SNL 2007 [DIRS 176828], Section 6.7.1), which provides an example calculation of the probability of seismically induced drift collapse during an 80-year period immediately after repository closure. The inputs used came from the output DTNs from the multiscale model (SNL 2007 [DIRS 181383]). The source DTNs required for the inputs in Section 6.5.1 are given in Table 4.1-15. The numerical meshes of the 2-D LDTH models of partial to full drift collapse apply the dimensions from the LDTH submodels in DTN: LL0705PA038MST.030 [DIRS 182332].

Table 4.1-15. Source DTNs for the Respective Models Used in Section 6.5.1

Model Type	Case Description	Percolation-Flux / Host-Rock Thermal Conductivity Case	Source DTN(s)
2-D LDTH	Base-case, nominal	P10	LL0702PA014MST.069 [DIRS 179591]
2-D LDTH	Base-case, partial to full drift collapse	P10	LL0702PA014MST.069 [DIRS 179591] LL0705PA038MST.030 [DIRS 182332] LL0702PA027MST.082 [DIRS 179590]

NOTE: The base-case models are those using the base-case heat-generation tables.

4.2 ACCEPTANCE CRITERIA

YMRP acceptance criteria (NRC 2003 [DIRS 163274]) applicable to this report are identified in Section 3.3 of the TWP (BSC 2006 [DIRS 179791]). In particular, the requirements identified in 10 CFR 63.114 (a), (b), (e), and (f) are identified. There are no U.S. Department of Energy (DOE) orders applicable to the scope of work identified in the TWP.

The following lists give *applicable* parts of the acceptance criteria shown, which are addressed in this report. Where differences exist with the text from the YMRP (NRC 2003 [DIRS 163274], Section 2.2.1.3), the omitted criteria information is determined to be not addressed by this report. Also, note that the criteria presented here are different than in the TWP. The criteria presented in

the TWP (BSC 2006 [DIRS 179791], Section 3.3) are not all applicable; the criteria presented here are the only criteria that apply, and thus this can be considered a deviation from the TWP as noted in Section 1 of this report.

Degradation of Engineered Barriers (NRC 2003 [DIRS 163274], Section 2.2.1.3.1.3)—from 10 CFR 63.114(a), (b), (e), (f):

Acceptance Criterion 1 – System Description and Model Integration Are Adequate:

(1) The total system performance assessment adequately incorporates important design features, physical phenomena, and couplings, and uses consistent and appropriate assumptions throughout the degradation of engineered barriers abstraction process.

(2) Assessment abstraction of the degradation of engineered barriers uses assumptions, technical bases, data, and models that are appropriate and consistent with other related U.S. Department of Energy abstractions. For example, the assumptions used for degradation of engineered barriers should be consistent with the abstractions of the quantity and chemistry of water contacting waste packages and waste forms (Section 2.2.1.3.3); climate and infiltration (Section 2.2.1.3.5); and mechanical disruption of waste packages (Section 2.2.1.3.2). The descriptions and technical bases provide transparent and traceable support for the abstraction of the degradation of engineered barriers.

(3) The descriptions of engineered barriers, design features, degradation processes, physical phenomena, and couplings that may affect the degradation of the engineered barriers are adequate. For example, materials and methods used to construct the engineered barriers are included, and degradation processes, such as uniform corrosion, pitting corrosion, crevice corrosion, stress corrosion cracking, intergranular corrosion, microbially influenced corrosion, dry-air oxidation, hydrogen embrittlement, and the effects of wet and dry cycles, material aging and phase stability, welding, and initial defects on the degradation modes for the engineered barriers are considered.

(4) Boundary and initial conditions used in the total system performance assessment abstractions are propagated consistently throughout the abstraction approaches. For example, the conditions and assumptions used in the degradation of engineered barriers abstraction are consistent with those used to model the quantity and chemistry of water contacting waste packages and waste forms (Section 2.2.1.3.3); climate and infiltration (Section 2.2.1.3.5); and mechanical disruption of waste packages (Section 2.2.1.3.2).

(5) Sufficient technical bases for the inclusion of features, events, and processes related to degradation of engineered barriers in the total system performance assessment abstractions are provided.

(7) Guidance in NUREG–1297 and NUREG–1298 (Altman et al. 1988 [DIRS 103597]; Altman et al. 1988 [DIRS 103750]), or other acceptable approaches, is followed.

Mechanical Disruption of Engineered Barriers (NRC 2003 [DIRS 163274], Section 2.2.1.3.2.3)—from 10 CFR 63.114(a), (b), (e), (f):

Acceptance Criterion 1 – System Description and Model Integration Are Adequate:

(1) Total system performance assessment adequately incorporates important design features, physical phenomena, and couplings, and uses consistent and appropriate assumptions throughout the mechanical disruption of engineered barrier abstraction process.

(2) The description of geological and engineering aspects of design features, physical phenomena, and couplings, that may affect mechanical disruption of engineered barriers, is adequate. For example, the description may include materials used in the construction of engineered barrier components, environmental effects (e.g., temperature, water chemistry, humidity, radiation, etc.) on these materials, and mechanical-failure processes and concomitant failure criteria used to assess the performance capabilities of these materials. Conditions and assumptions in the abstraction of mechanical disruption of engineered barriers are readily identified and consistent with the body of data presented in the description.

(4) Boundary and initial conditions used in the total system performance assessment abstraction of mechanical disruption of engineered barriers are propagated throughout its abstraction approaches.

(5) Sufficient data and technical bases to assess the degree to which features, events, and processes have been included in this abstraction are provided.

Quantity and Chemistry of Water Contacting Waste Packages and Waste Forms (NRC 2003 [DIRS 163274], Section 2.2.1.3.3.3)—from 10 CFR 63.114(a), (b), (e), (f):

Acceptance Criterion 1 – System Description and Model Integration Are Adequate:

(1) Total system performance assessment adequately incorporates important design features, physical phenomena, and couplings, and uses consistent and appropriate assumptions throughout the quantity and chemistry of water contacting engineered barriers and waste forms abstraction process.

(2) The abstraction of the quantity and chemistry of water contacting engineered barriers and waste forms uses assumptions, technical bases, data, and models, that are appropriate and consistent with other related U.S. Department of Energy abstractions. appropriate and consistent with other related U.S. Department of Energy abstractions. For example, the assumptions used for the quantity and chemistry of water contacting engineered barriers and waste forms are consistent with the abstractions of "Degradation of Engineered Barriers" (Section 2.2.1.3.1.3); "Mechanical Disruption of Engineered Barriers (Section 2.2.1.3.2); "Radionuclide Release Rates and Solubility Limits" (Section 2.2.1.3.4); "Climate and Infiltration" (Section 2.2.1.3.5); and "Flow Paths in the Unsaturated Zone" (Section 2.2.1.3.6). The descriptions and

technical bases provide transparent and traceable support for the abstraction of quantity and chemistry of water contacting engineered barriers and waste forms.

(3) Important design features, such as waste package design and material selection, backfill, drip shield, ground support, thermal loading strategy, and degradation processes, are adequate to determine the initial and boundary conditions for calculations of the quantity and chemistry of water contacting engineered barriers and waste forms.

(4) Spatial and temporal abstractions appropriately address physical couplings (thermal-hydrologic-mechanical-chemical). For example, the U.S. Department of Energy evaluates the potential for focusing of water flow into drifts, caused by coupled thermal-hydrologic mechanical-chemical processes.

(5) Sufficient technical bases and justification are provided for total system performance assessment assumptions and approximations for modeling coupled thermal-hydrologic-mechanical-chemical effects on seepage and flow, the waste package chemical environment, and the chemical environment for radionuclide release. The effects of distribution of flow on the amount of water contacting the engineered barriers and waste forms are consistently addressed, in all relevant abstractions.

(6) The expected ranges of environmental conditions within the waste package emplacement drifts, inside the breached waste packages, and contacting the waste forms and their evolution with time are identified. These ranges may be developed to include: (i) the effects of the drip shield and backfill on the quantity and chemistry of water (e.g., the potential for condensate formation and dripping from the underside of the shield); (ii) conditions that promote corrosion of engineered barriers and degradation of waste forms; (iii) irregular wet and dry cycles; (iv) gamma-radiolysis; and (v) size and distribution of penetrations of engineered barriers.

(7) The model abstraction for quantity and chemistry of water contacting engineered barriers and waste forms is consistent with the detailed information on engineered barrier design and other engineered features. For example, consistency is demonstrated for: (i) dimensionality of the abstractions; (ii) various design features and site characteristics; and (iii) alternative conceptual approaches. Analyses are adequate to demonstrate that no deleterious effects are caused by design or site features that the U.S. Department of Energy does not take into account in this abstraction.

(8) Adequate technical bases are provided, including activities such as independent modeling, laboratory or field data, or sensitivity studies, for inclusion of any thermal-hydrologic-mechanical-chemical couplings and features, events, and processes.

(10) Likely modes for container corrosion (NRC 2003 [DIRS 163274], Section 2.2.1.3.1) are identified and considered in determining the quantity and chemistry of water entering the engineered barriers and contacting waste forms. For example, the model abstractions consistently address the role of parameters, such as pH, carbonate

concentration, and the effect of corrosion on the quantity and chemistry of water contacting engineered barriers and waste forms.

(12) Guidance in NUREG–1297 and NUREG–1298 (Altman et al. 1988 [DIRS 103597]; Altman et al. 1988 [DIRS 103750]), or other acceptable approaches, is followed.

Acceptance Criterion 2 – Data Are Sufficient for Model Justification:

(2) Sufficient data were collected on the characteristics of the natural system and engineered materials to establish initial and boundary conditions for conceptual models of thermal-hydrological-mechanical-chemical coupled processes, that affect seepage and flow and the engineered barrier chemical environment.

Acceptance Criterion 3 – Data Uncertainty Is Characterized and Propagated through the Model Abstraction:

(1) Models use parameter values, assumed ranges, probability distributions, and bounding assumptions that are technically defensible, reasonably account for uncertainties and variabilities, and do not result in an under-representation of the risk estimate.

(3) Input values used in TSPA are consistent with the boundary conditions and assumptions associated with the design concepts for the Yucca Mountain site. Reasonable or conservative ranges of parameters or functional relations are established.

4.3 CODES, STANDARDS, AND REGULATIONS

This work scope will provide information required as SAR content in 10 CFR 63.21(c)(10). The verbatim wording of 63.21(c)(10) states that the SAR must include:

> An assessment of the anticipated response of the geomechanical, hydrogeologic, and geochemical systems to the range of design thermal loadings under consideration, given the pattern of fractures and other discontinuities and the heat transfer properties of the rock mass and water.

INTENTIONALLY LEFT BLANK

5. ASSUMPTIONS

5.1 POSTCLOSURE HEAT SHARING IN OPEN DRIFTS

This assumption was used in developing the emplacement sequences that are qualified in Appendix B for use in Section 6.1, and is inherited by this analysis. The loading sequence analysis performed by post-processing the ELWS case output from the TSM study is described in *Total System Performance Assessment Data Input Package for Requirements Analysis for EBS In-Drift Configuration* (SNL 2007 [DIRS 179354], Table 4-4, Parameter 05-03). That study applied the following "loading rules" in developing emplacement sequences:

- 2.0 kW/m maximum average thermal line-load at emplacement, averaged over any seven adjacent waste packages
- 18.0 kW maximum waste package power at emplacement.

The study assumed that, by applying these rules, the postclosure drift wall temperature would be limited to 200°C, although direct simulation of drift wall temperature using a range of host-rock thermal conductivity values was not performed. This assumption was based originally on assessment of previous simulations (BSC 2006 [DIRS 179686], Section 7), which used mean thermal properties for the host rock and found peak postclosure drift wall temperatures to be well under 200°C.

Confirmation Status: This assumption is confirmed by analysis, using 10th percentile values for thermal conductivity of the lower lithophysal (Tptpll) unit, in Section 6.3 of this report.

5.2 PRECLOSURE DRIFT WALL TEMPERATURE LIMIT FOR NORMAL OPERATIONS

Operational arrangements (e.g., temporary adjustments to the preclosure ventilation rate) will limit preclosure drift wall temperatures as specified in *Yucca Mountain Conceptual Design Report* (DOE 2006 [DIRS 176937]). Section 2.4.3.20.1.1 of that report states that preclosure drift wall temperature "shall be less than 96°C (205°F) and shall not exceed 200°C (392°F) at any time during preclosure, allowing for off-normal events of limited duration." This report (Section 6.1) is limited in scope to postclosure temperature limits, and therefore does not address this requirement.

Confirmation Status: None required. This is a preclosure requirement.

5.3 ADEQUACY OF WASTE PACKAGE DIMENSIONAL DATA

The waste package lengths used in the TSM study (SNL 2007 [DIRS 179354], Table 4-4, Parameter 05-03), and in DTNs: MO0705WASTELIM.000 [DIRS 181570] and MO0707ELWSDNSL.000 [DIRS 183774], are slightly different from current baseline values presented in Table 4.1-1 of this report.

Rationale: For consistency, the same length dimensions used in the TSM study are used in this report (Section 6.1 and 3-D analyses in Section 6.4.2). A summary and comparison of waste package length values is shown in Table 5-1. The relative differences in waste package lengths are much less significant than the relative uncertainties in waste package heat output (for example, see Output DTN: MO0705SUPPCALC.000, folder: \Select Hot and Cold Cases, file: *Hottest 3-7 + Coolest WP 96-2 10Jul07.xls*, worksheet: "Hottest Segments 96-2") and the properties of the host rock (Table 4.1-2). Similar justification is offered in *Initial Radionuclides Inventory* (SNL 2007 [DIRS 180472], Section 5.13[a]).

Confirmation Status: None required; justified in this report.

Table 5-1. Comparison of Waste Package Lengths Used in Analyses

Waste Package Type – This Report	Length (m)	Waste Package Type – Baseline	Length (m)
TAD Canister[a] (i.e., PWR, BWR, WPNavyL, STP)	5.85	TAD Canister[b]	5.8501
Codisposal-Long[a] (i.e., WPCodisposeL, WPMCO)	5.22	Codisposal-Long[b] (i.e., 5 DHLW/DOE SNF-LONG)	5.3039
Codisposal-Long[a] (i.e., WPNavy)	5.21		
Codisposal-Short[a] (i.e., WPCodispose)	3.59	Codisposal-Short[b] (i.e., 5 DHLW/DOE SNF-SHORT)	3.6974

[a] Output DTN: MO0705SUPPCALC.000, folder: \Select Hot and Cold Cases, file: *Hottest 3-7 + Coolest WP 96-2 10Jul07.xls*, worksheet: "WP_Emplaced 96."
[b] See Table 4.1-1.

5.4 THERMAL PROPERTIES OF ALLUVIUM AND CRYSTAL-RICH TIVA/POST-TIVA

The thermal conductivity of alluvium at the ground surface is assumed to be the same as that of the crystal-rich Tiva/Post-Tiva stratum, for the drift wall peak temperature analysis developed in Section 6.3. Also, the specific heat values for the alluvium and crystal-rich Tiva/Post-Tiva are assumed to be the same as for the Tpcun layer (Tpcp geologic framework unit; Table 4.1-7).

Rationale: Thermal conductivity and specific heat measurements for the alluvium and crystal-rich Tiva/Post-Tiva layers are not currently available. Using the thermal properties of the next rock layer below is reasonable because these layers are thin, at the top of the stratigraphic column, and are far removed from the host rock. Also, the peak drift wall temperature analysis in Section 6.3 involves simulations that run for only 200 years, which means that the temperatures and heat flow in these top layers are virtually unaffected by repository heating during the simulation period. Finally, the same assumption was used in *Repository Twelve Waste Package Segment Thermal Calculation* (BSC 2006 [DIRS 179686], Section 3.1.15), and its use here is consistent.

Confirmation Status: None required; justified in this report.

5.5 GEOMECHANICAL MODELING ASSUMPTION

Section 6.4.1 of this report presents thermomechanical analysis based on previous analyses and subject to a key assumption (BSC 2004 [DIRS 166107], Section 5). The description and justification for the applicable assumption is summarized below, and the reader is referred to the previous report for additional details. Note that the assumption identified below was selected as most directly related to the purpose of this report.

5.5.1 Thermal Expansion

Thermal expansion values used in the underlying layers (CHn1 and CHn2) under the repository units (TSw2) are assumed to be equal to those for the repository layers (BSC 2004 [DIRS 166107], Section 5.1.3).

Rationale: This assumption is used because the test data from the underlying units are limited. Temperature changes in the these layers are small, and the resulting thermal stresses are negligible.

Confirmation Status: Justified by analysis; does not require further confirmation.

5.6 THERMAL-HYDROLOGIC MODELING ASSUMPTIONS

Sections 6.2 and 6.4.2 of this report present thermal-hydrologic analyses based on the multiscale model, which are subject to some of the assumptions identified for that model (SNL 2007 [DIRS 181383], Section 5). The descriptions and justifications for the applicable assumptions are summarized in Table 5-2, and the reader is referred to the multiscale report for additional details. Note that the multiscale assumptions identified here were selected as most directly related to the purpose of this report.

5.7 GEOCHEMICAL MODELING ASSUMPTIONS

Section 6.4.3 of this report presents hydrogeochemical analyses based on the NFC model, which are subject to some of the assumptions identified for that model (SNL 2007 [DIRS 177412], Section 5). The descriptions and justifications for the applicable assumptions are summarized in Table 5-3, and the reader is referred to the previous report for additional details. Note that the assumptions identified here were selected as most directly related to the purpose of this report.

Table 5-2. Summary of Thermal-Hydrologic Modeling Assumptions

Assumption	Description	Reference
Ground-Surface Relative Humidity	The relative humidity at the ground surface above the repository is assumed to be 100%.	SNL 2007 [DIRS 181383], Section 5.1.1
Barometric Pressure Fluctuations at the Ground Surface	Barometric pressure fluctuations at the ground surface above the repository are assumed to be insignificant, so pressure at the ground surface is held constant.	SNL 2007 [DIRS 181383], Section 5.1.3
Hydrologic Properties of the Intragranular Porosity in the Invert Materials	The hydrologic properties of the intragranular porosity of the invert materials are assumed to be the same as those of the matrix of the lower lithophysal (Tptpll or tsw35) host rock.	SNL 2007 [DIRS 181383], Section 5.3.1.2
Pseudo-Permeability in the Emplacement Drifts	The gas-filled cavity between the drip shield and drift wall is represented as a porous medium with 100% porosity and pseudo-permeability of 1.0×10^{-8} m^2.	SNL 2007 [DIRS 181383], Section 5.3.1.7
Tortuosity for Binary Gas-Phase Diffusion	Appropriate values for the tortuosity factor are selected for the matrix and fracture continuum on the basis of the parameter range given by de Marsily (1986 [DIRS 100439], p. 233).	SNL 2007 [DIRS 181383], Section 5.3.1.9
Permeability of Host Rock at Emplacement Drift Wall	The permeability of the host rock at the drift wall surface is assumed to be unaffected by the presence of Bernold-style sheets used in the ground support system.	SNL 2007 [DIRS 181383], Section 5.3.1.10
Residual Saturation of the Intergranular Porosity of the Invert Ballast	Residual saturation for the intergranular porosity of the invert is assumed to be the same as that of the fractures (0.01) of the Tptpll host-rock unit.	SNL 2007 [DIRS 181383], Section 5.3.1.11[a]
Partitioning Thermal Conductance and Mass Density between Dual Continua	Thermal conductivity and mass density are apportioned from the bulk values, based on the fracture porosity.	SNL 2007 [DIRS 181383], Section 5.3.2.3
Thermal Properties of the Lumped Drip-Shield/Waste Package Heat Source in LDTH Models	The drip shield and waste package are represented as a lumped monolithic heat source in the LDTH modeling approach, with properties that are mass-weighted averages.	SNL 2007 [DIRS 181383], Section 5.3.2.4
Average Waste Package Diameter and Location above Invert	A value of 2.0085 m is assumed for the diameters of all waste packages in 3-D thermal-hydrologic analyses, based on a weighted average for the arrangement of the postclosure thermal reference case. The location of the waste package centerline above the invert surface is taken to be 1.218 m, corresponding to the average package diameter.	SNL 2007 [DIRS 181383], Section 6.2.8[a]
Mass Transport in the Longitudinal Direction along Emplacement Drifts	The use of 2-D models to investigate peak mid-pillar temperature is conservative, because it tends to over-estimate the predicted temperatures.	SNL 2007 [DIRS 181383], Section 5.7

Table 5-3. Summary of Geochemical Modeling Assumptions

Assumption	Description	Reference
Repository Location	NFC model results calculated using averaged rock properties for the four host rock units, and thermal properties for the lower lithophysal (Tptpll) host-rock unit, are applicable to all lithologies intersected by the repository drifts.	SNL 2007 [DIRS 177412], Section 5.7
Representative Distribution of Seepage Water Compositions	NFC model simulations using the four selected starting waters adequately represent all possible seepage waters.	SNL 2007 [DIRS 177412], Section 5.2.2
Pore-Water Transport Velocity through the NFC Model Domain	Pore-water transport times through the NFC model domain are calculated assuming plug flow through host rock with uniform, representative rock properties, supported by a series of numerical simulations using a dual-permeability transport analysis.	SNL 2007 [DIRS 177412], Section 5.2.3
Feldspar Dissolution Rate	Temperature is the dominant factor controlling the effective feldspar dissolution rate in the NFC model. This implicitly assumes that the alkali feldspar accessible surface area does not change with time.	SNL 2007 [DIRS 177412], Section 5.2.4
Host Rock Saturation Value for Thermal Conductivity and Heat Capacity	The in situ water saturation of the host rock is assumed to be 90.5% for the purpose of calculating far-field temperature.	SNL 2007 [DIRS 177412], Section 6.3.2.4.3

5.8 LIQUID WATER SATURATION OF HOST-ROCK UNITS

The initial water saturation of the stratigraphic layers is assumed to be approximately 90.5%, for the purpose of calculating the mid-pillar temperatures in Section 6.1.3 and the effective heat capacity in Appendix C. This value is typical for the range of observations from the densely welded host-rock units, based on the range of matrix saturation data used to calibrate unsaturated-zone hydrologic properties (SNL 2007 [DIRS 179545]; the repository horizon is within the TSw plateau region of Figures 6-1, 6-3, 6-5, and 6-7). There is uncertainty of up to approximately 10% on average matrix saturation (from the error bars on the figures), but the thermal properties evaluated in this report (thermal diffusivity and heat capacity; Section 6.1 and Appendix C) are relatively insensitive to this range. The choice of 90.5% initial matrix saturation is also consistent with previous analyses (BSC 2004 [DIRS 169862], Sections 6.9 and 6.11; SNL 2007 [179196], Section 6.3.1). Hence, the choice of 90.5% matrix saturation for densely welded host rock is justified, and no confirmation is required.

INTENTIONALLY LEFT BLANK

6. ANALYSIS

Phase 1 activities described in the TWP (BSC 2006 [DIRS 179791]) include adoption of an estimated limiting waste stream (ELWS), which is a forecast of the likely sequence of waste packages that will be received at the Yucca Mountain repository, for use in evaluating the range of thermal loading conditions. The ELWS is slightly cooler overall, expressed as an average line load, than the postclosure thermal reference case used for total system performance assessment (TSPA). Waste package emplacement ("loading") rules are developed to control how the ELWS sequence would be emplaced underground, in a manner that provides assurance that the postclosure temperature limits will be met. Two realizations of the emplacement sequence are analyzed to determine the range of local thermal loading conditions (Section 6.1).

Supplementing Phase 1 is analysis of the sources of margin available to demonstrate that the postclosure temperature limits will be met as described in Section 6.2. Margin is provided by hydrologic quenching of mid-pillar temperature, and the drift-end and edge-drift effects particular to the repository layout. These sources of margin help ensure that the postclosure mid-pillar temperature limit can be met, given the uncertainty and variability of host-rock thermal conductivity.

The uncertainty of previous predictions of peak postclosure drift wall temperature is then evaluated (Section 6.3), given the range of host-rock thermal conductivity, and the range of thermal loading conditions identified in Section 6.1. This analysis shows that the peak postclosure drift wall temperature can be maintained at or below 200°C if the mid-pillar temperature limit criterion is met, and if necessary by implementing thermal management criteria.

Phase 2 activities to assess the responses of the geomechanical, hydrogeologic, and geochemical systems to the range of local thermal loading conditions are described in Section 6.4. These analyses evaluate the output of models that feed TSPA, when applied to the range of thermal loadings determined in Section 6.1. The descriptions consider model validity for the limiting cases analyzed, for included features, events, and processes (FEPs).

The impact of the anticipated range of thermal loading on FEP screening is evaluated in Section 6.5. This discussion focuses on excluded FEPs, and concludes that FEP screening decisions are generally valid over the full range of thermal conditions.

6.1 PHASE 1 THERMAL ANALYSES

6.1.1 Postclosure Temperature Limits

This report evaluates whether the following conditions will be met by the repository given the anticipated range of thermal loadings: (1) postclosure temperature limits (DOE 2006 [DIRS 176937], Section 4.6.5) will not be exceeded; and (2) modeling results used for postclosure TSPA and for screening of FEPs are representative and valid.

The postclosure temperature limits are:

- Mid-pillar temperature limit of 96°C (approximate boiling temperature of water at the repository elevation) to facilitate drainage of percolation water and condensate through the repository horizon.
- Peak postclosure drift wall temperature of 200°C to limit thermomechanical effects on drift opening stability.
- Waste package outer wall temperature limit of 300°C for 500 years, followed by 200°C for 9,500 years, to reduce Alloy 22 corrosion from certain metallurgical processes.
- Maximum commercial spent nuclear fuel (CSNF) cladding temperature of 350°C to limit degradation of cladding integrity due to thermal creep rupture.

These temperature limits have been used in the repository design basis, and in developing FEP screening justifications. The following paragraphs provide additional detail on the origin and current documentation of these limits.

Mid-Pillar – The mid-pillar temperature limit (96°C) is documented in *Yucca Mountain Project Conceptual Design Report* (DOE 2006 [DIRS 176937], Section 4.6.5). The mid-pillar limit is used in evaluating unsaturated zone FEPs (SNL 2007 [DIRS 181613]) and is called out in *Postclosure Modeling and Analyses Design Parameters* (BSC 2008 [DIRS 183627], Table 1, Parameter 05-03). The purpose of the mid-pillar limit is to preserve pathways for drainage of percolation flux and condensate between every pair of adjacent drifts in the repository. The 96°C limit corresponds to the approximate boiling temperature for water at the repository elevation.

Drift Wall – The drift wall temperature limit (200°C) has not been fully documented (see CR-7969) and warrants additional discussion here. The drift wall temperature limit (200°C) is described in *Yucca Mountain Project Conceptual Design Report* (DOE 2006 [DIRS 176937], Section 4.6.5), and is also called out in *Postclosure Modeling and Analyses Design Parameters* (BSC 2008 [DIRS 183627], Table 1, Parameter 06-02).

Thermal expansivity of welded tuff at temperatures up to 300°C was investigated by Brodsky et al. (1997 [DIRS 100653], Section 4.2) using laboratory tests. The coefficient of thermal expansion for welded tuff (including samples from the host rock units) was found to increase with temperature. Transitional temperature behavior was observed whereby thermal expansion (slope of strain vs. temperature) gradually increased near and above 200°C. The magnitude of strain hysteresis on cool-down was related to the maximum temperature to which each sample was exposed. Transition behavior was attributed to physical changes in the rock, including mineral-phase transitions (Nimick and Connolly 1991 [DIRS 100690]) and dilation caused by differential thermal expansion. Unconfined thermal expansivity of silicate rocks generally increases with temperature (Hardin and Chesnut 1997 [DIRS 150043], Section 2.4). Dilation results from nonuniform expansion of constituent grains, which causes the formation of new microcracks or the opening of pre-existing microcracks (Cooper and Simmons 1977

[DIRS 183072]). In most of the tests reported by Brodsky et al. (1997 [DIRS 100653]), expansion reversed on cooling, but permanent elongations of as much as 0.4% were observed for some samples.

Increased thermal expansivity is indicative of micro-cracking from differential, thermally induced strains, and cracking can reduce rock strength. In addition, increased expansivity increases the rate at which thermal stress is produced on heating, although the associated reductions in deformation moduli tend to offset this effect. The observation of transitional temperature behavior in laboratory testing of samples from the host rock units is the reason that the 200°C drift wall temperature limit is imposed. The drift wall temperature limit will confine the extent of permanent changes in rock characteristics that could impact drift opening stability. It is noted that drift wall temperatures of 200°C, and rock mass temperatures greater than 250°C, were achieved in the Drift Scale Test with only minor effects observed (SNL 2007 [DIRS 177414], Sections 6.3.1.2 and 6.3.3.7).

Mineral phase transformations have been identified as mechanisms contributing to transitional behavior; however, the changes occur gradually in laboratory tests, and other mechanisms are very likely effective. Because the transitional behavior occurs gradually, and because rock mass strength varies over a wide range of anticipated conditions, no significant effect on drift opening stability is likely to occur if the drift wall temperature limit is exceeded. Effects on drift opening stability are analyzed in Section 6.4.1.

Waste Package Outer Barrier – The waste package outer barrier postclosure temperature limit is found in *Project Design Criteria Document* (BSC 2006 [DIRS 178308], Section 6.2.2), and in *Postclosure Modeling and Analyses Design Parameters* (BSC 2008 [DIRS 183627], Table 1, Parameter 06-03). The limit is developed in *Aging and Phase Stability of the Waste Package Outer Barrier* (BSC 2004 [DIRS 171924], Section 8). The waste package outer barrier temperature limit is used in evaluating waste package FEPs (BSC 2005 [DIRS 174995], Sections 6.2.8, 6.2.13, 6.2.23, and 6.2.27).

CSNF Cladding – The 350°C postclosure limit is found in *Project Design Criteria Document* (BSC 2006 [DIRS 178308], Section 6.2.1), and is also discussed in *Postclosure Modeling and Analyses Design Parameters* (BSC 2008 [DIRS 183627], Table 1, Parameter 06-04), where it is supported by reference to other sources. The cladding temperature limit is used in evaluating cladding FEPs (SNL 2007 [DIRS 181613]). It is noted that whereas the cladding temperature limit is intended to preserve cladding integrity, the TSPA assumes that no fuel rod in CSNF waste packages has full integrity (SNL 2007 [DIRS 178871], Section 6.3.7).

Further documentation of the postclosure temperature limits is provided in *Basis of Design for the TAD Canister-Based Repository Design Concept* (BSC 2006 [DIRS 177636]).

6.1.2 Thermal Reference Case for TSPA, and the Estimated Limiting Waste Stream

The postclosure thermal reference case comprises a likely inventory of wastes to be received at Yucca Mountain, and a representative arrangement of waste packages (“unit cell”) for use by TSPA. The unit cell is a repeating sequence of eight waste packages that is used in the multiscale model (SNL 2007 [DIRS 181383]) to represent waste package variability in the

thermal-hydrologic simulations for TSPA. The average thermal output of the postclosure reference case for TSPA (i.e., the unit-cell average lineal thermal load) retains the same average line-load function used in previous models that support TSPA (SNL 2007 [DIRS 180472], Section 5.15[a]). The inventory is compiled, and the unit cell is developed, in *Initial Radionuclide Inventories* (SNL 2007 [DIRS 180472], Section 6.2[a]).

The postclosure reference case includes the assumption of instantaneous emplacement of all waste packages, followed by 50 years of preclosure ventilation (SNL 2007 [DIRS 181383], Section 5.2.3). The project schedule calls for initial operation in November 2016 (fiscal year 2017), with a total preclosure period of 100 years, including at least 50 years of forced ventilation after emplacement is complete (DOE 2006 [DIRS 176937], Sections 2.4.3.9.2, 3.4, and 4.6.5). For the postclosure thermal reference case, the "instantaneous" emplacement event is assigned at calendar year 2067 so that closure corresponds to the schedule in the conceptual design report (DOE 2006 [DIRS 176937]).

The ELWS was selected from cases run in *Total System Performance Assessment Data Input Package for Requirements Analysis for EBS In-Drift Configuration* (SNL 2007 [DIRS 179354], Table 4-4, Parameter 05-03); and also in DTNs: MO0705WASTELIM.000 [DIRS 181570] and MO0707ELWSDNSL.000 [DIRS 183774], which simulate constraints imposed by contracts between the DOE and the nuclear power utilities, and the operational processes of waste selection, canisterization, and transport to Yucca Mountain. Note that data was extracted from DTN: MO0705WASTELIM.000 [DIRS 181570], and is located in DTN: MO0707ELWSDNSL.000 [DIRS 183774] and qualified in Appendix B. The particular case selected used the following criteria:

- Transportation, aging, and disposal (TAD) canisters could be shipped as hot as 22 kW (the current limit on licensed transportation casks).

- Youngest fuel available would be shipped first from the utilities, with a minimum age of 5 years out of reactor (YFF5).

The ELWS represents a sequence of waste packages that will be received at Yucca Mountain during a period of approximately 35 years (depending on the emplacement scheme as discussed below) starting in 2017. Thus, the ELWS includes the total numbers of waste packages of different types. For each waste package, the ELWS includes key dimensions, and a thermal decay function based on the radionuclide inventory it contains (SNL 2007 [DIRS 179354], Table 4-4, Parameter 05-03). Qualification of the ELWS data for input to this study (DTN: MO0707ELWSDNSL.000 [DIRS 183774]) is addressed in Appendix B.

The postclosure thermal reference case encompasses the average lineal thermal output of the ELWS, considering instantaneous power output (Figure 6.1-1). There are two reasons for this: (1) the ELWS combines hotter CSNF with cooler HLW packages, and (2) the postclosure reference case is delayed to 2067 to represent the conceptual design schedule. To address the possibility that the waste stream (same waste packages) could be emplaced underground in less than 50 years, Figure 6.1-1 also shows the postclosure reference case shifted 17 years earlier in time (from 2067 to 2050). This curve is very close to the ELWS, when presented as an average line load. The postclosure reference case thus defines an operating thermal envelope for the

repository, which may be very close to the ELWS, but only in an overall average sense that does not take local variability into account. Variability in the ELWS emplacement sequences (Section 6.1.3) contributes to local thermal loading conditions that exceed the average for the postclosure thermal reference case.

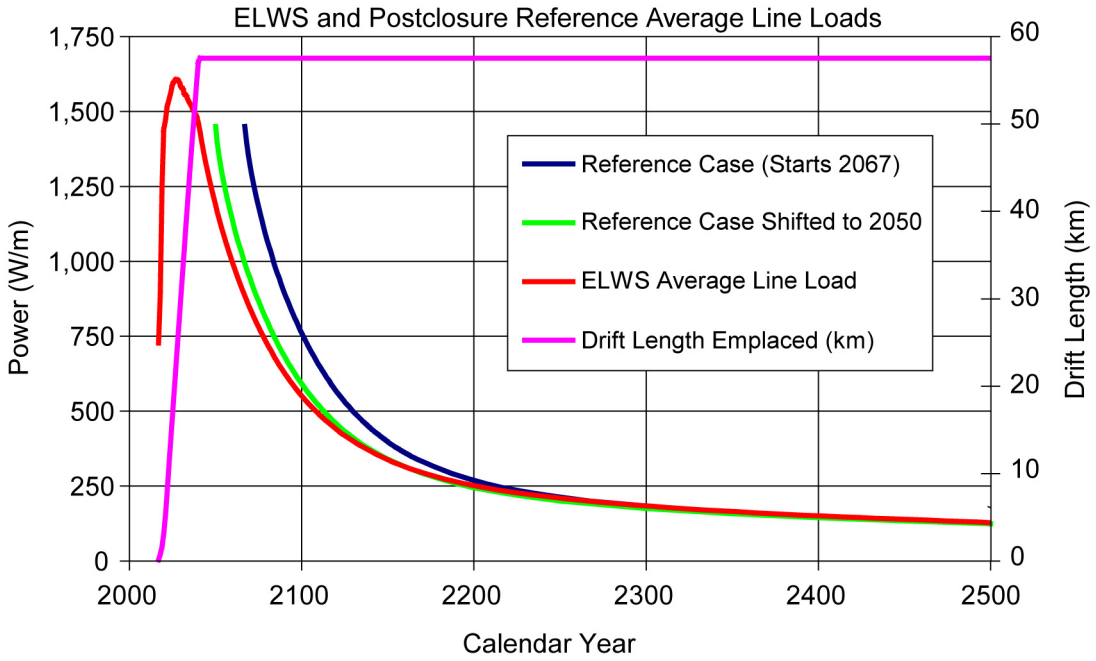

Source: Output DTN: MO0705SUPPCALC.000, folder: \YFF5_22 Envelope, file: *Average Line Load.xmcd.xls.*

NOTE: Shifting the reference to begin at year 2050 is done for illustrative purposes, for comparison to the ELWS.

Figure 6.1-1. Comparison of Average Lineal Power Decay Functions

6.1.3 Postclosure Peak Mid-Pillar Temperature

When this study was planned, the mid-pillar temperature limit was thought to be limiting, among all the postclosure temperature limits (SNL 2007 [DIRS 179196], Section 7; see Section 6.3 for discussion of limiting temperature criteria). To investigate the peak mid-pillar temperatures associated with the range of thermal loadings, a conduction-only method was developed. The approach is based on that used for the condensation model (SNL 2007 [DIRS 181648], Section 6.3), the ventilation model (BSC 2004 [DIRS 169862]), and the thermal loading flexibility analysis (SNL 2007 [DIRS 179196], Sections 6.3 through 6.6). The approach used here is simplified, permitting thousands of calculations corresponding to individual waste packages, and tailored to the calculation of mid-pillar (and drift wall) temperature.

In its simplest form the analysis method superimposes parallel line heat sources representing emplacement drifts, in an infinite space occupied by a conductive solid. The temperature is calculated at the center of a pillar between two drifts, flanked by a sufficient number of additional drifts on both sides. A uniform initial temperature is assigned to the host rock. Hydrologic processes are neglected as a simplification, which is justified because hydrology always tends to produce cooler conditions. Thermal stratigraphy in the unsaturated zone, and

thermal boundary conditions at the water table and the ground surface, are neglected as model simplifications, which is justified because the mid-pillar temperature occurs before there is much influence from these features. A fixed ventilation efficiency of 86% is used, consistent with previous studies (BSC 2004 [DIRS 169862], Table 8-2; temporal and spatial average for 800-m drifts). This value may slightly under-estimate heat removed by ventilation (by a few percent) based on more recent analysis using the ventilation model (SNL 2007 [DIRS 179196], Section 6.3.2).

The result of the peak mid-pillar temperature calculation is an index of thermal energy density for each waste package (waste package index – mid-pillar, or WPIMP) that takes into account its time-varying thermal output, and the thermal properties of the host rock, to represent the contribution of each package to mid-pillar temperature. As an index, the result does not need to be highly accurate, but it has sufficient relative accuracy to compare waste package contributions to heating, and it is shown to be a conservative approach for determining that the mid-pillar temperature limit will be met.

The mid-pillar index (WPIMP) for any particular waste package is defined as the resultant peak mid-pillar temperature if the entire repository is loaded with identical packages with those thermal characteristics. Thus, the index shows whether a particular package can possibly produce over-limit temperatures. If all waste packages have mid-pillar indices less than 96°C, then it is obvious that the peak mid-pillar temperature limit will be met everywhere that the host-rock properties apply.

Line-Source Calculation Method for WPIMP – The mid-pillar temperature is determined for an instantaneous infinite line source in an infinite medium from an analytic equation (Carlsaw and Jaeger 1959 [DIRS 100968], Section 10.3):

$$T(\Delta x, \Delta z, t)\big|_{Line\ Source} = T_0 + \frac{Q_{Line}}{4(\pi \kappa t)} e^{-\left\{\frac{(\Delta x^2 + \Delta z^2)}{4\kappa t}\right\}} \qquad \text{(Eq. 6.1-1)}$$

where

T_0 = initial (ambient background) temperature (25 °C).

t = time (sec), such that the heat source occurs at $t = 0$.

Q_{Line} = instantaneous line heat source strength ($K \cdot m^2$), defined as lineal power (W/m) times source duration (sec), divided by the product of bulk density (kg/m^3) and specific heat (J/kg·K). The source duration must be short compared to the heat transport time.

κ = thermal diffusivity (m^2/sec).

Δx, Δz = distances from the line source in x and z directions (m) with the origin of the coordinate system at the drift centerline.

For a time-varying heat source such as a repository drift with an average line thermal load, Equation 6.1-1 is convolved with the thermal decay curve to yield the temperature as a function of time and distance from the line source (see Carlsaw and Jaeger 1959 [DIRS 100968], Equation 3, p. 261):

$$T(\Delta x, \Delta z, t)\big|_{Time\ Varying\ Line\ Source} = T_0 + \int_0^t \frac{Q_{Line}(\tau)}{4(\pi\kappa)(t-\tau)} e^{-\left\{\frac{(\Delta x^2+\Delta z^2)}{4\kappa(t-\tau)}\right\}} d\tau \qquad \text{(Eq. 6.1-2)}$$

where

τ = integration time-variable.

$Q_{Line}(\tau)$ = time-varying line heat source strength function (thermal decay curve).

If the thermal decay curve is a discrete time series, the convolution is numerical. If the decay curve can be represented by a fitted function, the convolution can be performed analytically. In evaluating the ELWS, the numerical approach is used for every waste package in the ELWS, with discrete decay curves from DTN: MO0707ELWSDNSL.000 [DIRS 183774] (file: *WP_Decay_70K22kw_011707_DS.xls*). For exposition of mid-pillar temperature behavior in this section, an analytical solution is used based on a thermal decay function fitted to the average line load decay history for the postclosure thermal reference case (Output DTN: MO0705SUPPCALC.000, folder: \Other Supporting Files, file: *Reference Line Load Fit.xls*).

For the analysis in this section, the thermal properties of the host rock are chosen to represent the mean properties of the lower lithophysal (Tptpll) unit with 90.5% in situ liquid saturation, 14.86% matrix porosity, and 8.83% lithophysal porosity (Table 4.1-4). Thermal diffusivity is defined by Carslaw and Jaeger (1959 [DIRS 100968], Section 1.6) as $\kappa = K_{th} / \rho C_p$, where K_{th} is thermal conductivity (W/m-K), ρ is density (kg/m^3), and C_p is specific heat (J/kg-K). The estimation approach for thermal diffusivity follows that of *Thermal Management Flexibility Analysis* (SNL 2007 [DIRS 179196], Section 6.3 and Appendix A). The volume of liquid water is corrected for both the lithophysal and matrix porosities, because the lithophysal pores are so large that they always have zero liquid saturation. The density and specific heat for liquid water are assigned values of 982.3 kg/m^3 and 4,186 J/kg-K, respectively, interpolated from handbook values at a representative temperature of 62°C (335 K approximately halfway between 23°C and 96°C; Incropera and DeWitt 2002 [DIRS 163337], Table A.6). The grain density and grain specific heat for the rock are taken to be 2,550 Kg/m^3 and 930 J/kg-K, respectively, consistent with previous studies (SNL 2007 [DIRS 179196], Section 4.1.13.4). The resulting value of thermal diffusivity, rounded to two significant figures and used in this analysis, is 7.7×10^{-7} m^2/sec.

The z-direction is chosen to be vertical, and Δx = the pillar half-width of 40.5 m (Section 4.1.1). In this section every waste package is assumed to have thermal decay characteristics of the average line load for the postclosure reference case (Table 4-1.1). This assumption facilitates analysis of the effect of waste package position, including the effect of thermal decay, without the complication of package-to-package variability in heat output. Also, the average line-load

decay curve for the postclosure reference case has a similar shape to that for the hotter waste packages in the ELWS for which the index methodology is most useful.

The calculation includes the contribution from four drifts on each side of the desired mid-pillar location (by summing the results with appropriate Δx values).

$$T(\Delta x|_i, \Delta z|_i, t)\Big|_{Time\ Varying\ Line\ Sources} = T_0 + 2 \cdot \sum_{i=1}^{N_D} \int_0^t \frac{Q_{Line}(\tau)}{4(\pi\kappa)(t-\tau)} e^{-\left\{\frac{(\Delta x_i^2 + \Delta z_i^2)}{4\kappa(t-\tau)}\right\}} d\tau \quad \text{(Eq. 6.1-3)}$$

Four drifts on each side of the mid-pillar location to be evaluated are represented by the summation (N_D = 4) which is doubled to represent both sides. The mid-pillar temperature history for the average ELWS line load, using the mean thermal conductivity and other properties for the lower lithophysal (Tptpll) host-rock unit (Section 4.1.1), is shown in Figure 6.1-2.

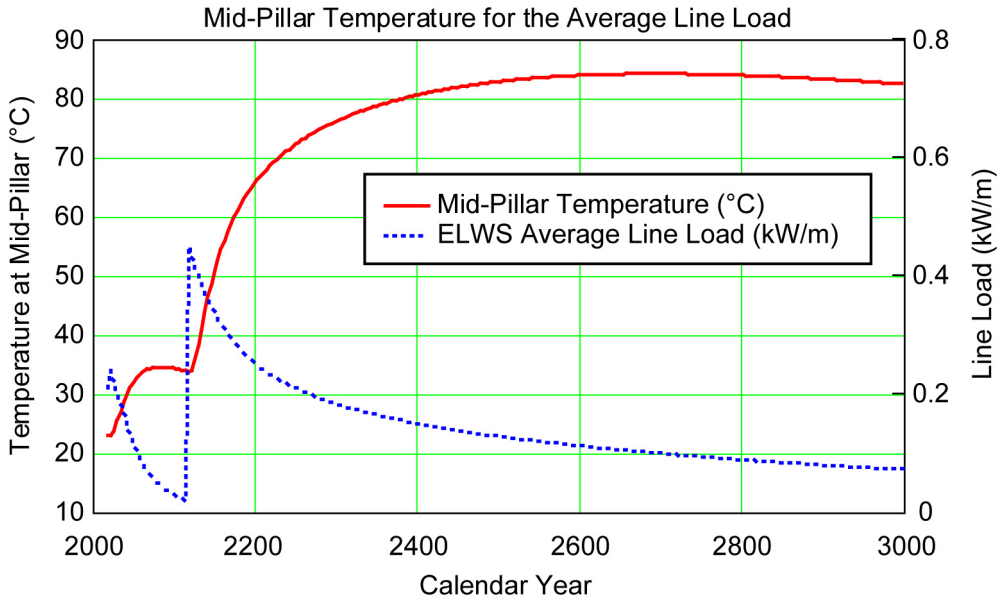

Source: Output DTN: MO0705SUPPCALC.000, folder: \YFF5_22 Envelope, file: *Unit Pulse Solution for the Calculation of the Average MidPillar Temperatures Rev01.xmcd*.

NOTE: Mid-pillar temperature calculated using the mean wet thermal conductivity for the lower lithophysal host-rock unit.

Figure 6.1-2. ELWS Average Line Load and Mid-Pillar Temperature

The mid-pillar index (WPIMP) is calculated using Equation 6.1-3, and is the peak mid-pillar temperature if the entire repository (approximated by 8 drifts, each represented by an infinite line source) is filled with identical waste packages. The WPIMP takes into account differences in thermal decay rates among waste packages of different types. Importantly, mid-pillar temperature increases within a few hundred years after closure of the repository, and is then very "flat" near the peak. This behavior is useful because the peak WPIMP temperatures for different types of waste packages can be compared, or averaged together, without concern for the time at which the peak occurs. It is slightly conservative to take the average of peak WPIMP values for

adjacent waste packages, corresponding to different peak times, since this maximizes the contribution from every waste package to the computed mid-pillar temperature estimate.

A histogram of WPIMP values for all 10,394 waste packages in the ELWS, using mean thermal properties of the lower lithophysal (Tptpll) host-rock unit, is shown in Figure 6.1-3. Approximately half of the waste packages in the ELWS have WPIMP values that exceed the limit of 96°C. These packages will be emplaced with, and adjacent to, cooler packages so that the local peak mid-pillar temperature is limited. This section describes use of the running average of mid-pillar index values as a "loading rule" for generating emplaced sequences from the ELWS, to ensure that the mid-pillar limit is met.

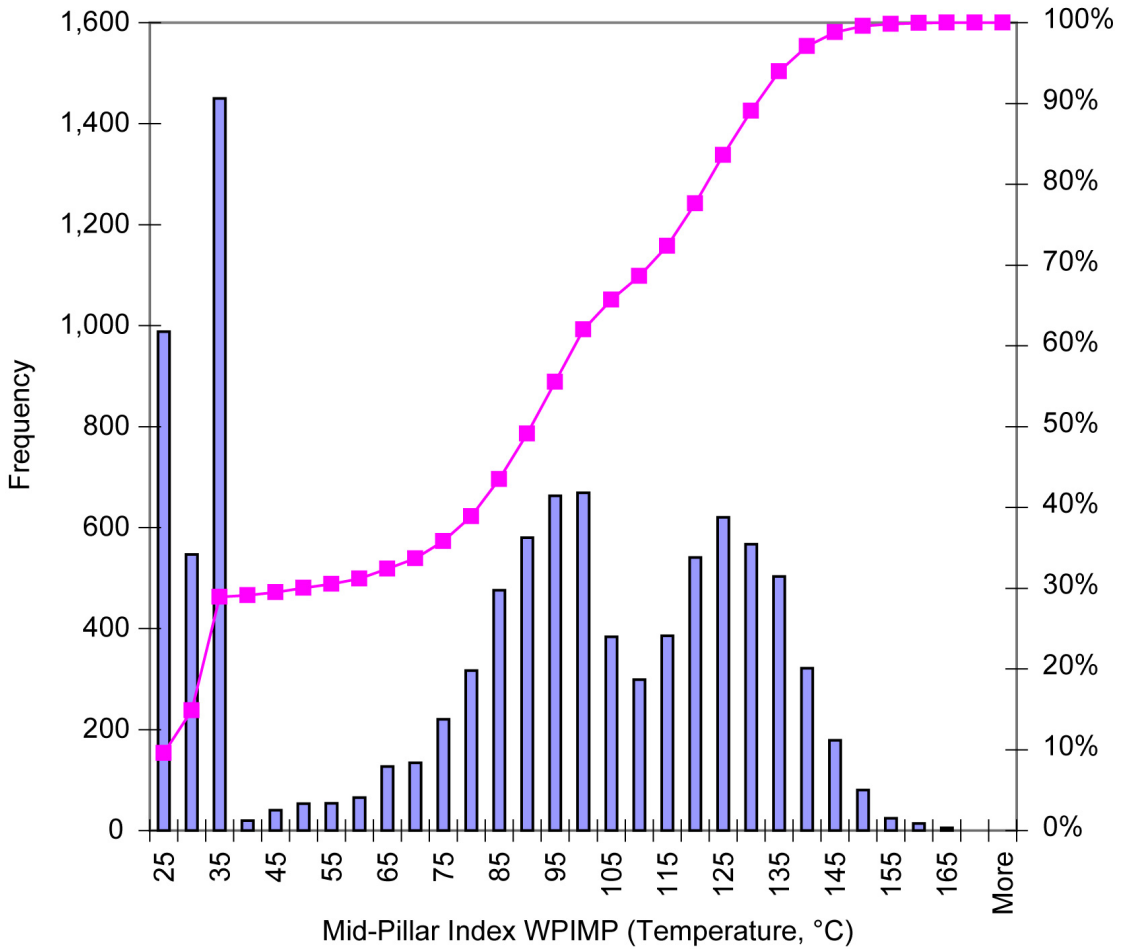

Source: Output DTN: MO0705SUPPCALC.000, folder: \YFF5_22 Envelope, file: *Worksheet in Histogram of Peak Mid Pillar Temperatures Rev02.xmcd.xls*.

NOTE: WPIMP indices calculated using the mean wet thermal conductivity for the lower lithophysal host-rock unit.

Figure 6.1-3. Histogram of Peak Mid-Pillar Temperature for the ELWS Case

Uncertainty and Variability of Rock Thermal Properties – The mid-pillar temperature or WPIMP index for each waste package depends on the thermal diffusivity (κ) for the host rock. Whereas κ is directly proportional to thermal conductivity and inversely related to density and specific heat ($\kappa = K_{th}/\rho C_p$), this means that WPIMP is actually a distributed parameter that depends on the host stratigraphic unit, and the uncertainty of K_{th} for each unit.

For WPIMP calculations, the wet thermal conductivity values for the host rock are used (Section 4.1.1). Thermal-hydrologic modeling has shown that dryout around the emplacement drifts typically extends to a distance on the order of 10 m from the drift centerline (SNL 2007 [DIRS 181383], Table 6.3-40). The host rock beyond this distance, in the pillar and above and below the drift opening, remains at high liquid saturation on the order of 90% or greater (SNL 2007 [DIRS 181383], Table 6.3-1). Accordingly, the wet value (saturation of 100%) is a suitable approximation for calculating this index. The effect of dryout on thermal conductivity and temperature is substantially limited to the dryout zone and the drift within it.

To characterize the impact of uncertainty and variability, a Monte Carlo analysis was performed to recalculate the histogram of WPIMP values (Figure 6.1-3) for each unit, sampling values of thermal conductivity using the same weighted sampling scheme developed for the multiscale model (SNL 2007 [DIRS 181383]). The thermal conductivity values (Table 4.1-2) and the sampling weights (Table 4.1-3) are combined to produce new histograms for each host-rock unit (Figure 6.1-4). The results indicate similar distributions with up to 15°C difference among host rock units, and dominance by the lower lithophysal unit (comprising 85% of the repository area).

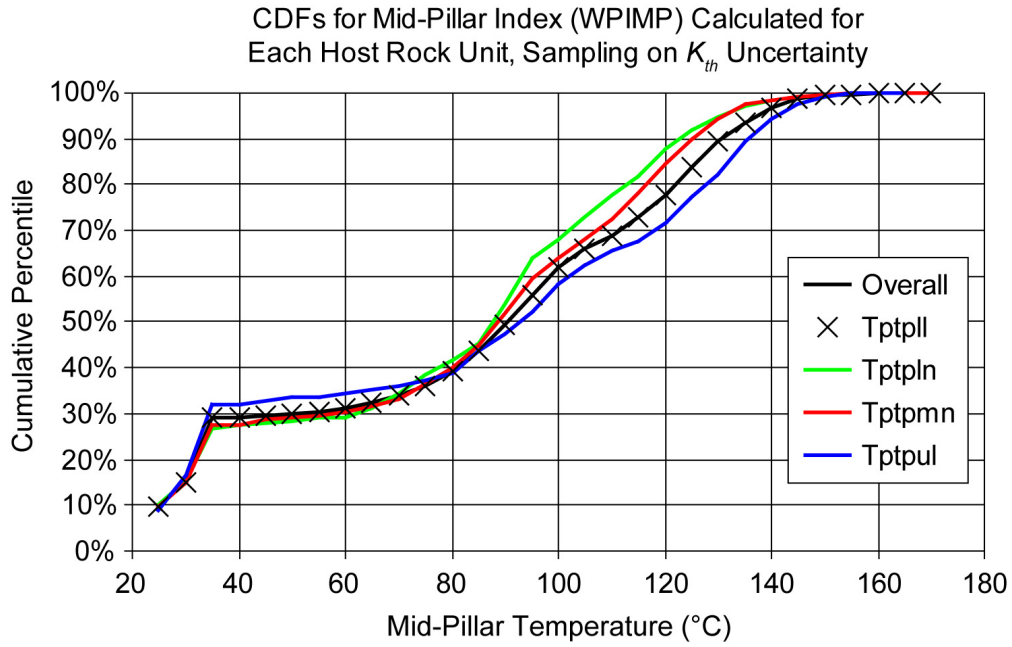

Source: Output DTN: MO0705SUPPCALC.000, folder: \Composite Histogram, file: *Worksheet in Mid Pillar Temperature Index Composite Histogram.xmcd.xls*.

NOTE: WPIMP indices calculated for each host-rock unit, sampling on the weighted distribution of 10th percentile, mean, and 90th percentile values of the wet thermal conductivity for the unit.

Figure 6.1-4. Cumulative Distribution Functions for the WPIMP Index for Each Host-Rock Unit

Further Discussion of the Mid-Pillar Index (WPIMP) Calculation Method – More distant drifts do not contribute significantly to the mid-pillar peak temperature calculated in the manner of Figure 6.1-2. The peak temperature from line sources at various distances, calculated from Equation 6.1-2, shows that the effect from the pair of drifts in the fifth position (at a distance 3.5 times the drift spacing) on overall peak temperature is approximately 1.3% of the total (Output DTN: MO0705SUPPCALC.000, folder: \Other Supporting Files, file: *Four drift justification.xmcd*). When the timing of the peak temperatures is taken into account, the peaks from the more distant drifts arrive later than the dominant peak from the closest drift. For example, the effect from the fifth drift evaluated at 2,365 years, instead of 647 years, is approximately 8.8% of the total from all drifts (Output DTN: MO0705SUPPCALC.000, folder: \Other Supporting Files, file: *Four drift justification.xmcd*). Contributions from the closer drifts thus dominate the mid-pillar temperature response at approximately 400 to 700 years when the peak temperature occurs. The same conclusion reached for drifts beyond the fourth can also be made for waste packages with axial separation greater than approximately 300 m. The effect of constant temperature at the ground surface or the water table can be represented using image sources (Carslaw and Jaeger 1959 [DIRS 100968], Section 10.10) hundreds of meters away, and therefore the same conclusion applies to the effects from these boundaries on the peak mid-pillar temperature. Thus, the line-source approximation for emplacement drifts is a reasonable representation for WPIMP, i.e., the maximum mid-pillar temperature near the repository center.

The following point-source analysis shows that the running average methodology mentioned in this section gives a valid, and likely conservative, result with respect to mid-pillar temperature.

Point-Source Calculation Method for Individual Waste Packages – For this analysis each waste package in a drift must be considered independently, so a point-source (rather than line-source) geometry is used for calculating mid-pillar temperature (Carlsaw and Jaeger 1959 [DIRS 100968], Section 10.2):

$$T(\Delta x, \Delta y, \Delta z, t)\big|_{Point\ Source} = T_0 + \frac{Q_{Point}}{8(\pi\kappa t)^{3/2}} e^{-\left\{\frac{(\Delta x^2+\Delta y^2+\Delta z^2)}{4\kappa t}\right\}} \qquad \text{(Eq. 6.1-4)}$$

where

t = time (sec), such that the heat pulse occurs at $t = 0$.

Q_{Point} = instantaneous point heat source strength ($K \cdot m^3$), defined as power (W) times source duration (sec) divided by the product of bulk density (kg/m^3) and specific heat (J/kg·K). The source duration must be short compared to the heat transport time.

κ = thermal diffusivity (m^2/sec).

Δx, Δy, Δz = distances from the source in x, y, and z directions (m) with the origin of the coordinate system located on the drift centerline, at the mid-point of the waste package for which the effect is evaluated.

Although the point-source solution can be integrated to represent finite line sources, the mid-pillar location is far enough from the drift that each waste package can be adequately represented by a point source (this will be demonstrated in the analysis below). For a time-varying heat source such as a repository drift with an average line thermal load, Equation 6.1-4 is convolved with the thermal decay curve to yield the temperature as a function of time and distance from the line source:

$$T(\Delta x, \Delta y, \Delta z, t)\big|_{TimeVaryingPoint Source} = T_0 + \int_0^t \frac{Q_{Point}(\tau)}{8(\pi\kappa)^{3/2}(t-\tau)^{3/2}} e^{-\left\{\frac{(\Delta x^2+\Delta y^2+\Delta z^2)}{4\kappa(t-\tau)}\right\}} d\tau \quad \text{(Eq. 6.1-5)}$$

where

τ = integration time-variable.

$Q_{Point}(\tau)$ = time-varying point heat source strength function (thermal decay curve).

Summing the waste packages present in four drifts on each side of a mid-pillar location, analogous to Equation 6.1-3, gives (from Carslaw and Jaeger 1959 [DIRS 100968], Section 10.4, Equation 1, p. 261):

$$T(\Delta x|_i, \Delta y|_j, t)\Big|_{Time\,Varying\,Point\,Sources} = T_0 + 2 \cdot \sum_{i=1}^{N_{Drift}} \sum_{j=1}^{N_{WP}} \int_0^t \frac{Q_{Point}(\tau)}{8(\pi\kappa)^{\frac{3}{2}}(t-\tau)^{\frac{3}{2}}} e^{-\left\{\frac{(\Delta x_i^2+\Delta y_j^2)}{4\kappa(t-\tau)}\right\}} d\tau \quad \text{(Eq. 6.1-6)}$$

The z-direction is vertical ($\Delta z = 0$), the x-direction is horizontal and perpendicular to drifts so that $\Delta x_i = 40.5$ m + (i-1)·81 m, and the y-direction is parallel to the drift axes. For this point-source analysis the waste packages are represented by point sources spaced at 6-m intervals, i.e., all waste packages are 6 m long, which is an appropriate simplification for sensitivity analysis. For drift length of 800 m, there are 133 such sources in each drift, for a total of 1,064. Each point source is assigned the thermal output and decay characteristics of the postclosure thermal reference case average line-load (Section 4.1.1) for the purpose of demonstrating that the point and line source equations produce similar results at the mid-pillar.

Equation 6.1-6 was solved numerically using Mathcad to estimate (see Output DTN: MO0705SUPPCALC.000, folder: \Other Supporting Files, file: *index concept 4.xmcd*) the contribution of each identical waste package (i.e., point source) in the array, to the peak temperature for the mid-pillar location at the center-point of the array. Figure 6.1-5 is a histogram of distances from the 1,064 sources to the center-point. Applying Equation 6.1-6 yields the point-source temperature history in Figure 6.1-6.

The mid-pillar temperature history calculated from superposition of 1,064 point sources is very similar to that calculated from superposition of infinite line sources (as done for the mid-pillar index WPIMP). Comparing the point-source and line-source curves in Figure 6.1-6, the results are indistinguishable at early time, but the point-source solution decays slightly faster because it does not have heat sources beyond the ends of the 800-m emplacement drifts. Thus, the WPIMP

is slightly conservative with respect to explicit point-source calculations with similar parameterization.

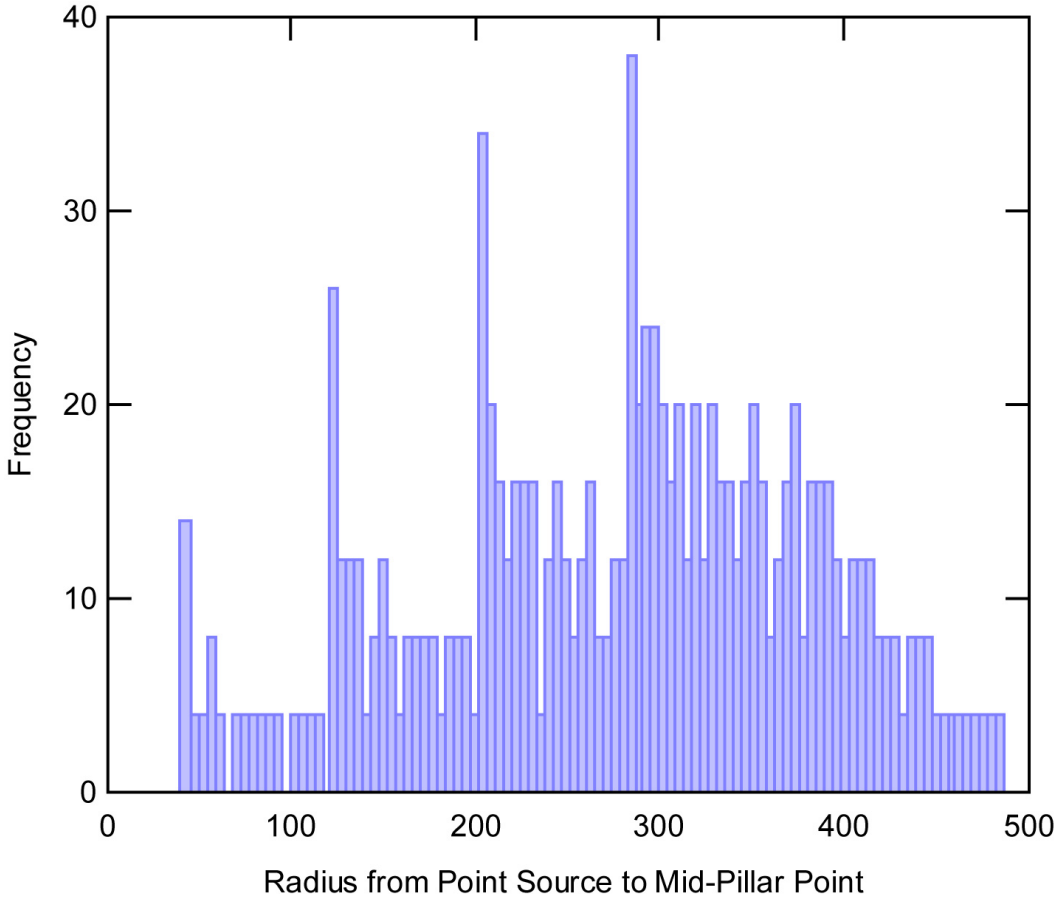

Source: Output DTN: MO0705SUPPCALC.000, folder: \Other Supporting Files, file: *index concept 4.xmcd*.

Figure 6.1-5. Histogram of Distances from 1,064 Waste Packages in the Eight Drifts Closest to a Mid-Pillar Location

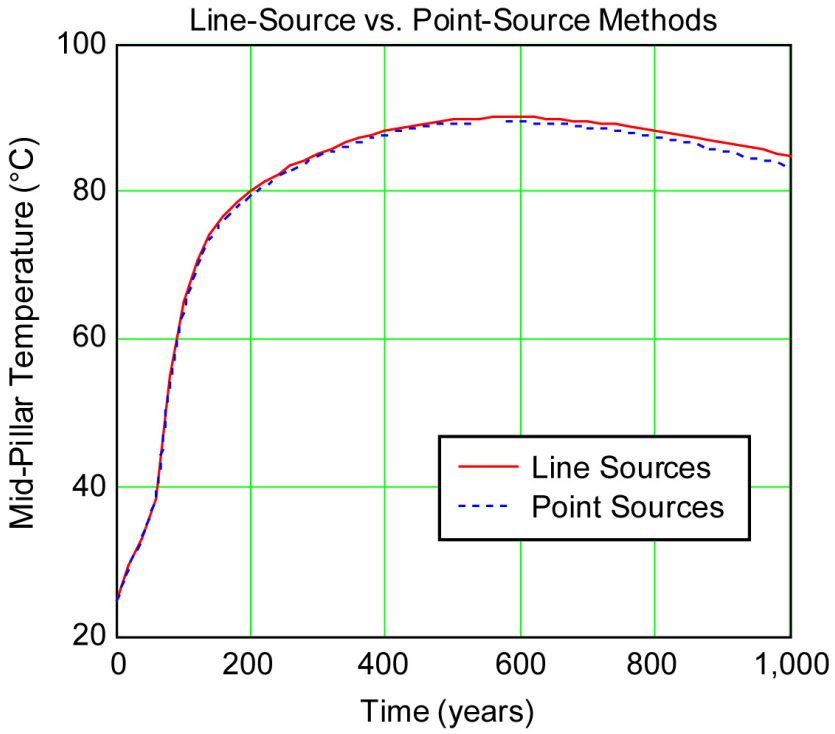

Source: Output DTN: MO0705SUPPCALC.000, folder: \Other Supporting Files, file: *index concept 4.xmcd*.

NOTES: Solid curve is line source solution (8 superposed infinite line sources); dashed curve is for point sources.

Calculated using the postclosure thermal reference case line load, which for the point-source result is assigned to 1,064 point sources, each representing one waste package with uniform 6-m length, and arrayed to represent 8 parallel drifts.

Use mean wet thermal conductivity for the lower lithophysal host-rock unit.

Figure 6.1-6. Comparison of Mid-Pillar Temperature Histories Calculated Using Line-Source and Point-Source Methods

Relative Contributions to Mid-Pillar Temperature – To understand the relative contributions of each waste package to the thermal response at any mid-pillar location, an analysis was performed to compare the contribution of each waste package, at selected times spanning the time period when peak mid-pillar temperature will occur. Rather than evaluate Equation 6.1-5 for every waste package, the temperature calculations represented by Equation 6.1-5 were performed for every bin of the histogram in Figure 6.1-5. The result for each bin was then weighted by the number of waste package locations for that bin. The calculations were repeated for a sequence of discrete time values, generating curves for temperature effect vs. distance, at each time value. Finally, the results for each time value were normalized, such that the sum of weighted temperature effects for all bins is unity. The plots of relative temperature effect vs. distance for selected time values are shown in Figure 6.1-7 (Output DTN: MO0705SUPPCALC.000, folder: \Other Supporting Files, file: *Normalized Time-Distance CalcsPlot.xls*).

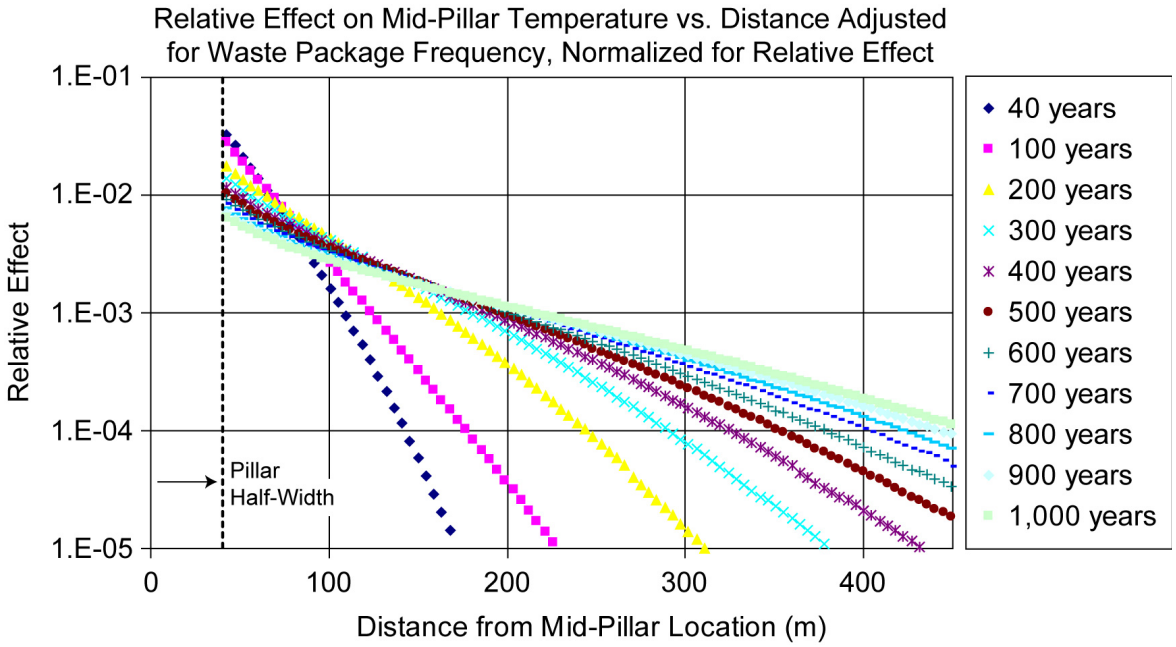

Source: Output DTN: MO0705SUPPCALC.000, folder: \Other Supporting Files, file: *Normalized Time-Distance Calcs.xls.*

NOTES: Calculated using the postclosure thermal reference case line load, assigned to 1,064 point sources each representing one waste package with uniform 6-m length, and arrayed to represent 8 parallel drifts.

Use the mean wet thermal conductivity for the lower lithophysal unit.

Figure 6.1-7. Relative Effect on Mid-Pillar Temperature from Waste Packages at a Range of Distances

Figure 6.1-7 shows that the closest waste packages in the nearest drifts ($\Delta x_i = 40.5$ m) exert the strongest effect on mid-pillar temperature. This is especially true for time less than 200 years, but continues throughout the period when peak mid-pillar temperature occurs (approximately 400 to 700 years; see Figures 6.1-2 and 6.1-6). The effect is attenuated with distance, so that beyond approximately 100 m (or roughly 20 package locations) the relative effect (which is time-dependent) is reduced by approximately a factor of 2 or more (i.e., all lines in Figure 6.1-7 decrease by approximately one third of a log unit, or more, from the pillar half-width to 100 m). The next furthest drifts, at a minimum distance of 121.5 m, have further reduced effect. When the peak mid-pillar temperature occurs (the curves for 400 through 700 years are bold) the effect from the nearest two drifts is greater than that from all other further drifts (three pairs included in calculations for Figure 6.1-7, which yields very similar results compared with four pairs for WPIMP and point-source sensitivity analyses discussed previously).

Simulation of Inhomogeneous Loading – The seven-package running average WPIMP approach implemented as a "loading rule" for emplacement sequences maintains the mid-pillar temperature at or below the limit everywhere in the repository because: (1) the pillar half-width (40.5 m) is sufficient to smear the individual responses of the closest packages, and (2) the running-average approach is applied everywhere in the repository, at every possible waste package position. The latter condition means that each waste package contributes to the running average WPIMP in seven adjacent seven-package segments. If all waste packages in the repository have a mid-pillar index less than the mid-pillar temperature limit, then it is obvious

that the mid-pillar limit will be met everywhere. However, the same condition is also met if the local, running average WPIMP is less than the mid-pillar temperature limit, even if some individual waste package WPIMP values exceed the limit.

To demonstrate the "smearing" effect of the pillar half-width on individual waste package heats, a simple simulation was done by increasing and decreasing the thermal output of the seven closest waste packages in one of the nearest drifts (Table 6.1-1). The heat output of three packages was doubled, corresponding approximately to a WPIMP value of 165, which is near the maximum on the histogram for the ELWS (Figure 6.1-3). This comparison is derived by letting the repository-average peak mid-pillar temperature for the ELWS be 96°C, which is 73°C greater than the ambient background of 23°C. Adding 73°C to 96°C yields 169°C, which is the approximate upper limit of the WPIMP values on Figure 6.1-3. Hence doubling the heat output for a particular package-source is approximately equivalent to the maximum range of the WPIMP index for the ELWS waste stream, for use in this sensitivity analysis.

Table 6.1-1. Multipliers Used on Seven Packages Closest to the Mid-Pillar Location

Δx (m)	Δy (m)	Multiplier (m)
40.5	–18	0.4
40.5	–12	2
40.5	–6	0.1
40.5	0	2
40.5	6	0.1
40.5	12	2
40.5	18	0.4

The heat output of the remaining four waste packages in the segment was reduced so that all seven waste packages average to the postclosure reference case line load. The resulting mid-pillar temperature history (Figure 6.1-8) is indistinguishable from the curve calculated using Equation 6.1-6 with uniform point-sources everywhere. The seven-package running average is actually conservative, because a longer running-average operator could be used as suggested by Figure 6.1-7, in which the relative effect from more than seven of the closest packages (extending to distances well in excess of 40.5 m) is nearly the same. In other words, the seven-package running average is more restrictive than needed to control mid-pillar temperature, which is shown on Figure 6.1-7 because at times from 400 to 700 years, waste package contributions are similar out to 100 m or more. Thus, a longer average could be used with similar effect. Note that the seven-package running average is used for the WPIMP loading rule, for simplicity, because it is also needed for the 2.0 kW/m average loading limit discussed below.

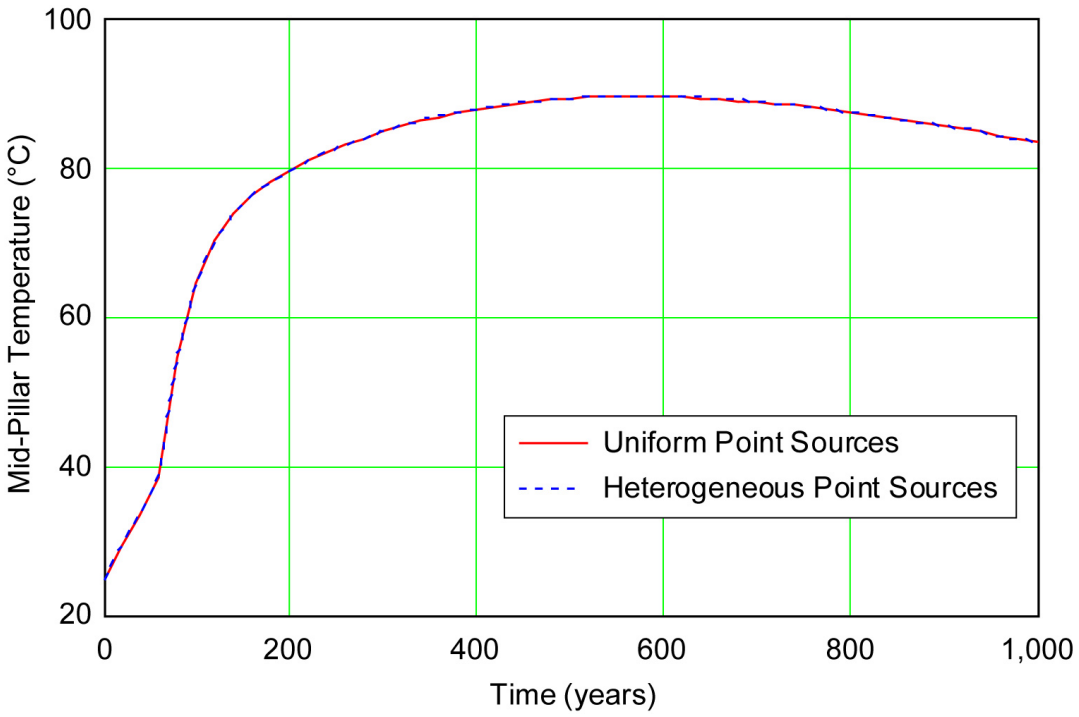

Source: Output DTN: MO0705SUPPCALC.000, fold er: \Other Supporting Files, file: *index concept 4.xmcd*.

NOTES: Solid curve is for uniform waste package heat output; overlying dashed curve is for modified nearby sources.

Calculated using the postclosure thermal reference case line load, assigned to 1,064 point sources each representing one waste package with uniform 6-m length, and arrayed to represent 8 parallel drifts.

Use mean wet thermal conductivity for the lower lithophysal host-rock unit.

Figure 6.1-8. Comparison of Mid-Pillar Temperature Calculated for Arrayed Uniform Point-Sources, with Increased and Decreased Output for the Seven Closest Waste Packages

Emplacement Sequences – Post-processing of the total system model output for the ELWS case was performed to produce two realizations of the emplaced sequence. These are the 85/4 case and the 96/2 case, which implement mid-pillar index (WPIMP) seven-package running average limits of 85°C and 96°C, respectively (emplacement sequences are found in DTN: MO0705WASTELIM.000 [DIRS 181570], file: *WP_Emplaced_ELWS_011707_23C_0501077.xls*). For the 85/4 case, the maximum amount of surface storage used to buffer the received waste packages before emplacement underground was equivalent to approximately 4 years of waste receipts at Yucca Mountain, while for the 96/2 case, storage equivalent to approximately 2 years of receipts was used. Further details of these cases are documented in the TSM study (SNL 2007 [DIRS 179354], Table 4-4, Parameter 05-03). Qualification of these input data including the emplacement sequences is addressed in Appendix B.

The emplacement sequence cases used the following "loading rules":

1. The seven-package running average of the mid-pillar index (WPIMP) was limited to either 85°C or 96°C.

2. 2.0 kW/m maximum average thermal line-load at emplacement, averaged over any seven adjacent waste packages.

3. 18.0 kW maximum waste package power at emplacement.

The latter two rules were implemented to constrain temperatures that would be reached in off-normal interruptions of preclosure forced ventilation (see SNL 2007 [DIRS 179354], Table 4-4, Parameter 05-03). They were also assumed to limit postclosure drift wall temperature to 200°C (Assumption 5.1).

The 85°C mid-pillar index running-average target was selected for the 85/4 case because this is the overall average WPIMP value for the ELWS, using the mean value of (wet) thermal conductivity for the lower lithophysal (Tptpll) host rock unit. In other words, this case represents the coolest possible thermal loading conditions. The sequences can be characterized as mixtures of CSNF and cooler DHLW waste packages, with more distribution of DHLW packages throughout the emplacement drifts. In the 96/2 case, the number of DHLW packages is the same, but many of them are emplaced later, after the CSNF is emplaced (see SNL 2007 [DIRS 179354], Table 4-4, Parameter 05-03). The next section describes the method used to identify the hottest and coolest segments within these sequences, using drift wall temperature calculations.

6.1.4 Postclosure Peak Drift Wall Temperature

The principal output from this section is the selection of hottest (and coolest) intervals within the as-emplaced ELWS for assessment of geomechanical, hydrogeologic, and geochemical responses (Section 6.4). The extent to which these responses can affect conditions within the emplacement drifts is determined by their effect on the host rock around the drift opening. Hence drift wall temperature is a better indicator of thermal effects on repository performance than far-field measures such as mid-pillar temperature.

Accordingly, the hottest intervals are selected using a measure of peak drift wall temperature, calculated using a modified form of Equation 6.1-3, to calculate drift crown temperature:

$$T(\Delta x|_i, \Delta z|_i, t)\Big|_{Time\ Varying\ Line\ Sources} = T_0 + \int_0^t \frac{Q_{Line}(\tau)}{4(\pi\kappa)(t-\tau)} e^{-\left\{\frac{(R^2)}{4\kappa(t-\tau)}\right\}} d\tau + 2 \cdot \sum_{i=1}^{N_D} \int_0^t \frac{Q_{Line}(\tau)}{4(\pi\kappa)(t-\tau)} e^{-\left\{\frac{(\Delta x_i^2 + R^2)}{4\kappa(t-\tau)}\right\}} d\tau \quad \text{(Eq. 6.1-7)}$$

where R is the drift radius. This approach takes the history of thermal decay into account, which is appropriate because decay history can vary greatly among CSNF waste packages during the first 50 to 150 years after emplacement when peak near-field temperatures will occur.

Calculation of the Drift Wall Index (WPIDW) – The peak drift wall temperature is calculated as an index of energy density for each waste package similar to the mid-pillar index (WPIMP) described previously. The WPIDW (waste package index – drift wall) is defined as the conduction-only, radial heat flow-only, drift wall temperature calculated using line sources with strength equivalent to each particular waste package, i.e., for a repository filled entirely with identical waste packages. Unlike the WPIMP index, the WPIDW index cannot be readily averaged along the drift as a predictor of peak postclosure drift wall temperature because the effects of axial heat sharing by natural convection and thermal radiation within the drift opening are not well described by a running average.

To calculate WPIDW, the thermal diffusivity for the host rock is needed. Unlike the WPIMP index, some representation of the effect of dryout is needed to avoid under-predicting the potential effect on local peak drift wall temperature from hotter waste packages. As a first approximation, an average of the wet and dry thermal conductivity values for the lower lithophysal (Tptpll) host-rock unit is used. This corresponds to 50% liquid saturation, and the specific heat is modified to include the corresponding amount of liquid water. This approach actually over-predicts temperature as shown in the sensitivity analysis presented in Section 6.2.2. In addition, the 10th percentile values of the Tptpll thermal conductivity are used (Section 4.1.1), which further avoids the potential for under-predicting local effects.

Drift wall temperature for the ELWS overall average line load is shown in Figure 6.1-9. This calculation implements Equation 6.1-7, superimposing four emplacement drifts on either side, and using the 10th percentile rock properties and 50% liquid saturation described above. The line load is reduced by ventilation for 74 years, with repository closure in calendar year 2117 (Output DTN: MO0705SUPPCALC.000, folder: \YFF5_22 Envelope, file: *Unit Pulse Solution for the Calculation of the Average Driftwall Temperatures Rev01.xmcd*). This ventilation duration would apply to the last few years of CSNF waste packages emplaced in the sequences identified in Section 6.1.3, with repository closure in 2117. The resulting peak drift wall temperature is approximately 160°C (less than the limit of 200°C) demonstrating that the drift wall temperature limit is met by the overall average thermal loading.

Repeating the calculation for each waste package in the ELWS, yields the histogram of WPIDW values shown in Figure 6.1-10. Approximately 10% of these values exceed 200°C, demonstrating that the drift wall temperature limit is not necessarily met for local thermal loading conditions, depending on the loading sequence.

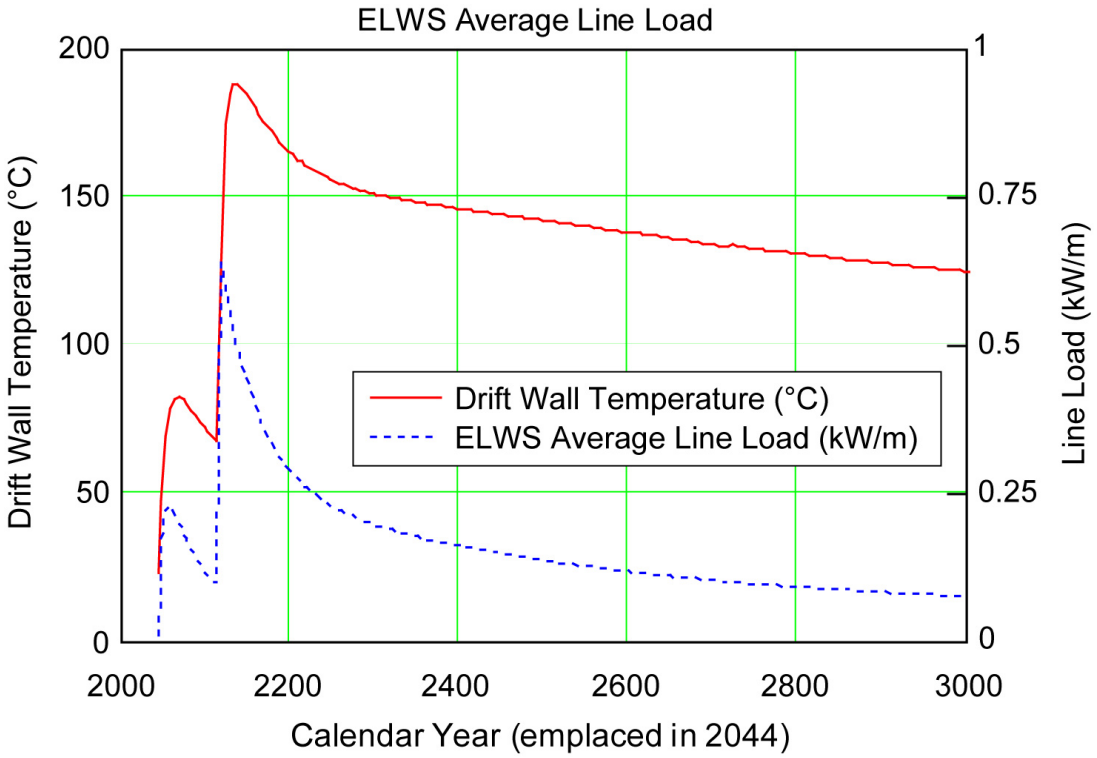

Source: Output DTN: MO0705SUPPCALC.000, folder: \Other Supporting Files, file: *Envelope Cases (line load).xmcd*.

NOTE: Drift wall temperature is calculated using nine superposed infinite line sources representing drifts, with the 10th percentile thermal conductivity values for the lower lithophysal host rock unit, and 50% matrix liquid saturation. Note that for drift wall temperature the sources represent nine drifts instead of the eight used for mid-pillar temperature, because the calculation is centered on a drift instead of on the center of a pillar.

Figure 6.1-9. ELWS Average Line Load and Corresponding Drift Wall Temperature

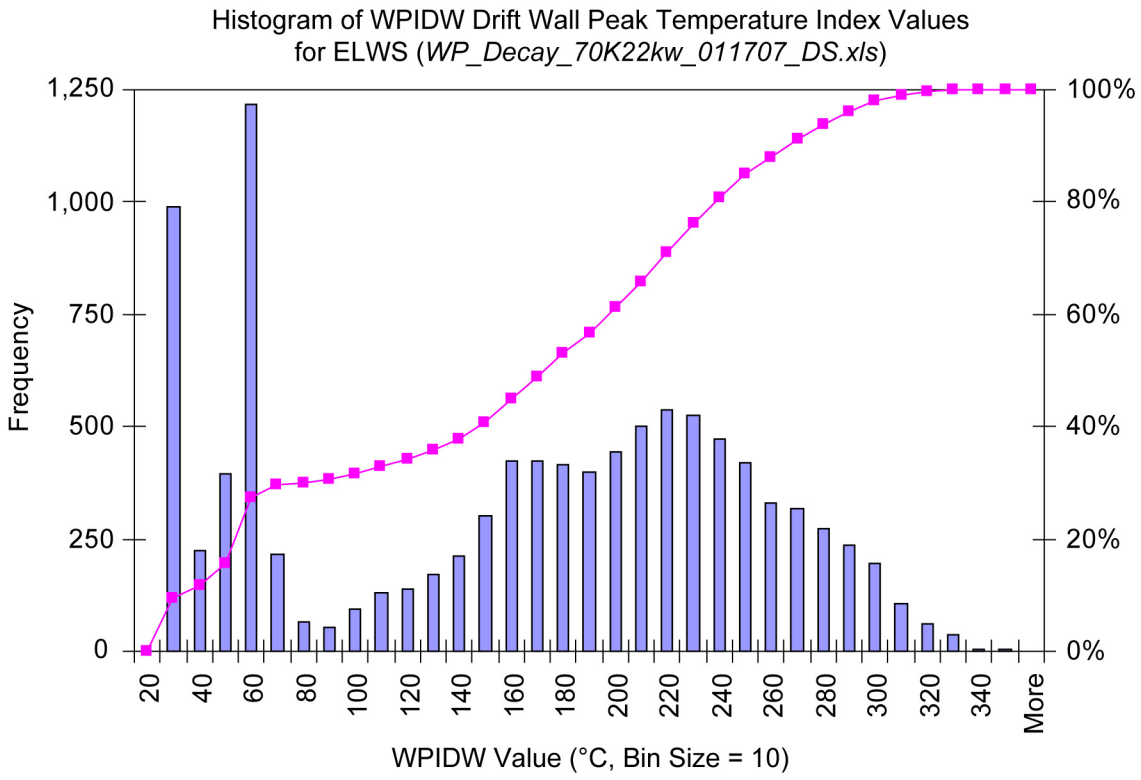

Source: Output DTN: MO0705SUPPCALC.000, folder: \YFF5_22 Envelope, file: *Worksheet in Histogram of Peak Driftwall Temperatures Rev01.xmcd.xls.*

NOTE: WPIDW index is calculated using nine superposed infinite line sources representing drifts, with the mean wet thermal conductivity for the lower lithophysal host rock unit. Note that for drift wall temperature the sources represent nine drifts instead of the eight used for mid-pillar temperature, because the calculation is centered on a drift instead of on the center of a pillar.

Figure 6.1-10. Histogram of Peak Drift Wall Temperatures for the ELWS Case

Justification for Use of WPIDW to Select Hottest Segments – Use of peak drift wall temperature as the selection measure for the hottest intervals in the as-emplaced ELWS sequences is justified by analysis of the variation of temperature in the radial direction above the drift crown. This calculation (Figure 6.1-11) is also performed using Equation 6.1-7, with the rock properties, liquid saturation, and ventilation duration described above (Output DTN: MO0705SUPPCALC.000, folder: \Other Supporting Files, file: *Envelope cases (line load).xmcd*). The peak drift wall temperature occurs at 105 years in this calculation, or 31 years after closure. Comparing the radial temperature profile at 105 years shows that WPIDW corresponds to the maximum temperatures in the rock within a few meters of the drift opening. At greater distances the peak temperature comes later than the peak at the drift wall. However, the WPIDW as defined is an adequate surrogate for the overall intensity of heating in the near field, if simulations of the near-field response are carried to appropriate duration (e.g., 1,000 years or longer).

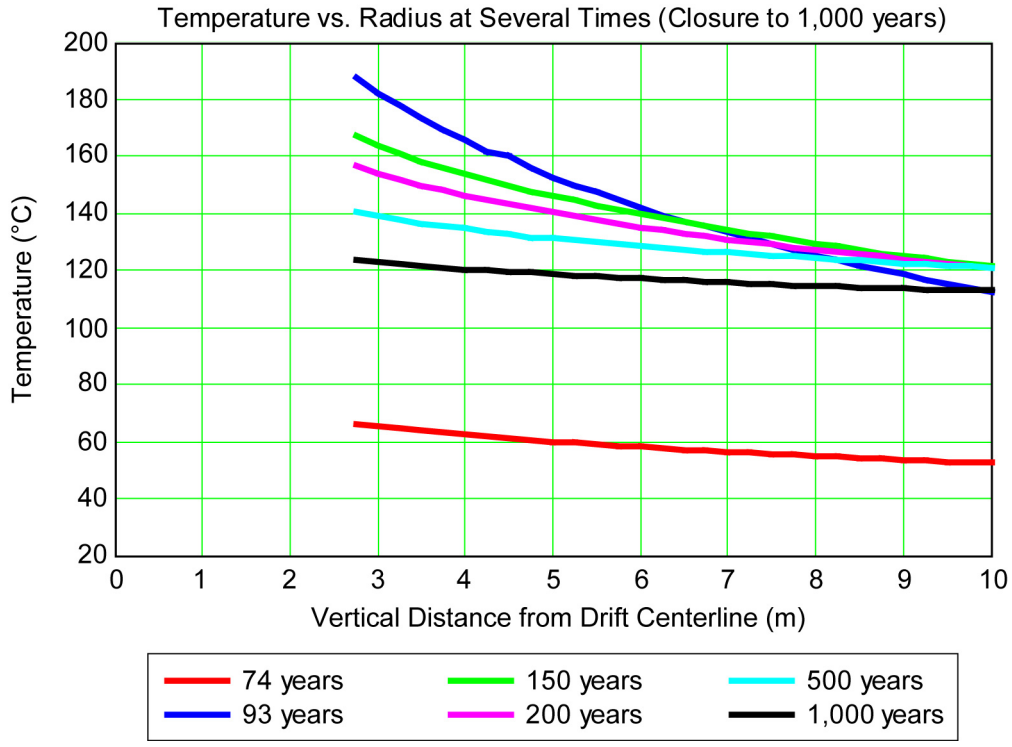

Source: Output DTN: MO0705SUPPCALC.000, fold er: \Other Supporting Files, file: *Envelope cases (line load).xmcd*.

NOTE: Temperature profiles are calculated using nine superposed infinite line sources representing drifts, with the 10th percentile thermal conductivity for the lower lithophysal host rock unit, and 50% liquid saturation.

Figure 6.1-11. Radial Variation of Temperature above the Drift Crown, for Average ELWS Thermal Load

Selection of Hottest Segments for Analysis – The WPIDW index was calculated for every waste package in the 85/4 and 96/2 emplacement sequences described previously. The WPIDW index sequences were then interrogated for the hottest local thermal conditions. The running average of seven consecutive waste packages is used to represent the maximum of the local average line load, as it would be likely to affect the near-field host rock. The hottest segments from the 85/4 and 96/2 emplacement sequences are shown in Table 6.1-2, and the associated line-loads (averaged over three or seven packages) are shown in Figure 6.1-12. All of these segments contain waste packages with hotter CSNF (i.e., relatively high burnup and young age) emplaced near the end of the operational period, with adjacent cooler DHLW waste packages to limit the local average thermal load. The hottest seven-package segment (Case 1) occurs in the 96/2 emplacement sequence.

Use of the seven-package running average to identify the hottest local thermal conditions is justified by reasoning similar to that in Section 6.1.3 (Figure 6.1-7). A finite-element (ANSYS) study is reported in *Repository Twelve Waste Package Segment Thermal Calculation* (BSC 2006 [DIRS 179686]), in which various arrangements of 12 waste packages (arrayed as 11 plus two half-packages, or 13 packages total) of representative types were simulated. The results show that axial variation of peak temperature just five meters into the drift wall is very small (generally less than 1°C) because of thermal radiation and natural convection in the drift, for all

waste package sequences considered (BSC 2006 [DIRS 179686], Section 7). This means that rock temperature at any location is strongly influenced by waste packages for some distance in both directions along the drift. This distance must be *at least* the length scale of variability in waste package heat output, for the waste package sequences used in the study. The waste package sequences were somewhat periodic, with patterns of high- and low-output waste packages repeating every five to seven package locations (BSC 2006 [DIRS 179686], Section 7).

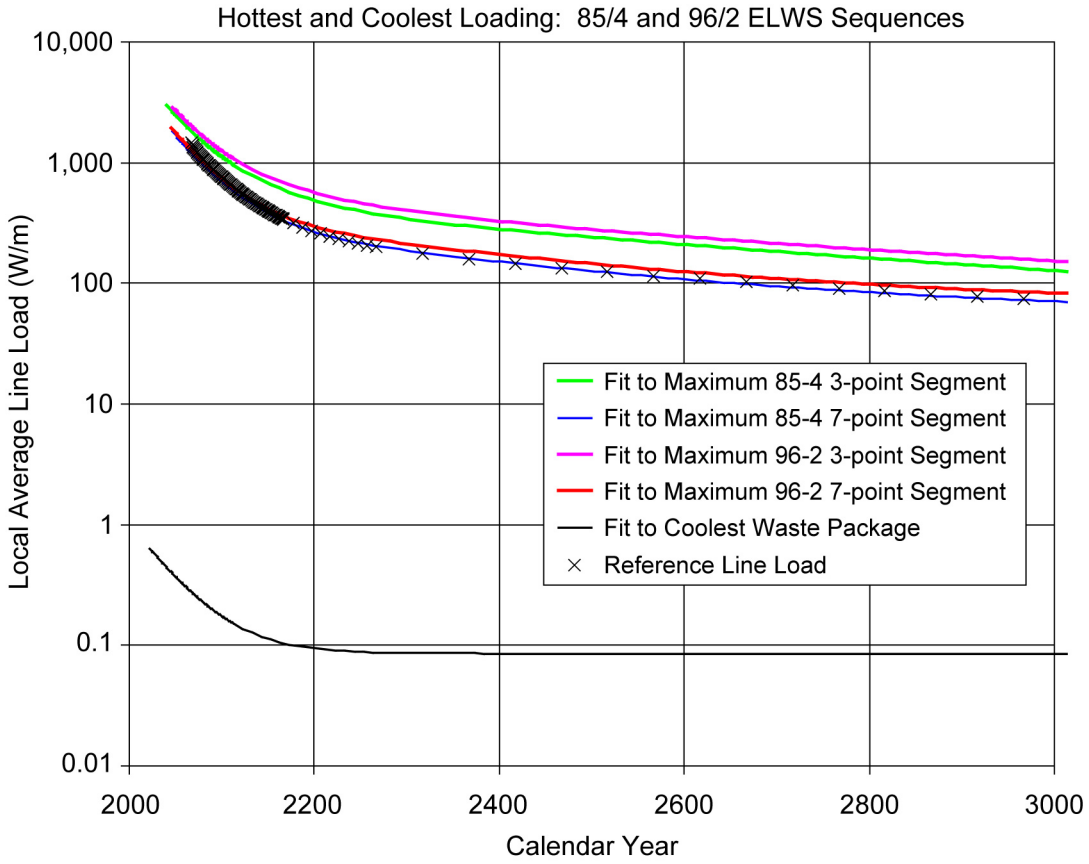

Source: Output DTN: MO0705SUPPCALC.000, folder: \Select Hot and Cold Cases, file: *Hottest + Coolest Comparison Plots.xls*.

Figure 6.1-12. Local Line Loads for the Hottest Segments from the 85/4 and 96/2 Emplacement Sequences, Compared with the Postclosure Reference Case

Another reason for using a seven-package running average of WPIDW, is that the ELWS emplacement sequences are already configured to limit the seven-package running-average line load at emplacement to 2.0 kW/m (Section 6.1.3; see also SNL 2007 [DIRS 179354], Table 4-4, Parameter 05-03). Thus, any larger number of consecutive waste packages must have the same limiting average line load and there is no reason to use a greater number to investigate local thermal loading conditions. Finally, it is noted that both the WPIMP loading rule and the WPIDW index used as the selection criterion are integrated measures that take into account differences in thermal decay rates among waste packages.

The maximum running average of WPIDW for three consecutive waste packages is also identified (Table 6.1-2) to represent extreme local thermal loading (Case 2). The hottest three-package segment also occurs in the 96/2 emplacement sequence. The equivalent line load for this maximum three-package segment (i.e., three packages averaged together) will not actually be expressed in the repository because of axial heat sharing with adjacent cooler locations as discussed above. The 13-package segment that includes the maximum three-package running average (Table 6.1-2) is representative of repository loading conditions. This segment is prepared for use in two- and three-dimensional analyses associated with this report because: (1) this segment coincides with the segment exhibiting maximum package-to-package variability (as discussed below), and (2) it represents an extreme case for use in two-dimensional sensitivity analyses.

Time-dependent ventilation efficiency associated with the three-package and seven-package segments is calculated for use in three-dimensional analyses (Section 6.4.2). Using the ventilation model (BSC 2004 [DIRS 169862]; Output DTN: MO0705SUPPCALC.000, folder: \Preclosure Ventilation, file: *Summary of Preclosure Ventilation for Thermal Envelope Studies.xmcd*), the ventilation efficiencies were calculated for average line loads corresponding to the three- and seven-package hottest intervals for the 96/2 emplacement sequence. The results are posted to the spreadsheets that describe these segments (Output DTN: MO0705SUPPCALC.000, folder: \Preclosure Ventilation,, files: *Preclosure Ventilation Results.xls*, *Hottest and Coolest Discrete Values 1E6 yr (ventilation).xls*, and *Hottest 3-7 + Coolest WP 96-2 10Jul07.xls*). From these ventilation model files, the results for the 800-m drift are selected for use because the efficiency is generally less than for the 600-m drift case (producing slightly hotter conditions).

Note that the 10th percentile dry and wet thermal conductivity values (and 50% liquid saturation) for the lower lithophysal host-rock unit are used to calculate these ventilation efficiencies, for consistency with the use of 10th percentile thermal conductivity to calculate peak temperatures. Use of a lower thermal conductivity for the rock actually increases efficiency (by increasing the drift wall temperature), which appears non-conservative with respect to modeling peak temperatures. However, the direct effect of lower thermal conductivity on postclosure temperature is much stronger than the effect of ventilation efficiency.

For two-dimensional analyses including the WPIMP and WPIDW index calculations (Section 6.1.3), a fixed value of 86% ventilation efficiency is used as a reasonable estimate of the spatial and temporal average. This is consistent with previous calculation of the WPIMP and WPIDW indices (Section 6.1.3), and with previous studies (SNL 2007 [DIRS 179196], Section 6.3).

Table 6.1-2. Hottest Segments from the 85/4 and 96/2 Emplacement Sequences

Waste Package Number	Waste Package Type	Emplaced Year	Year of Peak Drift Wall Temp.	WPIDW Peak Temp. (°C)	WPIDW Running Average	Waste Package Diameter (m)	Waste Package Length (m)
85/4 Sequence, Maximum of 3-point Running Average of WPIDW							
139829	WPMPC	2041	2142	261.4	225.1	1.882	5.85
140276	WPMPC	2041	2162	117.6	146.1	1.882	5.85
137600	WP	2041	2129	59.2	78.7	2.045	3.59
137603	WP	2041	2129	59.2	59.2	2.045	3.59
137607	WP	2041	2129	59.2	138.9	2.045	3.59
138026	WPMPC	2041	2143	298.4	216.1	1.882	5.85
138859	WPMPC	2041	2143	290.8	289.1	1.882	5.85
138998	WPMPC	2041	2142	278.1	234.7	1.882	5.85
139965	WPMPC	2041	2137	135.1	157.5	1.882	5.85
137613	WP	2041	2129	59.2	84.5	2.045	3.59
137615	WP	2041	2129	59.2	59.2	2.045	3.59
137617	WP	2041	2129	59.2	124.3	2.045	3.59
141174	WPMPC	2041	2153	254.4	201.8	1.882	5.85
85/4 Sequence, Maximum of 7-point Running Average of WPIDW							
141097	WPMPC	2043	2137	205.8	152.4	1.882	5.85
140003	WPMPC	2043	2137	204.5	152.4	1.882	5.85
138913	WPMPC	2043	2140	199.8	152.4	1.882	5.85
140299	WPMPC	2043	2140	200.9	161.6	1.882	5.85
138727	WP	2043	2127	25.7	161.5	2.045	5.22
138730	WP	2043	2127	25.7	161.7	2.045	5.22
140228	WPMPC	2043	2143	268.9	161.8	1.882	5.85
140990	WPMPC	2044	2137	205.4	152.4	1.882	5.85
141040	WPMPC	2044	2137	205.3	152.4	1.882	5.85
140001	WPMPC	2044	2137	201.0	152.4	1.882	5.85
139750	WPMPC	2044	2147	135.0	154.4	1.882	5.85
138733	WP	2044	2127	25.7	154.8	2.045	5.22
138735	WP	2044	2127	25.7	154.8	2.045	5.22
96/2 Sequence, Maximum of 3-point Running Average of WPIDW (Case 2)							
137226	WP	2046	2129	33.3	36.5	2.045	5.22
137230	WP	2046	2129	33.3	33.3	2.045	5.22
137233	WP	2046	2129	33.3	33.3	2.045	5.22
137236	WP	2046	2129	33.3	33.3	2.045	5.22
137239	WP	2046	2129	33.3	125.1	2.045	5.22
139805	WPMPC	2047	2146	308.7	215.3	1.882	5.85
140263	WPMPC	2047	2145	303.8	300.7	1.882	5.85
141183	WPMPC	2047	2144	289.6	206.3	1.882	5.85
137242	WP	2047	2129	25.5	113.5	2.045	5.22
137245	WP	2047	2129	25.5	25.5	2.045	5.22

Table 6.1-2. Hottest Segments from the 85/4 and 96/2 Emplacement Sequences (Continued)

Waste Package Number	Waste Package Type	Emplaced Year	Year of Peak Drift Wall Temp.	WPIDW Peak Temp. (°C)	WPIDW Running Average	Waste Package Diameter (m)	Waste Package Length (m)
137248	WP	2047	2129	25.5	25.5	2.045	5.22
137251	WP	2047	2129	25.5	113.2	2.045	5.22
140509	WPMPC	2047	2144	288.5	201.3	1.882	5.85
96/2 Sequence, Maximum of 7-point Running Average of WPIDW (Case 1)							
140352	WPMPC	2045	2140	169.9	164.7	1.882	5.85
140841	WPMPC	2045	2137	176.4	164.0	1.882	5.85
141057	WPMPC	2045	2141	155.3	164.1	1.882	5.85
140476	WPMPC	2045	2137	170.1	164.0	1.882	5.85
138059	WPMPC	2045	2141	160.3	162.1	1.882	5.85
137021	WPMPC	2045	2142	154.6	176.6	1.882	5.85
141172	WPMPC	2045	2140	161.2	178.8	1.882	5.85
138979	WPMPC	2045	2141	156.7	158.1	1.882	5.85
141205	WPMPC	2045	2144	278.2	177.0	1.882	5.85
141162	WPMPC	2045	2137	170.2	158.5	1.882	5.85
135370	WP	2045	2131	25.4	176.1	2.045	5.22
139795	WPMPC	2045	2145	292.4	157.4	1.882	5.85
135373	WP	2045	2131	25.4	160.8	2.045	5.22

Source: Output DTN: MO0705SUPPCALC.000, folder: \Select Hot and Cold Cases, file: *Hottest 3-7 + Coolest WP 96-2 10Jul07.xls*, worksheet: "Hottest Segments 96-2"; and file: *Hottest 3-7 + Coolest WP 85-4 10Jul07.xls*, worksheet: "Hottest Segments 85-4."

NOTES: Waste Package Number is for tracking within the total system model only.

WPMPC denotes multi-purpose (transportation, aging, and disposal) canister.

WP denotes DOE co-disposal package in both short and long configurations.

Shading indicates maximum running averages selected for analysis; the 13-package segment encompassing each maximum location is shown.

Waste package lengths differ slightly from the current baseline; see Assumption 5.3.

Hot-Cold Heterogeneity in the Emplacement Sequences – To support the evaluation of three-dimensional effects in heat transfer (Section 6.4.2), the occurrence of hot packages against cold ones was investigated for the 85/4 and 96/2 emplacement sequences. The sequences were processed to identify the segments with the maximum, absolute differences in WPIDW for adjacent packages in the following configurations:

- Maximum difference for any two adjacent waste packages ("1+1" result)
- Maximum difference in the average for any two waste packages together, compared with the average of two adjacent packages ("2+2" result)
- Maximum difference in the average for any three waste packages together, compared with the average of three adjacent packages ("3+3" result).

The results (Table 6.1-3) show that the maximum hot-cold heterogeneity is captured by the hottest segments identified above (Output DTN: MO0705SUPPCALC.000, folder: \Select Hot and Cold Cases, file: *Hottest 3-7 + Coolest WP 96-2 10Jul07.xls*, worksheet: "Analysis"; and file: *Hottest 3-7 + Coolest WP 85-4 10Jul07.xls*, worksheet: "Analysis"). In particular, the hottest running-average of three WPIDW values, from the 96/2 sequence, coincides with the maximum "2+2" and "3+3" heterogeneity in that sequence. Also, the hot-cold heterogeneity in the 96/2 sequence is greater than that in the 85/4 sequence. In accord with these results, there is no need to identify a separate segment for further investigation of hot-cold heterogeneity. Rather, the hottest three-point and seven-point segments from the 96/2 emplacement sequence (Table 6.1-2) already include the segments with the maximum "2+2" and "3+3" heterogeneity.

Table 6.1-3. Maximum Hot-Cold Heterogeneity in the 85/4 and 96/2 Emplacement Sequences

	WPIDW (°C)	Running Avg. WPIDW Three (°C)	Running Avg. WPIDW Seven (°C)	Running "1+1" WPIDW Abs. Diff. (°C)	Running "2+2" Avg. WPIDW Abs. Diff. (°C)	Running "3+3" Avg. WPIDW Abs. Diff. (°C)
85/4 Emplacement Sequence						
Maximum	307.86	264.54	161.83	268.36	237.50	230.60
Row # [a]	10132	6617	7523	7202	5578	5925
Minimum	23.06	25.13	25.91	0.00	0.00	0.00
Row # [a]	194[b]	956[b]	10231[b]	761[b]	7501[b]	10164[b]
96/2 Emplacement Sequence						
Maximum	308.68	300.66	178.75	282.66	272.89	275.15
Row # [a]	9308	9309	8653	10009	9308	9311
Minimum	23.06	24.36	25.36	0.00	0.00	0.00
Row # [a]	331[b]	330[b]	328[b]	333[b]	334[b]	343[b]

Source: Output DTN: MO0705SUPPCALC.000, folder: \Select Hot and Cold Cases, file: *Hottest 3-7 + Coolest WP 96-2 10Jul07.xls,* worksheet: "Analysis"; and file: *Hottest 3-7 + Coolest WP 85-4 10Jul07.xls*, worksheet: "Analysis."

[a] Row # indicates row number from worksheet listing sequence.
[b] For minimum values and differences, the row shown is the first in the sequence (i.e., earliest emplacement) for which the minimum condition occurs.

6.1.5 Postclosure Peak Waste Package Wall Temperature

If the drift wall temperature limit of 200°C is met, then the waste package wall temperature limit of 300°C (for 500 years; see Section 6.1.1) will be met for nominal (intact, or uncollapsed) conditions because the calculated difference between waste package and drift wall temperatures is generally less than 50°C. To evaluate this assertion, several cases from *Repository Twelve Waste Package Segment Thermal Calculation* (BSC 2006 [DIRS 179686], Section 7) were inspected to compare peak waste power at emplacement to the peak postclosure drift wall temperature at that waste package. The following cases were selected to investigate:

- The base case with 1.45 kW/m average line load at emplacement, 11.8 kW hottest package, convective boundary conditions representing preclosure ventilation, and uniform thermal loading within packages, i.e., no peaking factors (Case 2)

- Base case with 85% ventilation efficiency (closest to the value used in multiscale and the WPIMP and WPIDW calculations for this report) in lieu of convective conditions (Case 4b)
- Base case with thermal loads raised uniformly to average 1.75 kW/m (Case 6)
- Base case with one waste package increased to 16 kW at emplacement with fast decay (Case 11)
- Base case with slow decay for one 11.8 kW waste package (Case 12)
- Base case reordering with three hotter (11.8 kW) waste packages together (Case 14)
- Base case increasing waste package spacing from 0.1 m to 0.5 m, but increasing BWR waste package thermal output to maintain the average 1.45 kW/m line load (Case 17)
- Base case increasing package spacing to 0.5 m and increasing BWR thermal output to maintain 1.45 kW/m, with one waste package increased to 16 kW at emplacement with fast decay (Case 18)
- Base case increasing package spacing to 0.5 m and increasing BWR thermal output to maintain 1.45 kW/m, with one slow decay assigned to one 11.8 kW waste package (Case 19).

These cases were selected for this analysis to evaluate thermal loading, package arrangement, waste package spacing, and faster or slow decay. The cases not selected represented the effects of inhomogeneous heat generation within packages ("peaking"), off-normal loss of ventilation, zero-power packages, and different drift spacing. The effect of peaking was found to be minor, while loss of ventilation, zero-power, and different drift spacing are beyond the scope of this report.

The comparison shows that peak postclosure drift wall temperature is correlated with waste package power at emplacement (Figure 6.1-13). Thermal resistance (conductive, convective, and radiative) between the waste package and the drift wall is relatively constant over small ranges of temperature. This means that the temperature difference is approximately proportional to the local waste package power, and relatively insensitive to the temperature at the drift wall, which is controlled by host-rock thermal conductivity. Extrapolating the correlation to 18 kW (maximum permitted by ELWS "loading" rules; Section 6.1.3) shows that the waste package to drift wall temperature difference is approximately 50°C or less. A similar result would be obtained using different values of host-rock thermal conductivity. Hence these results show that if the drift wall temperature limit of 200°C is met, then the waste package outer barrier temperature will be substantially less than 300°C for open (intact) drifts. Similar temperature differences are reported for the multiscale model (SNL 2007 [DIRS 181383], Table 6.3-38). Collapsed-drift conditions are addressed in Assumption 5.4 (see SNL 2007 [DIRS 181383], Section 6.3.17[a]).

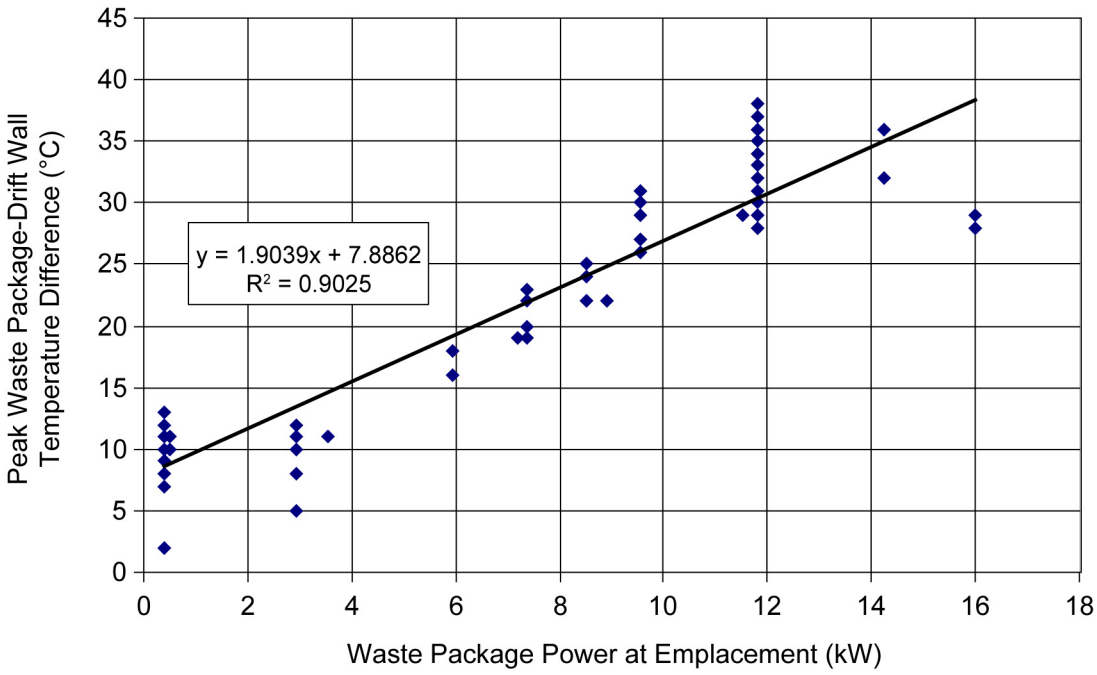

Source: Output DTN: MO0705SUPPCALC.000, folder: \Other Supporting Files, file: *12-WP study cases.xls*.

NOTE: Based on cases selected from BSC 2006 [DIRS 179686] as described in text.

Figure 6.1-13. Correlation of Peak Postclosure Drift Wall Temperature with Waste Package Power at Emplacement, from 12-Package Study

6.1.6 Postclosure Peak Spent Fuel Cladding Temperature

Interpretation of the design specifications for the TAD canister (DOE 2007 [DIRS 181403], Section 3.1.3) shows that peak postclosure cladding temperature for CSNF will be less than 350°C. This is because thermal output of CSNF waste packages will be less than 11.8 kW after closure. Thermal output of the hottest waste package in the ELWS drops below 11.8 kW at calendar year 2074, long before repository closure (DTN: MO0707ELWSDNSL.000 [DIRS 183774], file: *WP_Decay_70K22kw_011707_DS.xls*, worksheet: "WP_Decay," maximum from Column BV for nominal year 60, corresponding to calendar year 2074). Comparing to the TAD specification (DOE 2007 [DIRS 181403], Table 3.1-3) shows that, for 11.8 kW output, cladding temperature remains below 350°C (662°F) for canister wall temperature of 273°C (525°F). Simulations presented in Section 6.3 of this report show that the peak postclosure waste package wall temperature is significantly less than 200°C, using the 10th percentile thermal conductivity for the lower lithophysal (Tptpll) host rock unit. This leaves considerable margin (approximately 73°C) for the temperature difference required to propagate 11.8 kW from the TAD canister to the waste package outer barrier surface.

The potential significance of higher temperatures following partial or complete drift collapse is addressed in Section 6.5.1 of this report. That discussion focuses on waste package temperature, and the probability that seismically induced drift collapse could produce peak waste package temperature greater than 300°C, if a seismic event were to occur immediately after repository closure. The peak postclosure temperature of cladding in TAD canisters, if the waste package

outer barrier surface temperature is 300°C, can be estimated by extrapolating the TAD thermal performance implicit in the TAD specifications (DOE 2007 [DIRS 181403], Table 3.1-3). The temperature difference between the cladding and the TAD canister wall is linear, or nearly so, with respect to the waste package power output (Output DTN: MO0705SUPPCALC.000, folder: \Other Supporting Files, file: *TAD Temp. Extrapolation.xls*). This is expected because heat transfer from the cladding to the canister wall will be dominated by thermal conduction and thermal radiation (which exhibits nearly linear behavior over small temperature differences). Thus, the required maximum TAD surface temperature to maintain the cladding at 350°C or less is linear with respect to waste package thermal output. Fitting a linear trend to the data from the TAD specification, and extrapolating to the maximum waste package power at closure (6.73 kW; see DTN: MO0707ELWSDNSL.000 [DIRS 183774], file: *WP_Decay_70K22kw_ 011707_DS.xls*, worksheet: "WP_Decay," maximum from Column DJ), gives a required TAD canister surface temperature of 310°C or less, to maintain cladding at 350°C or less. This gives a margin of approximately 10°C for the temperature difference required to propagate 6.73 kW from the TAD canister to the waste package outer barrier surface. The waste package power continues to decay after closure, further increasing the temperature margin and providing reasonable assurance that the peak cladding temperature will remain below 350°C if the waste package surface temperature is at or below 300°C.

6.1.7 Summary of the Range of Design Thermal Loadings

Expressed as an average thermal line load, the range of design thermal loadings is bounded by the postclosure reference case (Figure 6.1-1), from the time when emplacement operations are complete (estimated to be in calendar year 2067) through 50 years of preclosure ventilation and beyond. For far-field thermal effects, e.g., in non-host-rock units or at the water table, the effects of variability among waste packages (decay history, ventilation time) are negligible. Thus, the postclosure reference case defines the thermal envelope for far-field analyses.

For near-field effects, the WPIMP index and the WPIDW index are developed and used to account for emplacement year and ventilation time, to evaluate whether postclosure thermal limits are likely to be met and to identify the hottest local thermal loading conditions for analysis. The maximum occurrence of the seven-package running average of the WPIDW index in the 96/2 emplacement sequence is selected as the hottest local condition (Case 1). It is possible that a repository drift could be loaded to a hotter condition; however, the hottest condition identified here and the methodology used provide a workable approach to evaluating and limiting thermal loading.

An additional sequence is identified for sensitivity testing, corresponding to the maximum occurrence of the three-package running average of the WPIDW index in the 96/2 sequence (Case 2). This case is realistic if the segment is evaluated in three dimensions with hot and cold waste packages, as in Section 6.4.2 of this report. It is much hotter, and not a realistic representation of local heating, if a three-package running average (over the hottest three packages) is used to derive a local line load. The local line load is used for sensitivity testing in Sections 6.4.1 and 6.4.3.

The coolest loading condition is caused by consecutively loading DHLW waste packages with low heat output. The minimum package output from both the 85/4 and 96/2 emplacement

sequences was selected to represent the coolest local loading conditions, and is nearly a zero-heat case especially after initial decay.

The thermal envelope defined in this section is for nominal postclosure conditions without drift collapse. The effects from drift collapse are evaluated in Sections 6.4.2 and 6.5, and also in *Multiscale Thermohydrologic Model* (SNL 2007 [DIRS 181383], Section 6.3.17[a]). Several assumptions are associated with these results as described in Section 5.

6.2 THERMAL-HYDROLOGIC MARGIN ANALYSIS FOR MID-PILLAR TEMPERATURE

Section 6.1.3 developed the WPIMP index, a measure of thermal energy density for each waste package, to show that ELWS emplacement sequences could be developed (the 85/4 and 96/2 sequences) that meet the mid-pillar postclosure temperature limit (96°C). This result was calculated for the mean value of wet thermal conductivity for the lower lithophysal host rock unit. The use of a wet (100% liquid saturation) value was justified qualitatively, and more support is provided in this section. The use of the mean value for thermal conductivity was representative, but the full distributions of WPIMP values for each host unit was also considered, taking into account the appropriate weighting of 10th and 90th percentile values (Figure 6.1-4).

This section evaluates the thermal-hydrologic margin, i.e., additional assurance that the mid-pillar temperature limit will be met, which is attributable to: (1) heat dissipation effects at the edge of the repository layout, and (2) the hydrological effects of percolation flux. Both of these ensure that the mid-pillar limit will be met through use of loading rules (Section 6.1.3), even considering the uncertainty in thermal conductivity and the variation among the host-rock units.

6.2.1 Thermal-Hydrologic Margin on Mid-Pillar Peak Temperature from Edge/End Cooling

Near the end of each emplacement drift, heat will tend to be conducted away from the repository, toward the unheated region outside the repository layout. Thus, it will be increasingly cooler toward the end of each drift, especially at the outer edges of the repository panels (a map is presented below in Figure 6.2-2). Also, where entire drifts define the edge of the repository layout, heat will be conducted away from the repository, producing cooler conditions. This thermal-hydrologic margin analysis is directed to the question of how much additional heat (expressed in terms of the WPIMP index) can be accommodated at the drift ends, and in the edge drifts, while still meeting the mid-pillar temperature limit.

The question was addressed using the analytical, thermal conduction-only solution for waste packages represented by point sources (Equation 6.1-6). Point sources were spaced at 6-m intervals, and heat generation was assigned corresponding to the overall average of the ELWS. Point sources were arrayed in 10 drifts, similar to the expository calculations of Section 6.1.3. The mean, wet thermal conductivity for the lower lithophysal (Tptpll) host-rock unit was used. Ventilation corrections were applied, and image sources were used to represent the cooling effect of constant temperature at the ground surface (Output DTN: MO0705SUPPCALC.000, folder: \YFF5_22 Envelope, file: *Interior Drift Methodology Rev04.xmcd*).

To investigate cooling at the ends of the drifts, first the profile of mid-pillar temperature was calculated for uniform, average loading of every drift (Figure 6.2-1). The resulting temperature profile is significantly lower for more than 100 m from the drift end, indicating the capacity to accommodate hotter waste packages. To investigate how much hotter, the heat output for waste packages within an interval at the end of every drift was multiplied by a constant factor. This factor was adjusted to raise the profile as much as possible without exceeding the prescribed limit (e.g., 85°C or 96°C). This was repeated for intervals of different size ranging up to 60 m (Figure 6.2-1). For discussion purposes, the last 10 waste packages occupying a length of approximately 50 m can be increased by a factor of 2.0 while meeting the same mid-pillar temperature limit.

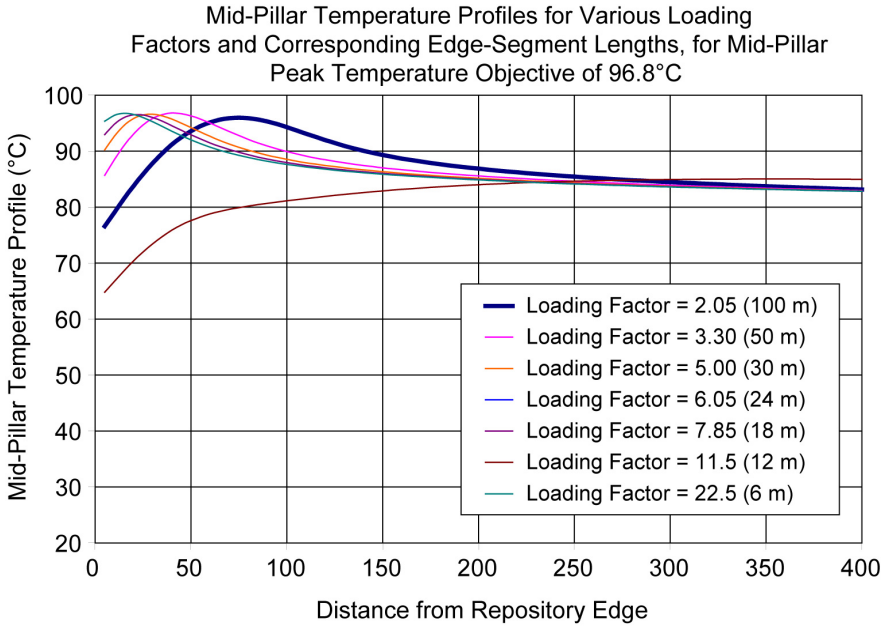

Source: Output DTN: MO0705SUPPCALC.000, folder: \YFF5_22 Envelope, file: *Worksheet in Interior Drift Methodology Rev04.xmcd.xls.*

Figure 6.2-1. Repository Edge Loading Effects for the ELWS Case, Using the 85°C Mid-Pillar Temperature Objective

To investigate cooling at edge drifts, the calculation was repeated for the last pillar flanked by two heated drifts (Output DTN: MO0705SUPPCALC.000, folder: \YFF5_22 Envelope, file: *Edge Drift Methodology.xmcd*). The edge drifts reside within the lower lithphysal (Tptpll) host rock unit, and the entire length of these drifts separately could accommodate waste with two times the heat output. This applies to the southernmost and northernmost drifts in the repository layout (Figure 6.2-2). The analysis was completed by recalculating the results for drift ends using the mean wet thermal conductivity for each host rock unit. A summary of results is presented in Figure 6.2-2, which plots the host-rock stratigraphy and the edge/end regions on the repository layout. Altogether, the combination of 10 packages at each drift end at the outside of the layout, plus the edge drifts, allows for emplacement of approximately 1,000 waste packages with substantially greater heat output (typically a factor of 2) while meeting the mid-pillar temperature limit.

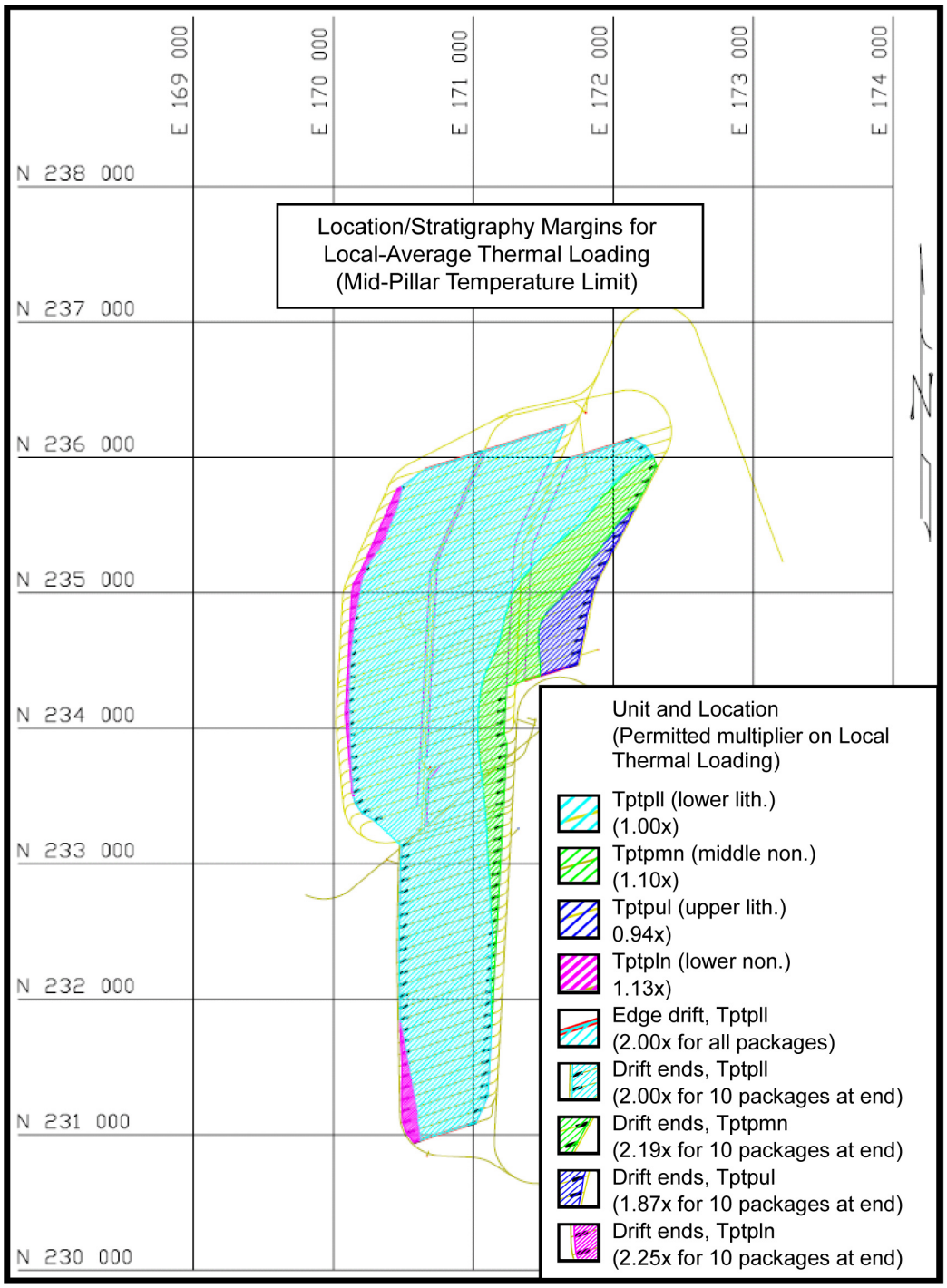

Source: Layout: BSC 2007 [DIRS 179640]; host-rock stratigraph y: BSC 2004 [DIRS 170029]; edge/end loading analysis: Output DTN: MO0705SUPPCALC.000, folder: \YFF5_22 Envelope, file: *Interior Drift Methodology Rev04.xmcd*.

Figure 6.2-2. Repository Edge/End Loading Thermal-Hydrologic Margin Map for the ELWS

6.2.2 Comparison of Analytical Solutions and Thermal-Hydrologic Simulations

The conclusions up to this point in this report are based on conduction-only analyses implemented using analytical solutions. Before analyzing the thermal margin on mid-pillar peak temperature from hydrologic effects (Section 6.2.3), this section examines the differences between conduction-only and two-dimensional thermal-hydrologic numerical solutions.

Inputs for the thermal-hydrologic simulations are described in Section 4.1.2, and generally conform to inputs used in the multiscale model (SNL 2007 [DIRS 181383], Table 4.1-1). The stratigraphy, physical properties, hydrologic properties, ground surface boundary conditions, and water table boundary conditions were taken directly from an LDTH submodel of the multiscale model (SNL 2007 [DIRS 181383], Section 6.2.6 and Table 4.1-1[a]). This LDTH location represents the majority of waste package locations, for which the repository drift is within the lower lithophysal (tsw35/tptpll) unit. The LDTH location is near the center of the repository footprint (SNL 2007 [DIRS 181383], Table 6.3-9 and Figure 6.3-1; location P2WR5C10). The percolation flux boundary condition and the average thermal line-load were varied parametrically as described below. Software used for this analysis consisted of NUFT v3.0s and mView v2.20 (Sections 3.1.3 and 3.1.4). For thermal conductivity of the lower lithophysal host-rock unit, the thermal-hydrologic margin analysis used preliminary values of 1.89 and 1.28 W/m-K for the wet and dry conditions, respectively, while the other analyses in this report and the multiscale model use mean values of 1.87 and 1.24 W/m-K. The differences are insignificant because the thermal-hydrologic margin analysis evaluates relative changes in thermal loading and flux. There are also some minor differences in thermal conductivity for the Tptpul, Tptpmn, and Tptpln units (Section 4.1.2), and these also are insignificant because the units are far removed from the repository horizon.

The thermal line-load function used in the thermal-hydrologic margin analysis was also preliminary and has minor differences from the ELWS average line-load (Figure 6.1-1). The updated function is comparable to the function used in this analysis (Figure 6.2-3). An impact evaluation was performed running the same case (with inputs described above and percolation flux of 3 mm/yr) using both of the line load functions (Figure 6.2-4). In addition, the updated host-rock thermal conductivity values were used in the analytical line-source solution (Equation 6.1-3), with thermal diffusivity calculated using both 50% and 100% liquid saturation, and without image sources, for comparison. The results show that the differences in the line-load functions are not significant because a few degrees in predicted temperature would not impact the derived relationships between percolation flux and changes in mid-pillar temperature.

The analytical conduction-only solutions are always hotter by roughly 10°C than the thermal-hydrologic simulations (Figure 6.2-4), which is appropriate considering the application of these solutions for calculating WPIMP and WPIDW indices. Also, the differences in these solutions using 50% and 100% liquid saturation are small, especially for mid-pillar temperature. Note that the conduction-only solutions produce peak mid-pillar temperatures somewhat earlier than the thermal-hydrologic simulations. This is because the stratigraphy in the numerical models includes lower conductivity layers above and below the host rock, which tend to trap heat in the host rock despite the use of constant temperature boundaries at the ground surface and the water table. In summary, the inputs for the thermal-hydrologic margin analysis (Section 6.2.3)

are reasonably representative for use in the study, and the conduction-only analytical solutions used to generate WPIMP and WPIDW are comparable to thermal-hydrologic simulations.

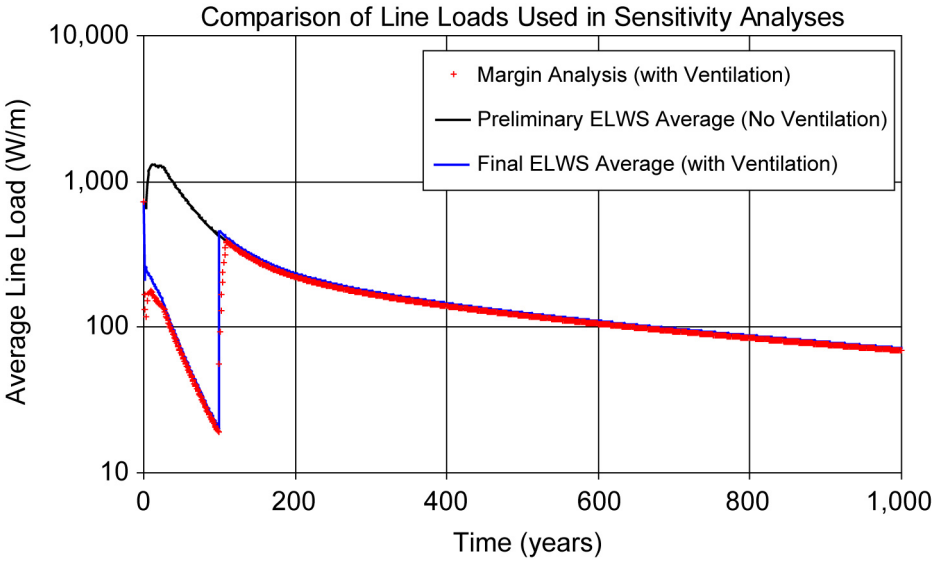

Source: Final ELWS average: Output DTN: MO 0705SUPPCALC.000, folder: \YFF5_22 Envelope, file: *Unit Pulse Solution for the Calculation of the Average Driftwall Temperatures Rev01.xmcd*; Thermal-hydrologic margin analysis: Output DTN: MO0707THERMHYD.000, file: *TH_P30_3mmyr_impact.xls.*

Figure 6.2-3. Thermal Line-Load History Used in Thermal-Hydrologic Simulations

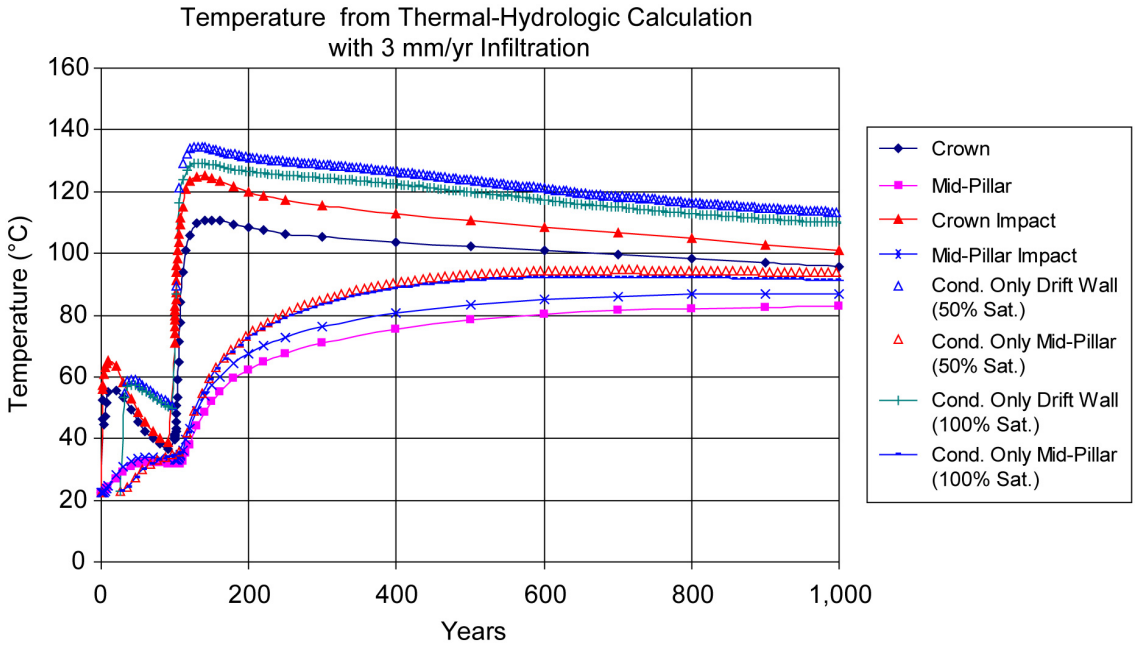

Source: Output DTN: MO0707THERMHYD.000, file: *TH_P30_3mmyr_impact.xls*.

Figure 6.2-4. Comparison of Temperature Histories (Mid-Pillar and Drift Wall) for Conduction-Only and Thermal-Hydrologic Simulations

Before investigating the effects of hydrology on peak mid-pillar temperature, a set of thermal hydrologic simulations was generated without hydrology, fixing the thermal conductivity at the wet value (i.e., 1.89 W/m-K for the host rock unit). The results (Figure 6.2-5) show that the peak temperature increases proportionally with increasing lineal heat load. The proportionality is consistent with the function of the $Q_{Line}(\tau)$ function in Equation 6.1-3. In the next section and its figures, the "T-only" plots are from simulations without hydrologic features, and correspond with Figures 6.2-6 to 6.2-8.

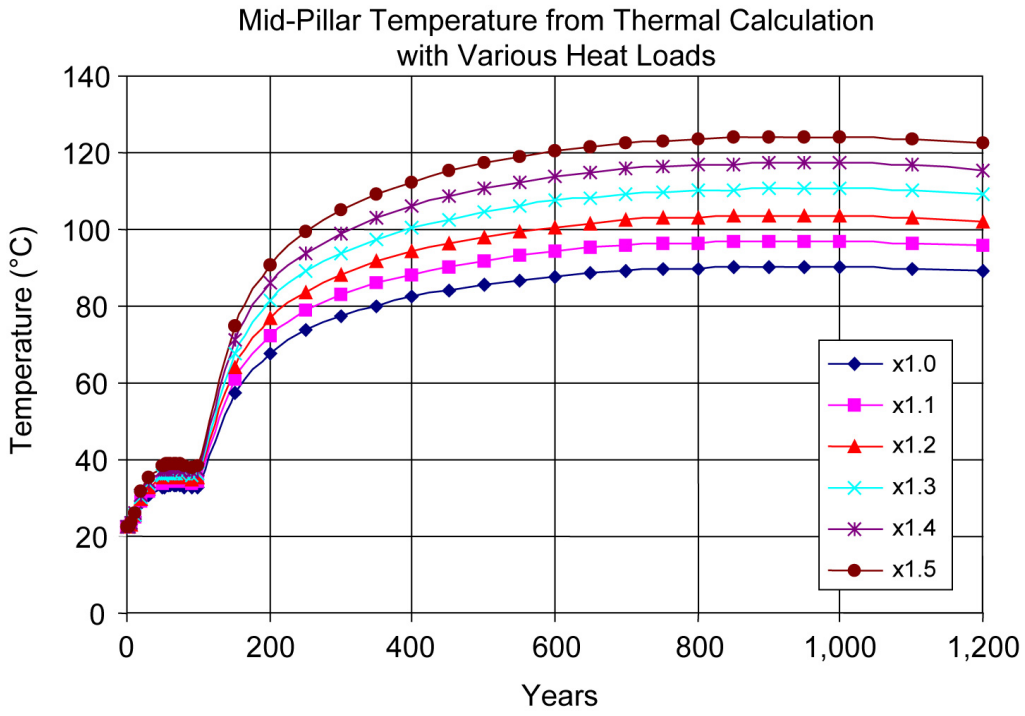

Source: Output DTN: MO0707THERMHYD.000, file: *TH_P30_1mmyr.xls*.

Figure 6.2-5. Mid-Pillar Temperature Calculated Using the Thermal-Hydrologic Simulation without Hydrologic Features, and Multiples of the Thermal Line Load

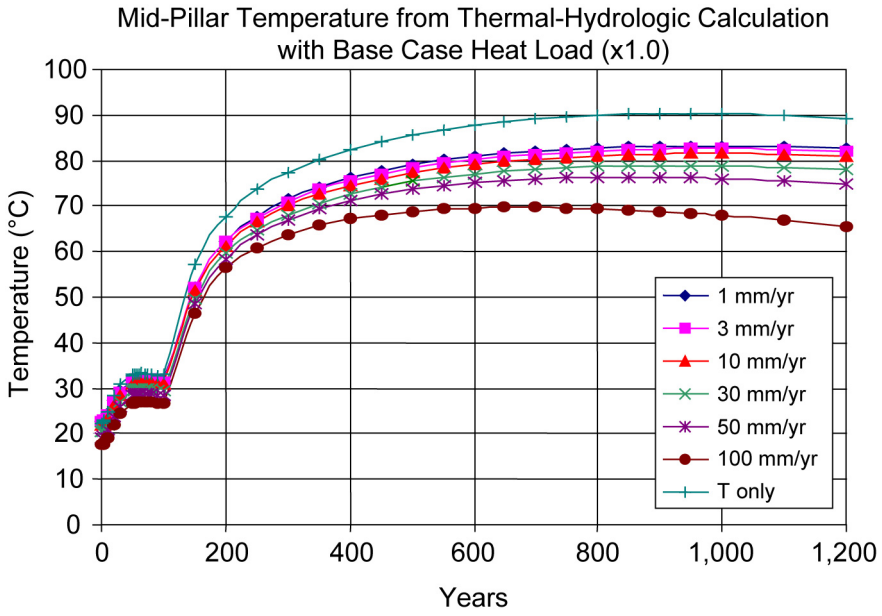

Source: Output DTN: MO0707THERMHYD.000, file: *TH1.0_P30.xls*.

Figure 6.2-6. Mid-Pillar Temperature for the Base Case Thermal Load, and Increasing Values of Percolation Flux

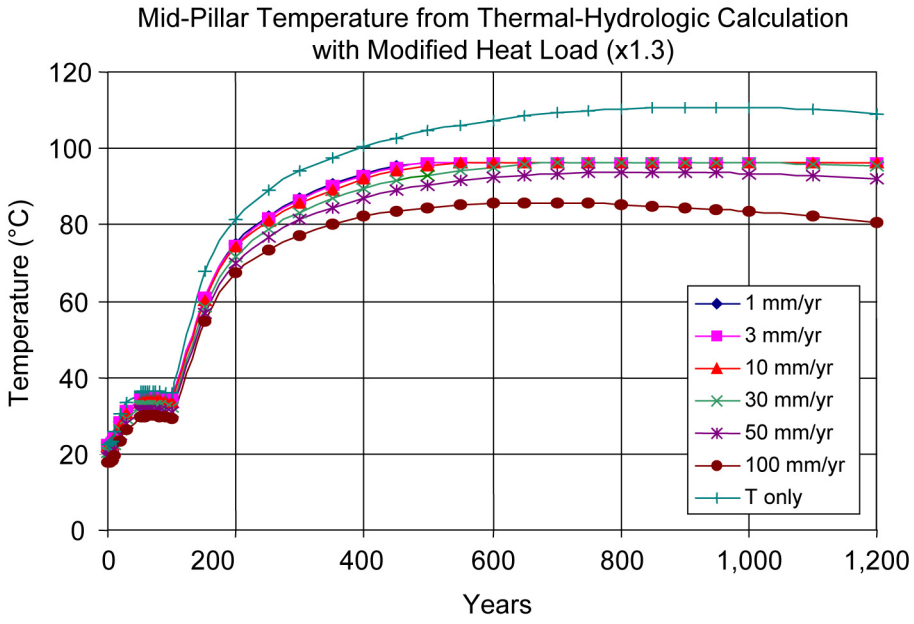

Source: Output DTN: MO0707THERMHYD.000, file: *TH1.3_P30.xls*.

Figure 6.2-7. Mid-Pillar Temperature for 1.3 Times the Base Case Thermal Load, and Increasing Values of Percolation Flux

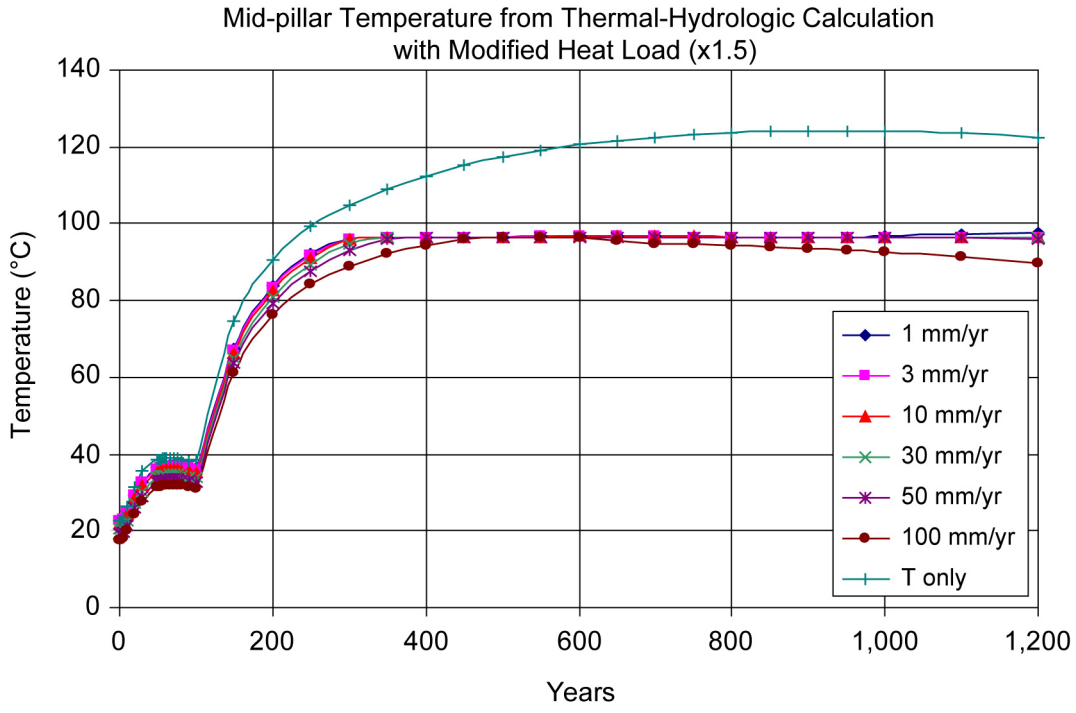

Source: Output DTN: MO0707THERMHYD.000, file: *TH1.5_P30.xls*.

Figure 6.2-8. Mid-Pillar Temperature for 1.5 Times the Base Case Thermal Load, and Increasing Values of Percolation Flux

6.2.3 Thermal-Hydrologic Margin on Mid-Pillar Peak Temperature from Hydrologic Effects

A series of thermal-hydrologic simulations was performed varying thermal line-loads and infiltration rates parametrically, to evaluate how much additional thermal loading can be accommodated while maintaining the mid-pillar temperature at the 96°C limit. Thermal loading was multiplied by factors of 1.0, 1.1, 1.2, 1.3, 1.4, 1.5, 1.6, 1.8, and 2.0. Percolation flux was set to 1 mm/yr, 3 mm/yr, 10 mm/yr, 30 mm/yr, 50 mm/yr, and 100 mm/yr. All possible combinations of these settings were run (Output DTN: MO0707THERMHYD.000). Additional simulations evaluated the effect of decreased host-rock thermal conductivity.

Comparisons between conduction-only and thermal-hydrologic simulations show the effect of percolation flux on peak mid-pillar temperature. This is shown through a series of mid-pillar temperature histories. As the flux increases (Figures 6.2-6 through 6.2-8), mid-pillar temperature is quenched, and the temperature differences between conduction-only and thermal-hydrologic simulations increase due to the temperature hold-up near 96°C. As the thermal load increases for a given value of flux (Figures 6.2-9 through 6.2-11), temperatures exceed the nominal 96°C boiling temperature only for the smallest flux values.

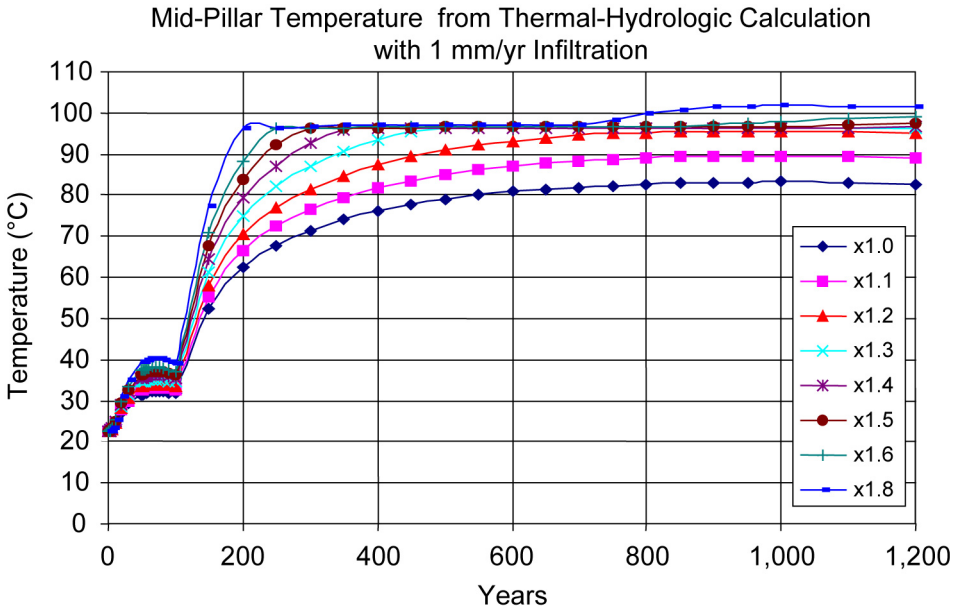

Source: Output DTN: MO0707THERMHYD.000, file: *TH_P30_1mmyr.xls*.

Figure 6.2-9. Mid-Pillar Temperature Histories for 1 mm/yr Infiltration Flux, and Increasing Multiples of the Thermal Load

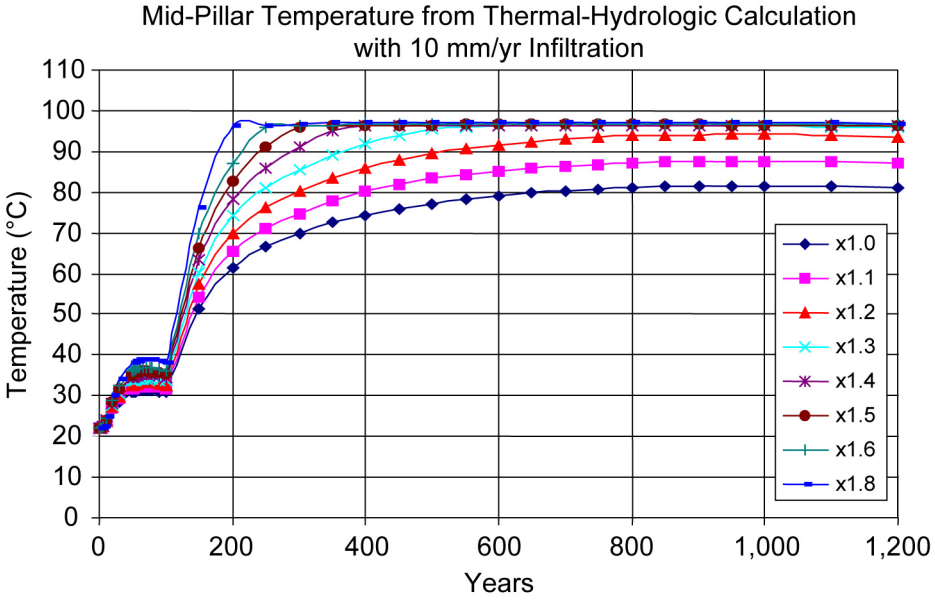

Source: Output DTN: MO0707THERMHYD.000, file: *TH_P30_10mmyr.xls*.

Figure 6.2-10. Mid-Pillar Temperature Histories for 10 mm/yr Infiltration Flux, and Increasing Multiples of the Thermal Load

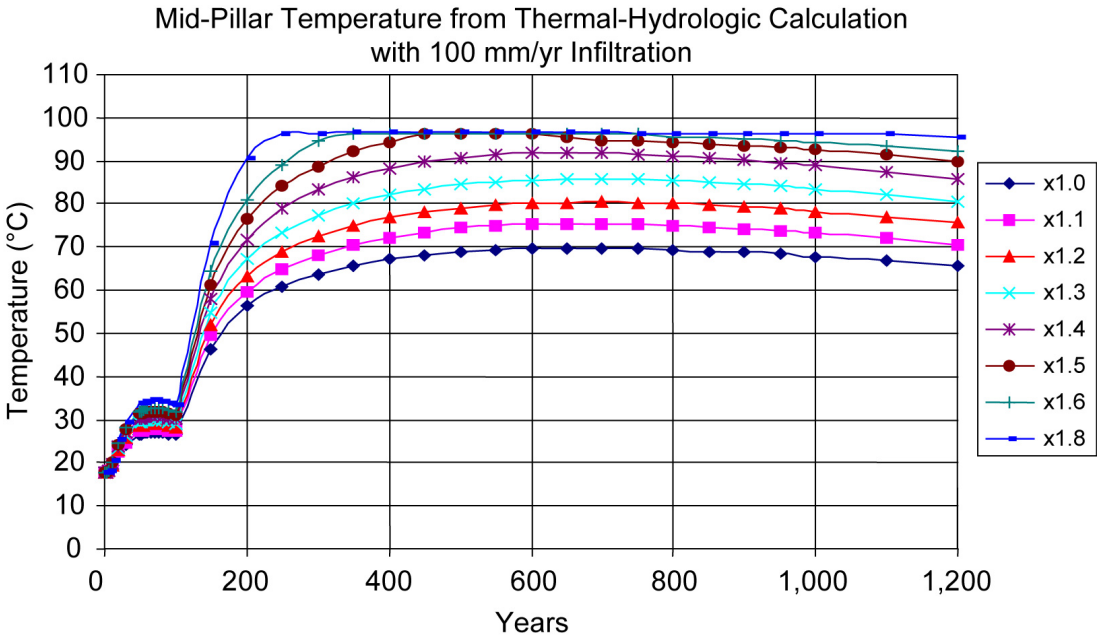

Source: Output DTN: MO0707THERMHYD.000, file: *TH_P30_100mmyr.xls*.

Figure 6.2-11. Mid-Pillar Temperature Histories for 100 mm/yr Infiltration Flux, and Increasing Multiples of the Thermal Load

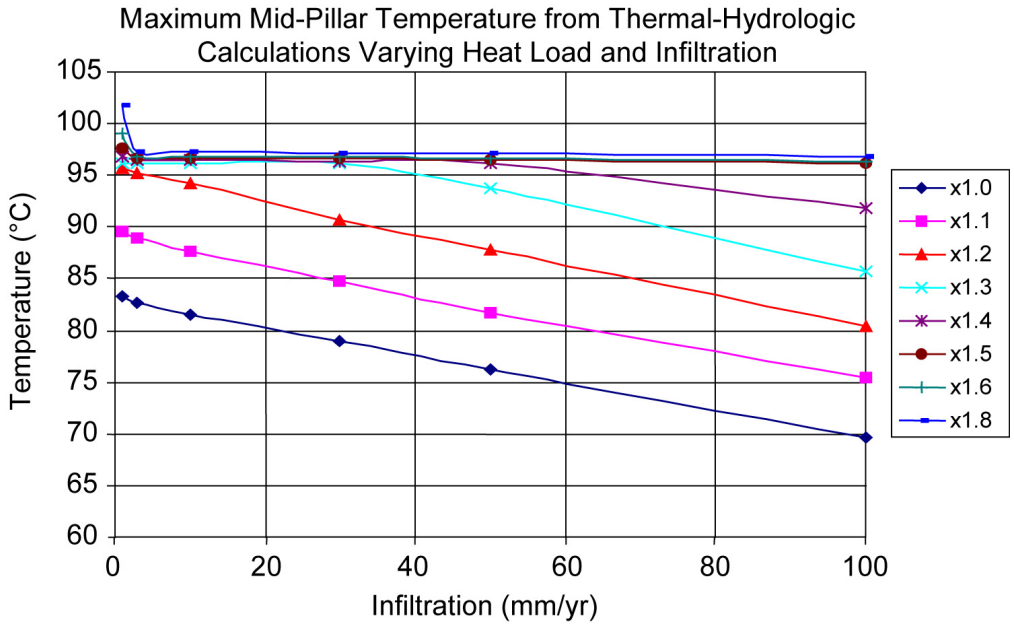

Source: Output DTN: MO0707THERMHYD.000, file: *max_min_temp.xls*.

Figure 6.2-12. Summary of Peak Mid-Pillar Temperature as a Function of Thermal Load and Percolation Flux

Note that while temperature hold-up near 96°C is common, there is not a sharp cutoff temperature. Vapor-pressure lowering implemented in the thermal-hydrologic simulation can slightly increase the local apparent boiling temperature due to capillarity at unsaturated conditions. The boiling temperature for water at the conditions in this thermal-hydrologic model is approximately 96.8°C.

Peak mid-pillar temperatures for the cases are summarized in Table 6.2-1. The boiling temperature was exceeded only for 1 mm/yr infiltration rate with heat load of at least 1.4 times the base case.

Table 6.2-1. Peak Mid-Pillar Temperatures from Thermal-Hydrologic Parametric Study

Maximum Mid-Pillar Temperature (°C)						
	Infiltration Rate					
Heat Load ×	1 mm/yr	3 mm/yr	10 mm/yr	30 mm/yr	50 mm/yr	100 mm/yr
1.0	83.22	82.64	81.55	78.89	76.24	69.65
1.1	89.58	88.93	87.62	84.79	81.74	75.38
1.2	95.60	95.22	94.17	90.71	87.72	80.41
1.3	96.19	96.19	96.17	96.15	93.82	85.79
1.4	96.85	96.45	96.44	96.29	96.22	91.88
1.5	97.67	96.64	96.65	96.59	96.40	96.22
1.6	98.98	96.82	96.84	96.80	96.72	96.31
1.8	101.76	97.25	97.25	97.19	97.13	96.82
2.0	104.09	97.78	97.83	97.73	97.55	97.31

Source: Output DTN: MO0707THERMHYD.000, folder: \Spreadsheets, file: *max_min_temp.xls.*

The relation between peak mid-pillar temperature, infiltration rate, and thermal loading is summarized in Figure 6.2-12 (for host-rock wet thermal conductivity of 1.89 W/m-K). Temperatures of 97°C or greater (i.e., significantly exceeding the nominal 96°C boiling temperature) are evident only for thermal loading greater than 1.4 times the base case, for infiltration as small as 1 mm/yr. Inspection of Figure 6.2-8 shows that this effect is equivalent to a margin of 20°C against thermal conduction-only behavior as represented by the WPIMP index.

In summary, these results show that there is substantial margin to meet the mid-pillar temperature limit, for infiltration flux of 1 mm/yr and greater. From Figures 6.2-6 through 6.2-8, the margin varies according to whether the thermal-hydrologic simulations predict boiling at the mid-pillar location. If boiling does occur, then the hydrologic effects produce temperatures at least 20°C cooler than predicted from thermal conduction only (Figure 6.2-8). Of the results shown in Figures 6.2-6 through 6.2-8, the most important is Figure 6.2-8, which shows 20°C of margin and demonstrates the capability of hydrologic processes to limit mid-pillar temperature. These results may be applied by observing that the WPIMP index (as calculated in Section 6.1.3) may be 20°C greater than the mid-pillar limit (nominal boiling temperature 96°C), if the infiltration flux is 1 mm/yr or greater, while preserving a drainage pathway through the pillar. Thus, the use of WPIMP calculated using the mean thermal conductivity for the lower lithophysal (Tptpll) unit (e.g., for mid-pillar temperature as shown in Figure 6.1-2) is robust with respect to lower values of thermal conductivity.

The 20°C margin is also useful to accommodate simplifications in the definition of the WPIMP index, which does not include lower-conductivity layers above and below the host rock which could trap heat and increase peak mid-pillar temperatures.

To elaborate this point, the mid-pillar temperature history was calculated for the postclosure thermal reference case, and the 10th percentile, mean, and 90th percentile values of the wet thermal conductivity for the lower lithphysal (Tptpll) unit (Figure 6.2-13). The calculated peak mid-pillar temperature values (corresponding to WPIMP) range from approximately 95°C to 103°C. This is within the 10°C margin (i.e., 96 + 10 = 106°C) afforded by hydrologic processes, so the mid-pillar temperature limit will be met if the infiltration flux is at least 3 mm/yr. If the flux were smaller, then condensate could slowly build up in the porosity of the pillar until the effective flux increased, quenching the mid-pillar temperature.

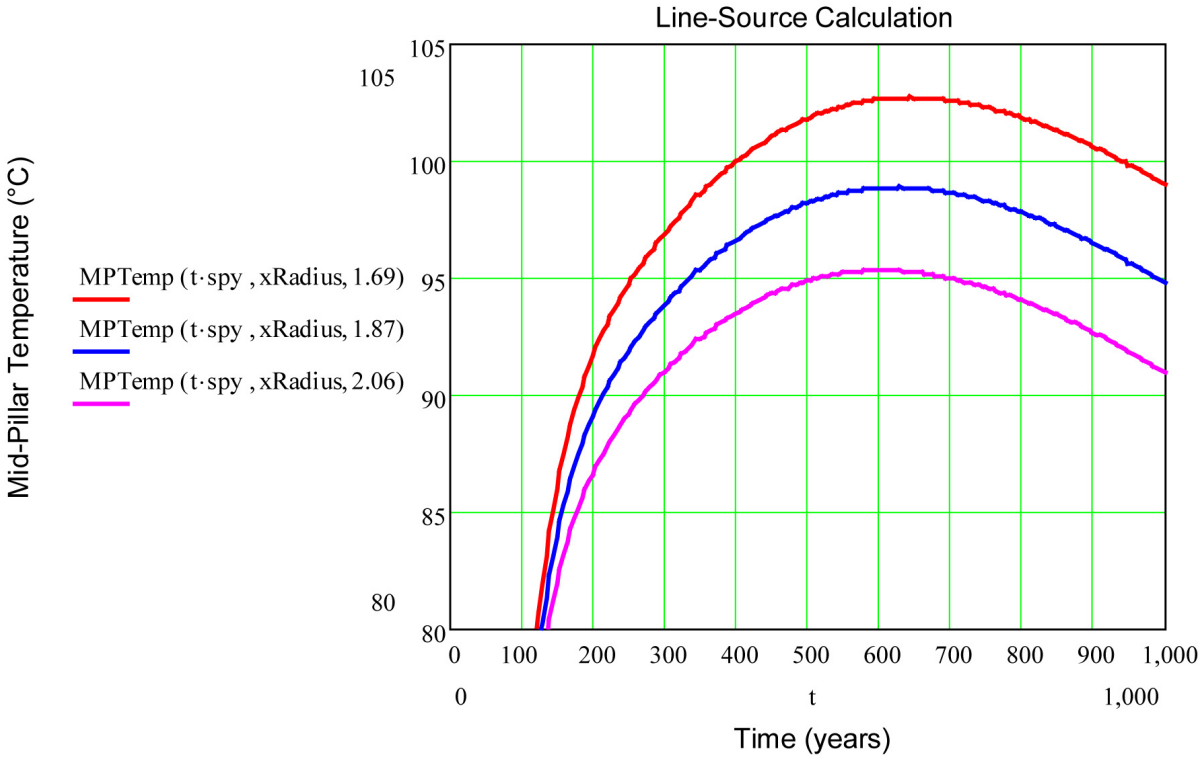

Source: Output DTN: MO0705SUPPCALC.000, fold er: \Other Supporting Files, file: *WPIMP vs. Kth.xmcd.*

NOTES: Thermal conductivity values of 1.69, 1.87, and 2.06 W/m-K correspond to the 10th percentile, mean, and 90th percentile values for the lower lithophysal (Tptpll) host unit.

Ventilation duration 50 years, efficiency 86%.

Figure 6.2-13. Mid-Pillar Temperature for a Line-Source Solution, Using the Postclosure Reference Thermal Load and Varying Host-Rock Thermal Conductivity

6.3 ANSYS ANALYSIS OF PEAK POSTCLOSURE DRIFT WALL TEMPERATURE

The purpose of this section is to produce high-resolution estimates of the peak postclosure temperatures of the drift wall and waste package, for comparison to the respective 200°C and 300°C limits (Section 6.1). The analysis approach uses ANSYS v8.0 (Section 3.1.2), a finite-element simulator, to implement thermal conduction in solids, and thermal radiation across the air spaces between the waste package and drip shield and between the drip shield and the drift wall. The ANSYS approach described here is essentially the same as the 3-D analysis developed in *Repository Twelve Waste Package Segment Thermal Calculation* (BSC 2006 [DIRS 179686]), which is justified because: (1) the approach is an implementation of standard engineering practice; and (2) the results can then be compared directly with the previous analysis, for the peak thermal conditions immediately after repository closure when the peak drift wall temperature occurs.

The ANSYS finite-element mesh resolution also produces greater accuracy in prediction of peak drift wall temperature than afforded by other methods such as the analytical solutions introduced in Section 6.1, or the thermal-hydrologic modeling described in Section 6.4.2.

Of the four cases run for this section, the first uses the previous model grid and thermal loading, but with lower values for host rock thermal conductivity (Scenario 1), and the second uses both the lower thermal conductivity and an improved function for host-rock heat capacity as derived in Appendix C (Scenario 2). These two runs serve the purpose of comparing the impacts from specific changes to the previous analysis. The third and fourth cases (Scenarios 3 and 4) are similar to the second, but with different waste package arrangements and thermal outputs, which include the 3-package and 7-package hottest segments from Section 6.1 (from the 96/2 emplacement sequence as presented in Table 6.1-2) with ventilation periods of 70 years and 72 years, respectively.

All four cases involve two time frames: preclosure and postclosure. The preclosure setup includes the effects from preclosure forced ventilation. Preclosure ventilation is implemented differently in Scenarios 1 and 2, compared with Scenarios 3 and 4 (see below). At closure, preclosure ventilation is turned off and the full heat output of the waste packages is applied, and the drip shield is introduced to the model grid. Note that simulation time steps must be constrained to small values around closure to ensure accuracy. ANSYS input and output files are available for inspection in Output DTNs: MO0709THERMAL1.000, MO0709THERMAL2.000, MO0709THERMAL3.000, and MO0709THERMAL4.000.

Postclosure heat transfer from the waste packages to the drip shield, and from the drip shield to the drift wall, occurs by thermal radiation only in the ANSYS analysis. The effects from natural convection and conduction through the gas phase are small, and are neglected in the analysis following the approach used in *Repository Twelve Waste Package Segment Thermal Calculation* (BSC 2006 [DIRS 179686], Section 6).

6.3.1 Scenario Descriptions

In this report, the first two cases (Scenarios 1 and 2) use exactly the same waste package arrangement as used in *Repository Twelve Waste Package Segment Thermal Calculation* (BSC 2006 DIRS 179686]), with the same thermal output, but with updated thermal properties of the host-rock material. A close-up of the model grid is shown in Figure 6.3-1. Symmetry boundary conditions (no heat flow by radiation or conduction) are applied at the ends. The 13-package arrangement (actually 11 plus two half-packages at the ends) is long enough that heat from waste packages near the middle is dissipated to the rock wall and not reflected at the ends. The third and fourth cases (Scenarios 3 and 4) use alternative waste package arrangements and thermal output as noted above. The grids for Scenarios 3 and 4 have the same connectivity, but are stretched to accommodate different waste package dimensions. Numbering of the waste packages for all cases is consistent with the previous analysis, as shown in Figure 6.3-1.

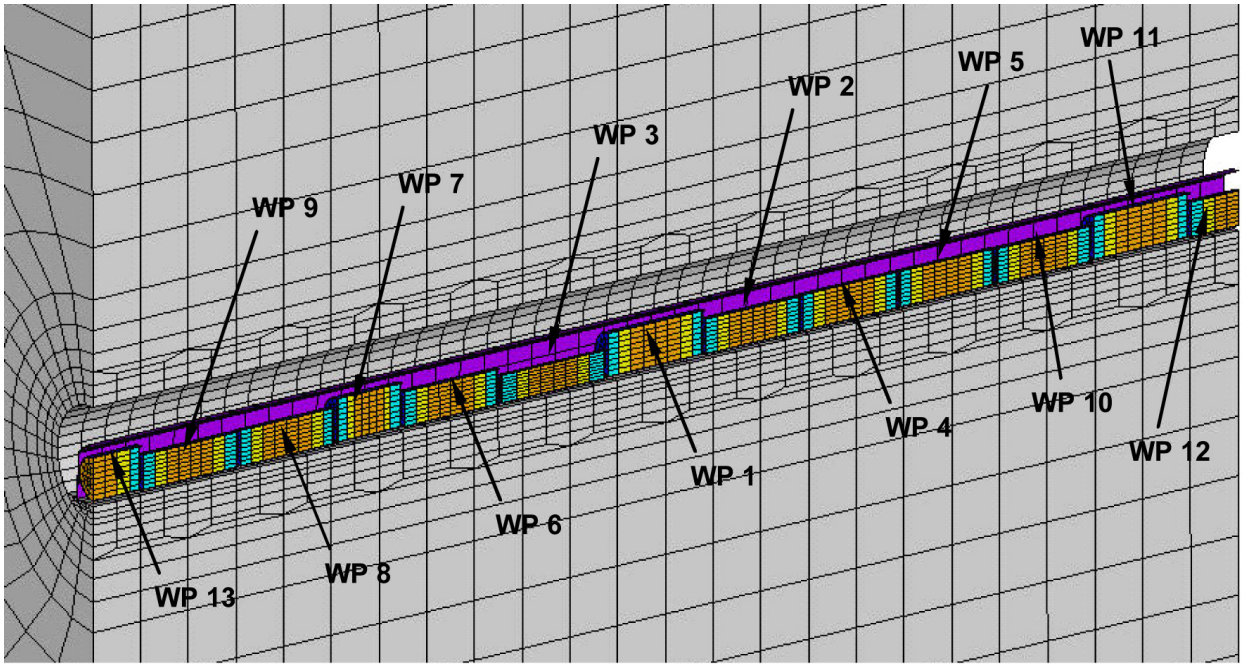

Source: BSC 2006 [DIRS 179686], Figure 4.

NOTE: WP = waste package. This figure is not to scale, applies to Scenarios 1 and 2 only (which replicate the waste package arrangement used previously), and is presented for illustrative purposes only.

Figure 6.3-1. Schematic of the ANSYS Grid for Waste Package Arrangements

The scenarios reported in this analysis are based on Case 1 from *Repository Twelve Waste Package Segment Thermal Calculation* (BSC 2006 [DIRS 179686]), but with different host-rock thermal properties, different waste package sizes and heat output, and different representation of preclosure ventilation.

Invert thermal properties used in this study are the same as used for all cases in *Repository Twelve Waste Package Segment Thermal Calculation* (BSC 2006 [DIRS 179686], Section 6.2.2). The invert lower layer was extended to achieve the updated overall invert height of 1.321 m for

all cases reported below, conforming to updated design information (SNL 2007 [DIRS 179354], Table 4-1).

Mesh refinement studies performed previously for Case 1 of the previous study (BSC 2006 [DIRS 179686], Attachment I) showed convergence after 1 refinement. Therefore, this analysis was performed using the same refined mesh.

The heat capacity values for the Tptpv3 unit for Scenarios 2, 3, and 4 were incorrectly transcribed into the input file *matprops09.dat* (Output DTNs: MO0709THERMAL2.000, MO0709THERMAL3.000 and MO0709THERMAL4.000). The correct values are for the specific heat are located in Table 4.1-7 with values of 907, 1,736, and 1,060 for the specific heat (J/kg) at temperatures (T) < 95°C, 95°C ≤ T ≥ 114°C, and T > 114°C, respectively. The incorrect values of 1,079.5, 6,340 and 930, for T < 95°C, 95°C ≤ T ≥ 114°C, and T > 114°C, respectively, were used in ANSYS as input. It should be noted these values exactly match the values for the unit (Tptpln) directly above the Tptpv3 and closely match the values for the unit (Tptpv2) directly below. The incorrect value for the specific heat is 16% different than the actual value for T < 95°C.

6.3.1.1 Scenario 1

The first case uses the 10th percentile wet and dry thermal conductivity values developed for the multiscale model (SNL 2007 [DIRS 181383], Section 6.2.13.3[a]). The ANSYS input file sets up a transition from wet to dry values when the local rock temperature is greater than 95°C (BSC 2006 [DIRS 179686], Table 8). Waste package and drip shield dimensions, and other thermal and physical properties, are consistent with the previous analyses (BSC 2006 [DIRS 179686], Sections 6.1 and 6.2).

Ventilation duration is 50 years consistent with the previous ANSYS analysis, and also with the postclosure thermal reference case described in Section 6.1. Heat removal by ventilation is represented using the same approach used in the previous Case 1, where ventilation is simulated via a convective boundary condition applied to the surfaces of the waste packages, the drift wall, and the invert surface (BSC 2007 [DIRS 179686], Section 6.3).

6.3.1.2 Scenario 2

The second case is identical to the first, but with the new host-rock effective heat capacity functions formulated to correct a conservatism identified with the functions used previously (Table 4.1-7; Appendix C; also see Output DTN: MO0709REVTHERM.000, file: *Summary of Thermal Properties.xls*).

6.3.1.3 Scenario 3

The third case is similar to the second, but using the waste package dimensions and heat outputs for the 3-package hottest segment for the 96/2 emplacement sequence (Table 6.1-2). The 13 waste packages bracketing the hottest segment of three are explicitly represented in the grid. The waste package dimensions and the assigned numbers are given in Table 6.3-3.

Table 6.3-1. Waste Package Dimensions for the Three-Package Hottest Segment (Scenario 3)

Position	Waste Package #	Length (m)	Diameter (m)
1	12	5.85	1.882
2	11	5.22	2.045
3	10	5.22	2.045
4	5	5.22	2.045
5	4	5.22	2.045
6	2	5.85	1.882
7	1	5.85	1.882
8	3	5.85	1.882
9	6	5.22	2.045
10	7	5.22	2.045
11	8	5.22	2.045
12	9	5.22	2.045
13	13	5.22	2.045

Source: Output DTN: MO0705SUPPCALC.000, folder: \Select Hot and Cold Cases, file: *Hottest 3-7 + Coolest WP 96-2 10Jul07.xls*, worksheet: "Hottest Segments 96-2."

NOTE: Waste Package # corresponds with position in Figure 6.3-1 order starting from right bottom, next right top, and so on right to left.

Preclosure ventilation is represented in this case by reducing the heat output of the waste packages, instead of using a convective boundary condition as described for Scenarios 1 and 2 (the convective boundary condition was turned off). Waste package heat output is decreased by the ventilation efficiency, a percentage of heat removed by air flow, calculated using the ventilation model (BSC 2004 [DIRS 169862]). The average line load for the three hottest waste packages constituting the 3-package segment was calculated (Output DTN: MO0705SUPPCALC.000, folder: \Select Hot and Cold Cases, file: *Hottest 3-7 + Coolest WP 96-2 10Jul07.xls*, worksheet: "Hottest Segments 96/2") and copied into another spreadsheet that implements the ventilation model (file: *Preclosure 3PtHottest.xls*, worksheet: "Heatgen_Vent"). The resulting time-dependent ventilation efficiency values were copied back into the original spreadsheet (file: *Hottest 3-7 + Coolest WP 96-2 10Jul07.xls*, worksheet: "Hottest Segments 96/2") for calculation of the decreased heat output values for each waste package in the 13-package sequence containing the hottest 3-package segment. The resulting heat output time series for each waste package are given as functions of time after emplacement, in Tables 6.3-1 through 6.3-7. Finally, this approach uses a local-average heat load to calculate ventilation efficiency, rather than the heat output of individual waste packages, which is consistent with the ventilation model, and is appropriate for the preclosure condition of rapid axial convection.

Table 6.3-2. Heat Output vs. Time for Waste Package #1 (Scenario 3)

Time (years)	Heat (kW)	Time (years)	Heat (kW)	Time (years)	Heat (kW)
0	1.10E+01	30.0	1.45E+00	126.0	3.97E+00
1.0	7.14E+00	35.0	1.29E+00	136.0	3.74E+00
2.0	5.65E+00	40.0	1.16E+00	146.0	3.54E+00
3.0	4.82E+00	45.0	1.05E+00	156.0	3.37E+00
4.0	4.27E+00	50.0	9.56E-01	166.0	3.23E+00
5.0	3.87E+00	55.0	8.72E-01	176.0	3.10E+00
6.0	3.57E+00	60.0	8.03E-01	186.0	2.99E+00
7.0	3.32E+00	65.0	7.40E-01	196.0	2.89E+00
8.0	3.12E+00	70.0	6.32E+00	206.0	2.80E+00
9.0	2.94E+00	76.0	5.91E+00	216.0	2.72E+00
10.0	2.80E+00	86.0	5.37E+00	226.0	2.64E+00
15.0	2.26E+00	96.0	4.92E+00	236.0	2.56E+00
20.0	1.91E+00	106.0	4.54E+00	246.0	2.49E+00
25.0	1.65E+00	116.0	4.23E+00	256.0	2.43E+00

Source: Output DTN: MO0705SUPPCALC.000, folder: \Select Hot and Cold Cases, file: *Hottest 3-7 + Coolest WP 96-2 10Jul07.xls*, worksheet: "Hottest Segments 96-2" (use row 27, starting with column AS for Waste Package 1 Heat).

NOTE: Year 0 corresponds to year of emplacement 2047.

Table 6.3-3. Heat Output vs. Time for Waste Package #2 (Scenario 3)

Time (years)	Heat (kW)	Time (years)	Heat (kW)	Time (years)	Heat (kW)
0	1.09E+01	30.0	1.42E+00	126.0	3.72E+00
1.0	7.09E+00	35.0	1.26E+00	136.0	3.50E+00
2.0	5.60E+00	40.0	1.13E+00	146.0	3.31E+00
3.0	4.77E+00	45.0	1.02E+00	156.0	3.15E+00
4.0	4.22E+00	50.0	9.22E-01	166.0	3.00E+00
5.0	3.83E+00	55.0	8.43E-01	176.0	2.89E+00
6.0	3.52E+00	60.0	7.70E-01	186.0	2.79E+00
7.0	3.28E+00	65.0	7.09E-01	196.0	2.69E+00
8.0	3.07E+00	70.0	6.05E+00	206.0	2.61E+00
9.0	2.90E+00	76.0	5.64E+00	216.0	2.53E+00
10.0	2.75E+00	86.0	5.09E+00	226.0	2.45E+00
15.0	2.21E+00	96.0	4.65E+00	236.0	2.39E+00
20.0	1.87E+00	106.0	4.28E+00	246.0	2.33E+00
25.0	1.61E+00	116.0	3.97E+00	256.0	2.27E+00

Source: Output DTN: MO0705SUPPCALC.000, folder: \Select Hot and Cold Cases, file: *Hottest 3-7 + Coolest WP 96-2 10Jul07.xls*, worksheet: "Hottest Segments 96-2" (use row 28, starting with column AS for Waste Package 2 Heat).

NOTE: Year 0 corresponds to year of emplacement 2047.

Table 6.3-4. Heat Output vs. Time for Waste Package #3 (Scenario 3)

Time (years)	Heat (kW)	Time (years)	Heat (kW)	Time (years)	Heat (kW)
0	1.08E+01	30.0	1.45E+00	126.0	4.07E+00
1.0	7.06E+00	35.0	1.29E+00	136.0	3.84E+00
2.0	5.59E+00	40.0	1.16E+00	146.0	3.65E+00
3.0	4.77E+00	45.0	1.05E+00	156.0	3.48E+00
4.0	4.23E+00	50.0	9.59E-01	166.0	3.33E+00
5.0	3.84E+00	55.0	8.79E-01	176.0	3.20E+00
6.0	3.54E+00	60.0	8.09E-01	186.0	3.09E+00
7.0	3.30E+00	65.0	7.48E-01	196.0	2.98E+00
8.0	3.09E+00	70.0	6.39E+00	206.0	2.89E+00
9.0	2.92E+00	76.0	6.00E+00	216.0	2.80E+00
10.0	2.78E+00	86.0	5.46E+00	226.0	2.72E+00
15.0	2.24E+00	96.0	5.02E+00	236.0	2.64E+00
20.0	1.90E+00	106.0	4.65E+00	246.0	2.57E+00
25.0	1.65E+00	116.0	4.34E+00	256.0	2.50E+00

Source: Output DTN: MO0705SUPPCALC.000, folder: \Select Hot and Cold Cases, file: *Hottest 3-7 + Coolest WP 96-2 10Jul07.xls*, worksheet: "Hottest Segments 96-2" (use row 26, starting with column AS for Waste Package 3 Heat).

NOTE: Year 0 corresponds to year of emplacement 2047.

Table 6.3-5. Heat Output vs. Time for Waste Packages #4, #5, #10, and #11 (Scenario 3)

Time (years)	Heat (kW)	Time (years)	Heat (kW)	Time (years)	Heat (kW)
0	1.75E-01	30.0	1.92E-02	126.0	1.60E-02
1.0	1.13E-01	35.0	1.64E-02	136.0	1.30E-02
2.0	8.91E-02	40.0	1.41E-02	146.0	1.10E-02
3.0	7.58E-02	45.0	1.22E-02	156.0	9.00E-03
4.0	6.69E-02	50.0	1.05E-02	166.0	7.00E-03
5.0	6.02E-02	55.0	9.08E-03	176.0	6.00E-03
6.0	5.53E-02	60.0	7.84E-03	186.0	5.00E-03
7.0	5.12E-02	65.0	6.89E-03	196.0	5.00E-03
8.0	4.78E-02	70.0	5.52E-02	206.0	5.00E-03
9.0	4.49E-02	76.0	4.80E-02	216.0	5.00E-03
10.0	4.23E-02	86.0	3.90E-02	226.0	5.00E-03
15.0	3.33E-02	96.0	3.10E-02	236.0	3.00E-03
20.0	2.71E-02	106.0	2.50E-02	246.0	3.00E-03
25.0	2.26E-02	116.0	2.00E-02	256.0	3.00E-03

Source: Output DTN: MO0705SUPPCALC.000, folder: \Select Hot and Cold Cases, file: *Hottest 3-7 + Coolest WP 96-2 10Jul07.xls*, worksheet: "Hottest Segments 96-2" (use row 29, starting with column AS for Waste Package 4, 5, 10,and 11 Heat).

NOTE: Year 0 corresponds to year of emplacement 2047.

Table 6.3-6. Heat Output vs. Time for Waste Packages #6, #7, #8, and #13 (Scenario 3)

Time (years)	Heat (kW)	Time (years)	Heat (kW)	Time (years)	Heat (kW)
0	7.15E-01	30.0	7.83E-02	126.0	6.60E-02
1.0	4.63E-01	35.0	6.70E-02	136.0	5.40E-02
2.0	3.65E-01	40.0	5.76E-02	146.0	4.40E-02
3.0	3.11E-01	45.0	4.96E-02	156.0	3.60E-02
4.0	2.74E-01	50.0	4.29E-02	166.0	3.00E-02
5.0	2.47E-01	55.0	3.70E-02	176.0	2.50E-02
6.0	2.26E-01	60.0	3.23E-02	186.0	2.10E-02
7.0	2.10E-01	65.0	2.81E-02	196.0	2.10E-02
8.0	1.95E-01	70.0	2.27E-01	206.0	2.10E-02
9.0	1.84E-01	76.0	1.96E-01	216.0	2.10E-02
10.0	1.73E-01	86.0	1.60E-01	226.0	2.10E-02
15.0	1.36E-01	96.0	1.27E-01	236.0	1.10E-02
20.0	1.11E-01	106.0	1.02E-01	246.0	1.10E-02
25.0	9.25E-02	116.0	8.20E-02	256.0	1.10E-02

Source: Output DTN: MO0705SUPPCALC.000, folder: \Select Hot and Cold Cases, file: *Hottest 3-7 + Coolest WP 96-2 10Jul07.xls*, worksheet: "Hottest Segments 96-2" (use row 21, starting with column AS for Waste Package 6,7,8 and 13 Heat).

NOTE: Year 0 corresponds to year of emplacement 2047.

Table 6.3-7. Heat Output vs. Time for Waste Package #12 (Scenario 3)

Time (years)	Heat (kW)	Time (years)	Heat (kW)	Time (years)	Heat (kW)
0	1.08E+01	30.0	1.41E+00	126.0	3.70E+00
1.0	7.03E+00	35.0	1.25E+00	136.0	3.49E+00
2.0	5.55E+00	40.0	1.12E+00	146.0	3.30E+00
3.0	4.73E+00	45.0	1.01E+00	156.0	3.13E+00
4.0	4.19E+00	50.0	9.17E-01	166.0	2.99E+00
5.0	3.80E+00	55.0	8.36E-01	176.0	2.87E+00
6.0	3.50E+00	60.0	7.65E-01	186.0	2.76E+00
7.0	3.25E+00	65.0	7.05E-01	196.0	2.67E+00
8.0	3.05E+00	70.0	6.01E+00	206.0	2.59E+00
9.0	2.88E+00	76.0	5.62E+00	216.0	2.51E+00
10.0	2.73E+00	86.0	5.07E+00	226.0	2.43E+00
15.0	2.20E+00	96.0	4.63E+00	236.0	2.36E+00
20.0	1.85E+00	106.0	4.27E+00	246.0	2.30E+00
25.0	1.60E+00	116.0	3.96E+00	256.0	2.24E+00

Source: Output DTN: MO0705SUPPCALC.000, folder: \Select Hot and Cold Cases, file: *Hottest 3-7 + Coolest WP 96-2 10Jul07.xls*, worksheet: "Hottest Segments 96-2" (use row 33, starting with column AS for Waste Package 12 Heat).

NOTE: Year 0 corresponds to year of emplacement 2047.

6.3.1.4 Scenario 4

The fourth case is similar to the third, but using the waste package dimensions and heat outputs for the 7-package hottest segment for the 96/2 emplacement sequence (Table 6.1-2). The 13 waste packages bracketing the hottest seven are explicitly represented in the grid. The waste package dimensions and the assigned numbers are given in Table 6.3-10.

Preclosure ventilation is represented in the same manner as for Scenario 3, but using calculated ventilation efficiency values specific to the average line load calculated for the 7-package segment (the convective boundary condition was turned off). The average line load for the seven hottest waste packages constituting the 7-package segment was calculated (Output DTN: MO0705SUPPCALC.000, folder: \Select Hot and Cold Cases, file: *Hottest 3-7 + Coolest WP 96-2 10Jul07.xls*, worksheet: "Hottest Segments 96/2") and copied into another spreadsheet that implements the ventilation model (file: *Preclosure 7PtHottest.xls*, worksheet: "Heatgen_Vent"). The resulting time-dependent ventilation efficiency values were copied back into the original spreadsheet (file: *Hottest 3-7 + Coolest WP 96-2 10Jul07.xls*, worksheet: "Hottest Segments 96/2") for calculation of the decreased heat output values for each waste package in the 13-package sequence containing the hottest 7-package segment. The resulting heat output time series for each waste package are given as functions of time after emplacement, in Tables 6.3-8 through 6.3-21.

Table 6.3-8. Waste Package Dimensions for the Seven-Package Hottest Segment (Scenario 4)

Position	Waste Package #	Length (m)	Diameter (m)
1	12	5.22	2.045
2	11	5.85	1.882
3	10	5.22	2.045
4	5	5.85	1.882
5	4	5.85	1.882
6	2	5.85	1.882
7	1	5.85	1.882
8	3	5.85	1.882
9	6	5.85	1.882
10	7	5.85	1.882
11	8	5.85	1.882
12	9	5.85	1.882
13	13	5.85	1.882

Source: Output DTN: MO0705SUPPCALC.000, folder: \Select Hot and Cold Cases, file: *Hottest 3-7 + Coolest WP 96-2 10Jul07.xls*, worksheet: "Hottest Segments 96-2."

NOTE: Waste Package # corresponds with position in Figure 6.3-1 order starting from right bottom, next right top, and so on right to left.

Table 6.3-9. Heat Output vs. Time for Waste Package #1 (Scenario 4)

Time (years)	Heat (kW)	Time (years)	Heat (kW)	Time (years)	Heat (kW)
0	6.72E+00	30.0	8.23E-01	118.0	1.97E+00
1.0	4.33E+00	35.0	7.25E-01	128.0	1.83E+00
2.0	3.41E+00	40.0	6.45E-01	138.0	1.71E+00
3.0	2.89E+00	45.0	5.77E-01	148.0	1.60E+00
4.0	2.55E+00	50.0	5.19E-01	158.0	1.52E+00
5.0	2.30E+00	55.0	4.69E-01	168.0	1.44E+00
6.0	2.11E+00	60.0	4.27E-01	178.0	1.38E+00
7.0	1.96E+00	65.0	3.89E-01	188.0	1.32E+00
8.0	1.84E+00	70.0	3.57E-01	198.0	1.28E+00
9.0	1.73E+00	72.0	3.19E+00	208.0	1.24E+00
10.0	1.64E+00	78.0	2.95E+00	218.0	1.20E+00
15.0	1.31E+00	88.0	2.63E+00	228.0	1.16E+00
20.0	1.10E+00	98.0	2.36E+00	238.0	1.13E+00
25.0	9.42E-01	108.0	2.15E+00	248.0	1.10E+00

Source: Output DTN: MO0705SUPPCALC.000, folder: \Select Hot and Cold Cases, file: *Hottest 3-7 + Coolest WP 96-2 10Jul07.xls*, worksheet: "Hottest Segments 96-2" (use row 62, starting with column AS for Waste Package 1 Heat).

NOTE: Year 0 corresponds to year of emplacement 2045.

Table 6.3-10. Heat Output vs. Time for Waste Package #2 (Scenario 4)

Time (years)	Heat (kW)	Time (years)	Heat (kW)	Time (years)	Heat (kW)
0	6.13E+00	30.0	7.79E-01	118.0	1.93E+00
1.0	3.98E+00	35.0	6.88E-01	128.0	1.79E+00
2.0	3.15E+00	40.0	6.13E-01	138.0	1.68E+00
3.0	2.68E+00	45.0	5.49E-01	148.0	1.58E+00
4.0	2.37E+00	50.0	4.96E-01	158.0	1.50E+00
5.0	2.15E+00	55.0	4.49E-01	168.0	1.43E+00
6.0	1.98E+00	60.0	4.09E-01	178.0	1.37E+00
7.0	1.84E+00	65.0	3.74E-01	188.0	1.31E+00
8.0	1.72E+00	70.0	3.44E-01	198.0	1.27E+00
9.0	1.62E+00	72.0	3.07E+00	208.0	1.23E+00
10.0	1.54E+00	78.0	2.85E+00	218.0	1.19E+00
15.0	1.23E+00	88.0	2.55E+00	228.0	1.15E+00
20.0	1.04E+00	98.0	2.30E+00	238.0	1.12E+00
25.0	8.91E-01	108.0	2.10E+00	248.0	1.09E+00

Source: Output DTN: MO0705SUPPCALC.000, folder: \Select Hot and Cold Cases, file: *Hottest 3-7 + Coolest WP 96-2 10Jul07.xls*, worksheet: "Hottest Segments 96-2" (use row 63, starting with column AS for Waste Package 2 Heat).

NOTE: Year 0 corresponds to year of emplacement 2045.

Table 6.3-11. Heat Output vs. Time for Waste Package #3 (Scenario 4)

Time (years)	Heat (kW)	Time (years)	Heat (kW)	Time (years)	Heat (kW)
0	5.82E+00	30.0	7.53E-01	118.0	1.92E+00
1.0	3.78E+00	35.0	6.66E-01	128.0	1.79E+00
2.0	3.00E+00	40.0	5.95E-01	138.0	1.68E+00
3.0	2.56E+00	45.0	5.34E-01	148.0	1.58E+00
4.0	2.27E+00	50.0	4.82E-01	158.0	1.50E+00
5.0	2.05E+00	55.0	4.38E-01	168.0	1.43E+00
6.0	1.89E+00	60.0	3.99E-01	178.0	1.37E+00
7.0	1.76E+00	65.0	3.66E-01	188.0	1.32E+00
8.0	1.65E+00	70.0	3.37E-01	198.0	1.28E+00
9.0	1.56E+00	72.0	3.01E+00	208.0	1.24E+00
10.0	1.48E+00	78.0	2.80E+00	218.0	1.20E+00
15.0	1.19E+00	88.0	2.51E+00	228.0	1.16E+00
20.0	9.98E-01	98.0	2.27E+00	238.0	1.13E+00
25.0	8.60E-01	108.0	2.08E+00	248.0	1.10E+00

Source: Output DTN: MO0705SUPPCALC.000, folder: \Select Hot and Cold Cases, file: *Hottest 3-7 + Coolest WP 96-2 10Jul07.xls*, worksheet: "Hottest Segments 96-2" (use row 61, starting with column AS for Waste Package 3 Heat).

NOTE: Year 0 corresponds to year of emplacement 2045.

Table 6.3-12. Heat Output vs. Time for Waste Package #4 (Scenario 4)

Time (years)	Heat (kW)	Time (years)	Heat (kW)	Time (years)	Heat (kW)
0	1.09E+01	30.0	1.40E+00	118.0	3.80E+00
1.0	7.08E+00	35.0	1.24E+00	128.0	3.56E+00
2.0	5.60E+00	40.0	1.11E+00	138.0	3.35E+00
3.0	4.77E+00	45.0	1.00E+00	148.0	3.16E+00
4.0	4.22E+00	50.0	9.08E-01	158.0	3.01E+00
5.0	3.83E+00	55.0	8.27E-01	168.0	2.88E+00
6.0	3.52E+00	60.0	7.57E-01	178.0	2.76E+00
7.0	3.27E+00	65.0	6.97E-01	188.0	2.65E+00
8.0	3.07E+00	70.0	6.45E-01	198.0	2.56E+00
9.0	2.90E+00	72.0	5.77E+00	208.0	2.48E+00
10.0	2.74E+00	78.0	5.39E+00	218.0	2.40E+00
15.0	2.20E+00	88.0	4.86E+00	228.0	2.33E+00
20.0	1.85E+00	98.0	4.44E+00	238.0	2.26E+00
25.0	1.60E+00	108.0	4.09E+00	248.0	2.20E+00

Source: Output DTN: MO0705SUPPCALC.000,folder: \Select Hot and Cold Cases, file: *Hottest 3-7 + Coolest WP 96-2 10Jul07.xls*, worksheet: "Hottest Segments 96-2" (use row 64, starting with column AS for Waste Package 4 Heat).

NOTE: Year 0 corresponds to year of emplacement 2045.

Table 6.3-13. Heat Output vs. Time for Waste Package #5 (Scenario 4)

Time (years)	Heat (kW)	Time (years)	Heat (kW)	Time (years)	Heat (kW)
0	7.71E+00	30.0	9.13E-01	118.0	2.06E+00
1.0	4.97E+00	35.0	8.01E-01	128.0	1.90E+00
2.0	3.91E+00	40.0	7.08E-01	138.0	1.76E+00
3.0	3.32E+00	45.0	6.30E-01	148.0	1.65E+00
4.0	2.92E+00	50.0	5.65E-01	158.0	1.55E+00
5.0	2.64E+00	55.0	5.09E-01	168.0	1.47E+00
6.0	2.42E+00	60.0	4.61E-01	178.0	1.40E+00
7.0	2.24E+00	65.0	4.19E-01	188.0	1.33E+00
8.0	2.10E+00	70.0	3.83E-01	198.0	1.28E+00
9.0	1.98E+00	72.0	3.41E+00	208.0	1.23E+00
10.0	1.87E+00	78.0	3.14E+00	218.0	1.19E+00
15.0	1.48E+00	88.0	2.78E+00	228.0	1.15E+00
20.0	1.23E+00	98.0	2.49E+00	238.0	1.11E+00
25.0	1.05E+00	108.0	2.25E+00	248.0	1.08E+00

Source: Output DTN: MO0705SUPPCALC.000, folder: \Select Hot and Cold Cases, file: *Hottest 3-7 + Coolest WP 96-2 10Jul07.xls*, worksheet: "Hottest Segments 96-2" (use row 65, starting with column AS for Waste Package 5 Heat).

NOTE: Year 0 corresponds to year of emplacement 2045.

Table 6.3-14. Heat Output vs. Time for Waste Package #6 (Scenario 4)

Time (years)	Heat (kW)	Time (years)	Heat (kW)	Time (years)	Heat (kW)
0	6.23E+00	30.0	7.95E-01	118.0	1.99E+00
1.0	4.05E+00	35.0	7.03E-01	128.0	1.85E+00
2.0	3.20E+00	40.0	6.26E-01	138.0	1.73E+00
3.0	2.73E+00	45.0	5.61E-01	148.0	1.63E+00
4.0	2.41E+00	50.0	5.06E-01	158.0	1.55E+00
5.0	2.19E+00	55.0	4.60E-01	168.0	1.47E+00
6.0	2.01E+00	60.0	4.18E-01	178.0	1.41E+00
7.0	1.87E+00	65.0	3.83E-01	188.0	1.36E+00
8.0	1.75E+00	70.0	3.53E-01	198.0	1.31E+00
9.0	1.65E+00	72.0	3.15E+00	208.0	1.27E+00
10.0	1.57E+00	78.0	2.92E+00	218.0	1.23E+00
15.0	1.26E+00	88.0	2.61E+00	228.0	1.19E+00
20.0	1.06E+00	98.0	2.36E+00	238.0	1.16E+00
25.0	9.10E-01	108.0	2.16E+00	248.0	1.13E+00

Source: Output DTN: MO0705SUPPCALC.000, folder: \Select Hot and Cold Cases, file: *Hottest 3-7 + Coolest WP 96-2 10Jul07.xls*, worksheet: "Hottest Segments 96-2" (use row 60, starting with column AS for Waste Package 6 Heat).

NOTE: Year 0 corresponds to year of emplacement 2045.

Table 6.3-15. Heat Output vs. Time for Waste Package #7 (Scenario 4)

Time (years)	Heat (kW)	Time (years)	Heat (kW)	Time (years)	Heat (kW)
0	7.21E+00	30.0	8.77E-01	118.0	2.09E+00
1.0	4.64E+00	35.0	7.76E-01	128.0	1.93E+00
2.0	3.65E+00	40.0	6.88E-01	138.0	1.80E+00
3.0	3.10E+00	45.0	6.15E-01	148.0	1.69E+00
4.0	2.73E+00	50.0	5.54E-01	158.0	1.60E+00
5.0	2.47E+00	55.0	5.01E-01	168.0	1.52E+00
6.0	2.26E+00	60.0	4.55E-01	178.0	1.45E+00
7.0	2.10E+00	65.0	4.15E-01	188.0	1.39E+00
8.0	1.96E+00	70.0	3.81E-01	198.0	1.34E+00
9.0	1.85E+00	72.0	3.40E+00	208.0	1.29E+00
10.0	1.76E+00	78.0	3.14E+00	218.0	1.25E+00
15.0	1.40E+00	88.0	2.79E+00	228.0	1.21E+00
20.0	1.17E+00	98.0	2.51E+00	238.0	1.18E+00
25.0	1.01E+00	108.0	2.28E+00	248.0	1.15E+00

Source: Output DTN: MO0705SUPPCALC.000, folder: \Select Hot and Cold Cases, file: *Hottest 3-7 + Coolest WP 96-2 10Jul07.xls*, worksheet: "Hottest Segments 96-2" (use row 59, starting with column AS for Waste Package 7 Heat).

NOTE: Year 0 corresponds to year of emplacement 2045.

Table 6.3-16. Heat Output vs. Time for Waste Package #8 (Scenario 4)

Time (years)	Heat (kW)	Time (years)	Heat (kW)	Time (years)	Heat (kW)
0	6.37E+00	30.0	7.65E-01	118.0	1.92E+00
1.0	4.08E+00	35.0	6.76E-01	128.0	1.79E+00
2.0	3.19E+00	40.0	6.03E-01	138.0	1.68E+00
3.0	2.70E+00	45.0	5.40E-01	148.0	1.59E+00
4.0	2.38E+00	50.0	4.87E-01	158.0	1.51E+00
5.0	2.14E+00	55.0	4.42E-01	168.0	1.45E+00
6.0	1.96E+00	60.0	4.03E-01	178.0	1.39E+00
7.0	1.82E+00	65.0	3.68E-01	188.0	1.34E+00
8.0	1.70E+00	70.0	3.39E-01	198.0	1.30E+00
9.0	1.60E+00	72.0	3.03E+00	208.0	1.26E+00
10.0	1.52E+00	78.0	2.81E+00	218.0	1.23E+00
15.0	1.21E+00	88.0	2.52E+00	228.0	1.20E+00
20.0	1.02E+00	98.0	2.28E+00	238.0	1.17E+00
25.0	8.74E-01	108.0	2.08E+00	248.0	1.14E+00

Source: Output DTN: MO0705SUPPCALC.000, folder: \Select Hot and Cold Cases, file: *Hottest 3-7 + Coolest WP 96-2 10Jul07.xls*, worksheet: "Hottest Segments 96-2" (use row 58, starting with column AS for Waste Package 8 Heat).

NOTE: Year 0 corresponds to year of emplacement 2045.

Table 6.3-17. Heat Output vs. Time for Waste Package #9 (Scenario 4)

Time (years)	Heat (kW)	Time (years)	Heat (kW)	Time (years)	Heat (kW)
0	7.86E+00	30.0	9.36E-01	118.0	2.16E+00
1.0	5.05E+00	35.0	8.22E-01	128.0	1.99E+00
2.0	3.97E+00	40.0	7.28E-01	138.0	1.85E+00
3.0	3.37E+00	45.0	6.50E-01	148.0	1.74E+00
4.0	2.97E+00	50.0	5.84E-01	158.0	1.64E+00
5.0	2.68E+00	55.0	5.27E-01	168.0	1.55E+00
6.0	2.46E+00	60.0	4.77E-01	178.0	1.48E+00
7.0	2.28E+00	65.0	4.35E-01	188.0	1.41E+00
8.0	2.13E+00	70.0	3.98E-01	198.0	1.36E+00
9.0	2.01E+00	72.0	3.55E+00	208.0	1.31E+00
10.0	1.90E+00	78.0	3.28E+00	218.0	1.26E+00
15.0	1.51E+00	88.0	2.91E+00	228.0	1.22E+00
20.0	1.26E+00	98.0	2.61E+00	238.0	1.18E+00
25.0	1.08E+00	108.0	2.36E+00	248.0	1.15E+00

Source: Output DTN: MO0705SUPPCALC.000, folder: \Select Hot and Cold Cases, file: *Hottest 3-7 + Coolest WP 96-2 10Jul07.xls*, worksheet: "Hottest Segments 96-2" (use row 57, starting with column AS for Waste Package 9 Heat).

NOTE: Year 0 corresponds to year of emplacement 2045.

Table 6.3-18. Heat Output vs. Time for Waste Package #10 (Scenario 4)

Time (years)	Heat (kW)	Time (years)	Heat (kW)	Time (years)	Heat (kW)
0	1.70E-01	30.0	1.88E-02	118.0	2.00E-02
1.0	1.10E-01	35.0	1.61E-02	128.0	1.60E-02
2.0	8.72E-02	40.0	1.38E-02	138.0	1.30E-02
3.0	7.41E-02	45.0	1.19E-02	148.0	1.10E-02
4.0	6.52E-02	50.0	1.03E-02	158.0	9.00E-03
5.0	5.91E-02	55.0	8.89E-03	168.0	7.00E-03
6.0	5.41E-02	60.0	7.77E-03	178.0	6.00E-03
7.0	5.01E-02	65.0	6.70E-03	188.0	5.00E-03
8.0	4.68E-02	70.0	5.89E-03	198.0	5.00E-03
9.0	4.39E-02	72.0	5.16E-02	208.0	5.00E-03
10.0	4.15E-02	78.0	4.50E-02	218.0	5.00E-03
15.0	3.25E-02	88.0	3.90E-02	228.0	5.00E-03
20.0	2.66E-02	98.0	3.10E-02	238.0	3.00E-03
25.0	2.22E-02	108.0	2.50E-02	248.0	3.00E-03

Source: Output DTN: MO0705SUPPCALC.000, folder: \Select Hot and Cold Cases, file: *Hottest 3-7 + Coolest WP 96-2 10Jul07.xls*, worksheet: "Hottest Segments 96-2" (use row 66, starting with column AS for Waste Package 10 Heat).

NOTE: Year 0 corresponds to year of emplacement 2045.

Table 6.3-19. Heat Output vs. Time for Waste Package #11 (Scenario 4)

Time (years)	Heat (kW)	Time (years)	Heat (kW)	Time (years)	Heat (kW)
0	1.09E+01	30.0	1.44E+00	118.0	4.05E+00
1.0	7.07E+00	35.0	1.28E+00	128.0	3.81E+00
2.0	5.61E+00	40.0	1.15E+00	138.0	3.59E+00
3.0	4.78E+00	45.0	1.04E+00	148.0	3.40E+00
4.0	4.24E+00	50.0	9.44E-01	158.0	3.24E+00
5.0	3.85E+00	55.0	8.62E-01	168.0	3.10E+00
6.0	3.54E+00	60.0	7.90E-01	178.0	2.98E+00
7.0	3.30E+00	65.0	7.29E-01	188.0	2.88E+00
8.0	3.09E+00	70.0	6.76E-01	198.0	2.78E+00
9.0	2.92E+00	72.0	6.05E+00	208.0	2.69E+00
10.0	2.77E+00	78.0	5.66E+00	218.0	2.61E+00
15.0	2.24E+00	88.0	5.14E+00	228.0	2.54E+00
20.0	1.89E+00	98.0	4.71E+00	238.0	2.47E+00
25.0	1.63E+00	108.0	4.35E+00	248.0	2.41E+00

Source: Output DTN: MO0705SUPPCALC.000, folder: Select Hot and Cold Cases, file: *Hottest 3-7 + Coolest WP 96-2 10Jul07.xls*, worksheet: "Hottest Segments 96-2" (use row 67, starting with column AS for Waste Package 11 Heat).

NOTE: Year 0 corresponds to year of emplacement 2045.

Table 6.3-20. Heat Output vs. Time for Waste Package #12 (Scenario 4)

Time (years)	Heat (kW)	Time (years)	Heat (kW)	Time (years)	Heat (kW)
0	1.70E-01	30.0	1.88E-02	118.0	2.00E-02
1.0	1.10E-01	35.0	1.61E-02	128.0	1.60E-02
2.0	8.72E-02	40.0	1.38E-02	138.0	1.30E-02
3.0	7.41E-02	45.0	1.19E-02	148.0	1.10E-02
4.0	6.52E-02	50.0	1.03E-02	158.0	9.00E-03
5.0	5.91E-02	55.0	8.89E-03	168.0	7.00E-03
6.0	5.41E-02	60.0	7.77E-03	178.0	6.00E-03
7.0	5.01E-02	65.0	6.70E-03	188.0	5.00E-03
8.0	4.68E-02	70.0	5.89E-03	198.0	5.00E-03
9.0	4.39E-02	72.0	5.16E-02	208.0	5.00E-03
10.0	4.15E-02	78.0	4.50E-02	218.0	5.00E-03
15.0	3.25E-02	88.0	3.90E-02	228.0	5.00E-03
20.0	2.66E-02	98.0	3.10E-02	238.0	3.00E-03
25.0	2.22E-02	108.0	2.50E-02	248.0	3.00E-03

Source: Output DTN: MO0705SUPPCALC.000, folder: \Select Hot and Cold Cases, file: *Hottest 3-7 + Coolest WP 96-2 10Jul07.xls*, worksheet: "Hottest Segments 96-2" (use row 68, starting with column AS for Waste Package 12 Heat).

NOTE: Year 0 corresponds to year of emplacement 2045.

Table 6.3-21. Heat Output vs. Time for Waste Package #13 (Scenario 4)

Time (years)	Heat (kW)	Time (years)	Heat (kW)	Time (years)	Heat (kW)
0	7.05E+00	30.0	8.73E-01	118.0	2.10E+00
1.0	4.56E+00	35.0	7.69E-01	128.0	1.94E+00
2.0	3.59E+00	40.0	6.84E-01	138.0	1.81E+00
3.0	3.05E+00	45.0	6.12E-01	148.0	1.71E+00
4.0	2.69E+00	50.0	5.51E-01	158.0	1.61E+00
5.0	2.43E+00	55.0	4.99E-01	168.0	1.53E+00
6.0	2.24E+00	60.0	4.53E-01	178.0	1.46E+00
7.0	2.07E+00	65.0	4.14E-01	188.0	1.40E+00
8.0	1.94E+00	70.0	3.80E-01	198.0	1.36E+00
9.0	1.83E+00	72.0	3.39E+03	208.0	1.31E+00
10.0	1.74E+00	78.0	3.14E+03	218.0	1.27E+00
15.0	1.39E+00	88.0	2.79E+03	228.0	1.23E+00
20.0	1.16E+00	98.0	2.51E+03	238.0	1.19E+00
25.0	9.99E-01	108.0	2.29E+03	248.0	1.16E+00

Source: Output DTN: MO0705SUPPCALC.000, folder: \Select Hot and Cold Cases, file: *Hottest 3-7 + Coolest WP 96-2 10Jul07.xls*, worksheet: "Hottest Segments 96-2" (use row 56, starting with column AQ for Waste Package 13 Heat).

NOTE: Year 0 corresponds to year of emplacement 2045.

6.3.2 Results of ANSYS Thermal Drift Analysis

The objective of this section was to determine the hottest postclosure drift wall temperature for the four cases described in Section 6.3.1. The results are presented as thermal-image snapshots, histories of the hottest and coolest temperatures at the drift wall, peak wall temperatures for each waste package, and snapshots of the axial profile of drift wall temperature. Histories are plotted for both preclosure and postclosure, and in-drift temperatures increase steeply at closure (at 50 years for Scenarios 1 and 2, 70 years for Scenario 3, and 72 years for Scenario 4).

The maximum drift wall temperature was determined to occur at or near the springline (a line parallel to the drift axis, at the same elevation as the drift axis). Calculated temperatures at the drift crown are slightly lower because the greater distance from the drip shield spreads the radiative flux. The lowest part of the drift wall (below the springline) is at a lower elevation than the centerline of the waste package, and thus receives less direct radiative heat flux than the springline. Accordingly, all drift wall temperature results are reported at the springline, and temperatures within the host rock are reported for locations that are oriented horizontally from the springline.

6.3.2.1 Scenario 1

From the analysis the hottest drift wall temperature achieved anywhere was 180.0°C, at the springline near waste package #2, at 25 years after closure (Output DTN: MO0709THERMAL1.000, file: *get_driftwall_axial_temps.out*, node 6317). The temperature history for this location through preclosure and postclosure is plotted in

Figure 6.3-2. The fine structure of this temperature history is attributable to interactions between adjacent waste packages with different thermal decay functions.

Peak temperatures at the drift wall were achieved everywhere in the model grid at this time. The smallest peak temperature of 173.6°C was adjacent to waste package #13 (Output DTN: MO0709THERMAL1.000, file: *get_driftwall_axial_temps.out*, node 6346). The temperature history for this location through preclosure and postclosure is plotted in Figure 6.3-3. The range of postclosure drift wall temperature throughout the 13-package segment is thus approximately 6°C at the peak (and less as temperatures decrease).

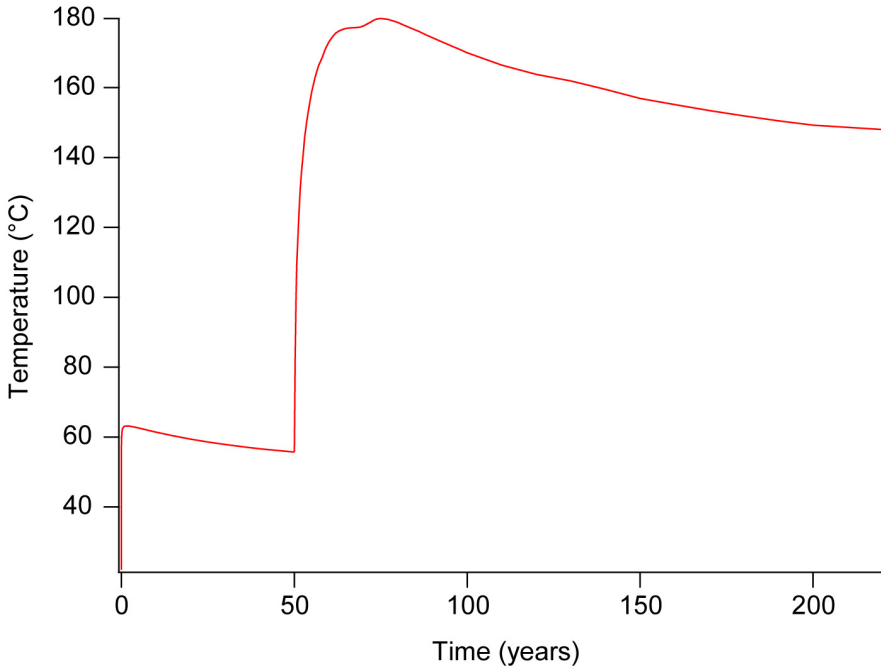

Source: Output DTN: MO0709THERMAL1.000.

NOTE: Temperature at node 6317 in the ANSYS grid, adjacent to waste package #2 (BSC 2006 [DIRS 179686], Table 39).

Figure 6.3-2. Hottest Peak Drift Wall (at the Springline) Temperature History, Scenario 1

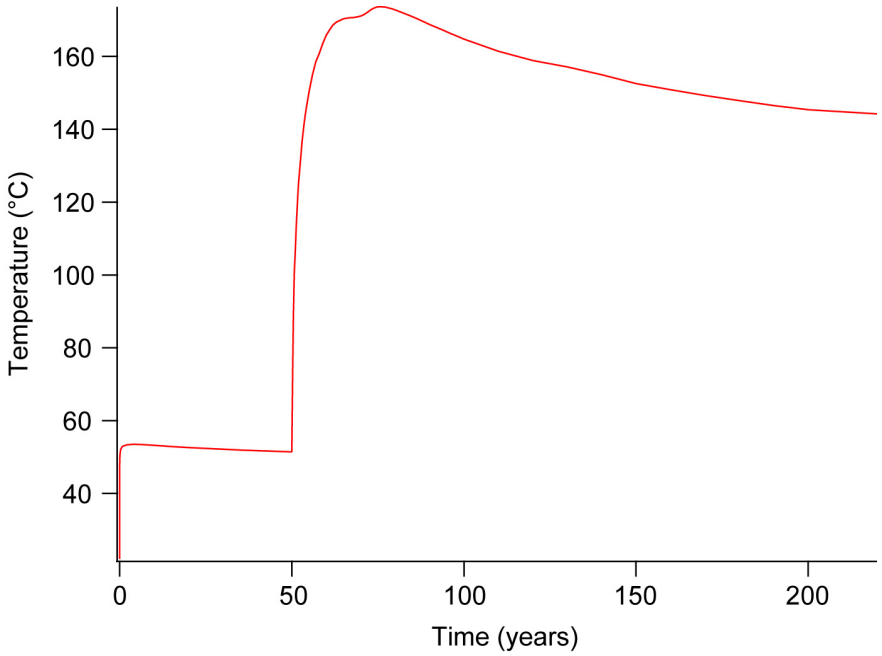

Source: Output DTN: MO0709THERMAL1.000.

NOTE: Temperature at node 6346 in the ANSYS grid, adjacent to waste package #13 (BSC 2006 [DIRS 179686], Table 39).

Figure 6.3-3. Coolest Peak Drift Wall (at the Springline) Temperature History, Scenario 1

The peak wall temperatures for all 13 waste packages, for Scenario 1, are shown in Figure 6.3-4. These results are comparable to the peak waste package temperatures calculated by the multiscale model (SNL 2007 [DIRS 181383], Table 6.3-49[a]) for the P10L case which uses the same 10th percentile value for host rock thermal conductivity.

An axial profile of the drift wall temperature (at the springline) at 75 years after emplacement (25 years after closure) is shown in Figure 6.3-5. This result is closely comparable to the Case 1 results from *Repository Twelve Waste Package Segment Thermal Calculation* (BSC 2006 [DIRS 179686], Figure 21), except that the temperatures are approximately 18°C higher because of the lower host rock thermal conductivity. In summary, the results obtained for Scenario 1 are closely comparable to Case 1 from the previous analysis, and the peak drift wall and waste package temperatures do not exceed their respective limits of 200°C and 300°C (Section 6.1).

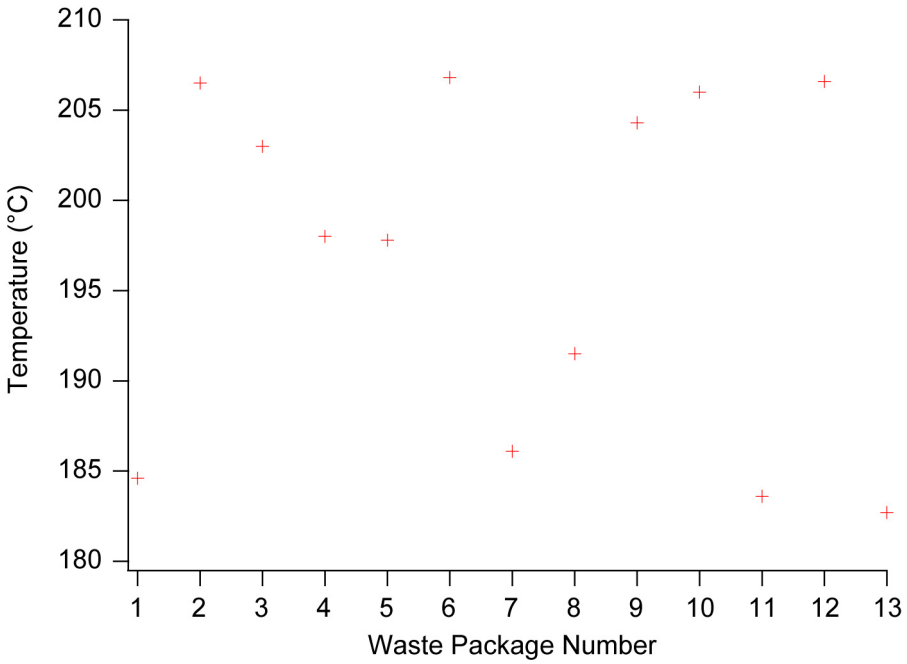

Source: Output DTN: MO0709THERMAL1.000.

NOTE: See BSC 2006 [DIRS 179686], Table 39, for waste package numbers and positions in the 13-package segment for Scenario 1.

Figure 6.3-4. Maximum Mid-Height Waste Package Wall Temperatures, Scenario 1

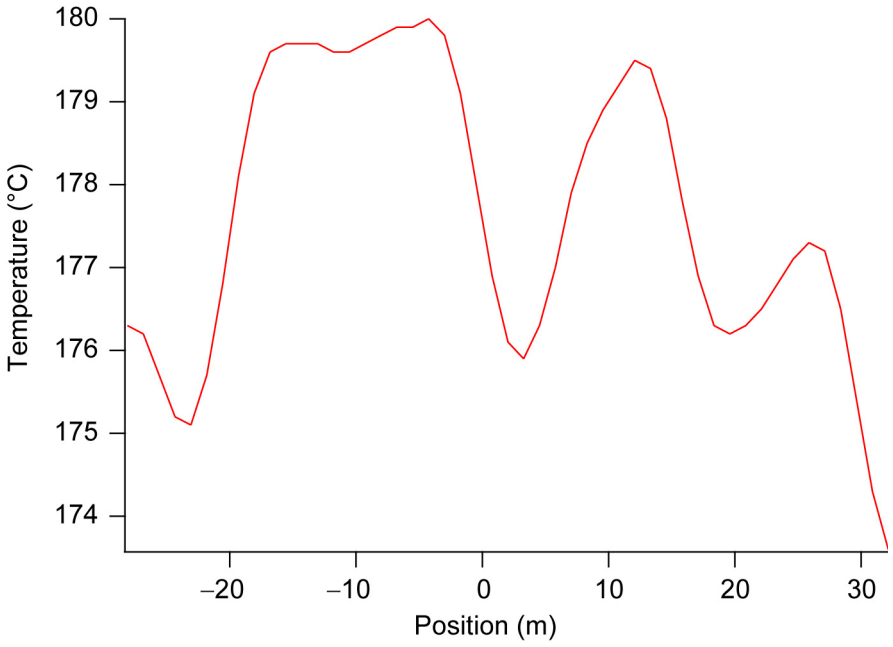

Source: Output DTN: MO0709THERMAL1.000.

NOTE: Position is plotted relative to the location of one end of waste package #1 (Figure 6.3-1).

Figure 6.3-5. Axial Profile of Drift Wall (Springline) Temperature at 75 Years, Scenario 1

6.3.2.2 Scenario 2

From the analysis the hottest drift wall temperature achieved anywhere was 168.1°C, at the springline near waste package #2, at 21 years after closure (Output DTN: MO0709THERMAL2.000, file: *get_driftwall_axial_temps.out*, node 6317). The temperature history for this location through preclosure and postclosure is plotted in Figure 6.3-6. Like Scenario 1, the fine structure of this temperature history is attributable to interactions between adjacent waste packages with different thermal decay functions.

Peak temperatures at the drift wall were achieved everywhere in the model grid at this time. The smallest peak temperature of 161.2°C was adjacent to waste package #13 (Output DTN: MO0709THERMAL2.000, file: *get_driftwall_axial_temps.out*, node 6346). The temperature history for this location through preclosure and postclosure is plotted in Figure 6.3-7. Like Scenario 1, the range of postclosure drift wall temperature throughout the 13-package segment, is thus approximately 6°C at the peak (and less as temperatures decrease).

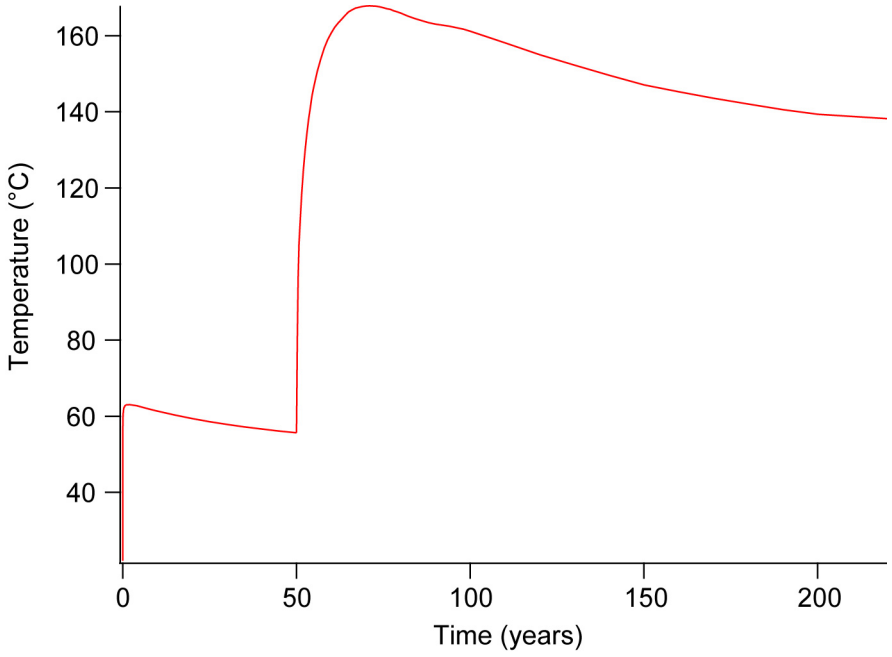

Source: Output DTN: MO0709THERMAL2.000.

NOTE: Temperature at node 6317 in the ANSYS grid, adjacent to waste package #2 (BSC 2006 [DIRS 179686], Table 39).

Figure 6.3-6. Hottest Peak Drift Wall (at the Springline) Temperature History, Scenario 2

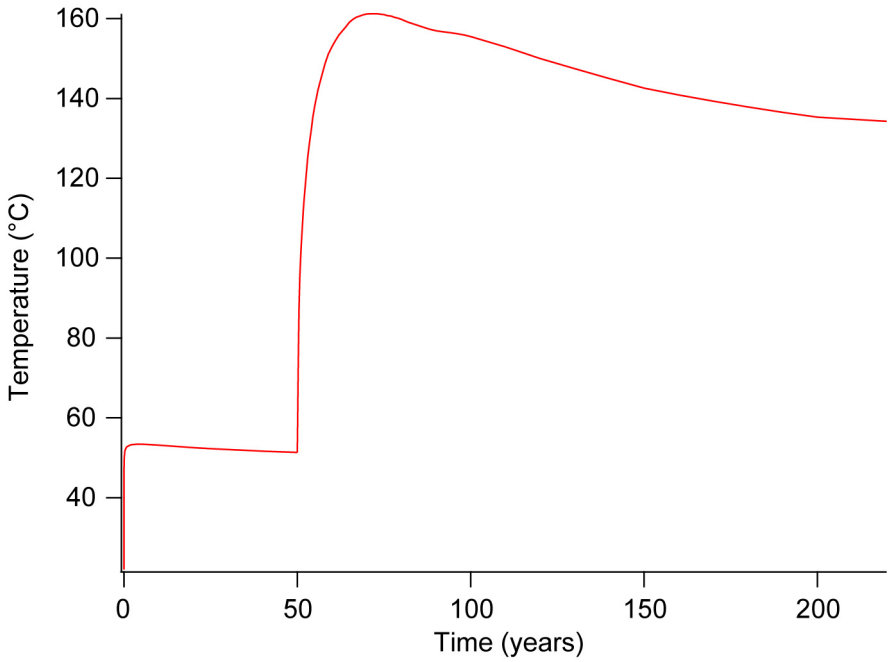

Source: Output DTN: MO0709THERMAL2.000.

NOTE: Temperature at node 6346 in the ANSYS grid, adjacent to waste package #13 (BSC 2006 [DIRS 179686], Table 39).

Figure 6.3-7. Coolest Peak Drift Wall (at the Springline) Temperature History, Scenario 2

The peak wall temperatures for all 13 waste packages, for Scenario 2, are shown in Figure 6.3-8. These results are comparable to the peak waste package temperatures calculated by the multiscale model (SNL 2007 [DIRS 181383], Table 6.3-49[a]) for the P10L case, and are also comparable to the values for Scenario 1 (Figure 6.3-4). From comparison of Figures 6.3-4 and 6.3-8, correction of the effective heat capacity function for the host rock (Appendix C) decreases the peak waste package temperature by approximately 12°C.

An axial profile of the drift wall temperature (at the springline) at 71 years after emplacement (21 years after closure) is shown in Figure 6.3-9. This result is closely comparable to the Case 1 results from *Repository Twelve Waste Package Segment Thermal Calculation* (BSC 2006 [DIRS 179686], Figure 21), and Scenario 1 (Figure 6.3-5), except that the temperatures are cooler. The peak temperature on Figure 6.3-9 is approximately 12°C cooler than Scenario 1 (Figure 6.3-5) because of the corrected heat capacity function. The peak temperature in Figure 6.3-9 is still approximately 6°C higher than Case 1 in *Repository Twelve Waste Package Segment Thermal Calculation* (BSC 2006 [DIRS 179686], Figure 21) because of the lower host rock thermal conductivity. In summary, overall the results obtained for Scenario 2 are closely comparable to Case 1 from the previous analysis, the peak drift wall and waste package temperatures do not exceed their respective postclosure limit, and the corrected heat capacity function produces significantly lower in-drift temperatures.

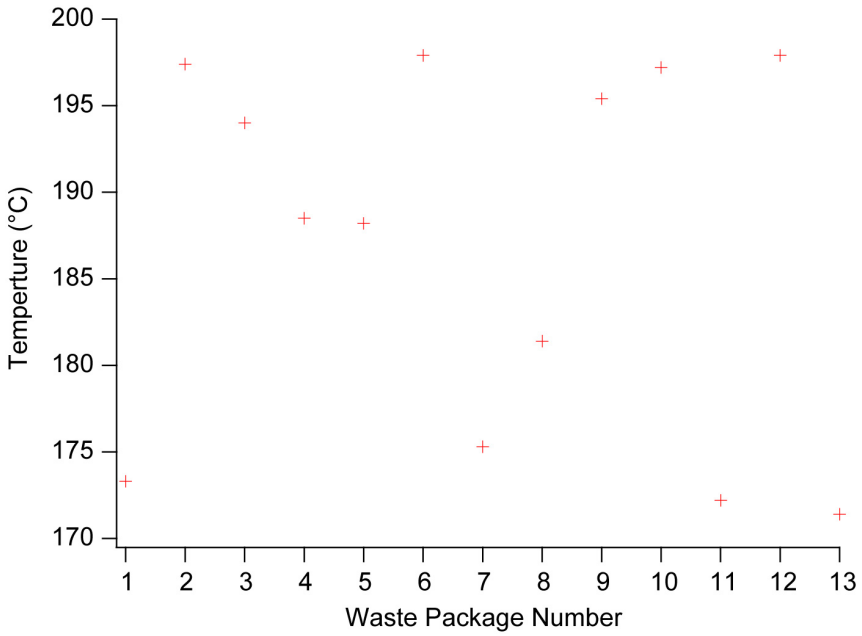

Source: Output DTN: MO0709THERMAL2.000.

NOTE: See BSC 2006 [DIRS 179686], Table 39, for waste package numbers and positions in the 13-package segment for Scenario 2.

Figure 6.3-8. Maximum Mid-Height Waste Package Wall Temperatures, Scenario 2

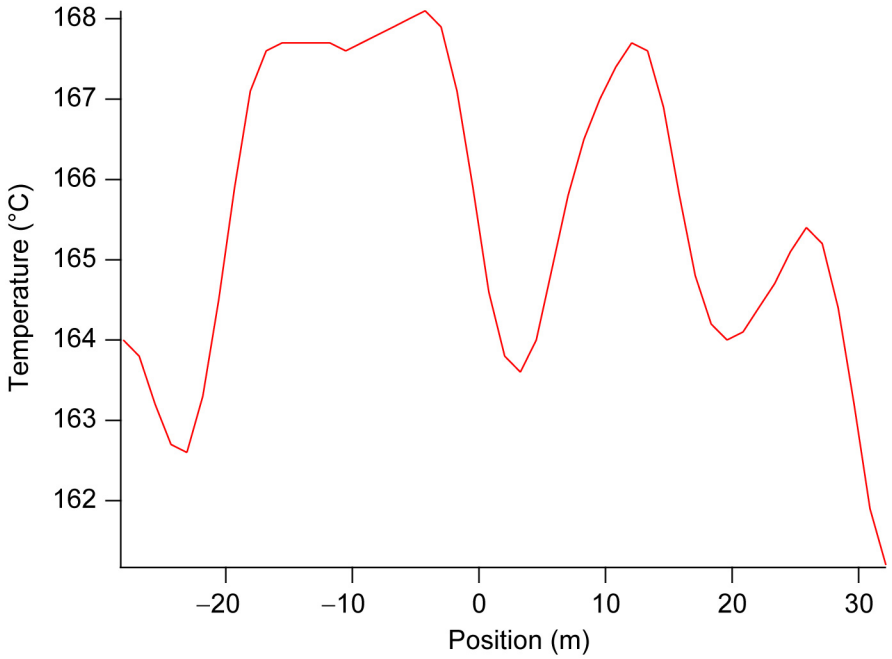

Source: Output DTN: MO0709THERMAL2.000.

NOTE: Position is plotted relative to the location of one end of waste package #1 (Figure 6.3-1).

Figure 6.3-9. Axial Profile of Drift Wall (Springline) Temperature at 71 Years, Scenario 2

6.3.2.3 Scenario 3

The thermal image along an axial, vertical cross-section through the drift is shown in Figure 6.3-10. The snapshot time (12 years after closure, following 70 years preclosure ventilation) corresponds closely with the time of the maximum peak temperature along the drift wall. From the analysis, the hottest drift wall temperature achieved anywhere was 134.2°C (Output DTN: MO0709THERMAL3.000; file: *base_case_post.out*, node 4264) located near waste package #1. The history (Figure 6.3-11) lacks the fine structure of Scenarios 1 and 2 (Figures 6.3-2 and 6.3-6) because the thermal loading for Scenario 3 is more homogeneous in the sense that fewer packages are placed next to packages with very different thermal output.

Peak temperatures at the drift wall were not achieved everywhere at this time in Scenario 3. The DHLW packages near the ends of the segment have much less initial power output, but slower decay, so the peak temperature is much lower but takes longer than 220 years after emplacement (the limit of Scenario 3) to develop. The smallest peak temperature for any waste package calculated in this analysis was 64.3°C, adjacent to waste package #12 (Output DTN: MO0709THERMAL3.000; file: *base_case_post.out*, node 4240). The temperature history for this location through preclosure and postclosure is plotted in Figure 6.3-12. Because Scenario 3 consists of concentrations of high-output CSNF packages and low-output DHLW packages, the range of postclosure drift wall temperature throughout the 13-package segment is greater than for other runs (on the order of 80°C when the peak temperature occurs, over a distance of several waste packages).

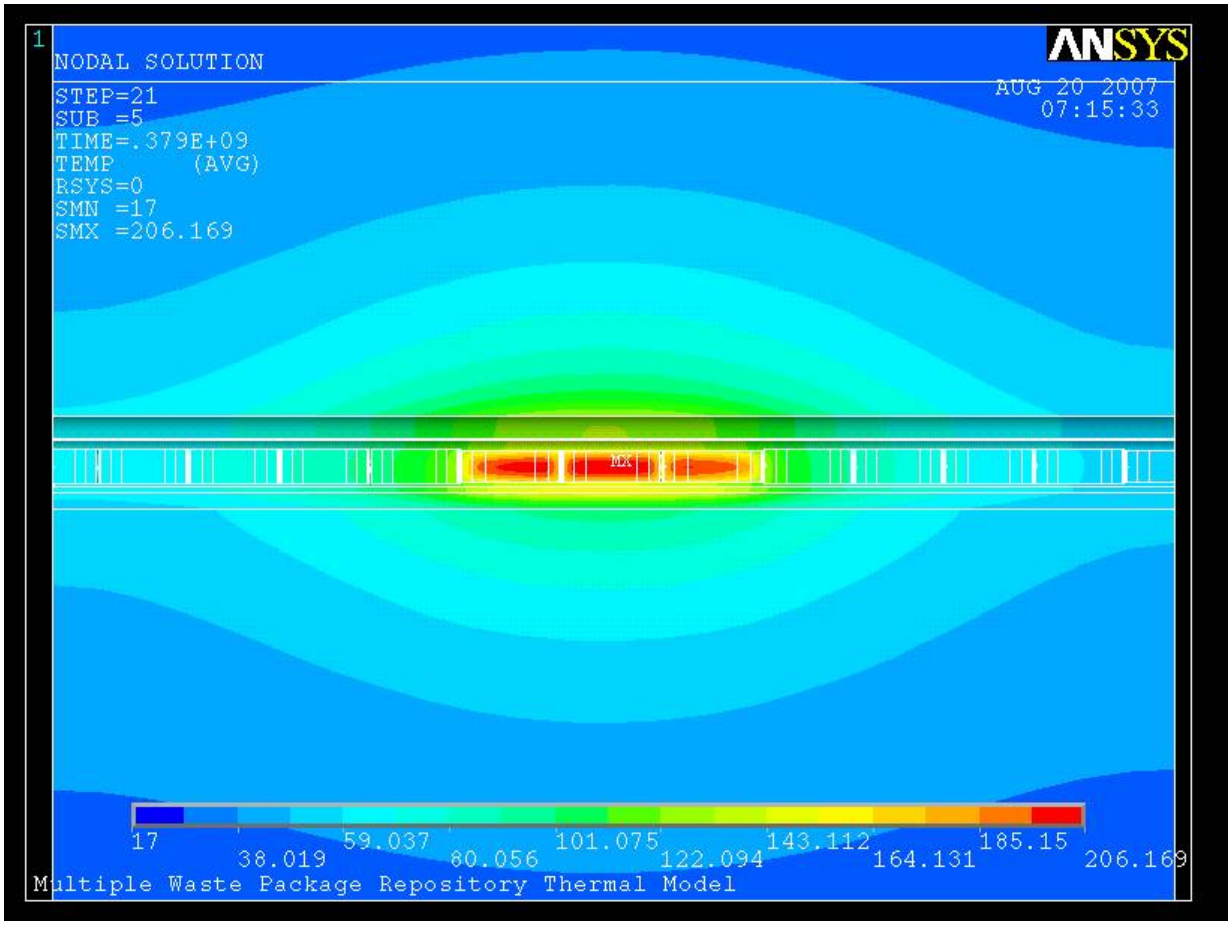

Source: Output DTN: MO0709THERMAL3.000.

NOTE: Provided for illustrative purposes; peak temperature information is given in the text.

Figure 6.3-10. Thermal Image of Peak Drift Wall Temperature, Scenario 3 at 12 Years after Closure

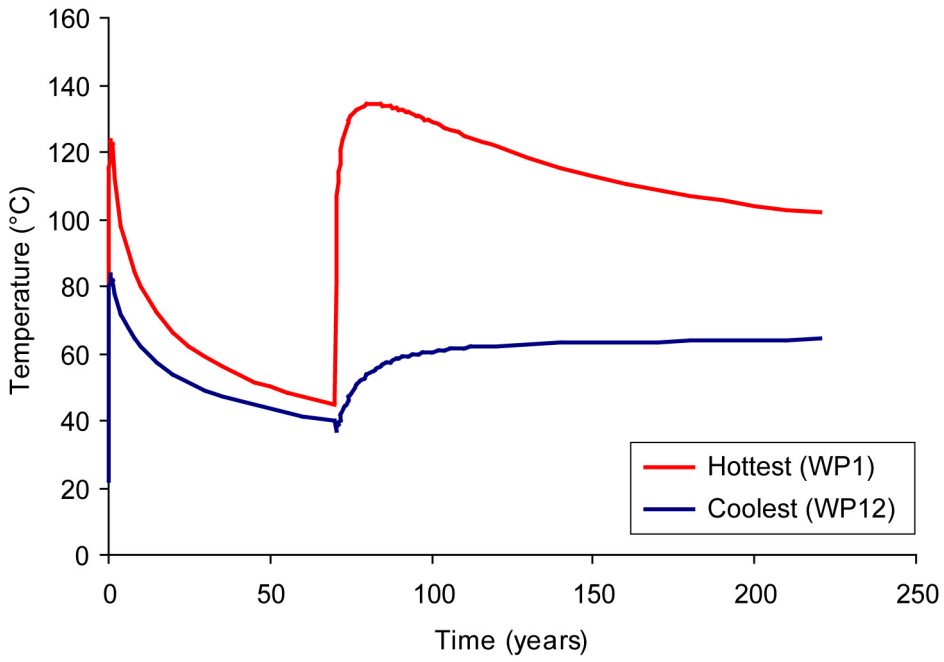

Source: Output DTN: MO0709THERMAL3.000.

NOTE: Hottest temperature is at node 4264 in the ANSYS grid, adjacent to waste package #1(Table 6.3-2). Coolest temperature is at node 4240, adjacent to waste package #12 (Table 6.3-7).

Figure 6.3-11. Hottest and Coolest Peak Drift Wall (at the Springline) Temperature History, Scenario 3

The peak wall temperatures for all 13 waste packages, for Scenario 3, are shown in Figure 6.3-12. For the three hottest waste packages, these results are approximately 35°C cooler than the peak package temperatures for Scenario 2 (Figure 6.3-8), indicating that axial heat sharing is effective over short distances (corresponding to one or two waste packages) in limiting peak waste package temperatures.

An axial profile of the drift wall temperature (at the springline) at 82 years after emplacement (12 years after closure, corresponding to the time of the peak drift wall temperature) is shown in Figure 6.3-13. This result also suggests that axial heat sharing is effective over distances corresponding to one or two waste packages. In summary, overall the results obtained for Scenario 3 show that even the hottest waste packages anticipated for the range of thermal loading (3-package hottest segment; Section 6.1) can readily meet the postclosure thermal limits.

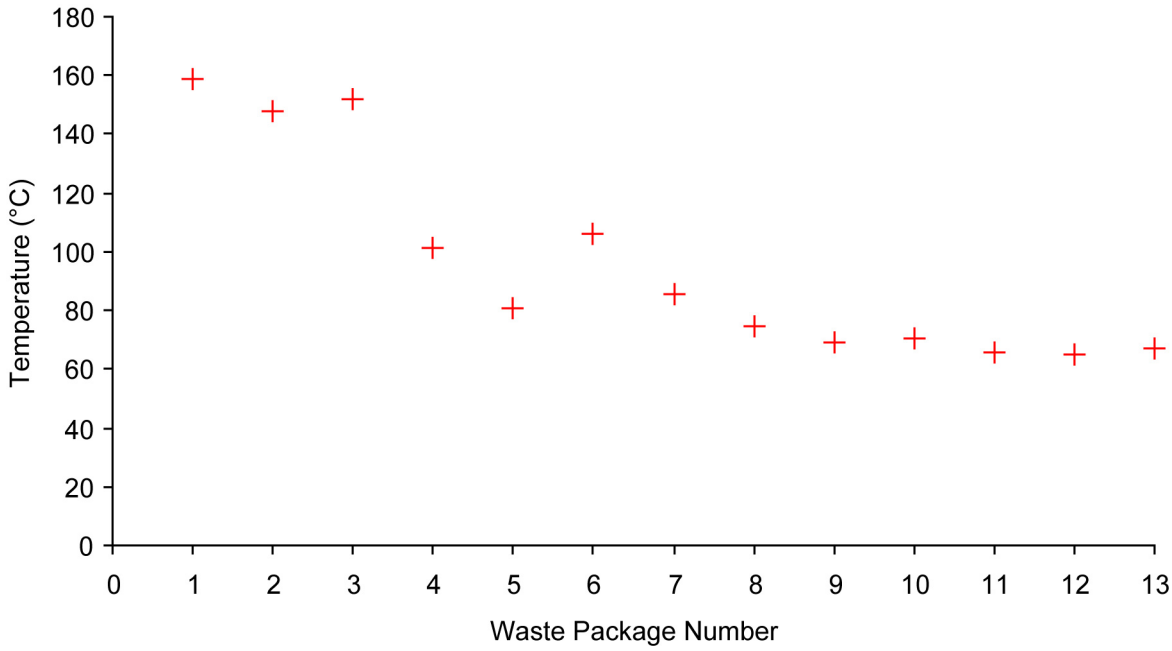

Source: Output DTN: MO0709THERMAL3.000.

Figure 6.3-12. Maximum Mid-Height Waste Package Wall Temperatures, Scenario 3

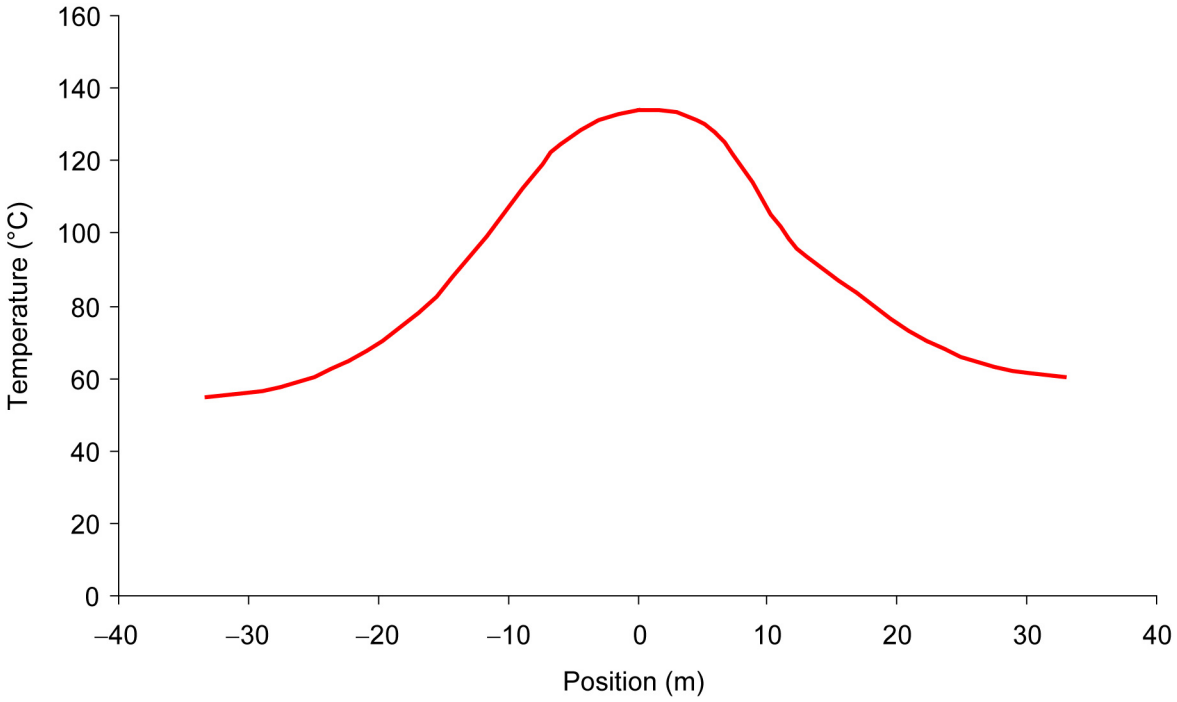

Source: Output DTN: MO0709THERMAL3.000.

NOTE: Position is plotted relative to the location of one end of waste package #1 (Table 6.3-3 and Figure 6.3-1).

Figure 6.3-13. Axial Profile of Drift Wall (Springline) Temperature at 82 Years, Scenario 3

6.3.2.4 Scenario 4

The thermal image along an axial, vertical cross-section through the drift is shown in Figure 6.3-14. The snapshot time (24 years after closure, following 72 years preclosure ventilation) corresponds closely with the time of the maximum peak temperature anywhere along the drift wall (Figure 6.3-15). From the analysis, the hottest drift wall temperature achieved anywhere was 160.3°C (Output DTN: MO0709THERMAL4.000; file: *base_case_post.out*, node 4256), located near waste package #4. Note that the temperature increases steeply at closure (here at 72 years). The history (Figure 6.3-15) lacks the fine structure of Scenarios 1 and 2 (Figures 6.3-2 and 6.3-6) because the peak temperature (package #4) occurs in a part of the segment where thermal loading is more homogeneous than in Scenarios 1 and 2.

Peak temperatures at the drift wall were not achieved everywhere at this time in Scenario 4, although the effect is much less pronounced than for Scenario 3. The smallest peak temperature for any waste package was 151.9°C, adjacent to waste package #12 (Output DTN: MO0709THERMAL4.000; file: *base_case_post.out*, node 4240). The temperature history for this location through preclosure and postclosure is also plotted in Figure 6.3-15. The range of postclosure drift wall temperature throughout the 13-package segment, is generally less than approximately 10°C throughout the time period simulated (comparing hottest and coolest curves in Figure 6.3-15).

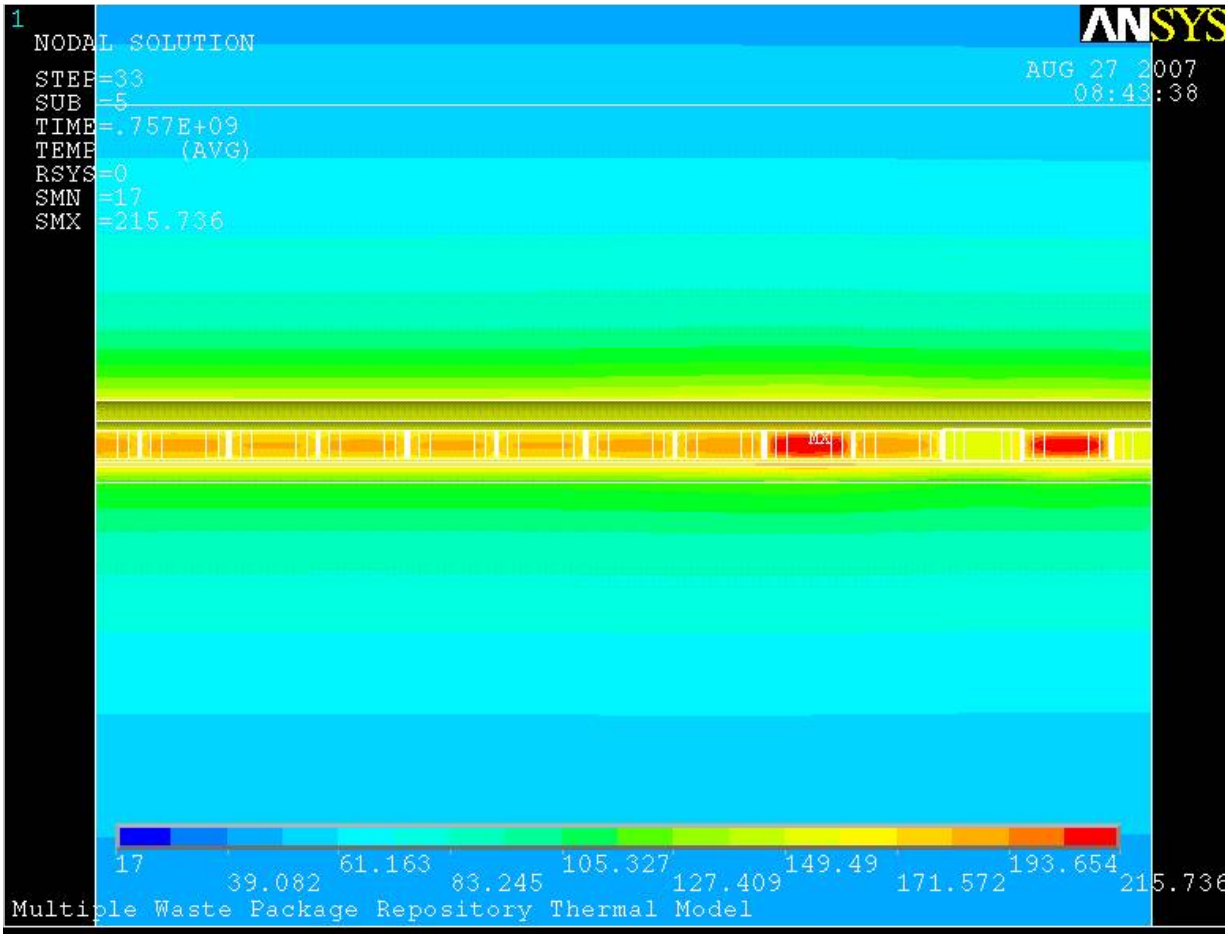

Source: Output DTN: MO0709THERMAL4.000.

NOTE: Provided for illustrative purposes; peak temperature information is given in the text.

Figure 6.3-14. Thermal Image of Peak Drift Wall Temperature, Scenario 4 at 24 Years after Closure

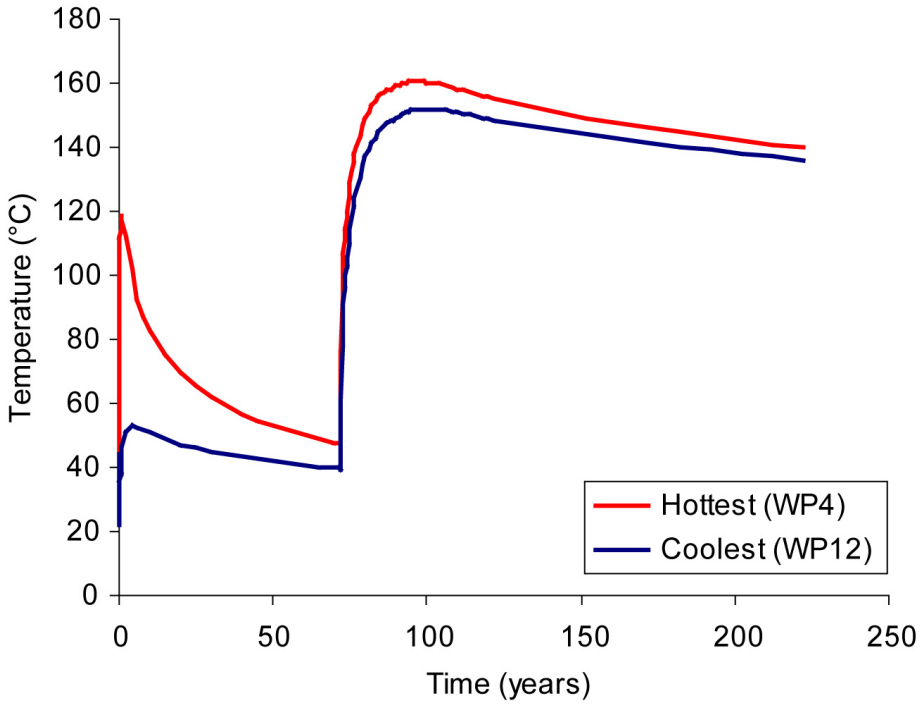

Source: Output DTN: MO0709THERMAL4.000.

NOTE: Hottest temperature is at node 4256 in the ANSYS grid, adjacent to waste package #4(Table 6.3-12). Coolest temperature is at node 4240, adjacent to waste package #12 (Table 6.3-20).

Figure 6.3-15. Hottest and Coolest Peak Drift Wall (at the Springline) Temperature History, Scenario 4

The peak wall temperatures for all 13 waste packages, for Scenario 4, are shown in Figure 6.3-16. For the seven hottest waste packages, these results are somewhat cooler than the peak package temperatures for Scenario 2 (Figure 6.3-8), indicating that axial heat sharing is effective over short distances (corresponding to one or two waste packages) in limiting peak waste package temperatures.

An axial profile of the drift wall temperature (at the springline) at 96 years after emplacement (24 years after closure, corresponding to the time of peak drift wall temperature) is shown in Figure 6.3-17. This result also suggests that axial heat sharing is effective over distances corresponding to one or two waste packages. In summary, overall the results obtained for Scenario 4 show that even the hottest segments for the anticipated range of thermal loading (7-package hottest segment; Section 6.1) can readily meet the postclosure thermal limits.

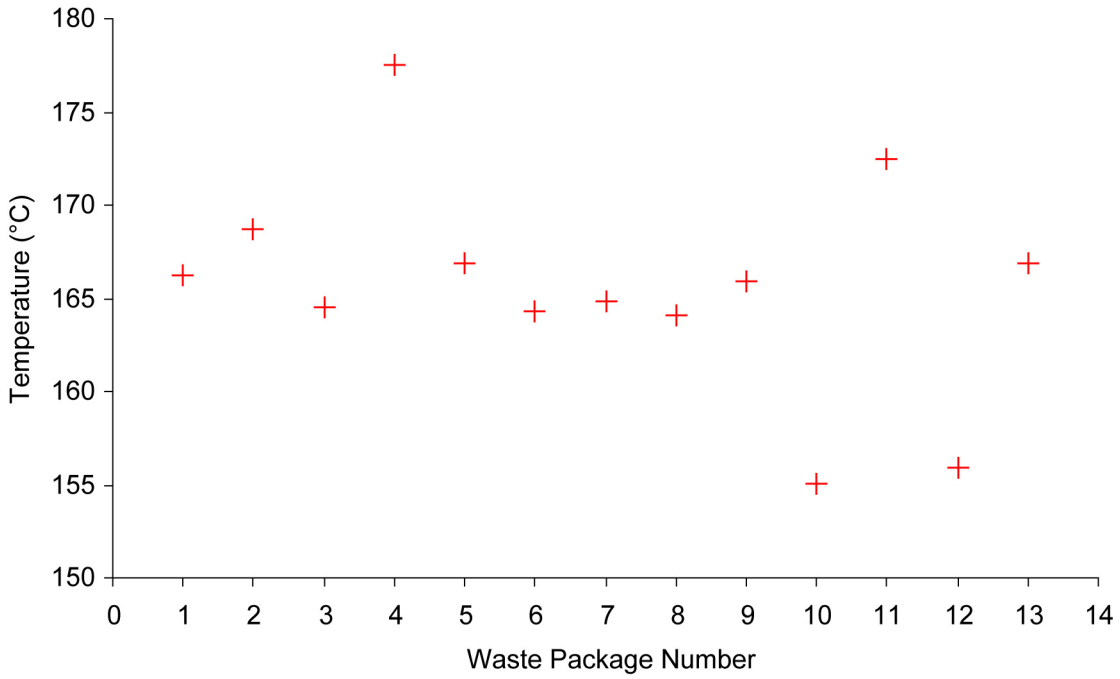

Source: Output DTN: MO0709THERMAL4.000.

Figure 6.3-16. Maximum Mid-Height Waste Package Wall Temperatures, Scenario 4

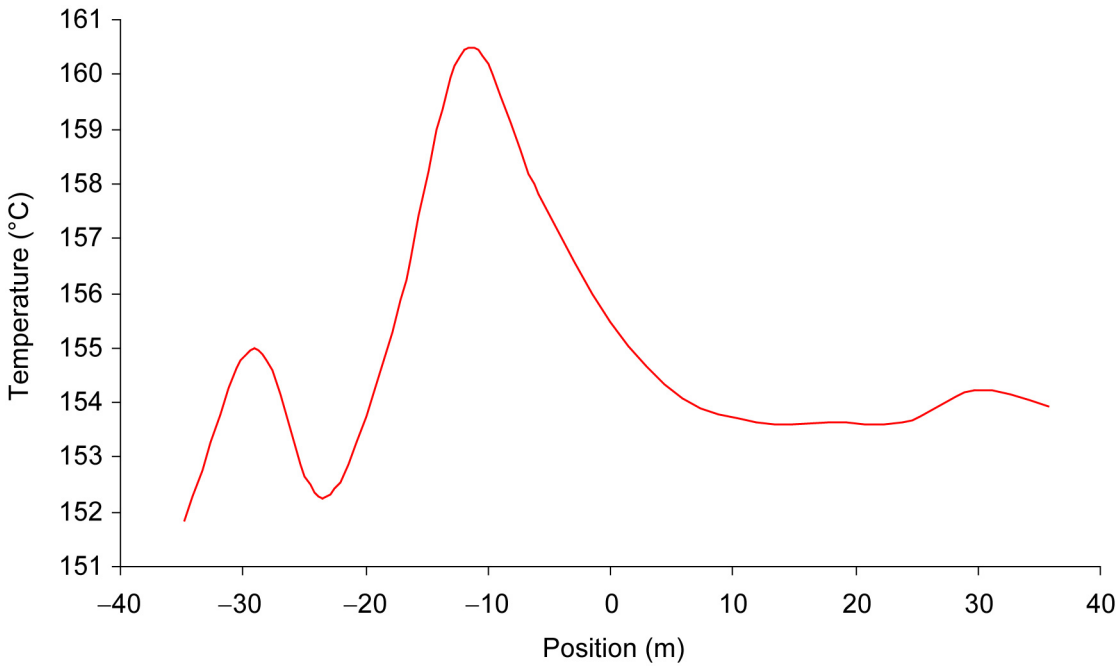

Source: Output DTN: MO0709THERMAL4.000.

NOTE: Position is plotted relative to the location of one end of waste package #1 (Table 6.3-10 and Figure 6.3-1).

Figure 6.3-17. Axial Profile of Drift Wall (Springline) Temperature at 96 Years, Scenario 4

6.3.2.5 Parameter Error Impact Sensitivity

One input transcription error was identified during checking of the ANSYS runs described in Section 6.3 of this report, and found to be insignificant to the results. Temperature-dependent heat capacity values for non-repository rock unit Tptpv3 were erroneously specified in the parameter input files for Scenarios 2 and 4. Comparison of the values used with the correct values is shown in Table 6.3-24. Note that the values for temperatures greater than 95°C are not used in the simulations, because the Tptpv3 is a far-field rock unit that never heats to sufficiently high temperature.

Table 6.3-22. Comparison with Corrected Values for Tptpv3 Unit Heat Capacity

Abbreviation	Geologic Framework Model Unit	Specific Heat (J/kg·K)
		T < 95°C
Values used in Scenarios 2 and 4		
Tptpv3	Tptpv3	1079.5
Correct values from DTN: SN0307T0510902.003 [DIRS 164196] (file: *rock_mass_heat_capacity(edited).xls*)		
Tptpv3	Tptpv3	907

To evaluate the impact of the different values for the lower temperature range (T < 95°C), a simulation was conducted using the NUFT v3.0s code, using an LDTH submodel from the multiscale model. The selected submodel was run with the heat capacity for the Tptpv3 unit (called the tsw38 unit in this submodel) set to each of the values shown in Table 6.3-24, and all other data the same as used for the margin analysis in Section 6.2 of this report. The distance between the repository and the tsw38 unit is approximately the same (about 100 m) as the distance in the ANSYS runs for Scenarios 2 and 4.

The results from this analysis (Output DTN: MO0711SENSTEST.000; summarized in file *Heat capacity impact.xls* in the root directory) show no difference (to four significant figures) in calculated temperatures at the repository horizon. Within the Tptpv3 (tsw38) unit itself, the temperature difference was on the order of 1°C or less at 100 years after emplacement, which is approximately when the peak temperatures occur in Scenarios 2 and 4. Accordingly, there is no impact from this transcription error on the peak drift wall and in-drift temperatures calculated using ANSYS for Scenarios 2 and 4.

6.3.3 Summary

The analysis presented here shows that all emplacement scenarios pass the Yucca Mountain Project design criteria. Of all four scenarios, the first scenario shows the highest drift wall and waste package temperatures. In the first scenario, only the thermal conductivity of the host rock is changed. The second highest temperatures are shown to be in Scenario 2, where the heat capacity values are changed along with the thermal conductivity of the host rock. In both of these cases, the waste packages and their placement have not changed. In addition, temperature trends are similar with the exception of the values.

The Scenario 3 and 4 results differ dramatically from those of Scenarios 1 and 2 The primary difference is the waste packages and placements are changed. The changes represent realistic waste package sizes and thermal outputs given updated information over the previous Scenarios 1 and 2. Scenarios 3 and 4 include the updated thermal conductivity and heat capacity of the host rock. The results show that Scenario 4 has the warmest waste package and drift wall temperature. The results of Scenario 4 show the heat input into the drift to be larger than that of Scenario 3. The result of the placement is emphasized by the spatial temperature plots shown in Figures 6.3-10 and 6.3-14, Scenarios 3 and 4 respectively. Both cases pass the design criteria and are acceptable waste packages for placement in the drift.

An analysis was re-run using non-Qualified software ANSYS version 11. A sample comparison of the different versions of ANSYS is also shown below in Figure 6.3-18.

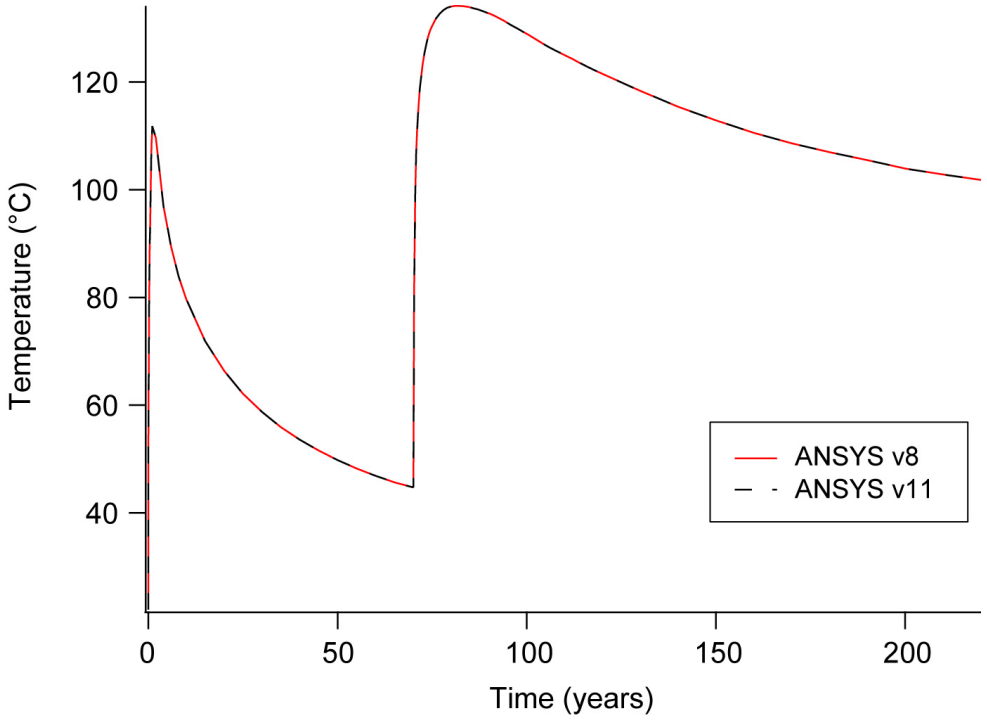

Source: Output DTN: MO0709THERMAL1.000.

Figure 6.3-18. Hottest Peak Drift Wall (at the Springline) Temperature History, Scenario 3

For all scenarios, the results of versions 8 and 11 are identical. The primary difference is runtime, but two factors need to be considered. The first factor is possibly an improvement in solver technology from ANSYS version 8 to 11. The second factor is an improvement in hardware. The calculations using ANSYS version 11 were performed on a local workstation versus a remote server. With the newer version of ANSYS, the speed-up was approximately three times over version 8 calculations.

6.4 PHASE 2 EVALUATIONS OF GEOMECHANICAL, HYDROGEOLOGIC, AND GEOCHEMICAL RESPONSES

This section evaluates the responses of the geomechanical, hydrogeologic, and geochemical systems to the range of design thermal loadings. The range is defined in Section 6.1.4. The results of the evaluation are summarized in Section 7.

The TWP (BSC 2006 [DIRS 179791], Section 2.1.2.2) lists a super-set of models that could be evaluated for Phase 2, and states the possibility that the scope could be reduced as appropriate. Accordingly, the following models in that list are not implemented in Phase 2 for the reasons given below:

- The ventilation model (BSC 2004 [DIRS 169862]) is not reevaluated because ventilation efficiency tends to increase with increased waste heat output, so that using the efficiency developed for the postclosure thermal reference case is slightly conservative with respect to meeting postclosure temperature limits.

- The convection and condensation models (SNL 2007 [DIRS 181648]) are not reevaluated because: (1) condensation is a minor effect as implemented in TSPA (SNL 2007 [DIRS 181648]); and (2) the potential for increased mass transport from convective mixing with increased thermal loading is small compared to the uncertainty associated with transport – for example, barometric pumping is not considered (SNL 2007 [DIRS 181648], Section 6.3).

- Three-dimensional thermal-hydrologic (TH) simulations are not included because 3-D effects are limited by heat sharing between waste packages, mostly by thermal radiation coupling from the waste package to the drip shield, and from the drip shield to the drift wall (Section 6.3). Heat conduction in the host rock further diffuses axial differences in drift wall temperature, which are insignificant at a distances of 1 m and 5 m into the rock (SNL 2007 [DIRS 181648], Section 6.1.3.2.3; BSC 2006 [DIRS 179686], comparing temperature histories in Section 7).

- Mountain-scale coupled processes (BSC 2005 [DIRS 174101) are not evaluated for the hottest thermal case identified in the ELWS because the far-field effect of the ELWS is shown to be similar to, and slightly cooler than, the postclosure thermal reference case for which the mountain-scale coupled process models were developed (Sections 6.4 through 6.6).

The remainder of this section focuses on thermomechanical, hydrogeologic (unsaturated and saturated zones), and geochemical responses. Both near-field and far-field responses are considered.

6.4.1 Geomechanical Response to Range of Design Thermal Loadings

This section applies methods of analysis developed for *Drift Degradation Analysis* (BSC 2004 [DIRS 166107]) to the limiting thermal loading cases identified in Section 6.1.4 of this report. These results, combined with the evaluation of features, events, and processes in Section 6.5,

provide the needed assessment of geomechanical system response to the anticipated range of thermal loading.

Stability of the emplacement drifts is analyzed for the two hottest cases identified in Section 6.1.4 of this report:

- Case 1 – The maximum effective local-average thermal line load (the 7-package average of the 7-package hottest segment from the 96/2 emplacement sequence)
- Case 2 – An extreme local-average line load for sensitivity testing (the 3-package average of the 3-package hottest segment from the 96/2 emplacement sequence).

Two-dimensional thermomechanical analysis was carried out for both cases assuming the line load to extend infinitely in the out-of-plane direction. Consequently, both analyses, particularly Case 2, overestimate far-field and long-term temperatures, thermally induced stresses, and the prospect for rock mass damage and rockfall. Coupled thermomechanical analysis is conducted in such a way that coupling is one-way, i.e., changes in temperature cause stress change, deformation, and damage in the rock. However, accumulation of rockfall around the drip shield and changes in the drift opening profile are not accounted for in the thermal analysis, which is carried out for the original intact drift configuration. Clearly, one-way coupling is inaccurate if there is significant rockfall. The amount of rockfall for all lithophysal rock-mass categories analyzed for Case 1 of the thermal line load is relatively small (Figures 6.4.1-4 through 6.4.1-6) and does not affect heat transfer; therefore, the coupling approximation is appropriate. For Case 2 results using rock properties from Categories 3 and 5 for the lithophysal rock mass, more rockfall accumulates around the drip shield, and the drift-opening profile changes (Figures 6.4.1-8 and 6.4.1-9). For such conditions, calculations based on the initial drift configuration are inaccurate. However, Case 2 is an extreme thermal load used for sensitivity analysis, to investigate a condition that produces impacts beyond any that could be realized in the repository. Case 1 captures the hottest conditions that would be encountered with the ELWS (i.e., maximum 7-package average power at emplacement conforming to the 2.0 kW/m loading rule; see Output DTN: MO0705SUPPCALC.000, folder: \Select Hot and Cold Cases, file: *Hottest 3-7 + Coolest WP 96-2 10Jul07.xls*, worksheet: "Hottest Segments 96-2," cell AQ52). Accordingly, Case 1 is bounding for this analysis, and one-way thermomechanical coupling is adequate for the intended use in this report.

6.4.1.1 Thermal Analysis Approach

Thermal analysis is conducted using an analytical solution constructed by time convolution of an analytical solution (Carslaw and Jaeger 1959 [DIRS 100968], Equation 1, Section 10.3.I) for heat conduction around an instantaneous, line heat source in an infinite medium. The temperature field T(x,z,t) around the analyzed emplacement drift is calculated using Equation (3), superimposing five drifts on either side (N_D = 5, giving more than adequate representation of far-field contributions compared to N_D = 4 used in Section 6.1.3). The origin of the coordinate system is the centerline of the analyzed drift. The temperature calculation (see Section 6.1.3, Equation 6.1-3) is implemented in Mathcad V13. The calculated drift wall temperature histories (evaluated at the springline) for 200 years after waste emplacement for thermal Cases 1 and 2 are shown in Figure 6.4.1-1. Whereas the thermal analysis does not include image sources to

constrain the ground-surface temperature, the cooling influence of the ground surface is negligible for the timeframe of peak near-field temperatures, and is conservatively neglected (higher temperatures) with respect to longer-term evaluation. Other differences between results from the conduction-only analytical solution and a numerical model of host-rock thermal evolution are discussed in Section 6.2.

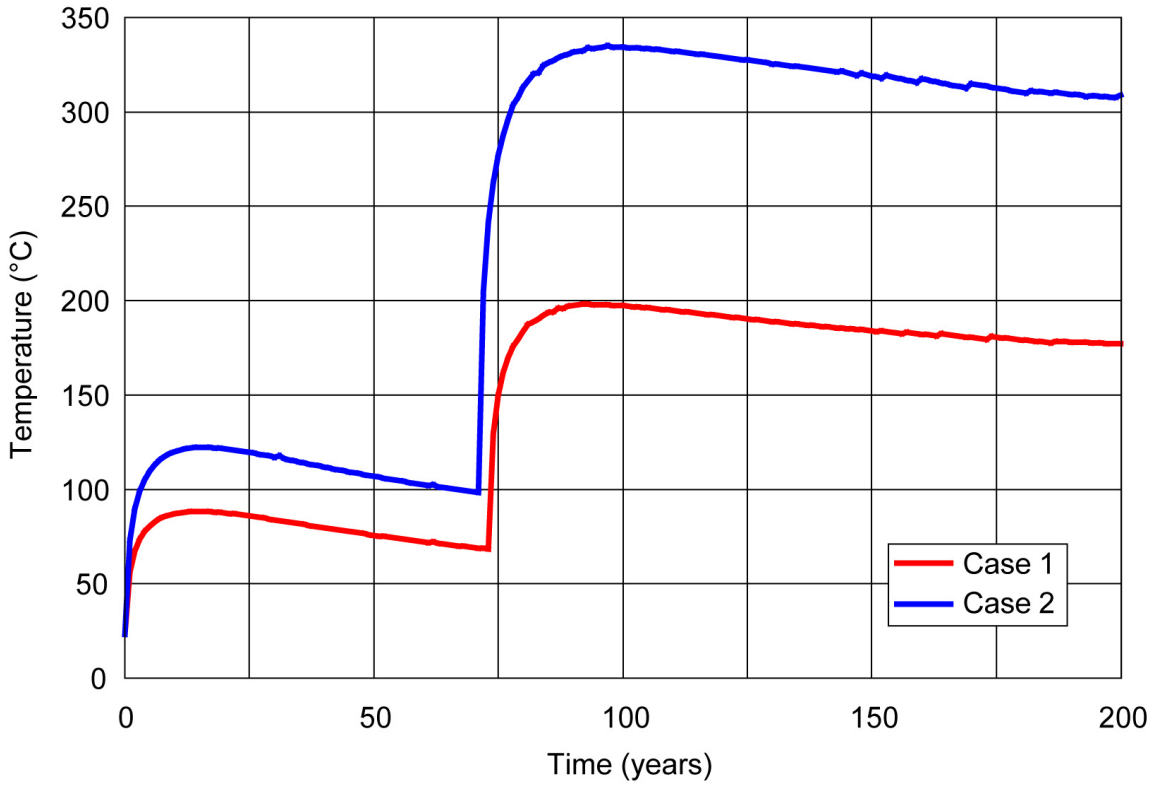

Source: Output DTN: MO0707THERMRES.000, file: *drift wall temperatures.xls.*

Figure 6.4.1-1. Drift Wall (Springline) Temperatures for the Two Cases of Line Load for 200 Years after Waste Emplacement

Drift stability analysis for Cases 1 and 2 temperature histories is carried out using the numerical software code UDEC (see Section 3.1.1). Although UDEC has the capability to perform heat conduction and coupled thermomechanical analysis, it is computationally more efficient to import into UDEC temperature fields as calculated in Mathcad. A sequence of temperature fields was generated in Mathcad for a rectangular grid, for a series of time slices after waste emplacement. The intervals between time slices are not uniform; they were selected so that incremental changes in drift wall temperature are of the order of 15°C or less to ensure that stress changes caused by temperature steps between time slices are relatively small. Temperature change is actually continuous, and the rock mass responds quasi-statically. The density of the spatial rectangular grid used to represent the temperature field is also not uniform. The grid is denser where greater temperature gradients are expected near the drift opening. The temperature fields as defined on the rectangular grid are imported into UDEC and interpolated to the mesh (grid) points for UDEC discretization. A detailed description of the methodology for temperature field transfer is provided in Appendix U of *Drift Degradation Analysis* (BSC 2004

[DIRS 166107]). The only difference is that, in the thermomechanical analysis discussed in the other report (BSC 2004 [DIRS 166107]), the temperature fields were generated using the numerical code NUFT; in the calculations discussed here, the temperature fields were generated based on the analytical solution implemented in Mathcad.

6.4.1.2 Mechanical Analysis Approach

Temperature fields are imported sequentially into UDEC for simulating the mechanical response of the rock mass. For each time slice, a new equilibrium state in the rock mass surrounding the emplacement drift is calculated, and the corresponding deformation, damage and rockfall are predicted. Time is not considered explicitly in the UDEC simulations because thermally induced deformation of the rock mass is quasi-static. Instead, time is defined implicitly in UDEC simulations through imported temperature fields. Thus, each UDEC equilibrium state corresponds to different time after waste emplacement. This methodology is consistent with that described in Section 6.4 of *Drift Degradation Analysis* (BSC 2004 [DIRS 166107]).

In the two-dimensional UDEC simulations the rock mass around the emplacement drift is represented as an assembly of Voronoi blocks, which have random polygonal shapes. The geometry of the UDEC numerical representation used in the calculations is shown in Figure 6.4.1-2. The blocks interact with each other through the interfaces. Initially, the interfaces are bonded together, i.e., assigned non-negative values for cohesion and tensile strength. Before any of the bonds break, the assemblage of polygonal blocks behaves as an elastic continuum. However, because the bond strength is finite, some interfaces could break as dictated by local stress conditions, which is equivalent to the formation of micro-fractures. With increased stress the fractures can propagate, and align or coalesce to form macroscopic fractures. Eventually the fractures can form loose and unstable blocks that fall under gravity. In this approach, the block shapes, and the pattern of interfaces between blocks, do not explicitly represent the structural discontinuities of the rock mass. Rather, the interfaces are randomly oriented and ubiquitous throughout the domain, and represent candidate locations for onset of micro-fracturing. They simply are modeling tools that facilitate realistic simulation of fracturing and damage in the rock mass. The average block size of the UDEC Voronoi assembly is approximately 0.3 m, which is consistent with the average spacing of joints and lithophysal cavities in the lithophysal rock mass, of the order of 0.1 to 0.3 m (BSC 2004 [DIRS 166107], Section 6.4.1.1).

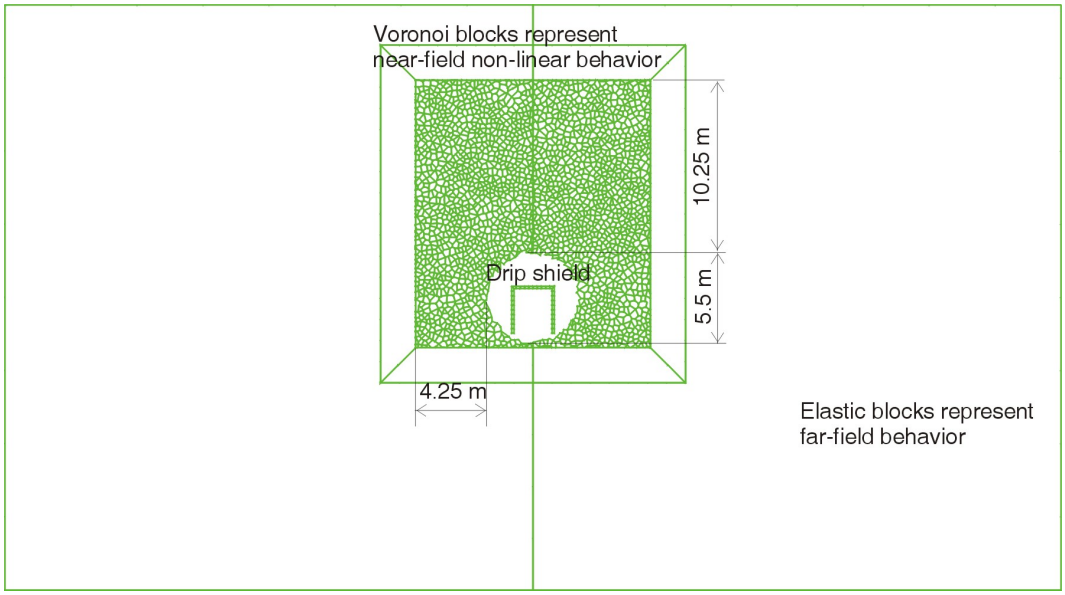

Source: BSC 2004 [DIRS 166107], Figure 6-116.

Figure 6.4.1-2. Geometry of the UDEC Lithophysal Rockfall Representation

One difficulty with using the Voronoi block approach is that the properties of Voronoi blocks (elastic properties and strength) and interfaces between the blocks (normal and shear stiffnesses, cohesion, friction angle and tensile strength) are microscopic properties, which generally cannot be calculated directly from macroscopic properties measured in the laboratory and in field tests. Instead, the microscopic properties have to be calibrated, which involves numerical simulation of relevant laboratory or field tests and adjusting of microscopic properties until the observed macroscopic behavior is matched qualitatively and quantitatively by the synthetic Voronoi block model. A detailed discussion of calibration of the UDEC Voronoi block model can be found in Sections 6.4.2.1 and 7.6 of *Drift Degradation Analysis* (BSC 2004 [DIRS 166107]).

The initial and boundary conditions for UDEC thermomechanical calculations are illustrated in Figure 6.4.1-3. The figure also illustrates the dimensions of the analyzed domain, which extends between two symmetry planes at the closest neighboring drifts on each side of the analyzed drift. Thus, the horizontal width of the domain is 81 m. The domain extends 30 m above and below the drift. The 60-m height of the analyzed domain is larger than the 35-m height used in the thermomechanical analysis for *Drift Degradation Analysis* (BSC 2004 [DIRS 166107], Figure 6-139) because of the increased temperatures considered in this analysis. As indicated in Figure 6.4.1-3, the in-situ stress state (before drift excavation) at the elevation of the drift centerline is given by vertical compressive stress of 7 MPa and horizontal compressive stress of 3.5 MPa (BSC 2004 [DIRS 166107], Section 6.3.1.1, p. 6-59). The symmetry boundary conditions (i.e., the rollers) are applied along the vertical boundaries, which coincide with symmetry planes. Rollers also are applied along the bottom boundary. The weight of the overburden above the top boundary of the simulated domain is applied as a stress boundary condition on the top boundary.

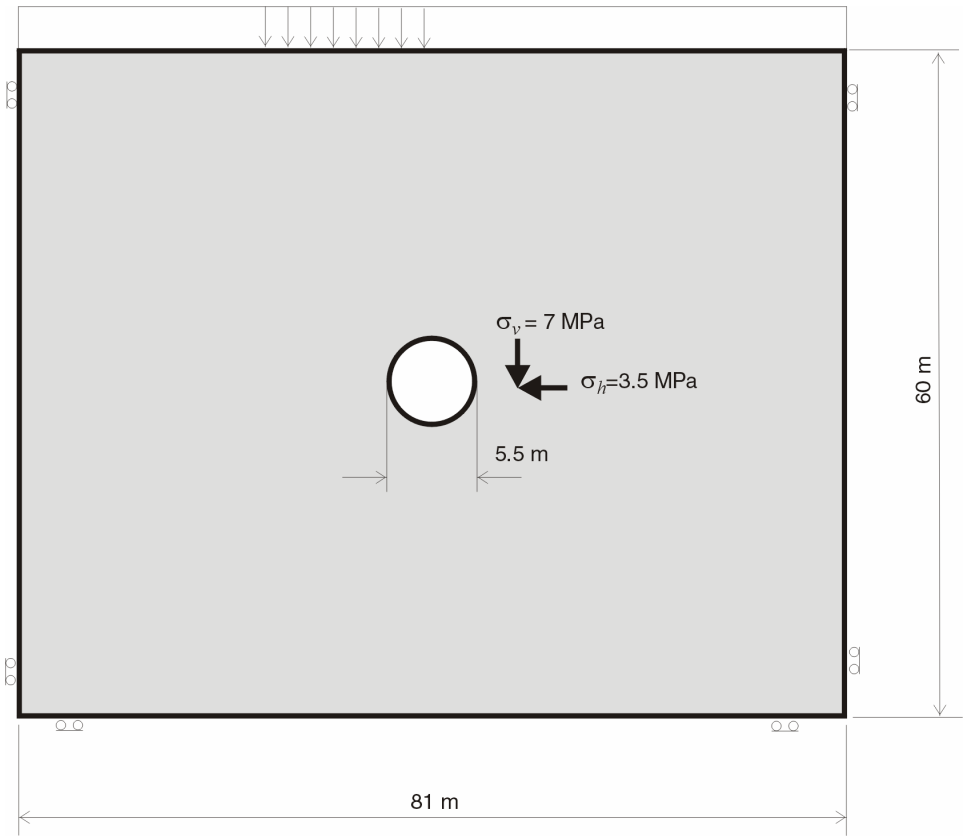

NOTE: Not to scale; presented for illustrative purposes only.

Figure 6.4.1-3. Geometry, Initial Conditions, and Boundary Conditions of the Domain Used in Mechanical Analysis

The numerical representation approximates the geometry and mechanical response of the drip shield. It has a rectangular outline (Figure 6.4.1-2) with height and width based on design information with an emplacement drift diameter of 5.5 m, and an emplacement drift spacing of 81 m (SNL 2007 [DIRS 179466], Table 4-1). The drip shield in this approximation is rigid and fixed in space. Such an approximation does not affect deformation and damage of the rock mass, but the presence of the drip shield is important, because it reduces the volume of open space available for rockfall, which can then fill with rubble sooner, preventing further rockfall.

This analysis pertains to the effect of thermal loading on the potential for rockfall. Seismic loading has the potential to generate far more rockfall (SNL 2007 [DIRS 176828], Section 6.7) than thermal loading alone as represented here. Dynamic damage to the drip shield and other features of the engineered barrier is much more likely to result from seismic ground motion than from rockfall cause by thermal loading. Accordingly, the approach applied here is to separate the effects of thermal loading from seismic consequences, and to evaluate aseismic rock conditions caused by thermal loading as they could exist before a seismic event occurs. Time-dependent deformation is not included in this analysis because, as shown in Section 6.4.2.3 (Figures 6.4.2-4 through 6.4.2-15), the hottest drift-wall temperature histories in intact drifts associated with the anticipated range of thermal loading cool down at a rate that is comparable to the reference case. These figures show that cooldown to a particular temperature is at most a few

hundred years slower, or a small fraction of the cooldown duration, compared to the reference case. Thus, although time-dependent deformation and rockfall may occur (BSC 2004 [DIRS 166107], Section 8.1 and Appendix S), the incidence will be comparable to the reference case thermal loading, and the effects will be greatest after thousands of years when cooldown is substantially complete.

6.4.1.3 Simulation Sequence

The simulations are initialized by applying the in situ stress boundary conditions to the domain without a drift opening. A drift opening is then introduced to simulate excavation, resulting in new equilibrium distributions of deformation and stress in the host rock. For thermomechanical analysis, the temperature fields are imported sequentially into UDEC for 40 different time slices up to 1,000 years after waste emplacement. The mechanical states of equilibrium deformation, damage, and stress in the rock around the emplacement drift are calculated for each time slice. The simulations for this analysis were stopped at 1,000 years after waste emplacement, because these and previous calculations (for the nominal thermal scenario; see BSC 2004 [DIRS 166107], Section 6.4.2.3) indicate that thermally induced rockfall is complete after 1,000 years.

6.4.1.4 Thermal-Mechanical Properties

The mechanical rock-mass property values assigned to five lithophysal rock categories spanning the range of rock quality (as mainly controlled by lithophysal porosity) are provided in Table 4.1-9. These categories were developed for earlier work presented in *Drift Degradation Analysis* (BSC 2004 [DIRS 166107], Table 6-41). Thermomechanical analyses for Cases 1 and 2 were carried out for lithophysal rock-mass Categories 1, 3, and 5, i.e., for the extremes and intermediate conditions, following the simplification used in the previous work (BSC 2004 [DIRS 166107], Section 6.4.2.2). The calibrated microscopic mechanical properties for the 0.3-m Voronoi blocks and interfaces between the blocks, used as inputs in the UDEC simulations, are listed in Table 4.1-10 for all lithophysal rock categories. These properties are based on the data sources and calibration procedure discussed in Section 6.4.1.2.2. The temperature-dependent coefficient of thermal expansion determined for the TSw2 thermomechanical unit (listed in Table 4.1-11) was used throughout the entire analyzed domain irrespective of the lithophysal rock-mass category.

6.4.1.5 Geomechanical Results

The results of the calculations for the Case 1 thermal line load are shown in Figures 6.4.1-4 through 6.4.1-6; the results for the Case 2 thermal line load are shown in Figures 6.4.1-7 through 6.4.1-9. The plots show conditions after 95 years for Case 1 and 97 years for Case 2, or approximately 25 years after closure, when the drift wall temperature is at or within a few degrees of maximum (see Figures 6.3-24 and 6.3-17, respectively). The plots also show conditions at the end of the simulations, after 1,000 years. The temperature contours and the magnitudes of maximum and minimum principal stresses are shown for the actual degraded configurations.

The results for Case 1 are similar to those for the nominal thermal case analyzed previously and discussed in Section 6.4.2.3.1 of *Drift Degradation Analysis* (BSC 2004 [DIRS 166107]). For Case 1, heating does not cause rockfall in Category 1 lithophysal rock (Figure 6.4.1-4). Fractured and distressed rock extends into the drift walls at the springline up to a depth of approximately 0.5 m (BSC 2004 [DIRS 166107], Section 7.6.6). However, that rock is already damaged due to the redistribution of the in situ stresses that occurs upon excavation. Thermal loading does not induce any additional damage, i.e., rockfall, for Category 1 rock.

Response to heating for Categories 3 and 5 is similar to Category 1 (Figures 6.4.1-5 and 6.4.1-6). For both categories, the thermal stress causes minor damage and rockfall from the drift crown, which occurs around the time of the maximum drift wall temperature. The maximum increase in thermally induced (compressive) stress is in the drift crown, and is associated with the vertical symmetry plane between the drifts (at which perpendicular displacements are restrained). The vertical direction is practically unrestrained, limiting changes in vertical compressive stress.

The reason that rockfall from the drift crown is predicted for rock Categories 3 and 5, while no rockfall is predicted in the poorest-quality lithophysal rock (Category 1), is explained by the ratio between the unconfined compressive strength, *UCS*, and the Young's modulus, *E* (see Section 6.4.2.3.1 of BSC 2004 [DIRS 166107]). Thermally induced stress change is proportional to Young's modulus, and the resistance of rock to damage and fracture is proportional to *UCS*. As the ratio decreases, thermally induced damage in the rock mass is expected to increase. Table 6.4.1-1 shows that the ratio decreases with increase in lithophysal rock-mass quality, making better rock-mass categories more susceptible to thermally induced damage and rockfall. The difference between the ratio for Categories 3 and 5 is relatively small; hence the similar rockfall is predicted.

Table 6.4.1-1. Strength-to-Stiffness Ratios for Lithophysal Rock-Mass Categories 1, 3, and 5

Lithophysal Rock-Mass Category	*UCS* / *E*
1	5.26×10^{-3}
3	1.85×10^{-3}
5	1.52×10^{-3}

Source: Calculated from the values in Table 4.1-9.

The results for Case 2, the extreme thermal line load, show an obvious increase in rockfall compared to Case 1 (Figures 6.4.1-7 through 6.4.1-9). However, the qualitative comparison of rockfall in different rock mass categories is similar to that in the Case 1 thermal line load. The least rockfall occurs for Category 1, and this rockfall comes mostly from the drift walls. Rockfall for Categories 3 and 5 is greater than that in Category 1, and comes mostly from the crown. However, in none of the analyzed cases does the drift collapse completely and fill with rubble. The reasons that a given temperature state initially causes damage and rockfall, which then stop as the rock mass reaches a state of thermomechanical equilibrium, include: (1) achievement of a new, more stable drift shape; and (2) the confining pressure of the accumulated rubble. For the cases shown in Figures 6.4.1-7 through 6.4.1-9, confining pressure is a factor only in the drift walls.

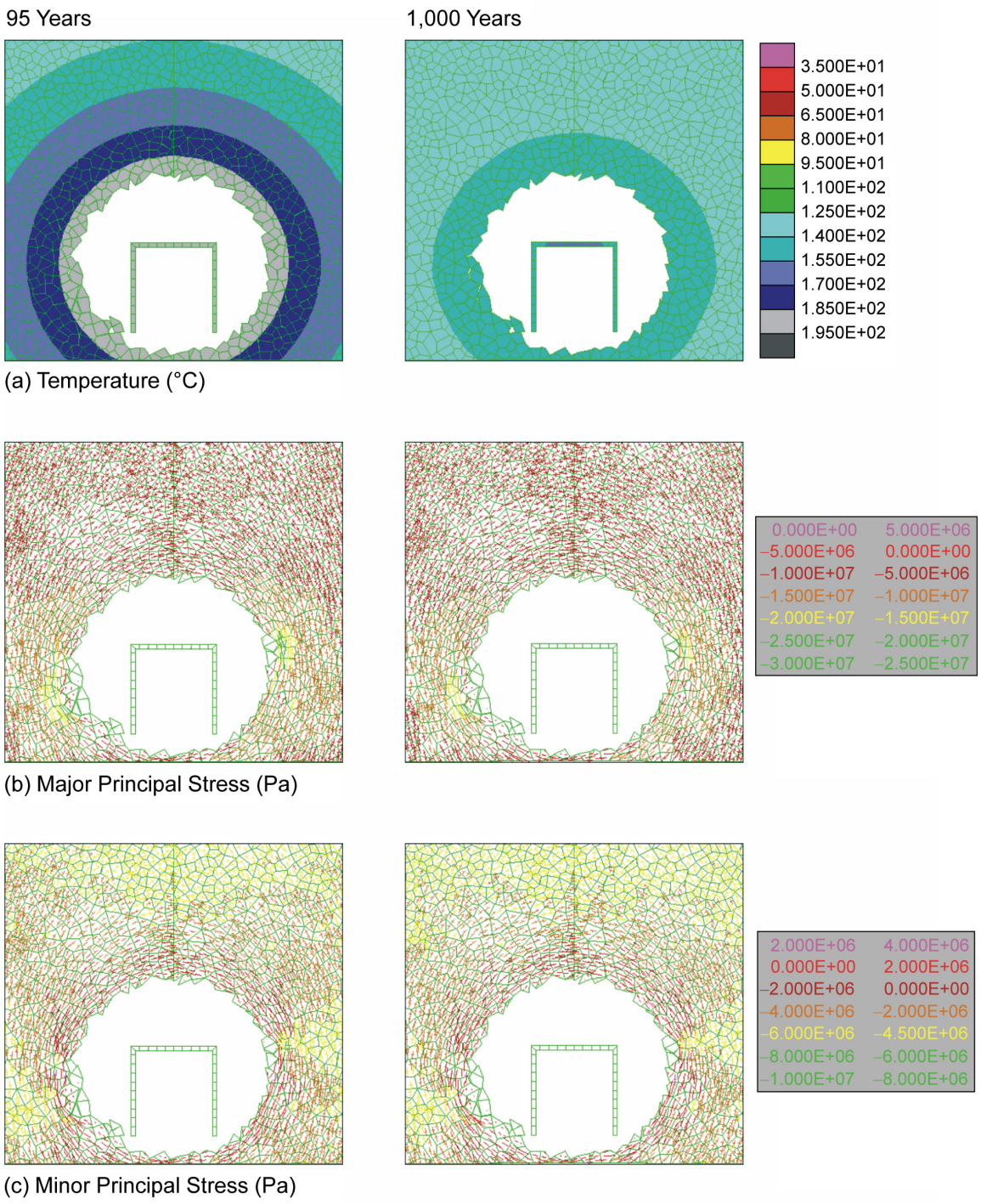

Source: Output DTN: MO0707THERMRES.000, folder: \Scenario 1\category 1, files: for 95 years see *case1jointing1age95temp.pcx*, *case1jointing1age95sig1.pcx*, and *case1jointing1age95sig2.pcx*; for 1,000 years see *case1jointing1age1000temp.pcx*, *case1jointing1age1000sig1.pcx*, and *case1jointing1age1000sig2.pcx*.

NOTE: Compressive stress is negative.

Figure 6.4.1-4. Drift Configuration, Temperatures, and Stresses for Case 1 of Thermal Load, Category 1 Lithophysal Rock Mass

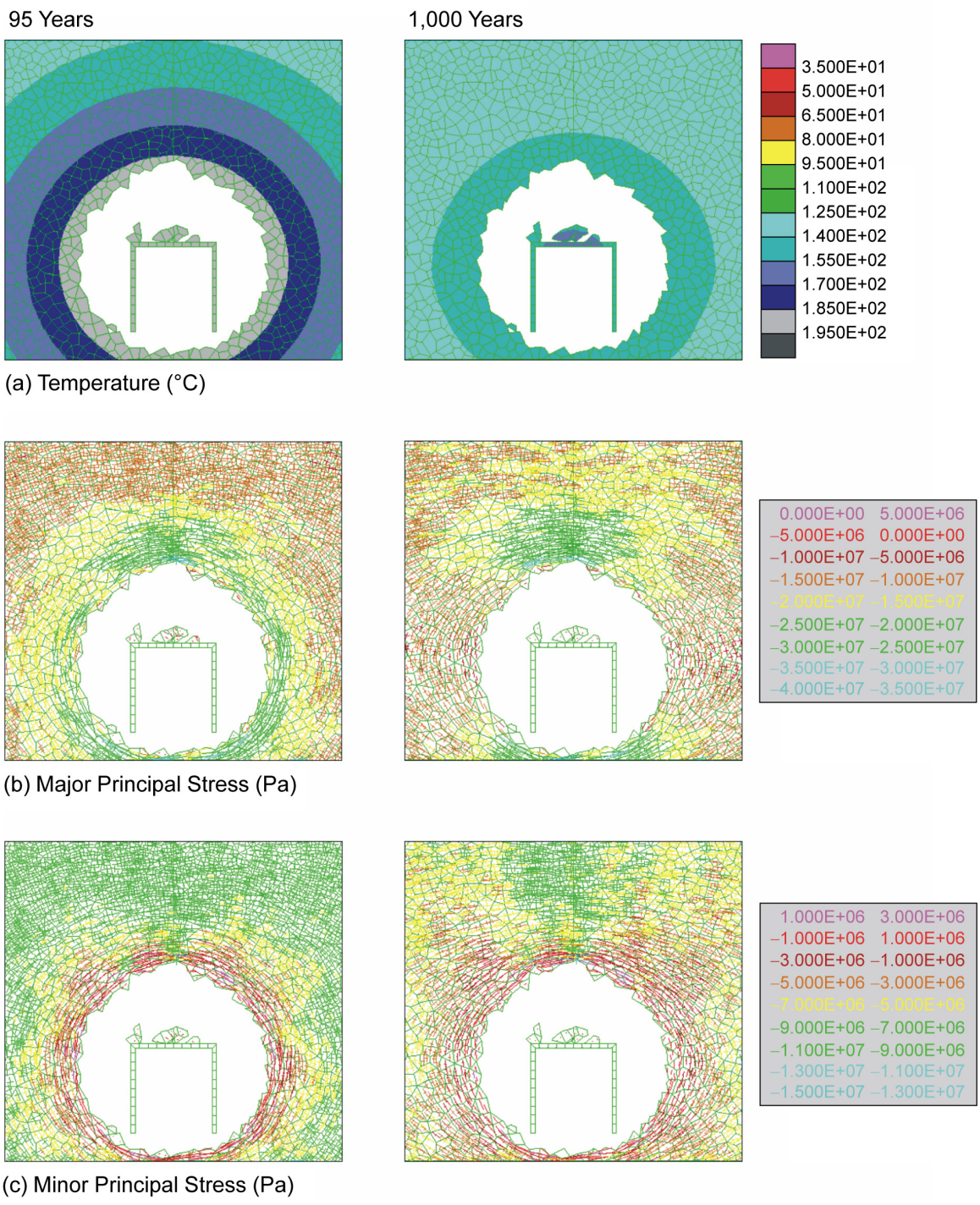

Source: Output DTN: MO0707THERMRES.000, folder: \Scenario 1\category 3, files: for 95 years see *case2jointing3age95temp.pcx*, *case2jointing3age95sig1.pcx*,and *case2jointing3age95sig2.pcx*; for 1,000 years see *case2jointing3age1000temp.pcx*, *case2jointing3age1000sig1.pcx*, and *case2jointing3age1000sig2.pcx*.

NOTE: Compressive stress is negative.

Figure 6.4.1-5. Drift Configuration, Temperatures, and Stresses for Case 1 of Thermal Load, Category 3 Lithophysal Rock Mass

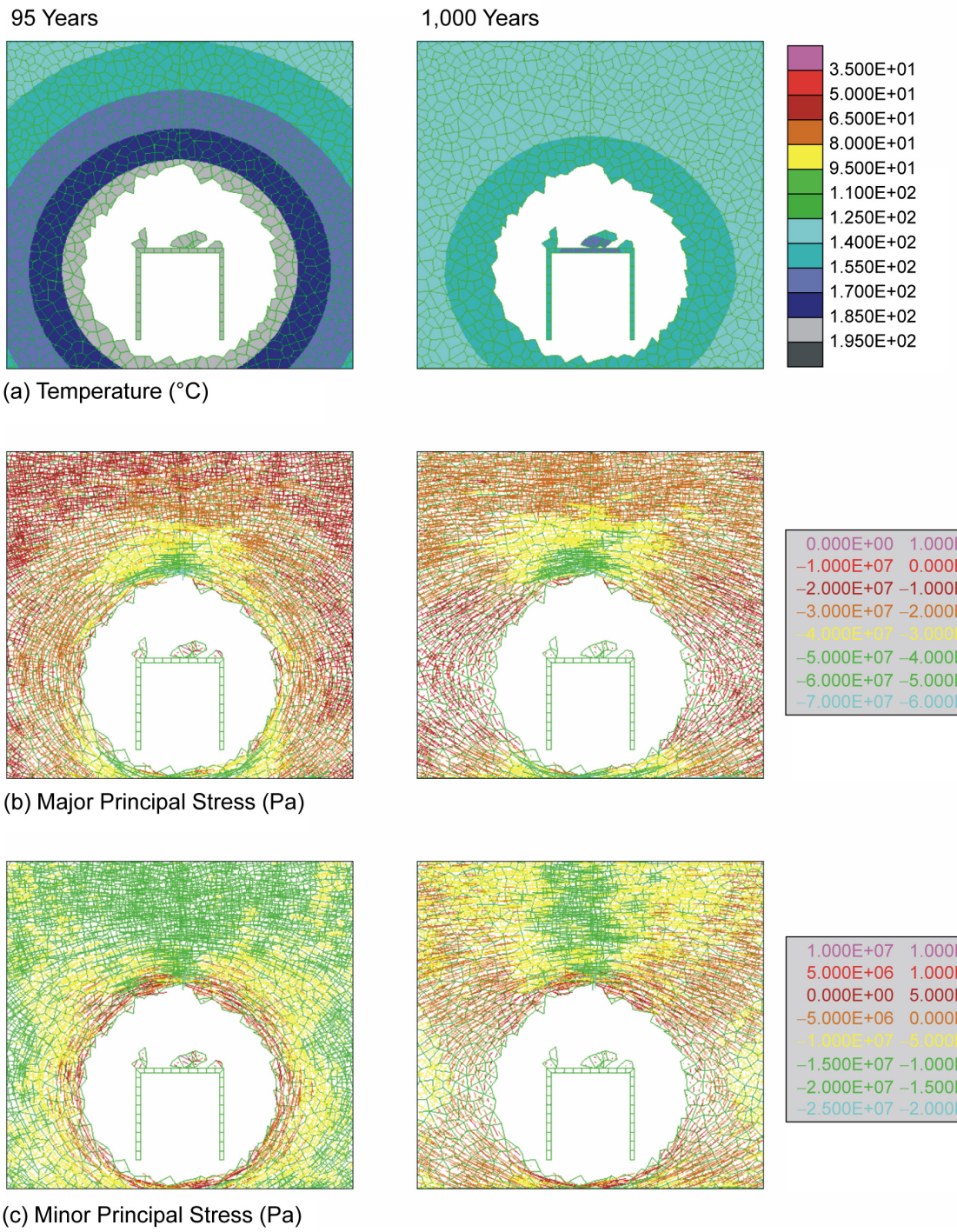

Source: Output DTN: MO0707THERMRES.000, folder: \Scenario 1\category 5, files: for 95 years see *case3jointing5age95temp.pcx*, *case3jointing5age95sig1.pcx*, and *case3jointing5age95sig2.pcx*; for 1,000 years see *case3jointing5age1000temp.pcx*, *case3jointing5age1000sig1.pcx*, and *case3jointing5age1000sig2.pcx*.

NOTE: Compressive stress is negative.

Figure 6.4.1-6. Drift Configuration, Temperatures, and Stresses for Case 1 of Thermal Load, Category 5 Lithophysal Rock Mass

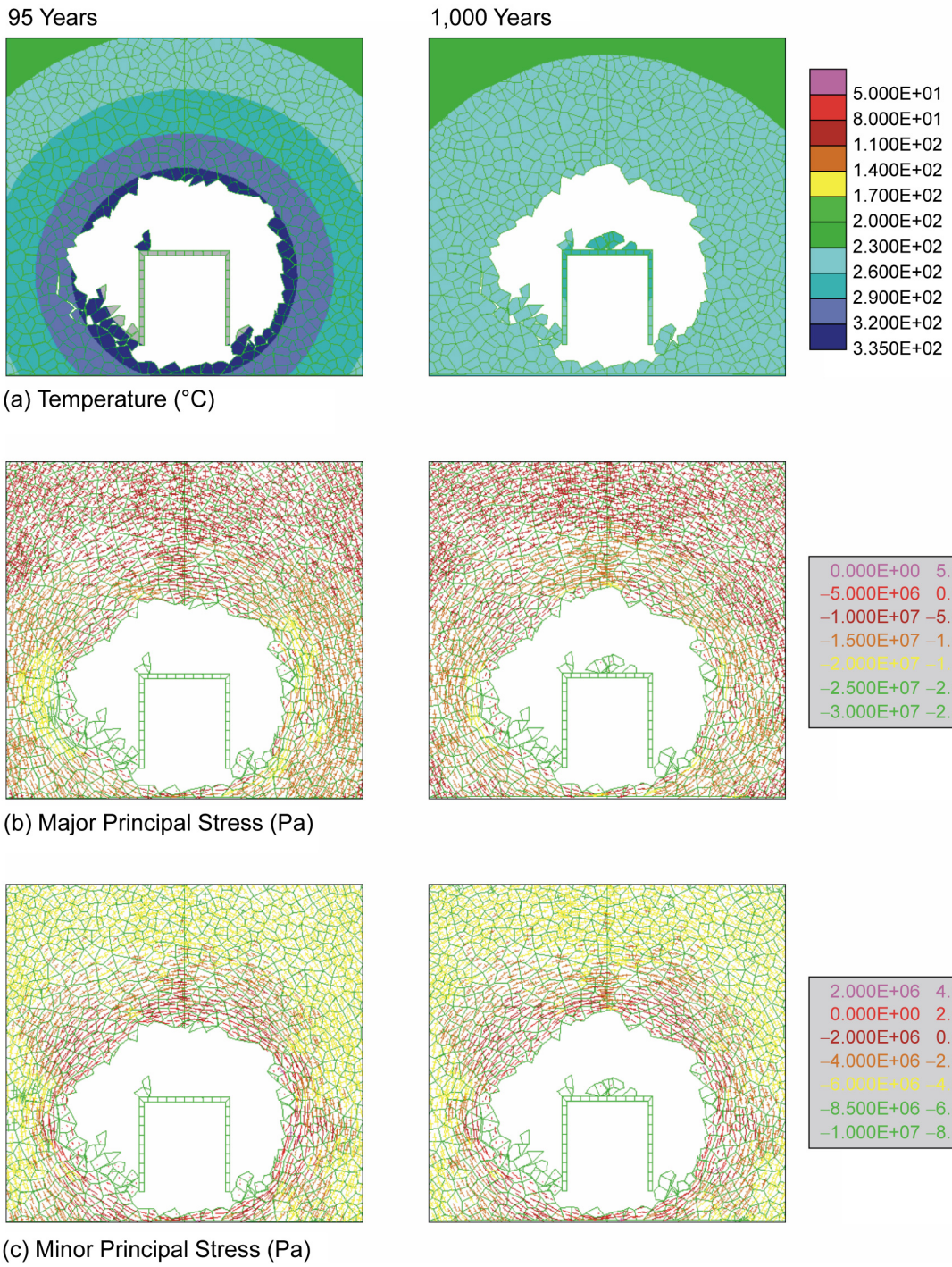

Source: Output DTN: MO0707THERMRES.000, folder: \Scenario 2\category 1, files: for 97 years see *case4jointing1age97sig1.pcx*, *case4jointing1age97sig2.pcx*, and *case4jointing1age97temp.pcx*; for 1,000 years see *case4jointing1age1000sig1.pcx*, *case4jointing1age1000sig2.pcx*, and *case4jointing1age1000temp.pcx*.

NOTE: Compressive stress is negative.

Figure 6.4.1-7. Drift Configuration, Temperatures, and Stresses for Case 2 of Thermal Load, Category 1 Lithophysal Rock Mass

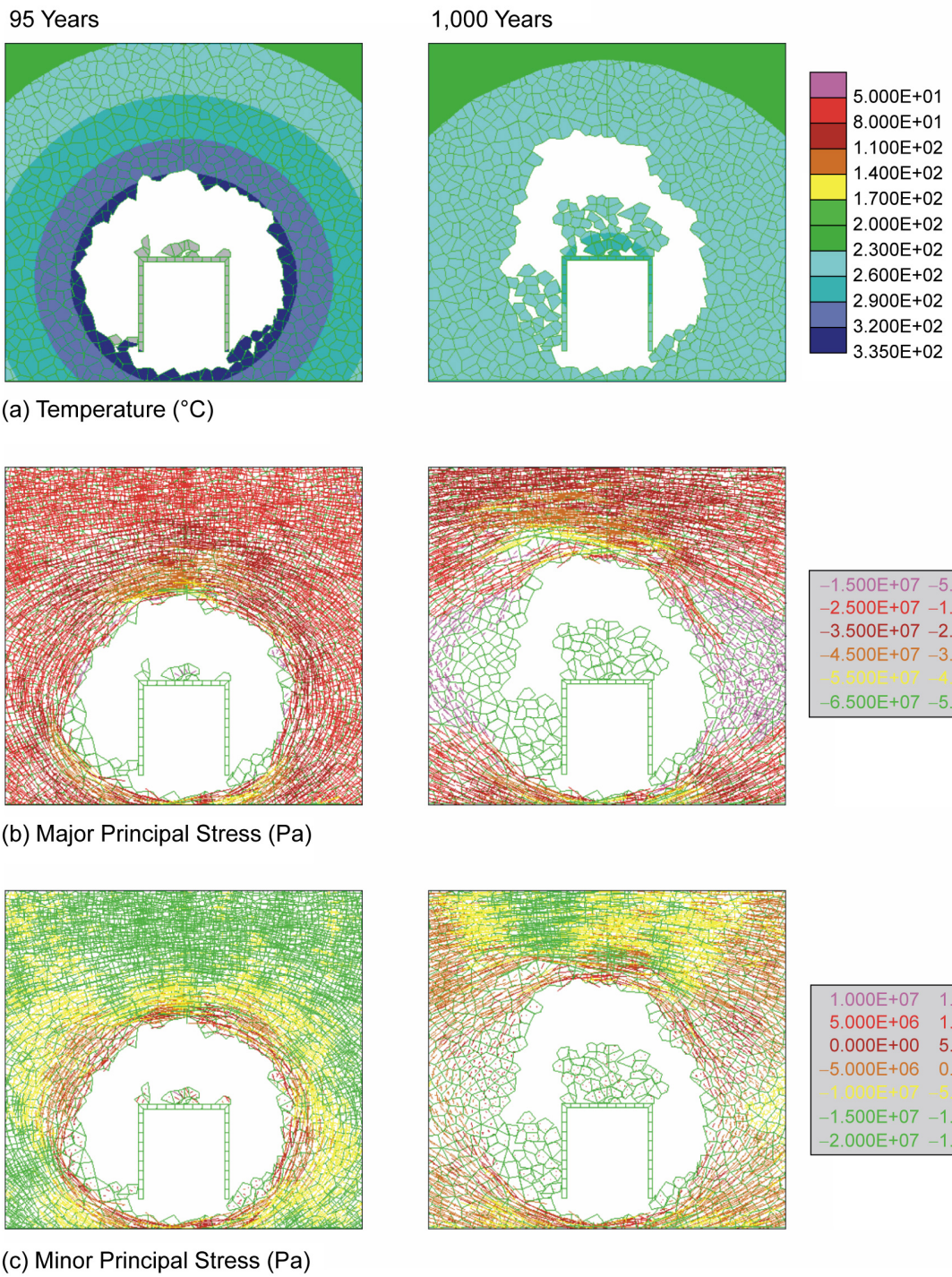

Source: Output DTN: MO0707THERMRES.000, folder: \Scenario 2\category 3, files: for 97 years see *case5jointing3age97sig1.pcx*, *case5jointing3age97sig2.pcx* and *case5jointing3age97temp.pcx*; for 1,000 years see *case5jointing3age1000sig1.pcx*, *case5jointing3age1000sig2.pcx*, and *case5jointing3age1000temp.pcx*.

NOTE: Compressive stress is negative.

Figure 6.4.1-8. Drift Configuration, Temperatures, and Stresses for Case 2 of Thermal Load, Category 3 Lithophysal Rock Mass

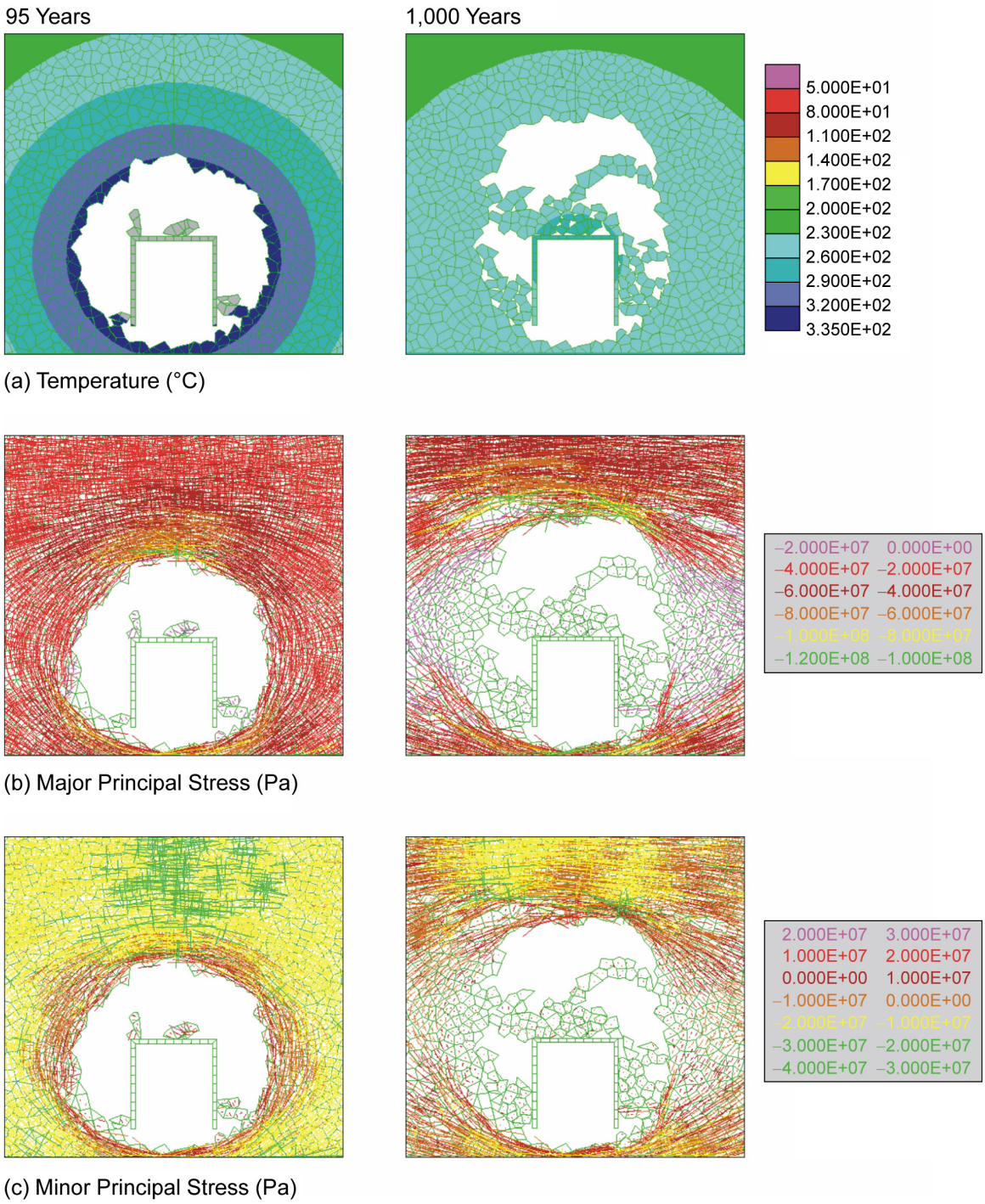

Source: Output DTN: MO0707THERMRES.000, folder: \Scenario 2\category 5, files: for 97 years see *case6jointing5age97sig1.pcx*, *case6jointing5age97sig2.pcx*, and *case6jointing5age97temp.pcx*; for 1,000 years see *case6jointing5age1000sig1.pcx*, *case6jointing5age1000sig2.pcx*, and *case6jointing5age1000temp.pcx*.

NOTE: Compressive stress is negative.

Figure 6.4.1-9. Drift Configuration, Temperatures, and Stresses for Case 2 of Thermal Load, Category 5 Lithophysal Rock Mass

6.4.1.6 Discussion

The maximum drift wall temperature calculated for the Case 1 thermal line load (~197°C in Figure 6.4.1-1) is similar to the maximum drift-crown temperature measured in the Drift Scale Test (DST), which reached approximately 200°C (Williams 2001 [DIRS 159516], Figure 1). The Drift Scale Test, which was conducted in the Tptpmn (middle nonlithophysal) unit, involved a 5-m diameter drift that was approximately 50 m in length. The drift was heated by electrically heated canisters within the drift itself, and by horizontal borehole heaters extending from the springline of the drift. In late 1999, some scaling of the rock from the crown was observed for the first time in a number of zones along the drift (Williams 2001 [DIRS 159516]). Zones of scaling appeared to be localized at the crown and not along the entire drift length, with maximum linear dimension in plan view of the order of 1 m. The loose rock fragments with thicknesses between 2 and 5 cm were held mostly by the wire mesh. Considering that on the scale of interest the unconfined compressive strength of the nonlithophysal rock mass is 70 MPa (BSC 2004 [DIRS 166107], Figure E-22) and the Young's modulus is 33.6 GPa (BSC 2004 [DIRS 166107], Section E3), the strength-to-stiffness ratio, $UCS / E = 2.08 \times 10^{-3}$, is very similar to the ratio for the better qualities of lithophysal rock, particularly Category 3. This means that the thermomechanical responses of Category 3 and 5 lithophysal rock in the repository will be similar to the response of the nonlithophysal rock in the DST.

Rockfall predicted for Categories 3 and 5 in the lithophysal rock for Case 1 thermal loads (Figures 6.4.1-5 and 6.4.1-6) will be similar to the observations from the DST (BSC 2004 [DIRS 166107], Figure 7-29) with respect to the minor amount of rockfall predicted. Note that minor rockfall does not significantly affect predicted engineered barrier temperatures, or produce significant drip shield damage. Also, minor rockfall is already factored into the seepage analysis (SNL 2007 [DIRS 181244], Section 6.2.4[a]). Rockfall volume observed in the DST may be somewhat less than predicted for lithophysal rock in the repository, because the strength-to-stiffness ratio in Categories 3 and 5 (lithophysal) is somewhat smaller than in the nonlithophysal rock. This comparison also suggests using Category 3 rockfall predictions as an upper-bound estimate of thermally induced rockfall in nonlithophysal host rock.

The effect of joints in the nonlithophysal rock mass, and their possible slip, on stability of large blocks is not accounted for in this approach. However, the analyses of drift stability in nonlithophysal rock in which jointing was represented explicitly (BSC 2004 [DIRS 166107], Section 6.3.1.3) showed that heating induced minor rockfall. This was true for both the nominal case (maximum drift wall temperature of 138°C; BSC 2004 [DIRS 166107], Section 6.2) and the thermal-properties sensitivity case (maximum drift wall temperature of 161°C; BSC 2004 [DIRS 166107], Section 6.2). In that study, the stress paths on selected joints (BSC 2004 [DIRS 166107], Figures 6-75, 6-76, 6-79, and 6-80) are parallel to, or moving away from, the joint slip line as the temperature increases. This implies that heating increases confinement on the joints more than shear forces. Therefore, no significant additional rockfall as a result of slip on pre-existing joints is expected in the nonlithophysal units for the Case 1 and 2 thermal line-loads analyzed here.

The calculations discussed here were carried out for short-term rock mass mechanical properties (including rock mass strength). Time-dependent strength decay could cause additional rockfall, particularly when combined with thermal stresses that last for thousands of years. The combined

effect of thermal stresses and time-dependent strength decay for the nominal temperature scenario has been analyzed, and the results are reported in *Drift Degradation Analysis* (BSC 2004 [DIRS 166107], Sections 6.4.2.4.2.6, S3.4.1, and S3.4.2). Figures S-38, S-39 and S-40 in Section S3.4.1 from that source (BSC 2004 [DIRS 166107]) show the evolution of damage and rockfall due to time-dependent strength decay for Categories 2, 3, and 5, respectively; the effects of both thermal stresses and time-dependent strength decay are shown in Figures S-42, S-43 and S-44 of Section S3.4.2 for the same rock categories. Thermal loading only (without time-dependent strength decay) caused practically no damage irrespective of lithophysal rock mass quality (BSC 2004 [DIRS 166107], Section 6.4.2.3.1). In all cases, the combined effects result in more rockfall, but there is a significant difference only for Category 5, in which no rockfall was predicted for either time-dependent or thermal-only analyses, while minor rockfall (2 m^3/m) accumulated from the combined effects. Extrapolating those observations to Case 1 analyzed here, it is reasonable to estimate that the increased rockfall volume attributable to time-dependent degradation would amount to approximately 2 m^3/m, at most, for all rock mass categories.

6.4.2 Hydrogeologic Response to Range of Design Thermal Loadings

This section applies two-dimensional (2-D) and three-dimensional (3-D) submodels from the multiscale model (SNL 2007 [DIRS 181383]) to simulation of thermal-hydrologic responses to the selected hottest loading conditions (Cases 1 and 2) identified in Section 6.1.4 of this report. These results, combined with the evaluation of features, events, and processes in Section 6.5, provide the needed assessment of hydrogeologic system response to the anticipated range of thermal loading.

6.4.2.1 Description of Thermal-Hydrologic Models

This section describes 2-D and 3-D TH analyses of the hottest 7-point and 3-point segments from the 96/2 emplacement sequence (Section 6.4.1). The TH model analyses are conducted for a simulation period of 10,000 years, and a location close to the repository center and within the UZ flow model "g_9" grid column (see SNL 2007 [DIRS 181383], Figure 6.2-17[a]). Besides being close to the repository center, this location is selected because it is within the predominant lower lithophysal host-rock unit (Tptpll, or tsw35 unit). The TH model analyses are conducted for three uncertainty cases selected from the multiscale model:

P10: 10th-percentile percolation flux with mean host-rock thermal conductivity
P10L: 10th-percentile percolation flux with low host-rock thermal conductivity
P90: 90th-percentile percolation flux with mean host-rock thermal conductivity.

As shown in Table 6.4.2-1, the location-specific percolation flux values at the "g_9" location are similar to the repository averages for the P10 and P90 cases (within 30%, with a much larger order-of-magnitude difference between P10 and P90 cases). The "g_9" location is therefore reasonably representative for use in sensitivity analyses involving the P10 and P90 cases.

Table 6.4.2-1. Percolation Flux Values at the UZ Flow Model "g_9" Location Compared with Repository Averages

Percolation-Flux Case	Percolation Flux (mm/yr)			
	Present-Day	Monsoonal	Glacial Transition	Post-10,000-Year
P10 at "g_9" location[a]	3.6	6.8	13.6	17.8
P10 average[b]	4.1	7.8	12.2	15.9
P90 at "g_9" location[c]	26.8	75.4	59.3	44.7
P90 average[b]	34.1	92.4	69.7	52.4

[a] DTN: LL0702PA014MST.069 [DIRS 179591].
[b] DTN: LL0705PA038MST.030 [DIRS 182332], folder: \Percolation, file: *chimName.dat*.
[c] DTN: LL0702PA020MST.075 [DIRS 179594].

The 2-D line-average-heat-source, drift-scale thermal-hydrologic (LDTH) model is used to calculate line-averaged TH behavior for the 96/2 emplacement sequence, for the selected hottest 7- and 3-point segments (Cases 1 and 2; Section 6.4.2.2). These results are compared to the 2-D results using the base-case average thermal load from *Multiscale Thermohydrologic Model* (SNL 2007 [DIRS 181383], Section 6.2.16).

This analysis also evaluates (Sections 6.4.2.3 and 6.4.2.4) the selected segments (Cases 1 and 2) using a 3-D discrete heat source, drift-scale, thermal-hydrologic (DDTH) modeling approach (similar to the DDT submodel; SNL 2007 [DIRS 181383], Section 6.2.17). This model domain contains 13 discrete waste packages: 11 full packages plus two halves at the ends of the domain. The general layout and boundary conditions for the DDTH domain are the same as used in ANSYS analyses discussed in Sections 6.1.4 and 6.3, as developed in *Repository Twelve Waste Package Segment Thermal Calculation* (BSC 2006 [DIRS 179686]). Symmetry conditions at each end of the domain represent repository-center conditions. The DDTH domain explicitly represents each waste package and the corresponding drip shield. As with the DDT submodel, the DDTH model applies an average waste package diameter to all waste packages. Unlike the DDT submodel, which explicitly represents in-drift thermal radiation, the DDTH model applied here uses an effective in-drift thermal conductivity approach which has been previously developed and justified (SNL 2007 [DIRS 181383], Section 6.2.19). The DDTH modeling approach is also used to evaluate peak temperatures after complete drift collapse (Section 6.4.2.5).

In addition, far-field effects are analyzed (Section 6.4.2.6) using a 2-D line-average-heat-source, drift-scale thermal-hydrologic (LDTH) model to calculate line-averaged TH behavior for the ELWS average line load. These results are compared to the 2-D results using the base-case average thermal load from *Multiscale Thermohydrologic Model* (SNL 2007 [DIRS 181383], Section 6.2.16).

6.4.2.2 2-D Model Results

Thermal-hydrologic responses for Cases 1 and 2 are first analyzed using the 2-D LDTH submodel from the multiscale model. For these runs, the hottest 7- and 3-package segments, respectively, are line-averaged over all 13 waste packages. The 7-package segment (Case 1)

represents typical thermal loading conditions, while the 3-package segment (Case 2) contains the hottest waste package in the ELWS, but mostly cooler DHLW packages.

Temperature and matrix liquid-phase saturation histories averaged around the drift wall are plotted for the P10, P10L, and P90 cases (Figures 6.4.2-1 through 6.4.2-3). Results for the 7-package segment (Case 1) are similar to the base case, which is expected because the line-load for Case 1 decays to 600 W/m at closure (calendar 2117; Output DTN: MO0705SUPPCALC.000, folder: \Select Hot and Cold Cases, file: *Hottest 3-7 + Coolest WP 96-2 10Jul07.xls*, worksheet: "Hottest Segments 96-2," cell DK52) whereas the postclosure reference case is at 592 W/m (at 50 years after emplacement; Output DTN: MO0705SUPPCALC.000, folder: \Other Supporting Files, file: *Reference Line Load Fit.xls*). Although the initial power for Case 1 is greater at emplacement, the ventilation period is longer. This finding of similarity with the postclosure reference case average line load is generally true for all 7-point segments in the emplacement sequences developed in Section 6.1, i.e., everywhere in the repository (except for cooler segments). This is because pillar drainage is an effective constraint for these sequences (implemented using the WPIMP index as described in Section 6.1), as it was for development of the postclosure reference case (DOE 2006 [DIRS 176937], Section 4.6.5).

The calculated results for the 3-package segment (Case 2) are much cooler (Figures 6.4.2-1 through 6.4.2.3) and generally do not predict formation of a dryout zone in the host rock.

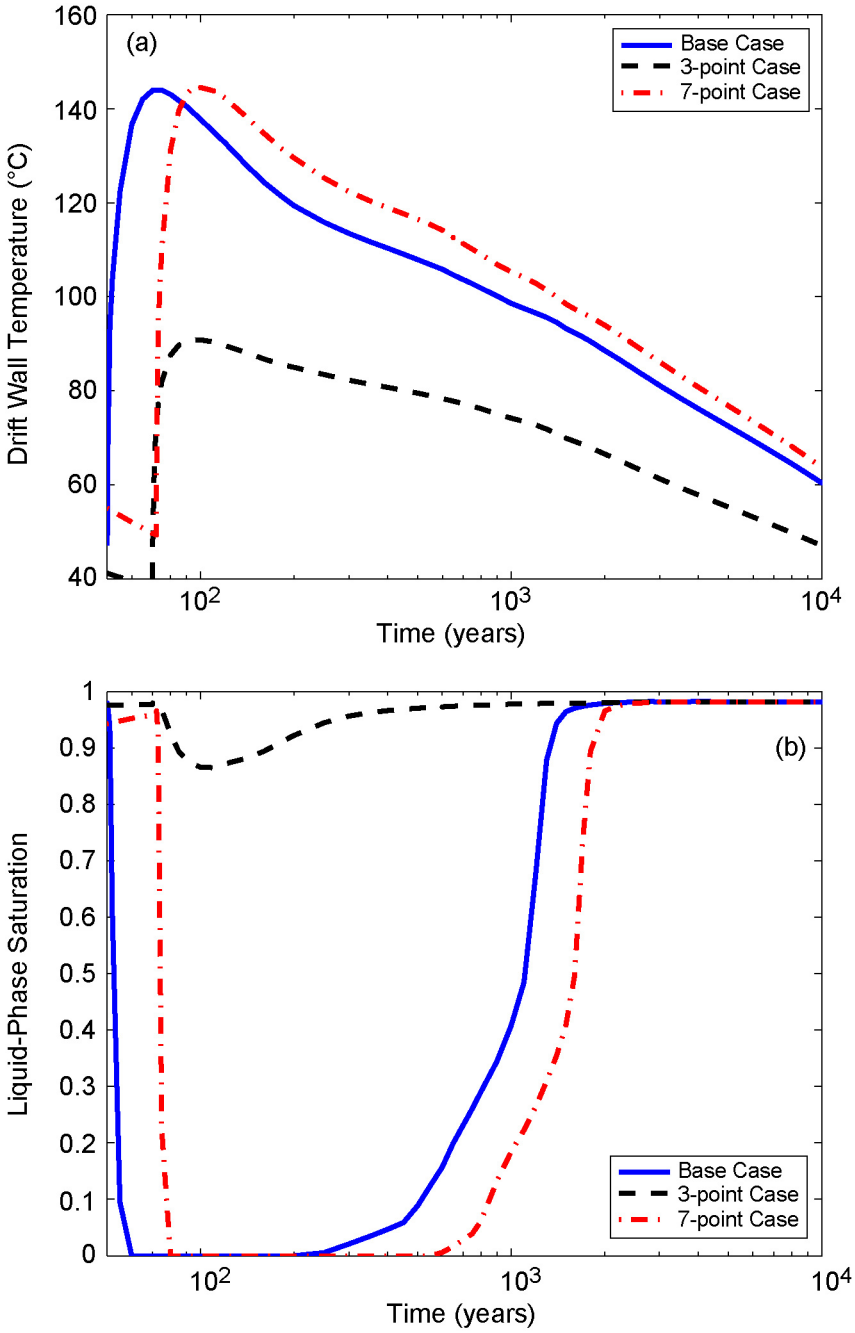

Source: Output DTN: MO0707TH2D3DDC.000, folder: /analyses/2D-LDTH, file: *P10-T-S.dat*.

NOTE: Drift wall temperature and matrix liquid-phase saturation histories for Case 1 and Case 2, plotted for the P10 percolation flux case with mean host-rock thermal conductivity. These results are from the 2-D LDTH analysis corresponding to the 13-package DDTH model (see text). Also plotted are the corresponding 2-D LDTH results for the postclosure reference case line load.

Figure 6.4.2-1. Line-Averaged Temperature (a) and Liquid-Phase Saturation at Drift Wall (b) for 96/2 3- and 7-Point Running-Average Sequences for the P10 Case

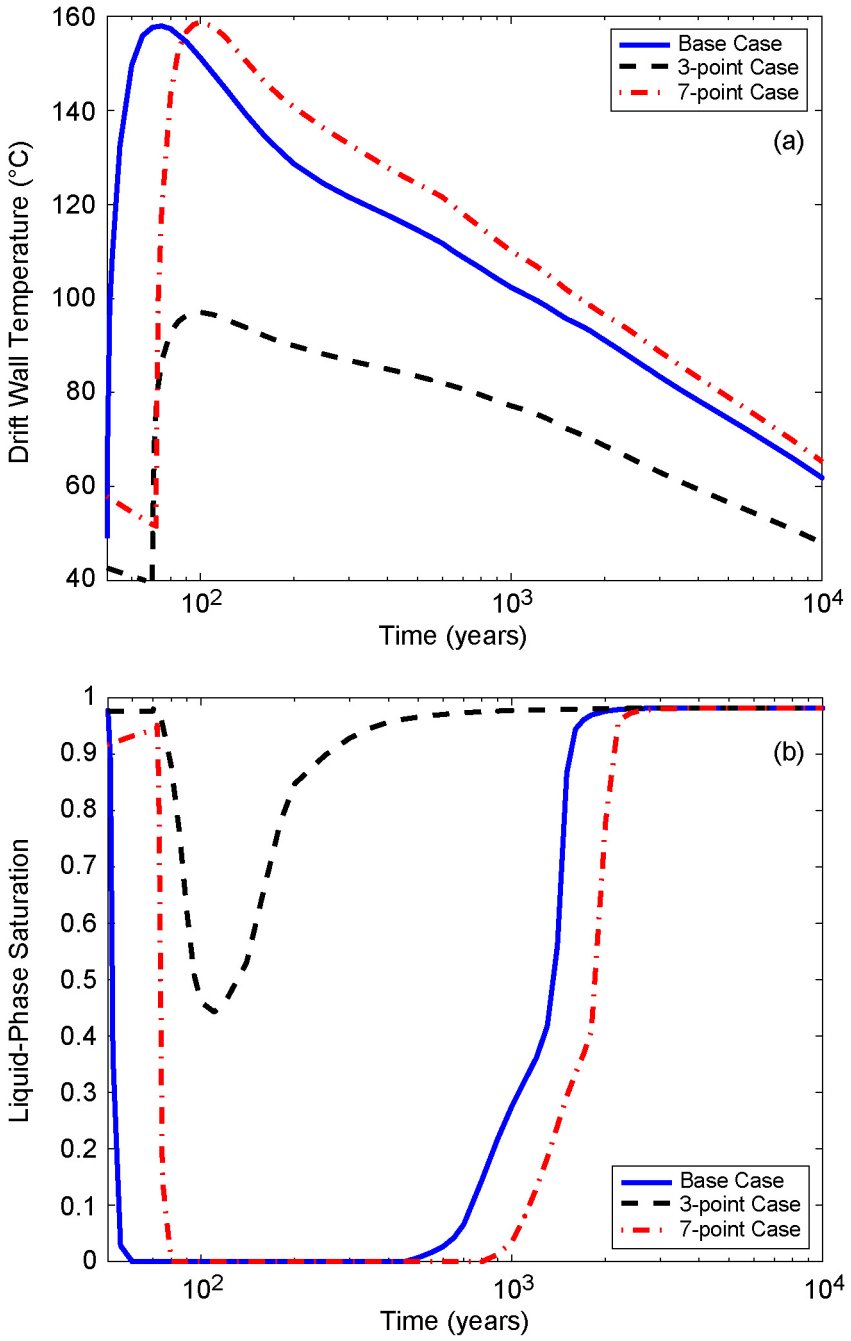

Source: Output DTN: MO0707TH2D3DDC.000, folder: /analyses/2D-LDTH, file: *P10L-T-S.dat*.

NOTE: Drift wall temperature and matrix liquid-phase saturation histories for Case 1 and Case 2, plotted for the P10 percolation flux case with low (10th percentile) host-rock thermal conductivity. These results are from the 2-D LDTH analysis corresponding to the 13-package DDTH model (see text). Also plotted are the corresponding 2-D LDTH results for the postclosure reference case line load.

Figure 6.4.2-2. Line-Averaged Temperature (a) and Liquid-Phase Saturation at Drift Wall (b) for 96/2 3- and 7-Point Running-Average Sequences for the P10L Case

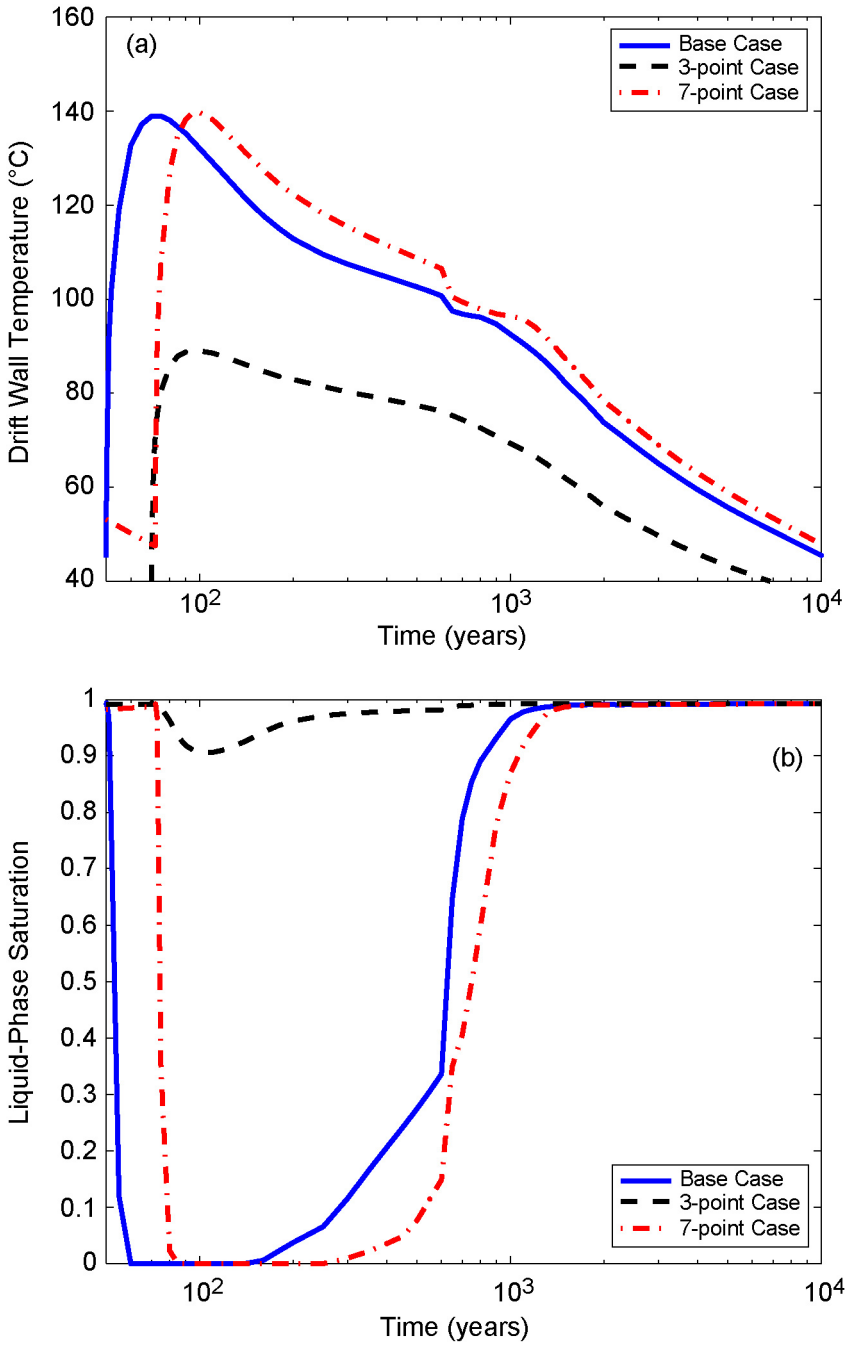

Source: Output DTN: MO0707TH2D3DDC.000, folder: /analyses/2D-LDTH, file: *P90-T-S.dat*.

NOTE: Drift wall temperature and matrix liquid-phase saturation histories for Case 1 and Case 2, plotted for the P90 percolation flux case with mean host-rock thermal conductivity. These results are from the 2-D LDTH analysis corresponding to the 13-package DDTH model (see text). Also plotted are the corresponding 2-D LDTH results for the postclosure reference case line load.

Figure 6.4.2-3. Line-Averaged Temperature (a) and Liquid-Phase Saturation at Drift Wall (b) for 96/2 3- and 7-Point Running-Average Sequences for the P90 Case

6.4.2.3 3-D Model Analysis of Temperature Range

The range of temperatures are analyzed for the 96/2 emplacement sequence, Case 1 (7-point) and Case 2 (3-point) segments selected in Section 6.1.4, using the DDTH model. For each case all 13 waste packages from Table 6.1-2 are represented explicitly, centered on the hottest 7-point or 3-point segments.

Figures 6.4.2-4 through 6.4.2-9 plot the minimum and maximum temperature histories for the 13 waste-package locations for the Case 1 (7-point) segment for four locations: (1) drift wall, (2) waste package, (3) 5 m above the crown of the drift, and (4) at the mid-pillar location between emplacement drifts. Also plotted is the temperature range from the corresponding base-case DDTH model. The peak drift wall and waste package temperatures are similar to the corresponding peak temperatures for the base case. The peak temperatures 5 m above the drift crown and at the mid-pillar location are greater for Case 1 than for the base case. The mid-pillar temperatures never exceed 96°C for either Case 1 or the base case. The similarity of temperature histories for Case 1 to the base case is demonstrated below in Figures 6.4.2-4 through 6.4.2-9.

Figures 6.4.2-10 through 6.4.2-15 plot the minimum and maximum temperature histories for the 13 waste package locations for the Case 2 (3-point) segment, for the same four locations. Also plotted is the temperature range from the corresponding base-case DDTH model. The Case 2 (3-point) segment produces similar, but cooler, maximum drift wall and waste package temperatures compared to the base case. The Case 2 segment produces much cooler maximum temperature histories 5 m above the drift crown and at the mid-pillar location, compared to the base case. All minimum temperature histories for Case 2 are much lower than those of the base case. These results are readily explained because the 13 waste packages in the Case 2 segment include only four CSNF packages, and the rest are much cooler DHLW packages.

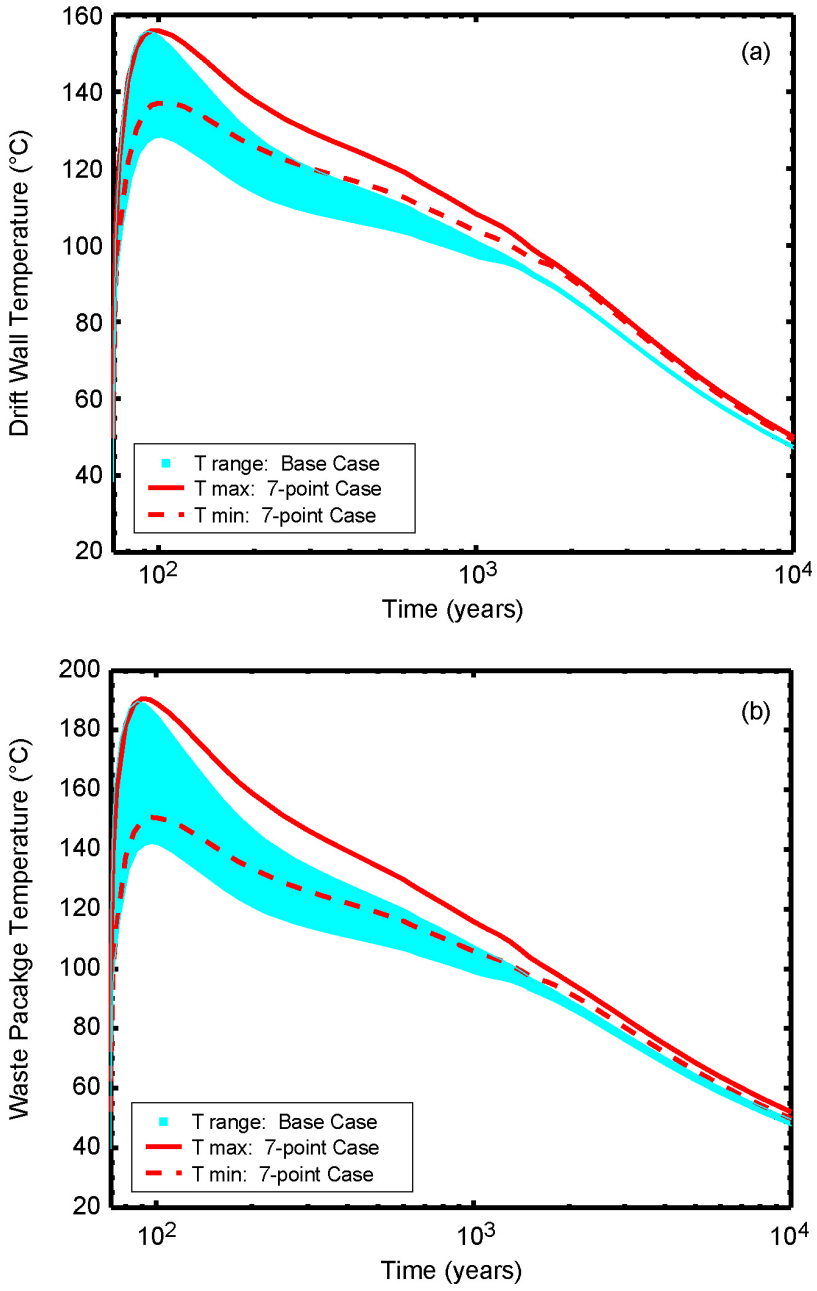

Source: Output DTN: MO0707TH2D3DDC.000, folder: /analyses/3D-DDTH, files: *p10-7wp-Tdw.dat, p10-7wp-Twp.dat, p10-7pt-Tdw.dat*, and *p10-7pt-Twp.dat*.

NOTE: The maximum and minimum temperature histories for Case 1 are plotted for the P10 percolation flux case with mean host-rock thermal conductivity. The temperature histories are from the 13-package DDTH model (see text). The temperature range for the corresponding base case (postclosure reference case) is shown in shaded blue, shifted so closure is at the same time as Case 1.

Figure 6.4.2-4. Temperature Range at Drift Wall (a) and Waste Package (b) for the Case 1 Segment, for the P10 Case

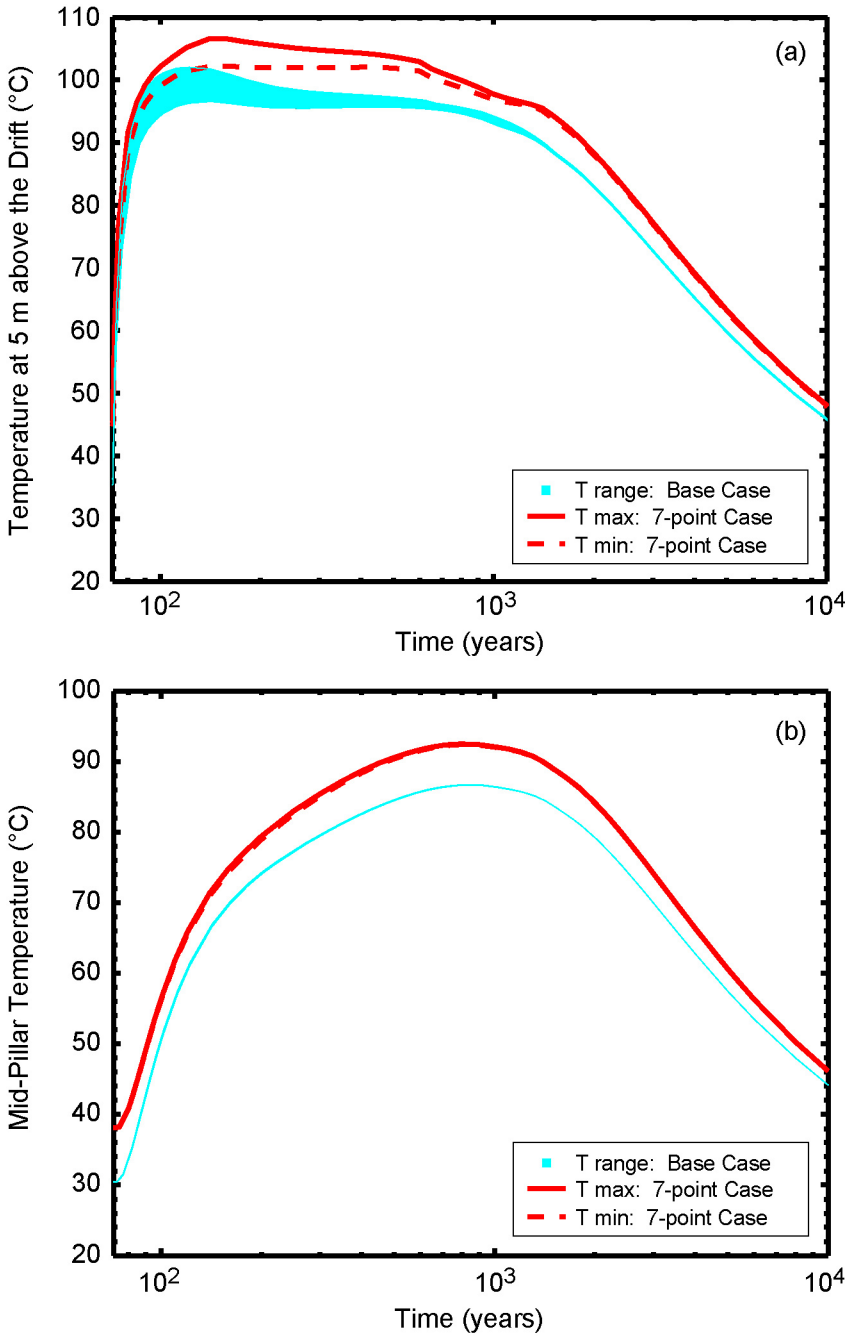

Source: Output DTN: MO0707TH2D3DDC.000, folder: /analyses/3D-DDTH, files: *p10-7wp-T_5m.dat*, *p10-7wp-Tpillar.dat*, *p10-7pt-T_5m.dat*, and *p10-7pt-Tpillar.dat*.

NOTE: The maximum and minimum temperature histories for Case 1 are plotted for the P10 percolation flux case with mean host-rock thermal conductivity. The temperature histories are from the 13-package DDTH model (see text). The temperature range for the corresponding base case (postclosure reference case) is shown in shaded blue, shifted so closure is at the same time as Case 1.

Figure 6.4.2-5. Temperature Range 5 m above the Crown of the Drift (a) and at the Mid-Pillar Location (b) for the Case 1 Segment, for the P10 Case

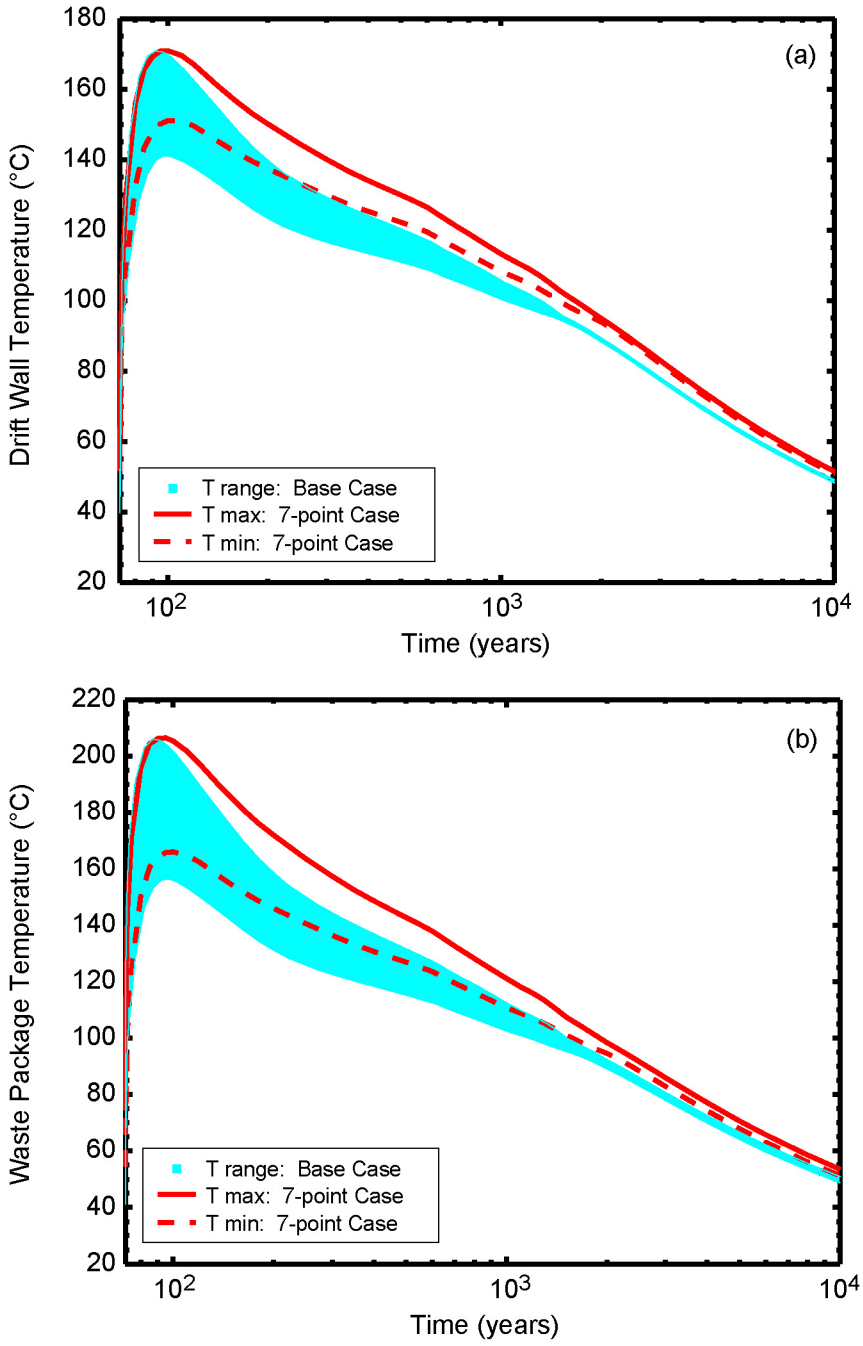

Source: Output DTN: MO0707TH2D3DDC.000, folder: /analyses/3D-DDTH, files: *p10L-7wp-Tdw.dat, p10L-7wp-Twp.dat, p10L-7pt-Tdw.dat*, and *p10L-7pt-Twp.dat*.

NOTE: The maximum and minimum temperature histories for Case 1 are plotted for the P10 percolation flux case with low (10th percentile) host-rock thermal conductivity. The temperature histories are from the 13-package DDTH model (see text). The temperature range for the corresponding base case (postclosure reference case) is shown in shaded blue, shifted so closure is at the same time as Case 1.

Figure 6.4.2-6. Temperature Range at Drift Wall (a) and Waste Package (b) for the Case 1 Segment, for the P10L Case

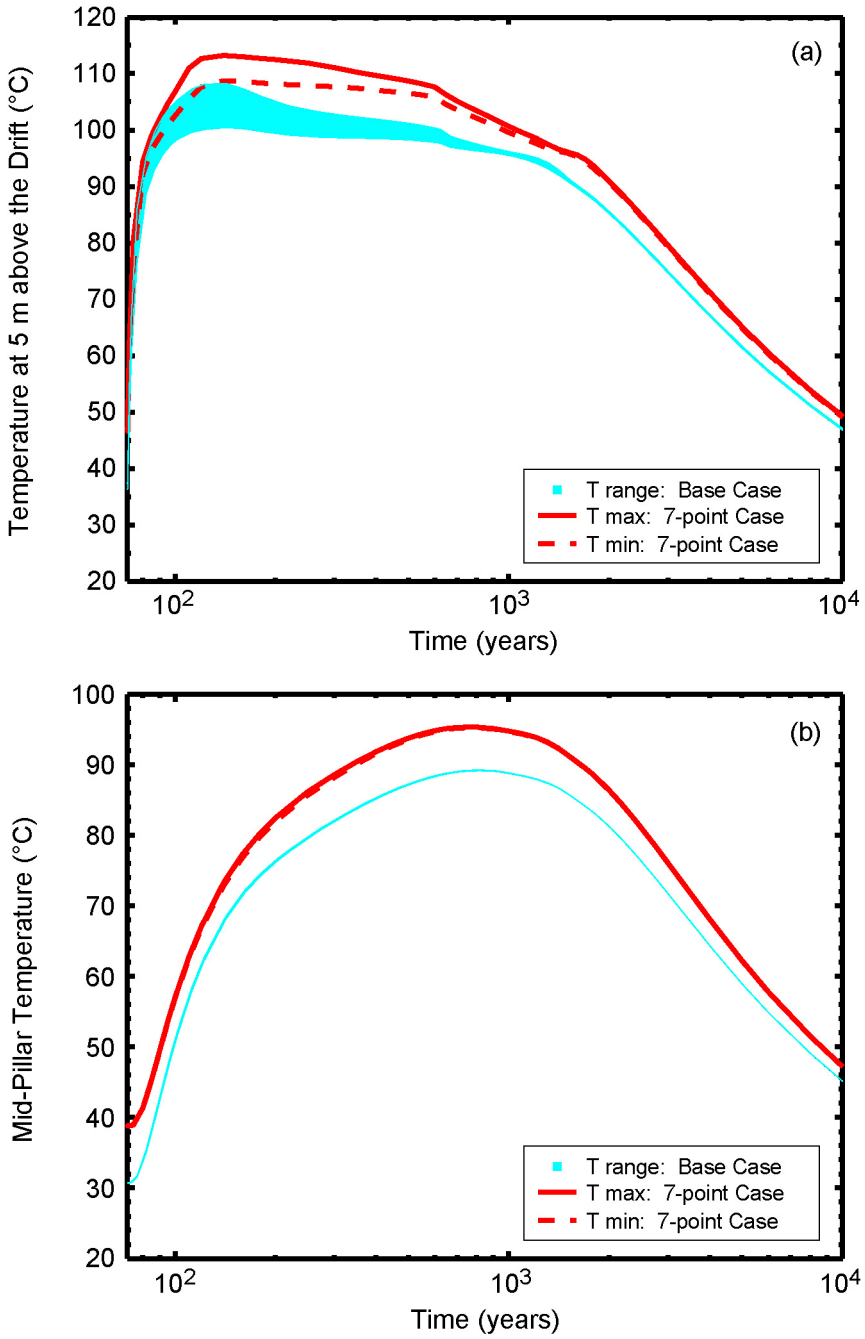

Source: Output DTN: MO0707TH2D3DDC.000, folder: /analyses/3D-DDTH, files: *p10L-7wp-T_5m.dat, p10L-7wp-Tpillar.dat, p10L-7pt-T_5m.dat*, and *p10L-7pt-Tpillar.dat*.

NOTE: The maximum and minimum temperature histories for Case 1 are plotted for the P10 percolation flux case with low (10th percentile) host-rock thermal conductivity. The temperature histories are from the 13-package DDTH model (see text). The temperature range for the corresponding base case (postclosure reference case) is shown in shaded blue, shifted so closure is at the same time as Case 1.

Figure 6.4.2-7. Temperature Range 5 m above the Crown of the Drift (a) and at the Mid-Pillar Location (b) for the Case 1 Segment, for the P10L Case

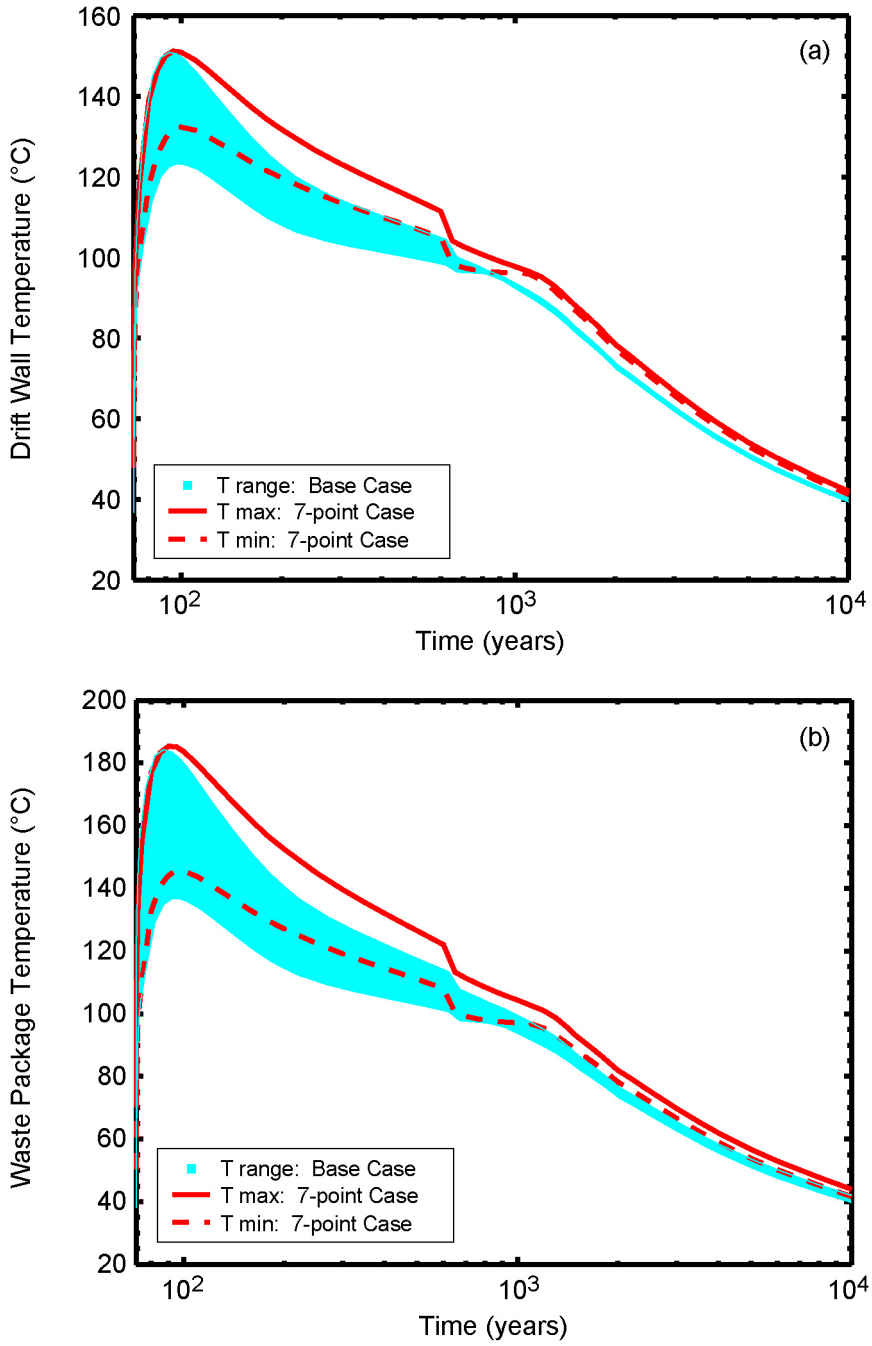

Source: Output DTN: MO0707TH2D3DDC.000, folder: /analyses/3D-DDTH, files: *p90-7wp-Tdw.dat, p90-7wp-Twp.dat, p90-7pt-Tdw.dat*, and *p90-7pt-Twp.dat*.

NOTE: The maximum and minimum temperature histories for Case 1 are plotted for the P90 percolation flux case with mean host-rock thermal conductivity. The temperature histories are from the 13-package DDTH model (see text). The temperature range for the corresponding base case (postclosure reference case) is shown in shaded blue, shifted so closure is at the same time as Case 1.

Figure 6.4.2-8. Temperature Range at Drift Wall (a) and Waste Package (b) for the Case 1 Segment, for the P90 Case

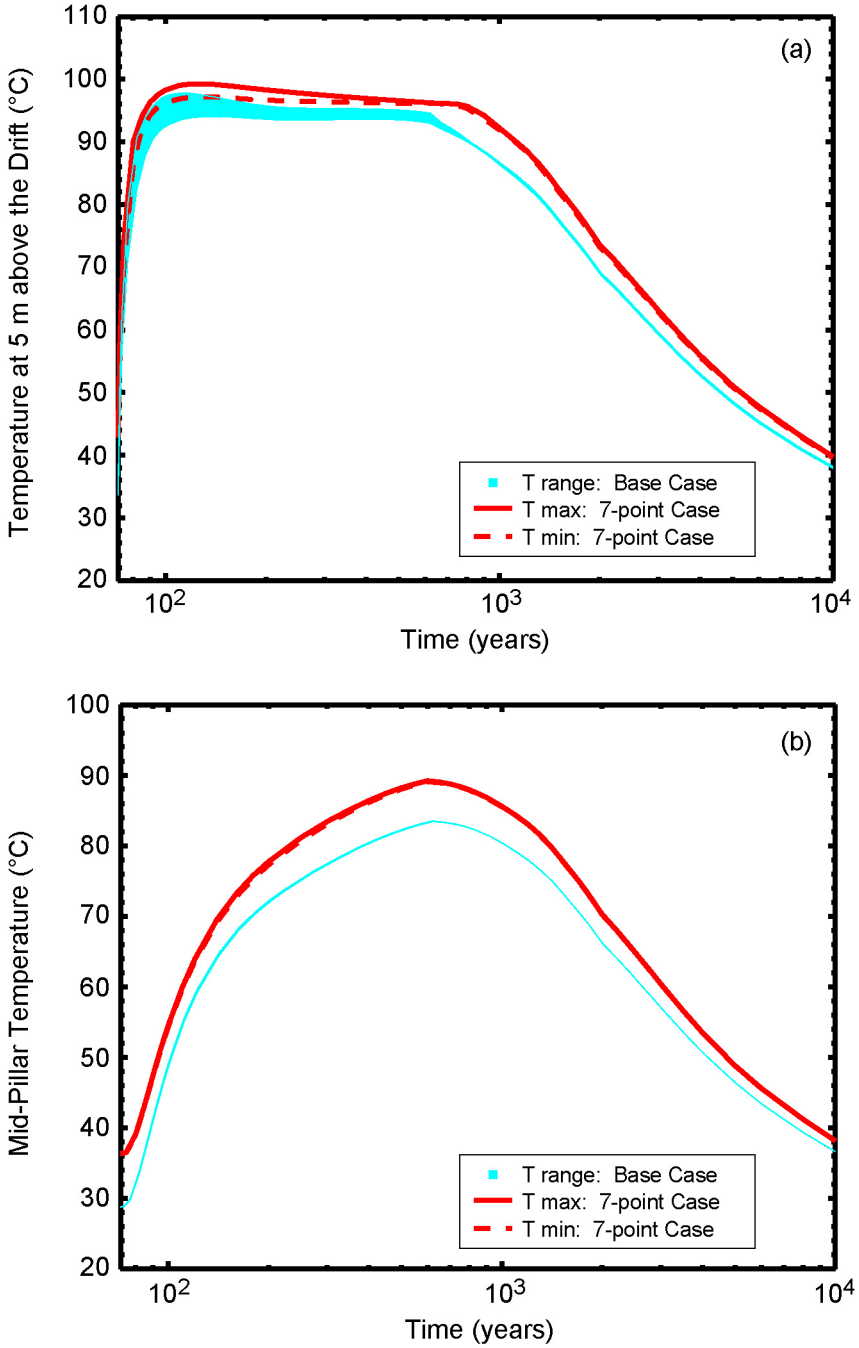

Source: Output DTN: MO0707TH2D3DDC.000, folder: /analyses/3D-DDTH, files: *p90-7wp-T_5m.dat, p90-7wp-Tpillar.dat, p90-7pt-T_5m.dat*, and *p90-7pt-Tpillar.dat*.

NOTE: The maximum and minimum temperature histories for Case 1are plotted for the P90 percolation flux case with mean host-rock thermal conductivity. The temperature histories are from the 13-package DDTH model (see text). The temperature range for the corresponding base case (postclosure reference case) is shown in shaded blue, shifted so closure is at the same time as Case 1.

Figure 6.4.2-9. Temperature Range 5 m above the Crown of the Drift (a) and at the Mid-Pillar Location (b) for the Case 1 Segment, for the P90 Case

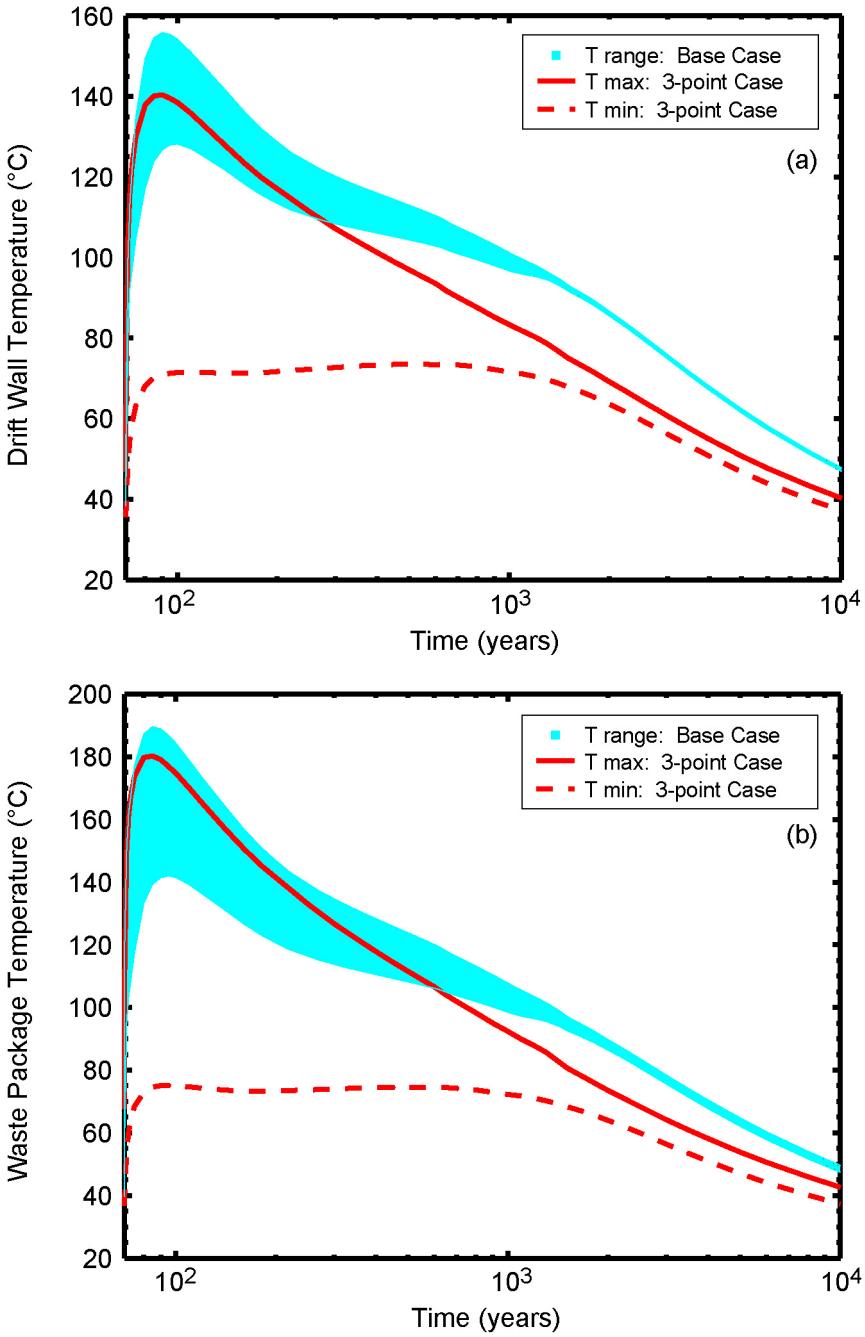

Source: Output DTN: MO0707TH2D3DDC.000, folder: /analyses/3D-DDTH, files: *p10-7wp-Tdw.dat, p10-7wp-Twp.dat, p10-3pt-Tdw.dat,* and *p10-3pt-Twp.dat*.

NOTE: The maximum and minimum temperature histories for Case 2 are plotted for the P10 percolation flux case with mean host-rock thermal conductivity. The temperature histories are from the 13-package DDTH model (see text). The temperature range for the corresponding base case (postclosure reference case) is shown in shaded blue, shifted so closure is at the same time as Case 2.

Figure 6.4.2-10. Temperature Range at Drift Wall (a) and Waste Package (b) for the Case 2 Segment, for the P10 Case

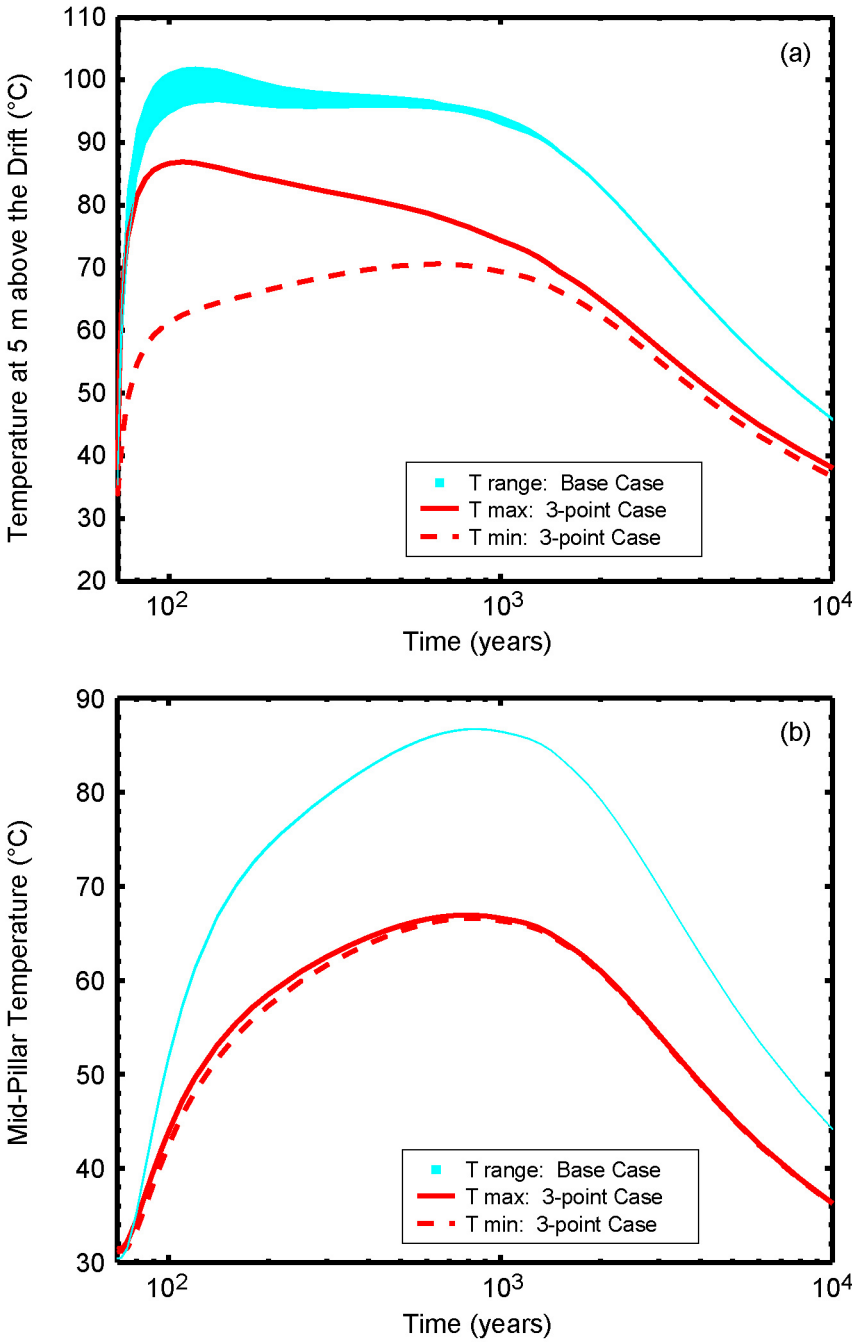

Source: Output DTN: MO0707TH2D3DDC.000, folder: /analyses/3D-DDTH, files: *p10-7wp-T_5m.dat, p10-7wp-Tpillar.dat, p10-3pt-T_5m.dat*, and *p10-3pt-Tpillar.dat*.

NOTE: The maximum and minimum temperature histories for Case 2 are plotted for the P10 percolation flux case with mean host-rock thermal conductivity. The temperature histories are from the 13-package DDTH model (see text). The temperature range for the corresponding base case (postclosure reference case) is shown in shaded blue, shifted so closure is at the same time as Case 2.

Figure 6.4.2-11. Temperature Range 5 m above the Crown of the Drift (a) and at the Mid-Pillar Location (b) for the Case 2 Segment, for the P10 Case

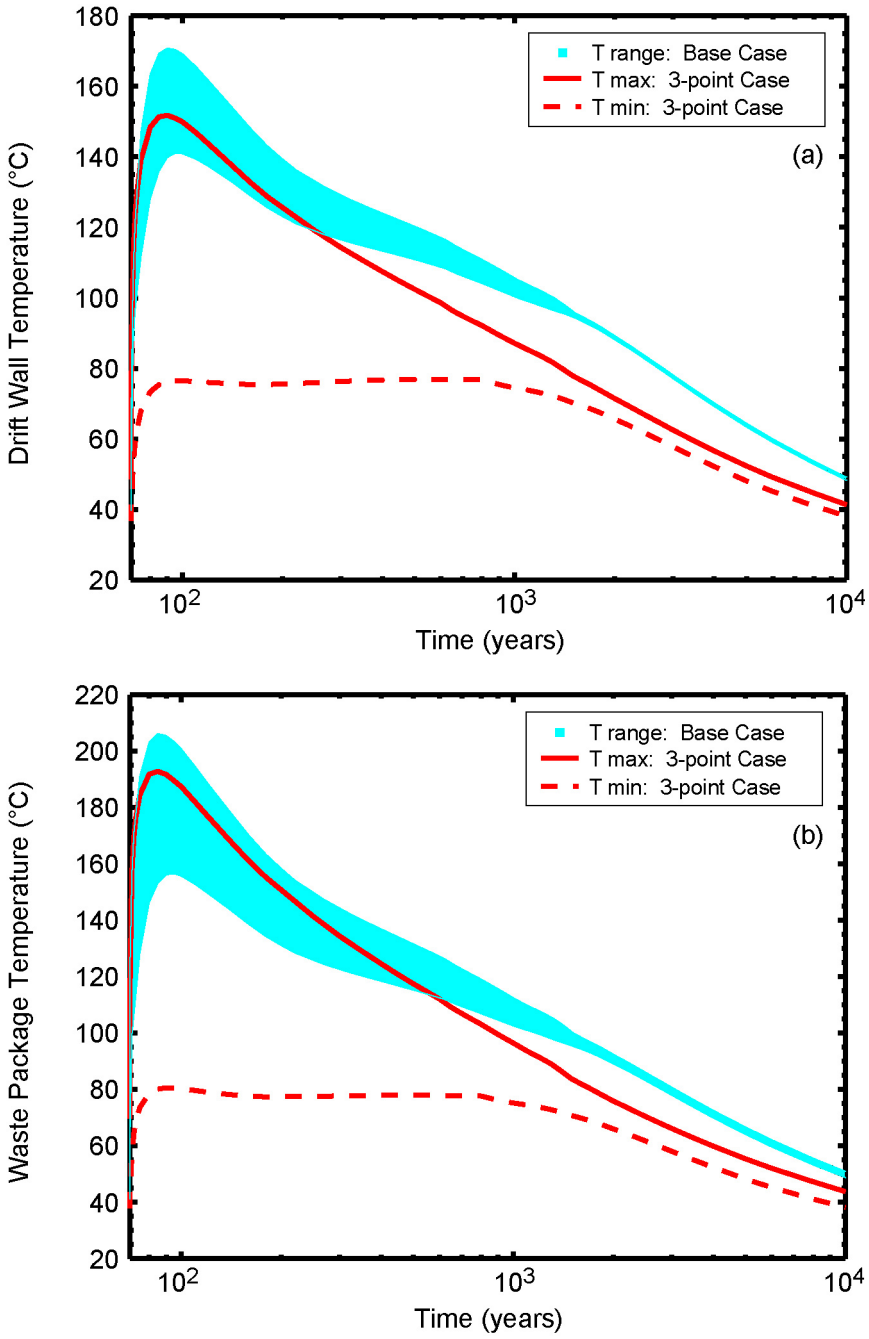

Source: Output DTN: MO0707TH2D3DDC.000, folder: /analyses/3D-DDTH, files: *p10L-7wp-Tdw.dat, p10L-7wp-Twp.dat, p10L-3pt-Tdw.dat*, and *p10L-3pt-Twp.dat*.

NOTE: The maximum and minimum temperature histories for Case 2 are plotted for the P10 percolation flux case with low (10th percentile) host-rock thermal conductivity. The temperature histories are from the 13-package DDTH model (see text). The temperature range for the corresponding base case (postclosure reference case) is shown in shaded blue, shifted so closure is at the same time as Case 2.

Figure 6.4.2-12. Temperature Range at Drift Wall (a) and Waste Package (b) for the Case 2 Segment for the P10L Case

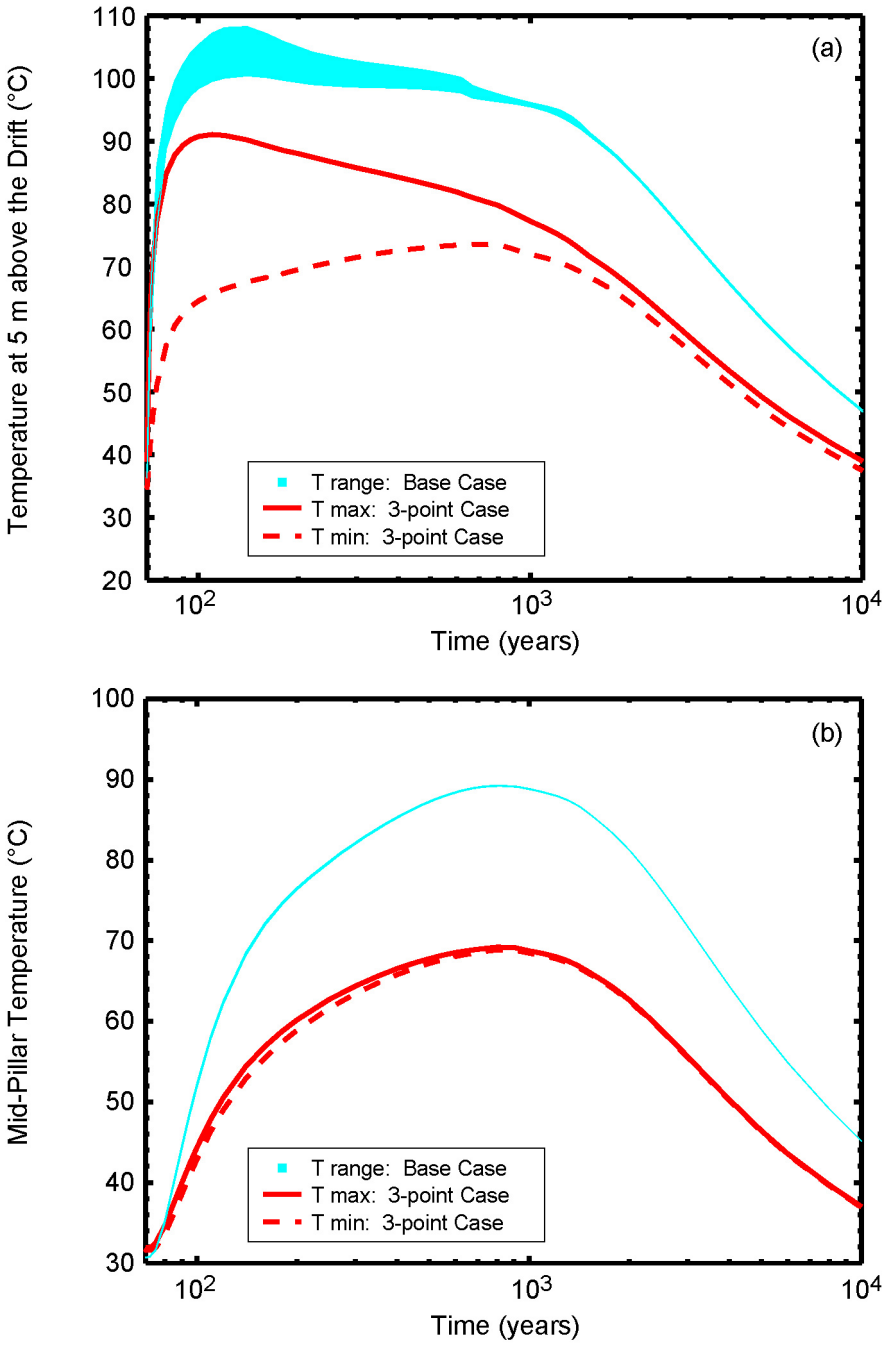

Source: Output DTN: MO0707TH2D3DDC.000, folder: /analyses/3D-DDTH, files: *p10L-7wp-T_5m.dat, p10L-7wp-Tpillar.dat, p10L-3pt-T_5m.dat*, and *p10L-3pt-Tpillar.dat*.

NOTE: The maximum and minimum temperature histories for Case 2 are plotted for the P10 percolation flux case with low (10th percentile) host-rock thermal conductivity. The temperature histories are from the 13-package DDTH model (see text). The temperature range for the corresponding base case (postclosure reference case) is shown in shaded blue, shifted so closure is at the same time as Case 2.

Figure 6.4.2-13. Temperature Range 5 m above the Crown of the Drift (a) and at the Mid-Pillar Location (b) for the Case 2 Segment for the P10L Case

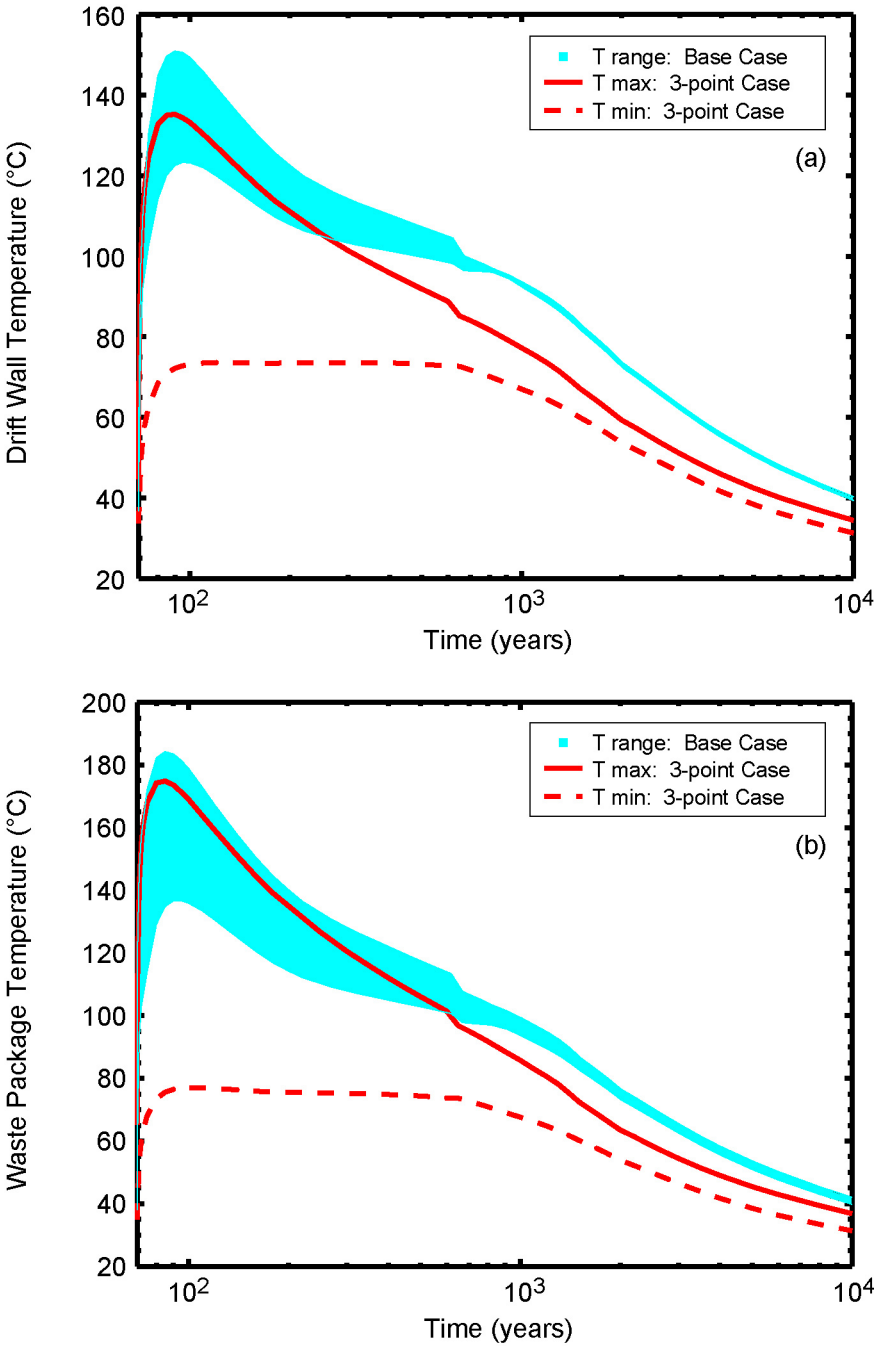

Source: Output DTN: MO0707TH2D3DDC.000, folder: /analyses/3D-DDTH, files: *p90-7wp-Tdw.dat, p90-7wp-Twp.dat, p90-3pt-Tdw.dat*, and *p90-3pt-Twp.dat*.

NOTE: The maximum and minimum temperature histories for Case 2 are plotted for the P90 percolation flux case with mean host-rock thermal conductivity. The temperature histories are from the 13-package DDTH model (see text). The temperature range for the corresponding base case (postclosure reference case) is shown in shaded blue, shifted so closure is at the same time as Case 2.

Figure 6.4.2-14. Temperature Range at Drift Wall (a) and Waste Package (b) for the Case 2 Segment for the P90 Case

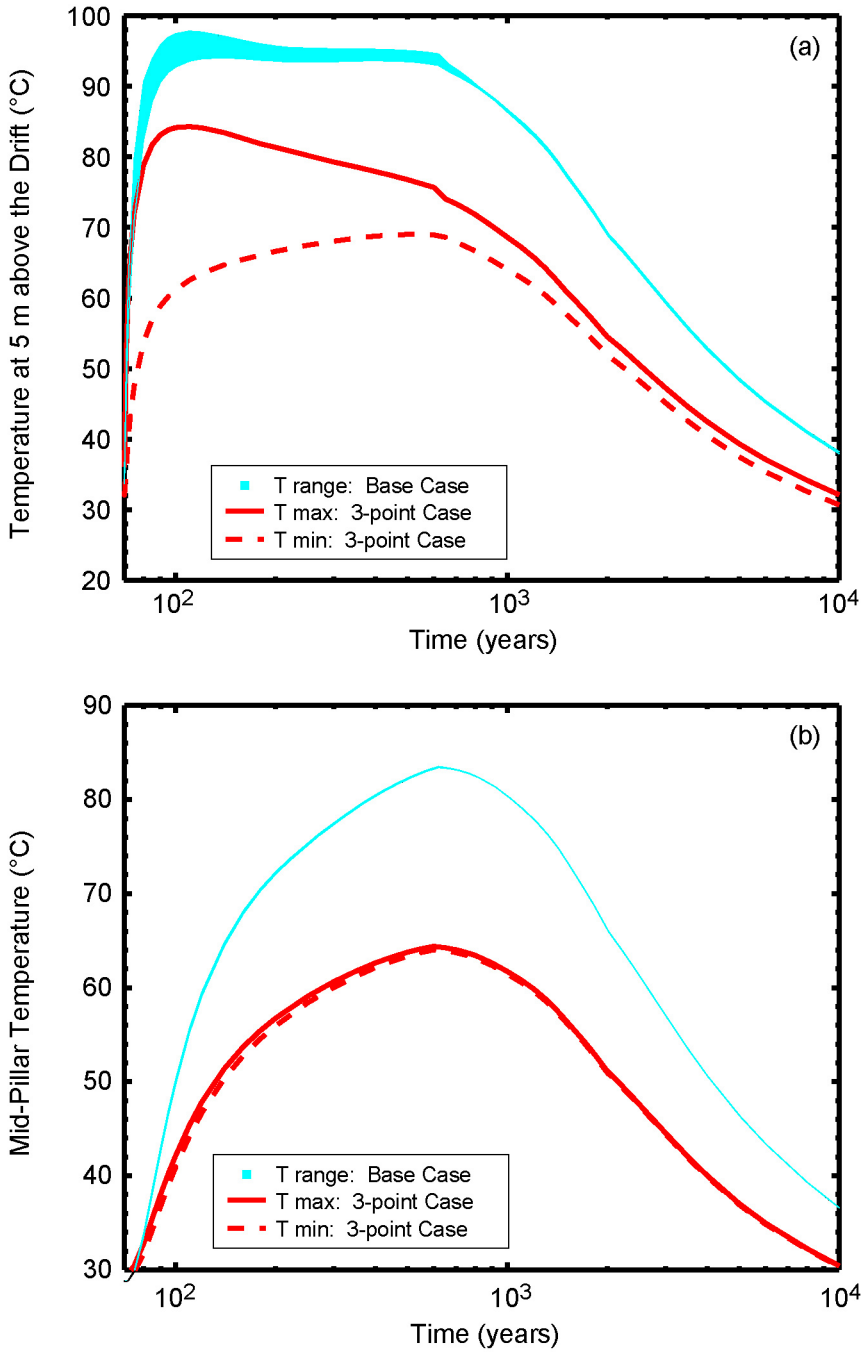

Source: Output DTN: MO0707TH2D3DDC.000, folder: /analyses/3D-DDTH, files: *p90-7wp-T_5m.dat, p90-7wp-Tpillar.dat, p90-3pt-T_5m.dat,* and *p90-3pt-Tpillar.dat*.

NOTE: The maximum and minimum temperature histories for Case 2 are plotted for the P90 percolation flux case with mean host-rock thermal conductivity. The temperature histories are from the 13-package DDTH model (see text). The temperature range for the corresponding base case (postclosure reference case) is shown in shaded blue, shifted so closure is at the same time as Case 2.

Figure 6.4.2-15. Temperature Range 5 m above the Crown of the Drift (a) and at the Mid-Pillar Location (b) for the Case 2 Segment for the P90 Case

6.4.2.4 3-D Model Analysis of Thermal-Hydrologic Behavior

In this section the DDTH model is used to address the potential for heating heterogeneity causing preferential condensate flow above the drift moving from hotter to cooler waste package locations. To evaluate this potential, the relationship between matrix liquid-phase saturation and temperature is examined at the crown of the drift. Figure 6.4.2-16 plots temperature and matrix liquid-phase saturation histories at the crown of the drift for the Case 1 segment, for the P10 case, while Figure 6.4.2-17 is the corresponding plot of matrix liquid-phase saturation as a function of temperature. The same trends observed for the P10 case occur for the P10L case as shown in Figures 6.4.2-18 and 6.4.2-19.

The plots of matrix liquid-phase saturation vs. temperature (Figures 6.4.2-17, 6.4.2-19, and 6.4.2-21 for Case 1; and Figures 6.4.2-23, 6.4.2-25, and 6.4.2-27 for Case 2) are designed to show how much the host rock has cooled, when rewetting occurs. When rewetting occurs at higher temperatures this signifies greater percolation flux above the drift crown. When two otherwise similar waste packages (e.g., two DHLW waste packages) in the DDTH 13-package models rewet at different temperatures, this indicates that adjacent, hotter waste packages are influencing the resaturation. If resaturation is accelerated, then the adjacent packages are contributing liquid flux as condensate. If resaturation is delayed, then the temperature effect from hotter adjacent packages is predominant. Note that matrix liquid-phase saturation vs. temperature is plotted only after the peak crown temperature has occurred.

For Case 1 the resaturation behavior proceeds similarly (as functions of temperature) for all waste packages (Figures 6.4.2-17, 6.4.2-19, and 6.4.2-21), as indicated by the coherent rewetting behavior for all waste packages. Note there are relatively few cooler packages in the Case 1 segment (Table 6.1-2), so the DHLW package locations are being heated by the adjacent hotter waste packages. Resaturation behavior is temperature-controlled, because the DHLW and CSNF (BWR and PWR) waste packages are rewetting as they cool, in a manner that is consistent across waste package types.

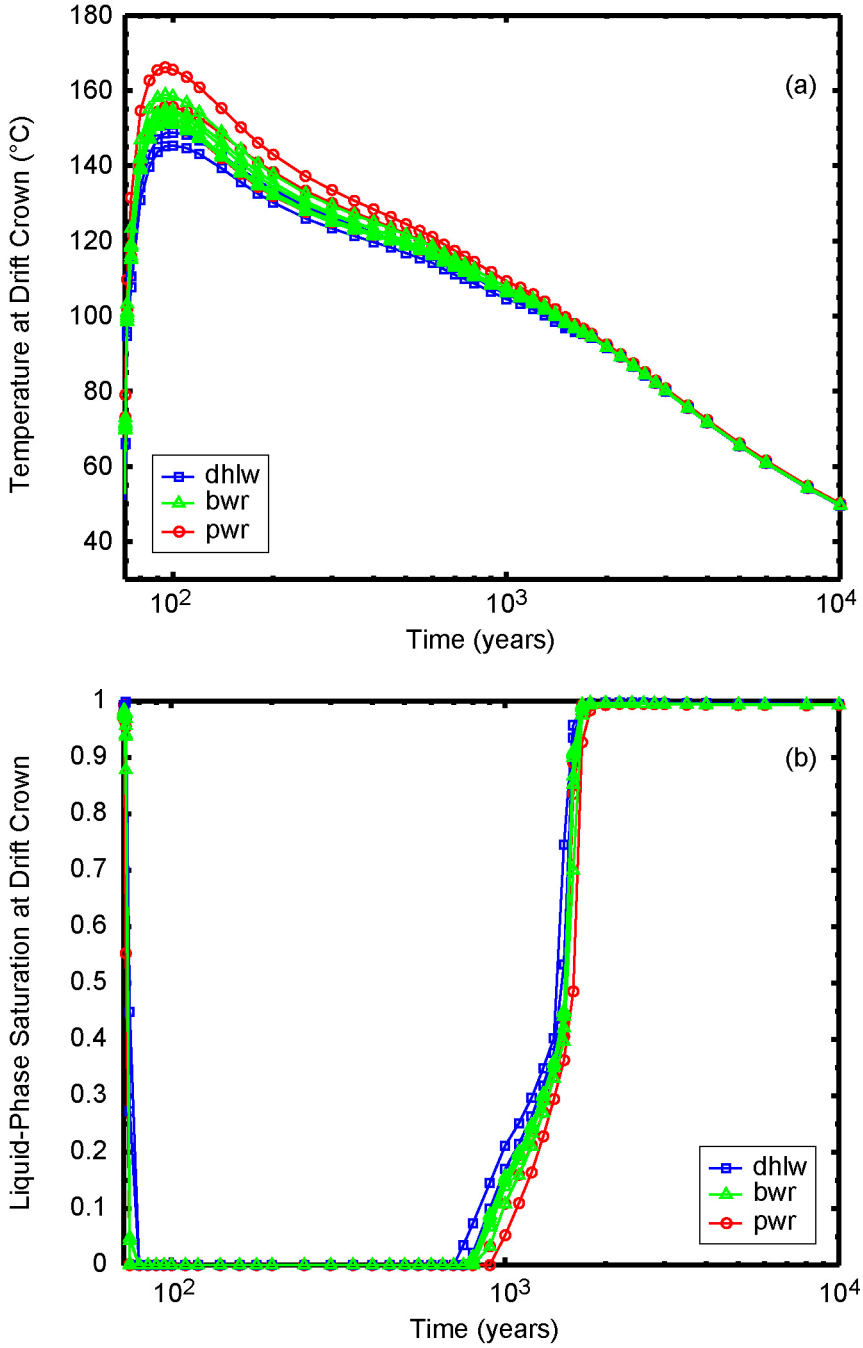

Source: Output DTN: MO0707TH2D3DDC.000, folder: /analyses/3D-DDTH, file: *p10-13wp-7pt-drift_crown_TS.dat*.

NOTES: Data plotted for the temperature and matrix liquid-phase saturation histories for the various waste packages in Case 1, for the P10 percolation flux case with mean host-rock thermal conductivity, from the 13-package DDTH model (see text).

The same symbols and colors are used respectively for the different DHLW, BWR, and PWR packages, because these packages have closely similar thermal characteristics for the Case 1 segment.

Figure 6.4.2-16. Temperature (a) and Liquid-Phase Saturation (b) at the Crown of the Drift for the Case 1 Segment, for the P10 Case

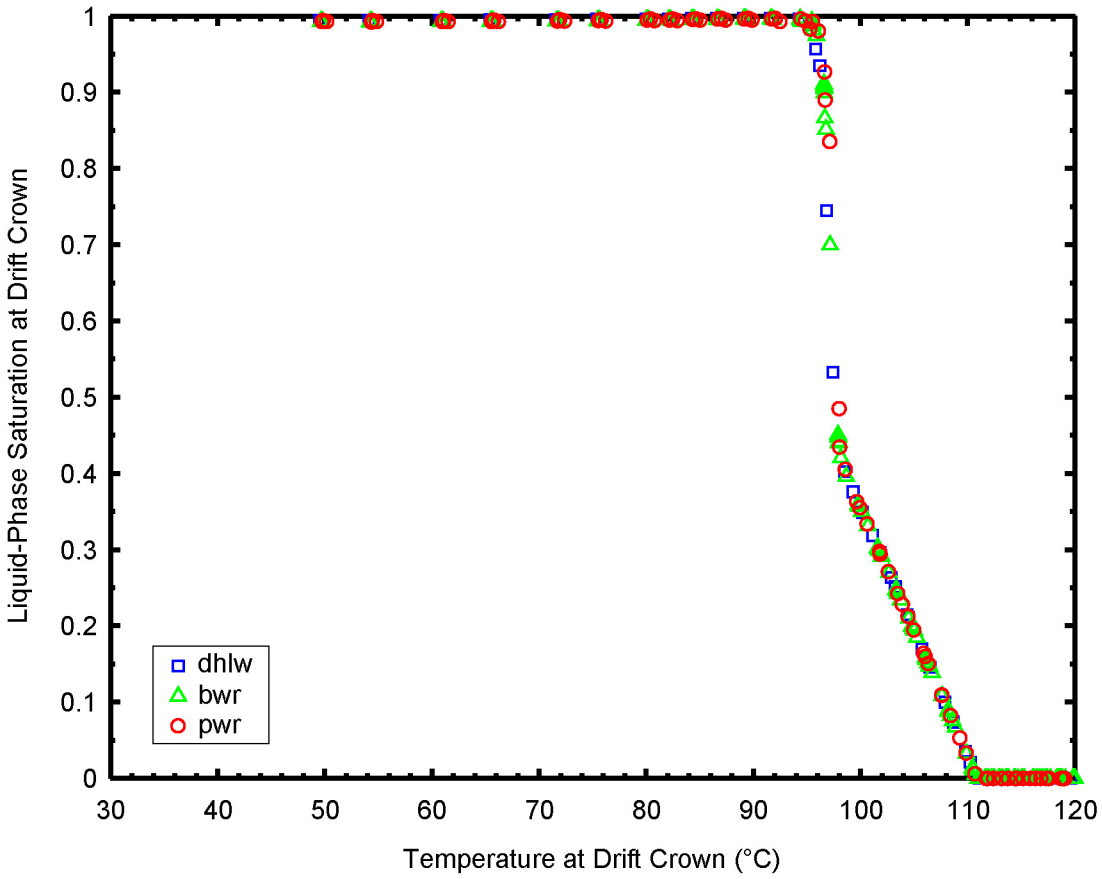

Source: Output DTN: MO0707TH2D3DDC.000, folder: /analyses/3D-DDTH, file: *p10-13wp-7pt-drift_crown_TS.dat*.

NOTES: Data plotted for the various waste packages in Case 1, for the P10 percolation flux case with mean host-rock thermal conductivity, from the 13-package DDTH model (see text).

The same symbols and colors are used respectively for the different DHLW, BWR, and PWR packages, because these packages have closely similar thermal characteristics for the Case 1 segment.

Figure 6.4.2-17. Liquid-Phase Saturation versus Temperature at the Crown of the Drift for the Case 1 Segment, for the P10 Case

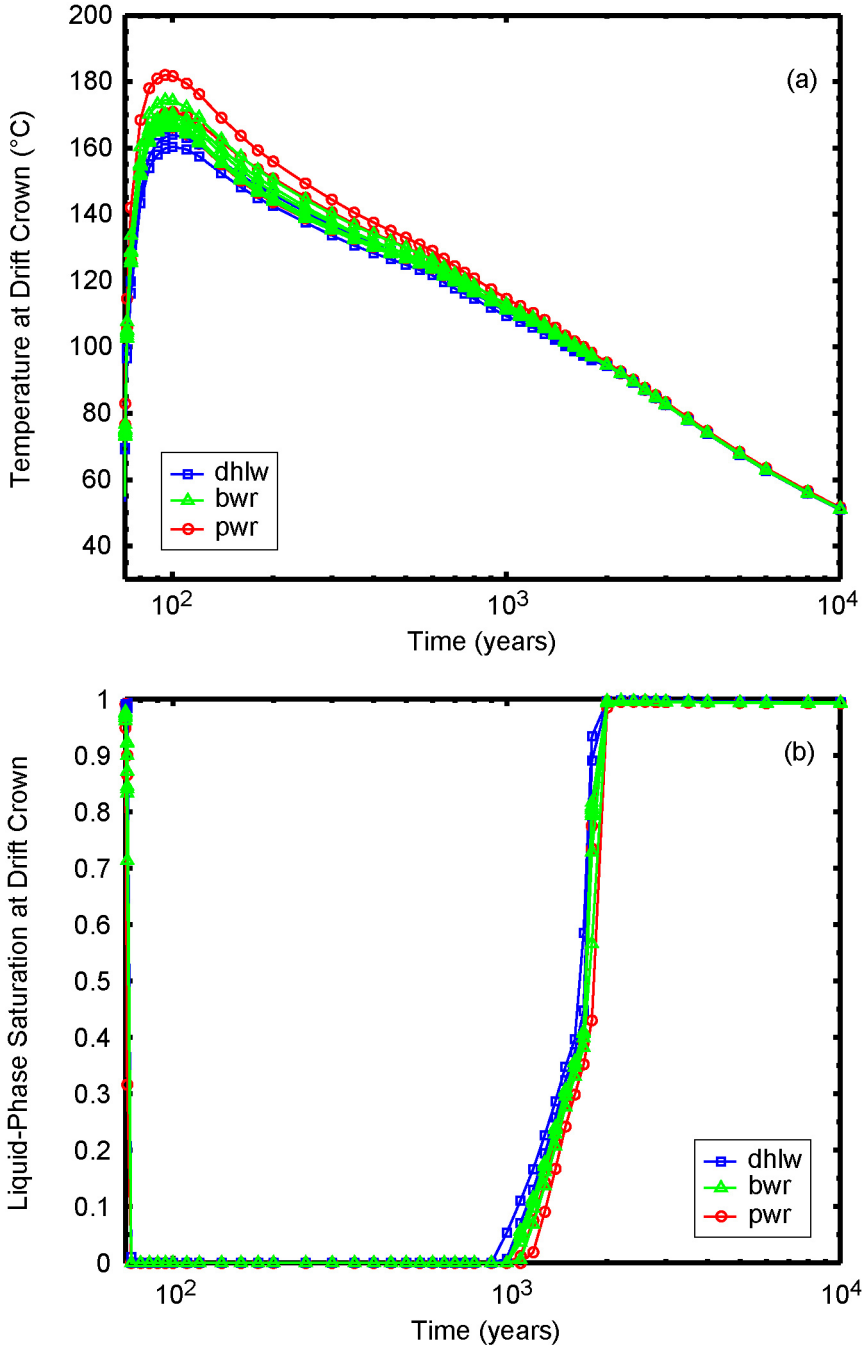

Source: Output DTN: MO0707TH2D3DDC.000, folder: /analyses/3D-DDTH, file: *p10L-13wp-7pt-drift_crown_TS.dat*.

NOTES: Data plotted for the temperature and matrix liquid-phase saturation histories for the various waste packages in Case 1, for the P10 percolation flux case with low (10th percentile) host-rock thermal conductivity, from the 13-package DDTH model (see text).

The same symbols and colors are used respectively for the different DHLW, BWR, and PWR packages, because these packages have closely similar thermal characteristics for the Case 1 segment.

Figure 6.4.2-18. Temperature (a) and Liquid-Phase Saturation (b) at the Crown of the Drift for the Case 1 Segment, for the P10L Case

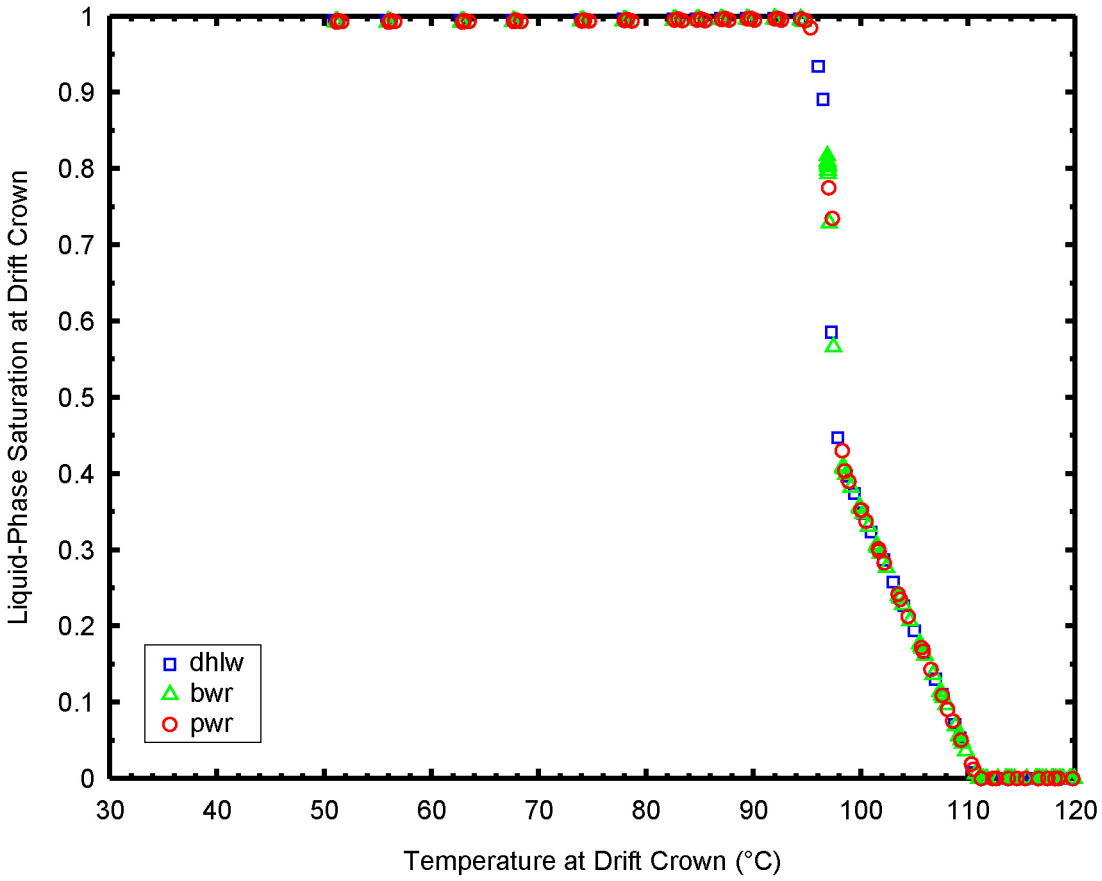

Source: Output DTN: MO0707TH2D3DDC.000, folder: ./analyses/3D-DDTH, file: *p10L-13wp-7pt-drift_crown_TS.dat*.

NOTES: Data plotted for the various waste packages in Case 1, for the P10 percolation flux case with low (10th percentile) host-rock thermal conductivity, from the 13-package DDTH model (see text).

The same symbols and colors are used respectively for the different DHLW, BWR, and PWR packages, because these packages have closely similar thermal characteristics for the Case 1 segment.

Figure 6.4.2-19. Liquid-Phase Saturation versus Temperature at the Crown of the Drift for the Case 1 Segment, for the P10L Case

Drift-crown temperature and matrix liquid-phase saturation histories for the Case 1 segment, for the P90 case (highest percolation flux among the cases presented), are plotted on Figure 6.4.2-20. The corresponding plot of matrix liquid-phase saturation as a function of temperature is Figure 6.4.2-21. Similar trends observed for the P10 and P10L cases occur for the P90 case, with some minor fluctuations caused by the greater percolation flux. The increased percolation flux when the monsoonal climate starts at 600 years quenches dryout and thermal-hydrologic processes in the host rock.

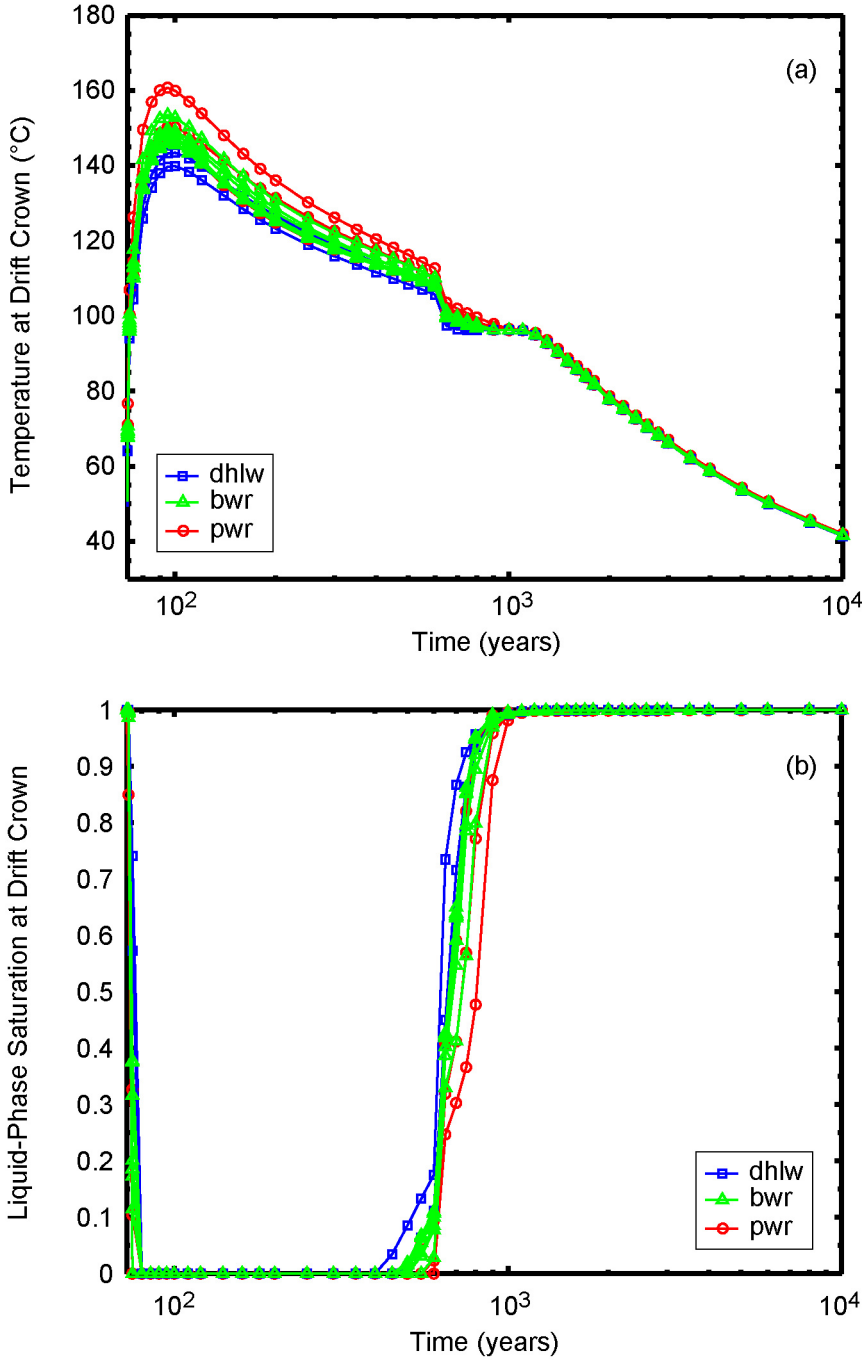

Source: Output DTN: MO0707TH2D3DDC.000, folder: /analyses/3D-DDTH, file: *p90-13wp-7pt-drift_crown_TS.dat*.

NOTES: Data plotted for the temperature and matrix liquid-phase saturation histories for the various waste packages in Case 1, for the P90 percolation flux case with mean host-rock thermal conductivity, from the 13-package DDTH model (see text).

The same symbols and colors are used respectively for the different DHLW, BWR, and PWR packages, because these packages have closely similar thermal characteristics for the Case 1 segment.

Figure 6.4.2-20. Temperature (a) and Liquid-Phase Saturation (b) at the Crown of the Drift for the Case 1 Segment, for the P90 Case

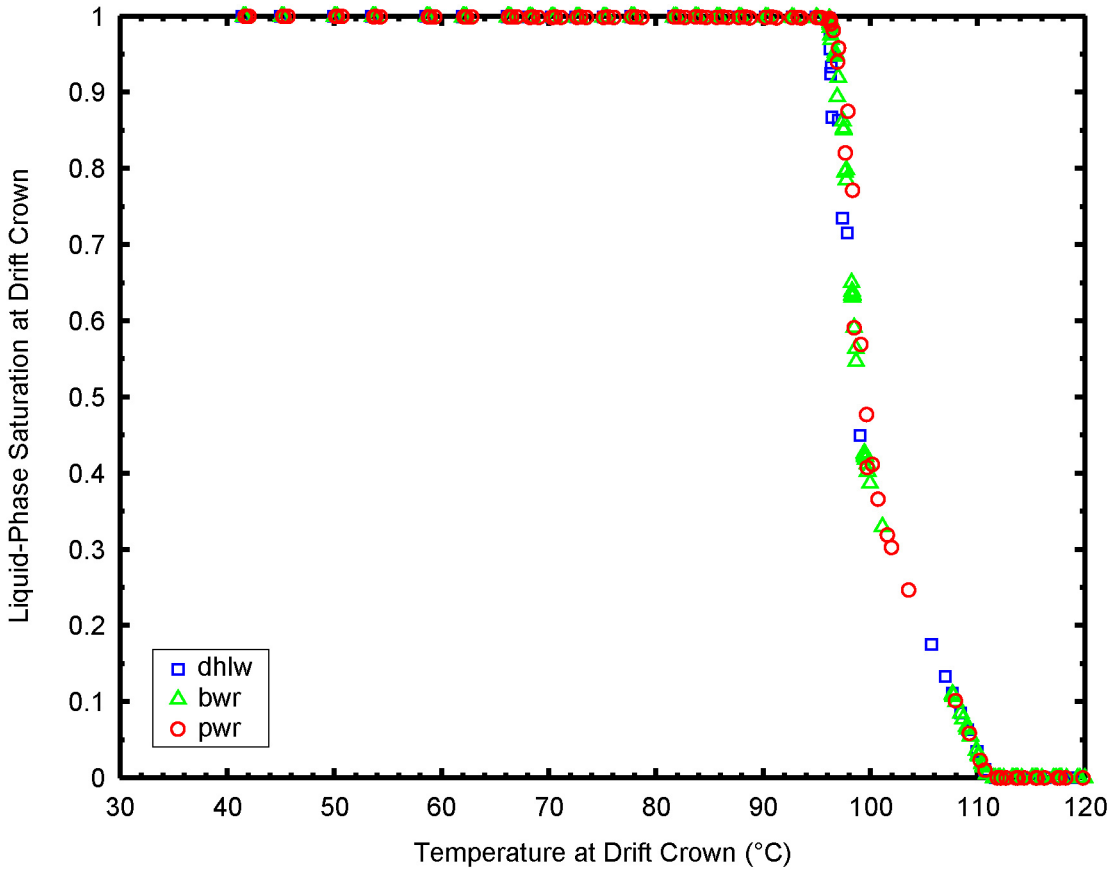

Source: Output DTN: MO0707TH2D3DDC.000, folder: /analyses/3D-DDTH, file: *p90-13wp-7pt-drift_crown_TS.dat.*

NOTES: Data plotted for the various waste packages in Case 1, for the P10 percolation flux case with mean host-rock thermal conductivity, from the 13-package DDTH model (see text).

The same symbols and colors are used respectively for the different DHLW, BWR, and PWR packages, because these packages have closely similar thermal characteristics for the Case 1 segment.

Figure 6.4.2-21. Liquid-Phase Saturation versus Temperature at the Crown of the Drift for the Case 1 Segment, for the P90 Case

The Case 2 segment includes relatively numerous DHLW packages, resulting in a wider range of temperature and matrix liquid-phase saturation histories (Figure 6.4.2-22) than for Case 1. In general, the DHLW packages adjacent to the CSNF packages (PWRs) experience the greatest rock dryout (these DHLW packages are shown in green, while those not adjacent are shown in blue). The relationship between matrix liquid-phase saturation and temperature (Figure 6.4.2-23) clearly shows the differences between different DHLW packages (by the spread of green vs. blue results). It also shows that all locations cool well below the boiling point (96°C) before substantial rewetting occurs, indicating that resaturation is temperature-controlled.

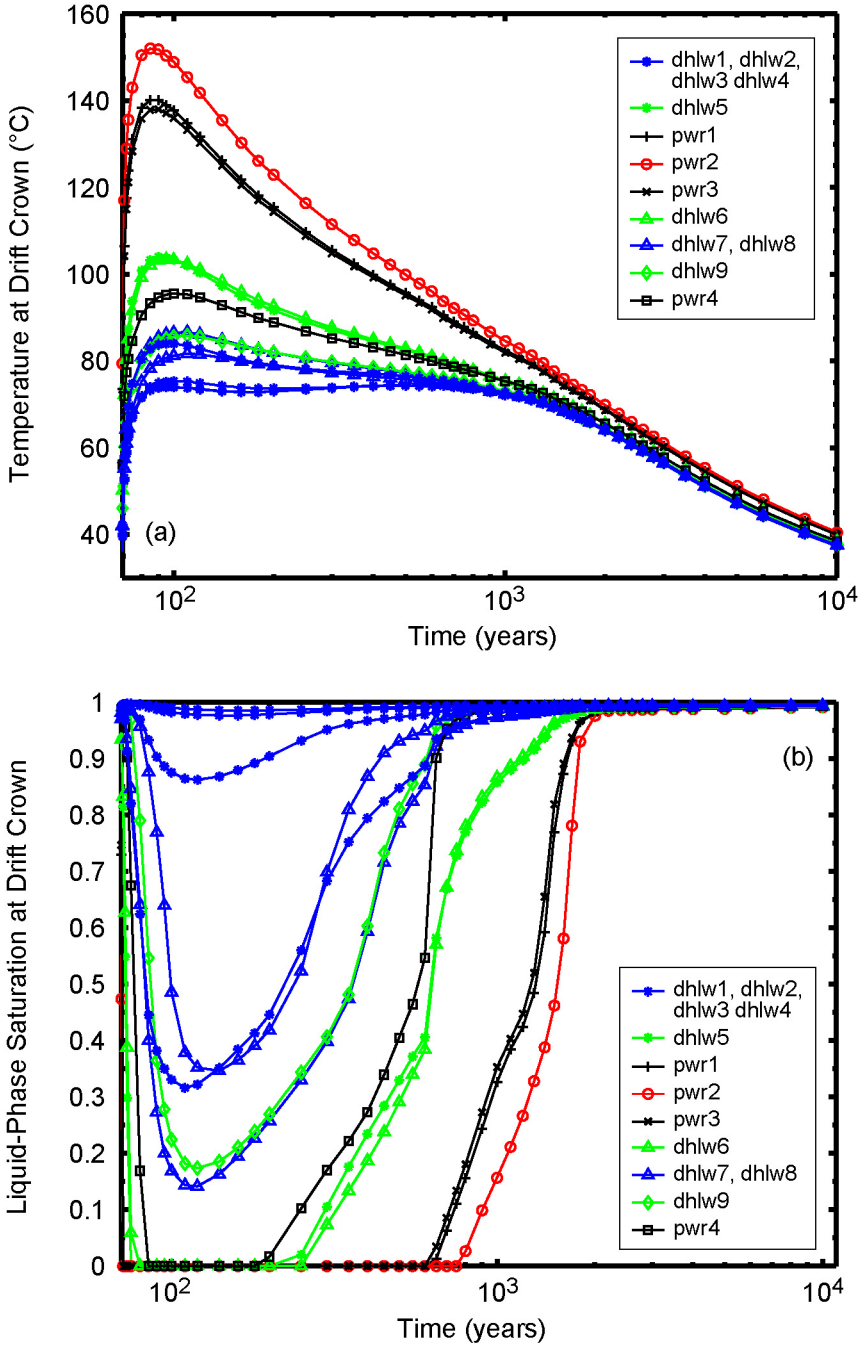

Source: Output DTN: MO0707TH2D3DDC.000, folder: /analyses/3D-DDTH, file: *p10-13wp-3pt-drift_crown_TS.dat.*

NOTE: The temperature and matrix liquid-phase saturation histories for Case 2 are plotted for the P10 percolation flux case with mean host-rock thermal conductivity, from the 13-package DDTH model (see text). DHLW waste packages plotted in green are those adjacent to PWR waste packages. The PWR waste packages plotted in black are those adjacent to DHLW waste packages.

Figure 6.4.2-22. Temperature (a) and Liquid-Phase Saturation (b) at the Crown of the Drift for the Case 2 Segment, for the P10 Case

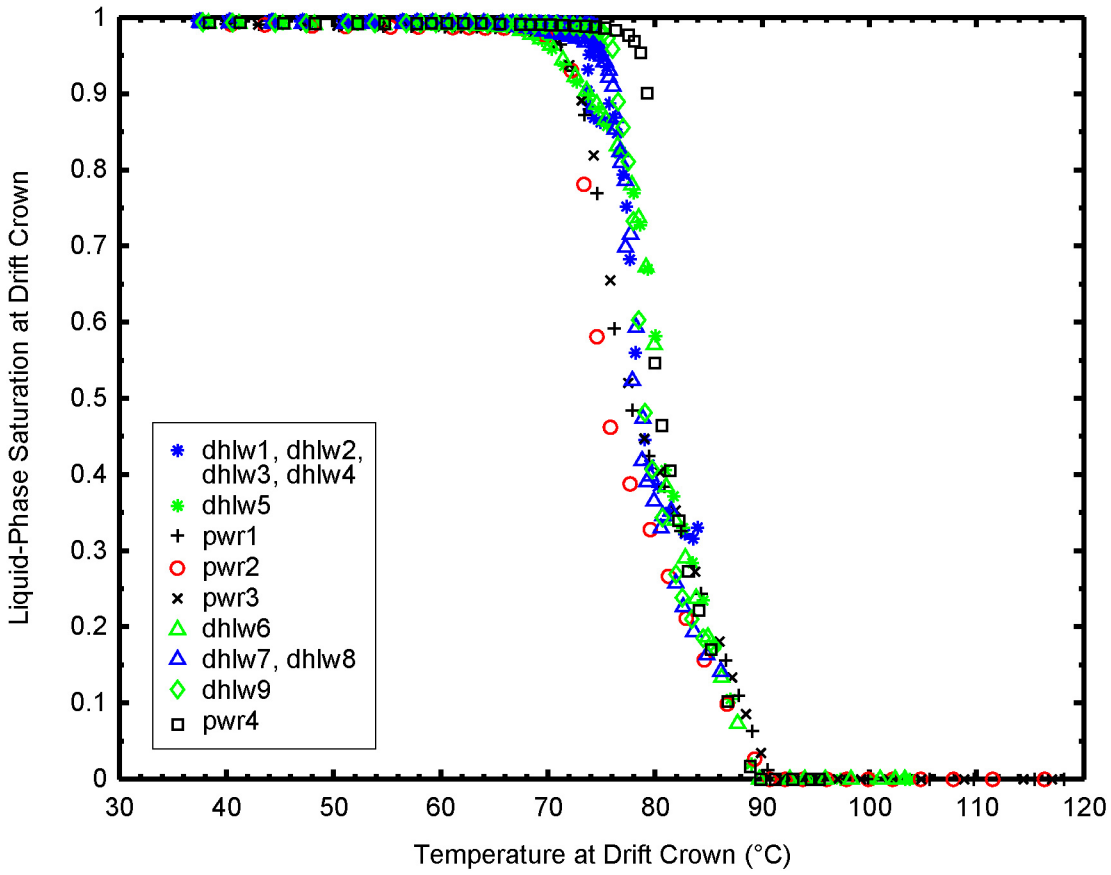

Source: Output DTN: MO0707TH2D3DDC.000, folder: /analyses/3D-DDTH, file: *p10-13wp-3pt-drift_crown_TS.dat.*

NOTE: The temperature versus matrix liquid-phase saturation for the Case 2 segment is plotted for the P10 (lowest) percolation flux case with mean host-rock thermal conductivity. The temperature and matrix liquid-phase saturation are from the 13-package DDTH model (with 11 full waste packages plus 2 half waste packages). DHLW waste packages plotted in green are those adjacent to CSNF (PWR) packages. The PWR packages plotted in black are those adjacent to DHLW packages. The relationship between matrix liquid-phase saturation and temperature is plotted after the peak crown temperature has occurred.

Figure 6.4.2-23. Liquid-Phase Saturation versus Temperature at the Crown of the Drift for the Case 2 Segment, for the P10 Case

Figure 6.4.2-24 plots temperature and matrix liquid-phase saturation histories at the crown of the drift for the Case 2 segment for the P10L case, with the lowest value of host-rock thermal conductivity. The corresponding plot of matrix liquid-phase saturation as a function of temperature is Figure 6.4.2-25. The same trends observed for the P10 case occur for the P10L case. Resaturation behavior is temperature-controlled, which is expected for the low-flux P10 condition.

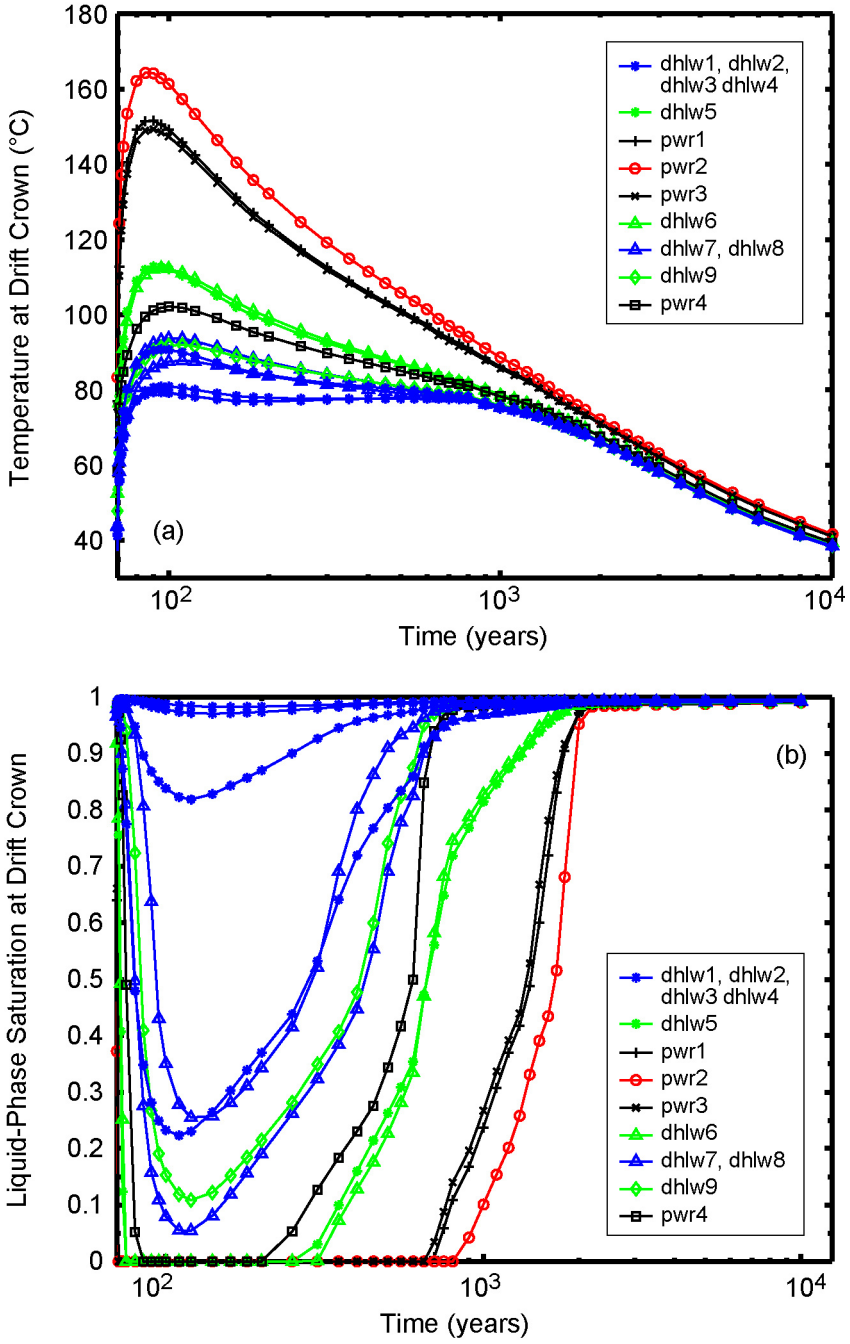

Source: Output DTN: MO0707TH2D3DDC.000, folder: /analyses/3D-DDTH, file: *p10L-13wp-3pt-drift_crown_TS.dat*.

NOTE: The temperature and matrix liquid-phase saturation histories for the 96/2 3-point running-average sequence is plotted for the P10L percolation flux case with low host-rock thermal conductivity. The temperature and matrix liquid-phase saturation histories are from the 13-package DDTH model (with 11 full waste packages plus 2 half waste packages). DHLW waste packages plotted in green are those adjacent to TAD (PWR) waste packages. The TAD (PWR) waste packages plotted in black are those adjacent to DHLW waste packages.

Figure 6.4.2-24. Temperature (a) and Liquid-Phase Saturation (b) at the Crown of the Drift for the Case 2 Segment, for the P10L Case

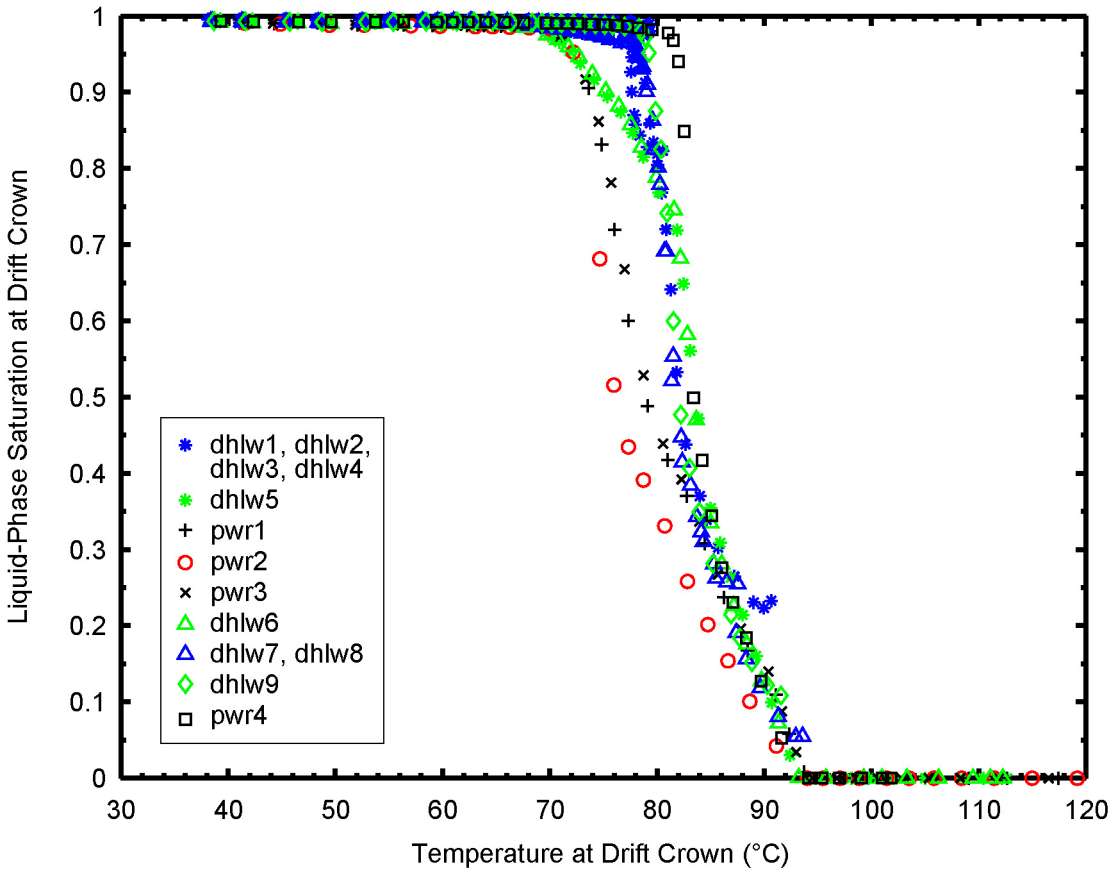

Source: Output DTN: MO0707TH2D3DDC.000, folder: /analyses/3D-DDTH, file: *p10L-13wp-3pt-drift_crown_TS.dat.*

NOTE: The temperature versus matrix liquid-phase saturation for the Case 2 segment is plotted for the P10 percolation flux case with low host-rock thermal conductivity. The temperature and matrix liquid-phase saturation are from the 13-package DDTH model (with 11 full waste packages plus 2 half waste packages). DHLW waste packages plotted in green are those adjacent to CSNF (PWR) packages. The PWR packages plotted in black are those adjacent to DHLW packages. The relationship between matrix liquid-phase saturation and temperature is plotted after the peak crown temperature has occurred.

Figure 6.4.2-25. Liquid-Phase Saturation versus Temperature at the Crown of the Drift for the Case 2 Segment, for the P10L Case

Figure 6.4.2-26 plots temperature and matrix liquid-phase saturation histories at the crown of the drift for the Case 2 segment for the P90 case (highest percolation flux among the cases presented). The corresponding plot of matrix liquid-phase saturation as a function of temperature is Figure 6.4.2-27. Results for this case are similar to the P10 and P10L cases, with some minor fluctuations related to the increased percolation flux. Rock dryout is substantially quenched by increased percolation flux when the monsoonal climate starts at 600 years. All waste packages have cooled well below the boiling point (96°C) before substantial rewetting occurs, indicating that resaturation is temperature-controlled.

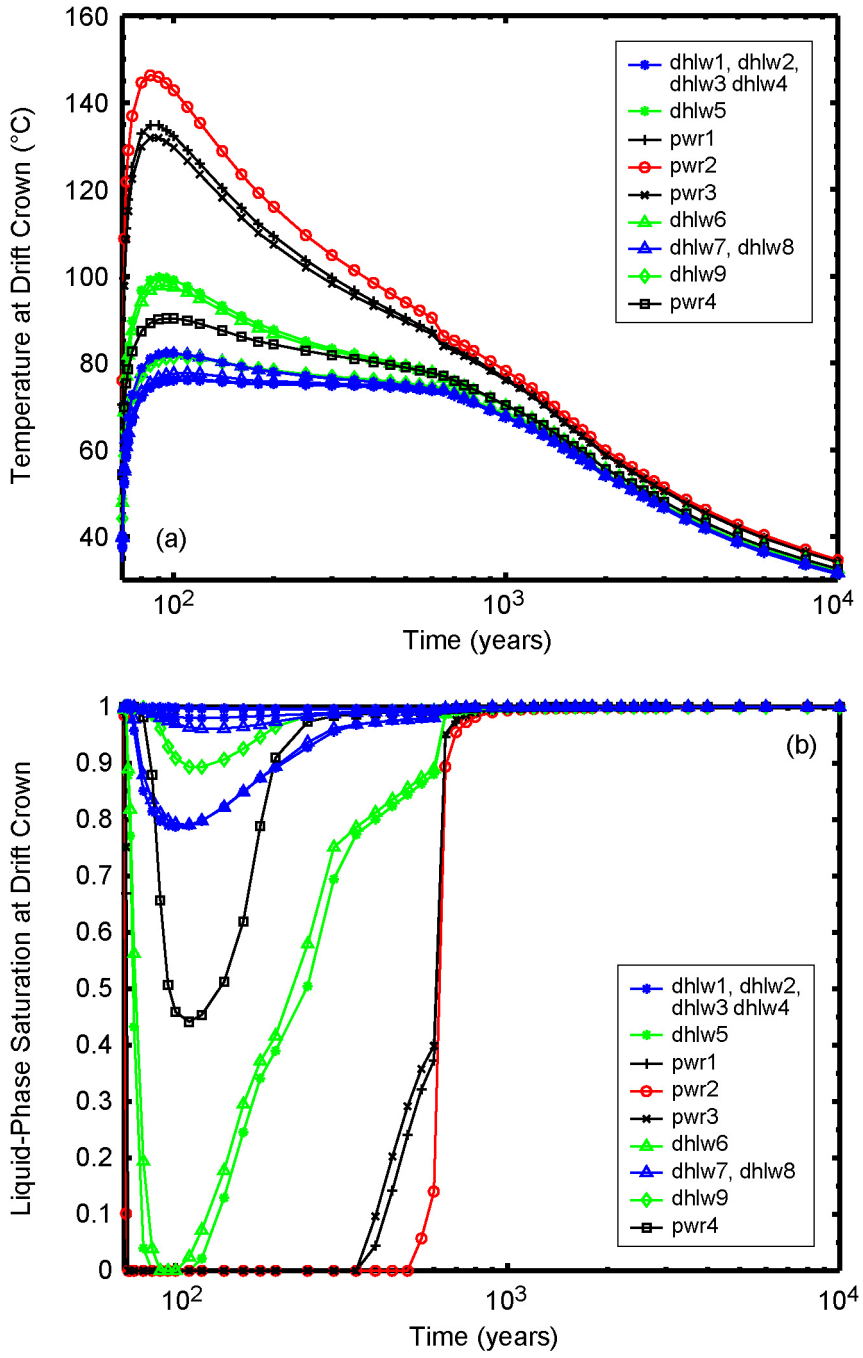

Source: Output DTN: MO0707TH2D3DDC.000, folder: /analyses/3D-DDTH, file: *p90-13wp-3pt-drift_crown_TS.dat.*

NOTE: The temperature and matrix liquid-phase saturation histories for the 96/2 3-point running-average sequence is plotted for the P90 percolation flux case with mean host-rock thermal conductivity. The temperature and matrix liquid-phase saturation histories are from the 13-package DDTH model (with 11 full waste packages plus 2 half waste packages). DHLW waste packages plotted in green are those adjacent to TAD (PWR) waste packages. The TAD (PWR) waste packages plotted in black are those adjacent to DHLW waste packages.

Figure 6.4.2-26. Temperature (a) and Liquid-Phase Saturation (b) at the Crown of the Drift for the Case 2 Segment, for the P90 Case

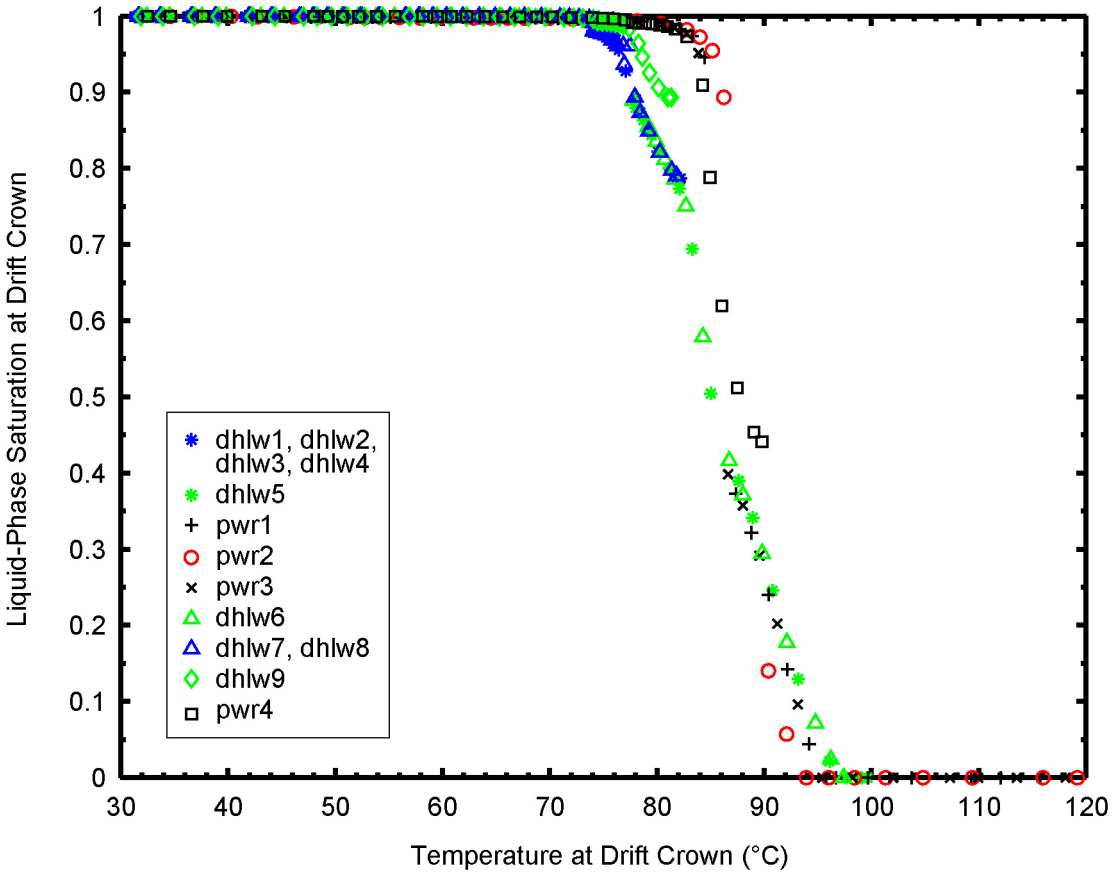

Source: Output DTN: MO0707TH2D3DDC.000, folder: /analyses/3D-DDTH, file: *p90-13wp-3pt-drift_crown_TS.dat.*

NOTE: The temperature versus matrix liquid-phase saturation for the Case 2 segment is plotted for the P90 (highest) percolation flux case with mean host-rock thermal conductivity. The temperature and matrix liquid-phase saturation are from the 13-package DDTH model (11 full waste packages plus 2 half waste packages). DHLW waste packages plotted in green are those adjacent to CSNF (PWR) packages. The PWR packages plotted in black are those adjacent to DHLW packages. The relationship between matrix liquid-phase saturation and temperature is plotted after the peak crown temperature has occurred.

Figure 6.4.2-27. Liquid-Phase Saturation versus Temperature at the Crown of the Drift for the Case 2 Segment, for the P90 Case

6.4.2.5 DDTH Model Analysis of Drift-Collapse Temperatures

The DDTH model runs for Cases 1 and 2 were repeated with modification of the model grid and materials properties, to simulate the effects from complete drift collapse. The approach is identical to that used for the multiscale model (SNL 2007 [DIRS 181383], Section 6.3.17[a]). The intention here is to evaluate the effect of local thermal loading on the peak waste package temperature, which is important for evaluating FEPs. In particular, the objective is to evaluate whether the temperature history for the hottest waste package is consistent with the screening justification for FEP 2.1.11.06.0A (Thermal sensitization of waste packages) as discussed in Section 6.5.

For the peak temperature of the hottest waste package, the DDTH runs were performed using the P10 percolation flux (lowest percolation flux among the cases presented), the low host-rock thermal conductivity, and the low rubble thermal conductivity function (SNL 2007 [DIRS 181383], Appendix XI). Using the multiscale approach to represent a drift collapse, a circular drift opening with twice the intact diameter is filled with rubble, corresponding to a bulking factor of approximately 20%.

The results (Figure 6.4.2-28) show that the hottest waste package will approach 380°C for Case 1, and 400°C for Case 2. These are somewhat hotter values than the 363°C value for the hottest waste package from the multiscale model using the postclosure reference case unit-cell arrangement (the hottest multiscale waste package is calculated in Output DTN: MO0707TH2D3DDC.000, file: *Hottest WP P10L_pwr1-3_collapse.xls*, using data from DTNs: LL0702PA013MST.068 [DIRS 180553], LL0702PA014MST.069 [DIRS 179591], LL0702PA022MST.077 [DIRS 179595], LL0702PA020MST.075 [DIRS 179594], LL0705PA032MST.028 [DIRS 182706], and LL0702PA027MST.082 [DIRS 179590]). Distribution functions for peak waste package temperature for all waste packages, for complete drift collapse immediately after repository closure, from the multiscale model are plotted in Figure 6.4.2-29. The figure shows that the global maximum peak temperature (363°C) is a very rare occurrence.

The temperatures exceed the 300°C maximum waste package temperature for the waste package (Section 6.1). However, as discussed in Section 6.5.1, the likelihood of waste package temperatures exceeding 300°C is small because the probability of the drift collapse during the thermal period is small.

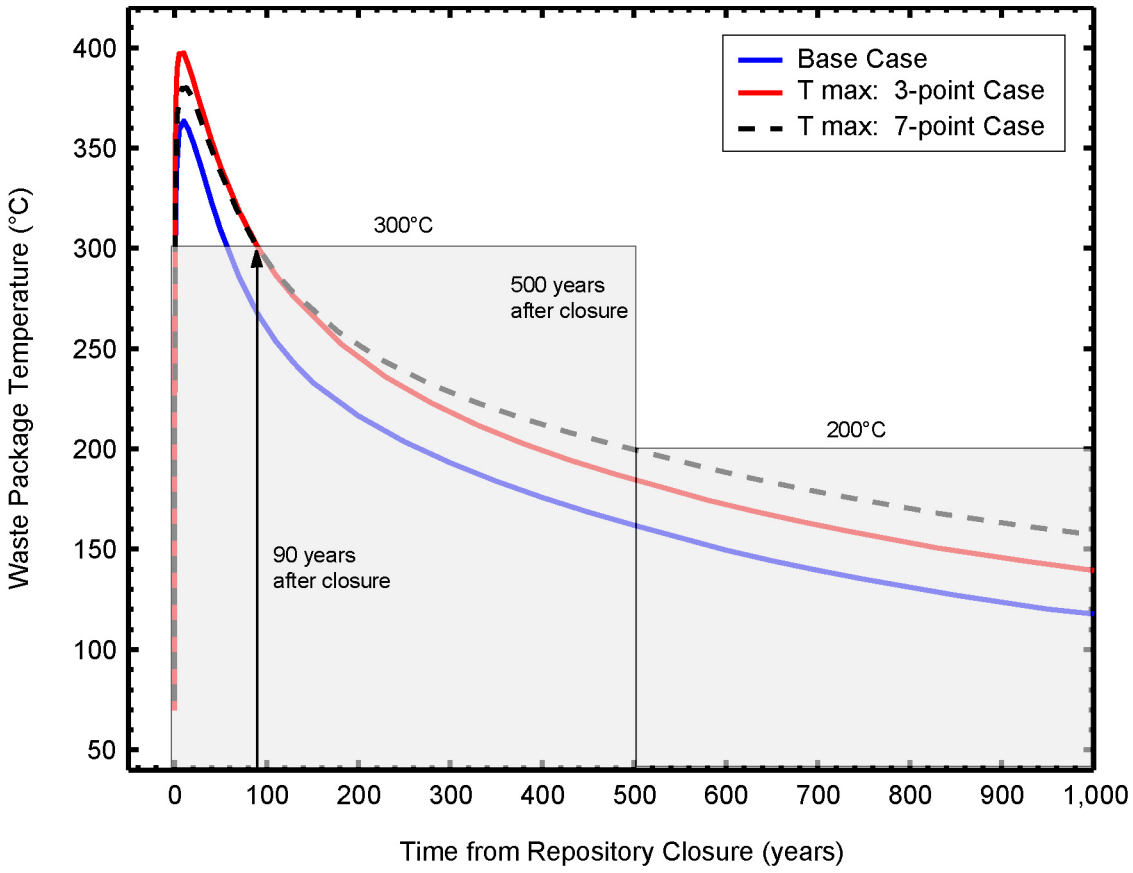

Source: Output DTN: MO0707TH2D3DDC.000, folder: /analyses/3D-Collasped-Drift, files: *p10L_pwr1-3_collapse.dat, p10L-collapse-lkt-3pt-Twp.dat*, and *p10L-collapse-lkt-7pt-Twp.dat*.

NOTES: Case 1 from the text corresponds to the 7-point case (hottest 7-package segment from Section 6.1.3), while Case 2 from the text is the 3-point case (hottest 3-package segment).

Temperature history is plotted for the hottest CSNF waste package (used in TSPA) from each of the 13 waste package segments (11 full waste packages plus 2 half waste packages) for Case 1 and Case 2, for the P10 percolation flux case with low host-rock thermal conductivity and low rubble thermal conductivity. The 90-year and 500-year windows are located with respect to these curves.

Also plotted is the temperature history for the hottest waste package from the multiscale model with drift-collapse (SNL 2007 [DIRS 181383], Section 6.3.17[a]), for the same properties and boundary conditions.

The time axis is expressed in years since emplacement, and not calendar time, for all curves plotted. Hence the base-case curve is not contemporaneous with the others and would be shifted approximately 20 years to the right for direct comparison to the other curves or to the time windows shown.

Figure 6.4.2-28. Temperature Histories for the Hottest Waste Packages in Collapsed-Drifts, from 3-D Results for Case 1, Case 2, and the Base-Case Multiscale Model

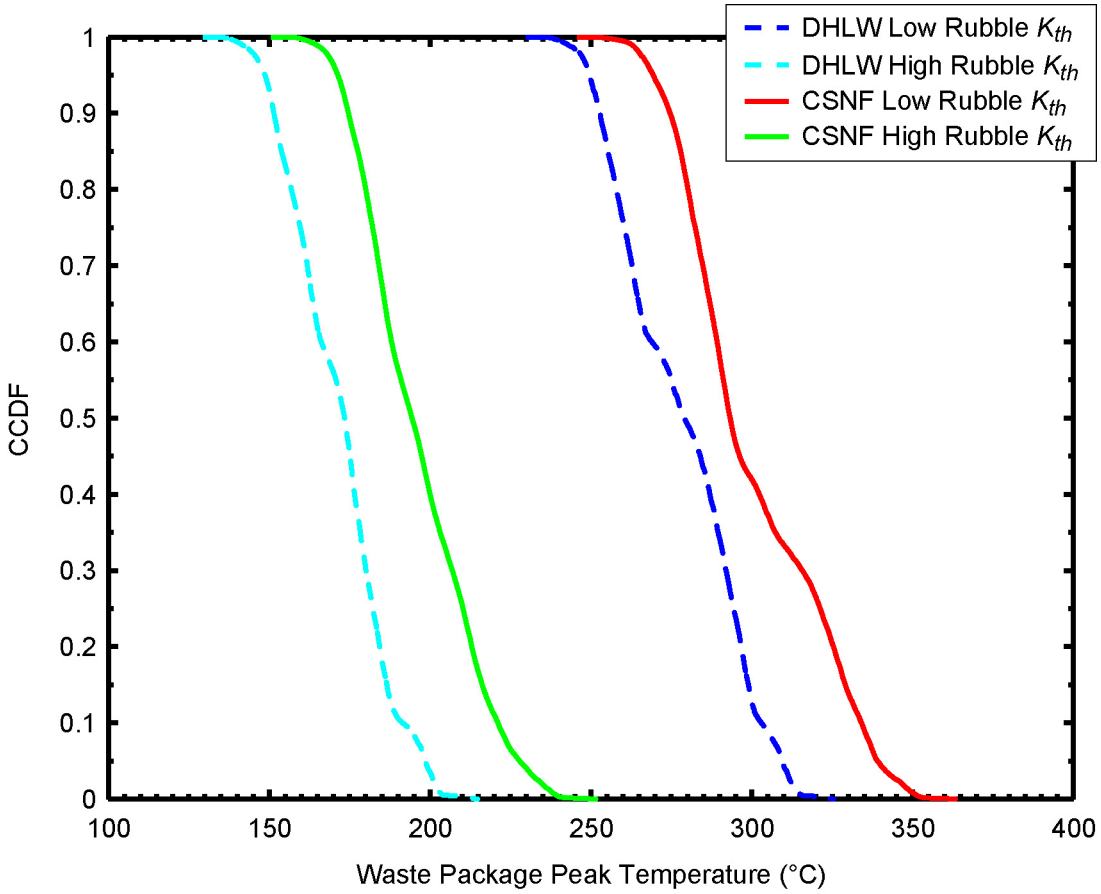

Source: Output DTN: MO0707TH2D3DDC.000, folder: /analyses/MSTHM-Collapsed-Drift, files: *Twp-peak-CCDF_Collapsed-Drift-DHLW-hkt.dat*, *Twp-peak-CCDF_Collapsed-Drift-CSNF-hkt.dat*, *Twp-peak-CCDF_Collapsed-Drift-DHLW.dat*, and *Twp-peak-CCDF_Collapsed-Drift-CSNF.dat*.

NOTES: All percolation flux/host-rock thermal conductivity ca ses from the multiscale model are represented in each CCDF, combined using appropriate weighting (SNL 2007 [DIRS 181383], Table 6.3-48[a]).

Results for DHLW and CSNF waste packages, and for low and high values of rubble effective thermal conductivity, are segregated to show differences.

Figure 6.4.2-29. Complementary Cumulative Distribution Functions for Peak Postclosure Waste Package Temperature, for the Drift-Collapse Case, for All Waste Packages

6.4.2.6 LDTH Model Analysis of Far-Field Thermal Response

The LDTH model is used to analyze the far-field thermal response comparing the global average line load for the ELWS to the average line load for the postclosure reference thermal base case (both thermal output histories are plotted on Figure 6.1-1). Figures 6.4.2-30 through 6.4.2-32 present the resulting temperature histories at the bottom of the PTn unit (overlying the host rock), the top of the CHn unit (underlying), and at the water table. Note that the lower boundary of the LDTH model domain is set 1,000 m below the water table (SNL 2007 [DIRS 181383]).

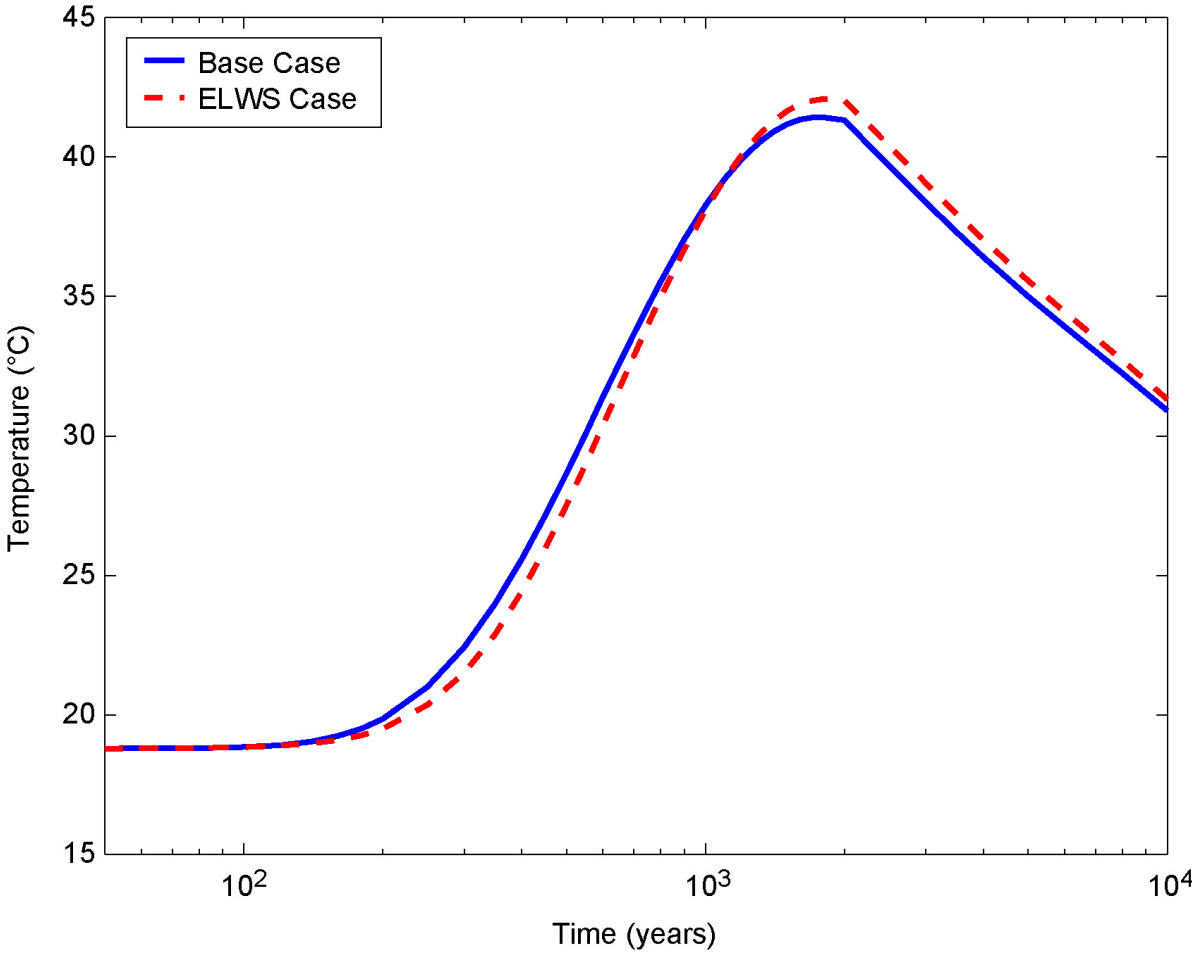

Source: Output DTN: MO0707TH2D3DDC.000, folder: /analyses/2D-LDTH, file: *P10-T_ELWS.dat.*

Figure 6.4.2-30. Temperature Histories for the Bottom of the PTn Unit, Comparing the ELWS Average Line Load with the Postclosure Reference Case Average Line Load

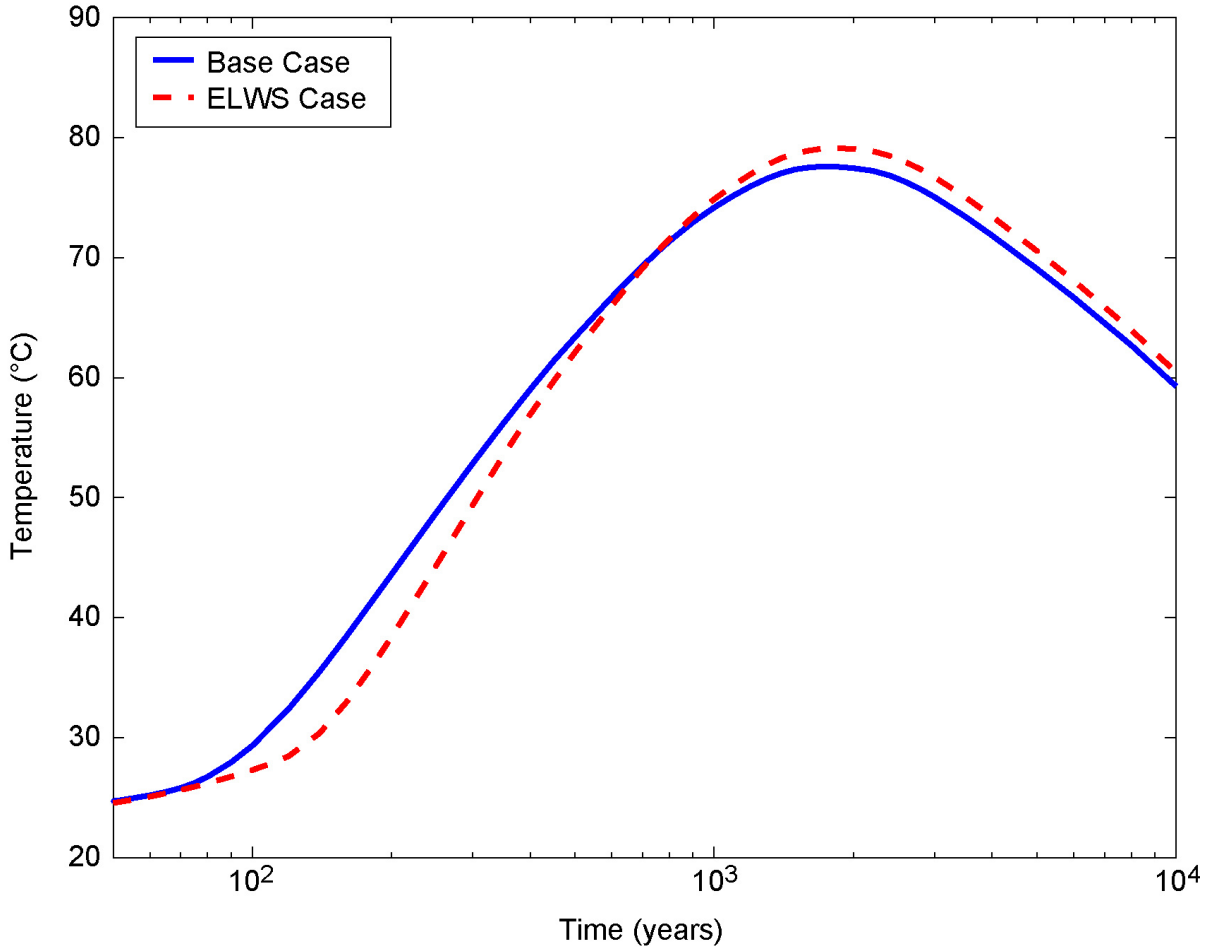

Source: Output DTN: MO0707TH2D3DDC.000, folder: /analyses/2D-LDTH, file: *P10-T_ELWS.dat.*

Figure 6.4.2-31. Temperature Histories for the Top of the CHn Unit, Comparing the ELWS Average Line Load with the Postclosure Reference Case Average Line Load

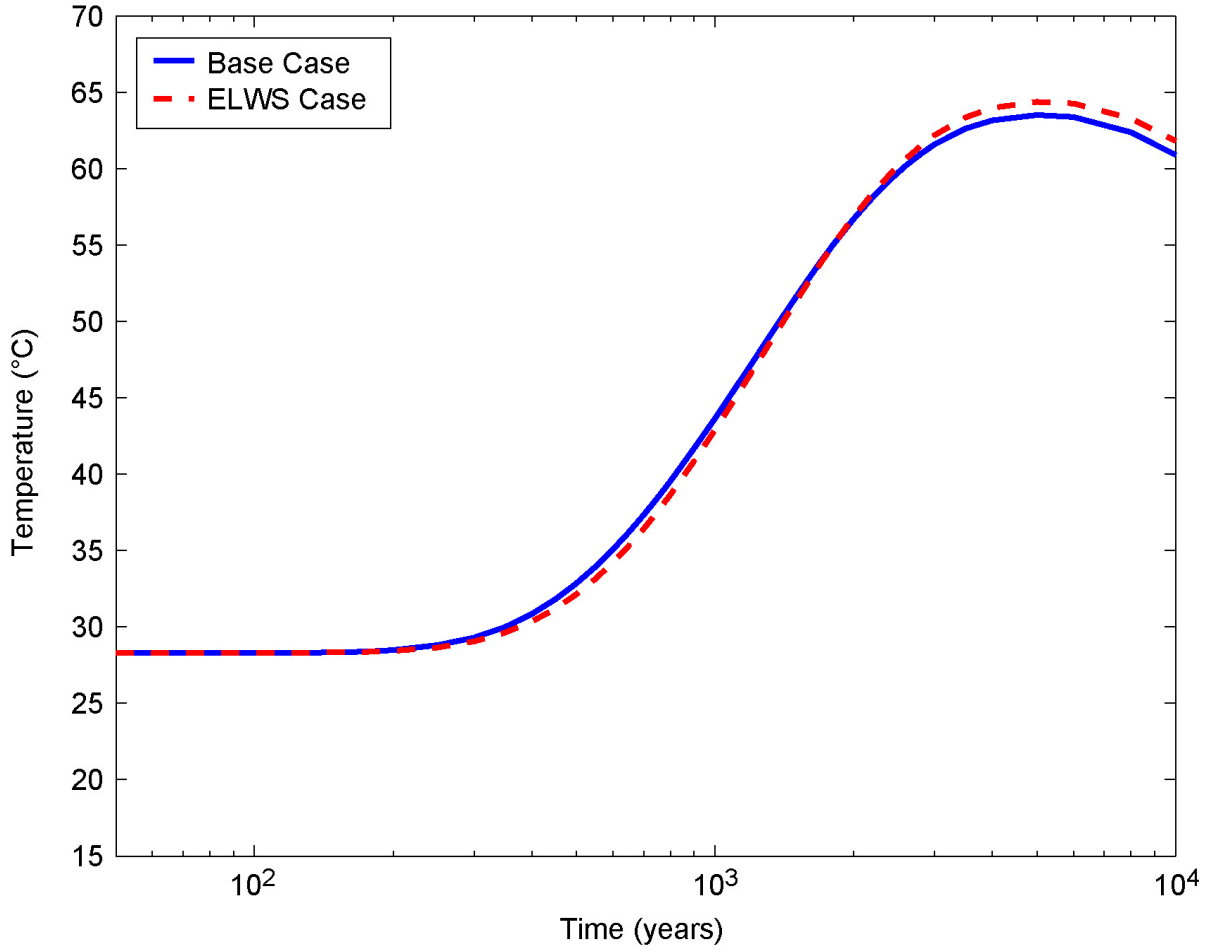

Source: Output DTN: MO0707TH2D3DDC.000, folder: /analyses/2D-LDTH , file: *P10-T_ELWS.dat.*

Figure 6.4.2-32. Temperature Histories at the Elevation of the Water Table, Comparing the ELWS Average Line Load with the Postclosure Reference Case Average Line Load

The base of the Paintbrush Tuff (PTn) unit for this location is 99.4 m below the ground surface and 211.1 m above the repository horizon. The peak temperature at this location (Figure 6.4.2-30) is slightly greater for the ELWS average than for the base case, within approximately 1°C, which is well within the range of uncertainty associated with thermal properties of the rock units. For the top of the CHn that is 85.2 m below the repository horizon and 193.3 m above the water table at this location, the peak temperature is slightly greater for the ELWS average than for the base case by approximately 2°C. The differences between results for the PTn and CHn are due to the proximity of the constant-temperature boundary condition at the ground surface, which limits the increase of rock temperatures. At the water table (Figure 6.4.2-32), which is 278.5 m below the repository horizon at this location, the peak temperature is approximately 1°C greater for the ELWS average than for the base case, and the peak occurs at approximately 5,000 years after closure. The smaller differences between these temperature histories are attributable to the delay time during which both line loads decay to small values and the thermal transients dissipate by diffusion.

These results support the statements in Sections 6.1 and 6.5 that the far-field temperature effects from the ELWS are closely comparable to, or less than, the postclosure reference base case.

6.4.2.7 Discussion

This section has demonstrated that, for nominal (intact drift) postclosure conditions, the loading arrangements selected from the ELWS will produce temperatures that comply with the postclosure temperature limits identified in Section 6.1. Case 1 represents the most likely maximum local thermal loading, and is slightly hotter than the postclosure reference case (Figures 6.4.2-4 through 6.4.2-9). The peak drift wall and waste package temperatures are similar (within a few degrees), but the post-peak temperatures are slightly hotter for Case 1. These results hold for the P10, P10L, and P90 cases, demonstrating the effects of percolation flux and host-rock thermal conductivity on peak temperature and temperature evolution.

For Case 2, the temperatures of individual waste packages are lower than for either Case 1 or the postclosure reference case (Figures 6.4.2-10 through 6.4.2-15). Whereas Case 2 includes the hottest waste package in the 96/2 emplacement sequence, that package is flanked by relatively numerous cooler DHLW packages in the Case 2 segment (Table 6.1-2).

On comparison with the 2-D LDTH results in Figures 6.4.2-1 through 6.4.2-3, the 3-D results show clearly that dimensionality and the arrangement of different types of waste packages need to be accounted for in predicting compliance with postclosure temperature limits. Peak temperatures from Figures 6.4.2-4 through 6.4.2-15 can be compared with the ANSYS finite-element analyses for Case 1 and Case 2, in Section 6.3.

The 3-D DDTH runs (Figures 6.4.2-16 through 6.4.2-27) and particularly the analysis of resaturation temperature (Figures 6.4.2-17, 6.4.2-19, 6.4.2-21, 6.4.2-23, 6.4.2-25, and 6.4.2-27), show that resaturation is temperature controlled. For the strongly heterogeneous waste package loading arrangement of Case 2, cooling histories for the DHLW packages depended on proximity to hotter CSNF packages, but resaturation of the host rock at each package was delayed until the rock temperature cooled to well below 96°C. From this it can be inferred that condensate flux was not focused on the cooler packages, but they were heated significantly by their neighbors.

For collapsed drifts, the analysis presented here shows peak waste package temperatures in the range from approximately 380°C to 400°C (Figure 6.4.2-28), compared to peak waste package temperature of 363°C for the postclosure reference base case. These results are conditioned on complete drift collapse at the time of closure. Also, they were calculated using the lower percolation flux (average for the emplacement area), lowest host-rock thermal conductivity, and lowest rubble thermal conductivity. Of these variables, the rubble effective thermal conductivity has by far the strongest influence on predicted waste package temperature.

Whereas these peak temperature values exceed the 300°C postclosure waste package temperature limit, the following mitigating factors apply:

- The low function for thermal conductivity for rubble (SNL 2007 [DIRS 181383], Appendix XI) is based on model calculations for spherical particles with 1-cm diameter, and total porosity of 30%, corresponding to a bulking factor of

approximately 20%. The bulking factor could be greater than 20%, and many of the voids are likely to be larger than those for 1-cm particles. Larger values of the bulking factor are associated with larger voids, and with a smaller drift collapse cavity, both of which contribute to better heat transfer. Hence the low rubble thermal conductivity is a bounding type value.

- Seismic-induced rockfall will be rare. This is because even with rockfall immediately after closure, and with bounding properties, waste package temperature will exceed 300°C for only 90 years or less (Figure 6.4.2-28). Drift collapse is three-dimensional and will not occur to equal extent for all waste packages due to the same seismic event, especially for lower-magnitude, higher-probability events. Also, partial collapse (analyzed in Section 6.5.1) will allow radiative transfer and convection in the remaining open volume (e.g., barometric pumping; SNL 2007 [DIRS 181648], Section 6.3).

- Peak waste package temperatures for drift collapse conditions can be lowered by extended ventilation (beyond the 72 years for Case 1 and 70 years for Case 2), as evaluated in *Thermal Management Flexibility Analysis* (SNL 2007 [DIRS 179196]). Although not evaluated in this report, peak waste package temperatures can also be lowered by increasing the end-to-end spacing of waste packages, for drift-collapse conditions as well as the nominal (intact drift) conditions identified in *Yucca Mountain Project Conceptual Design Report* (DOE 2006 [DIRS 176937], Section 4.6.5).

Hence peak waste package temperatures greater than 300°C will be relatively rare, occurring only for the hottest waste packages emplaced in lithophysal tuff, with the most unfavorable rubble thermal conductivity, after a seismic event of sufficient magnitude. This is also demonstrated by analogy to the base case results from the multiscale model, for which cumulative distributions of peak waste package temperature for complete drift collapse are plotted in Figure 6.4.2-29. Furthermore, measures have been identified that can be applied to the hottest waste packages to eliminate any significant possibility of exceeding 300°C in the event of drift collapse.

6.4.3 Geochemical Response to Range of Design Thermal Loadings

This section evaluates the geochemical responses for the Case 1 thermal loading conditions, representing local maximum loading as summarized in Section 6.1.7. Case 1 is selected because far-field evolution of water composition depends on average thermal loading conditions, and Case 1 represents such conditions more realistically than Case 2. Case 2, which is an extreme case dominated by three adjacent waste packages, is appropriate for use in evaluating process sensitivity in the very near-field (e.g., analyses in Sections 6.4.1 and 6.4.2). The responses are calculated using the near-field chemistry (NFC) model documented in *Engineered Barrier System: Physical and Chemical Environment* (SNL 2007 [DIRS 177412], Section 6.3.2). The results, combined with the evaluation of features, events, and processes in Section 6.5, provide the needed assessment of geochemical system response to the anticipated range of thermal loading.

6.4.3.1 Application of the Near-Field Chemistry Model

The NFC model is used to describe the compositions of potential seepage waters for the total system performance assessment (TSPA). It tracks a packet of water as it percolates downward through the thermal field above the drift, accounting for the cumulative effects of water–rock interactions in the devitrified, welded tuff (represented in the NFC model by the lower lithophysal Tptpll unit). The cumulative amount of alkali feldspar dissolution for such a packet (the "water–rock interaction parameter," or WRIP) is a function of temperature as it moves downward through the host rock, and also of the transport velocity and other factors. The composition when a packet arrives at the evaporation front around the drift is taken to be the composition of potential seepage into the drift. The evaporation front corresponds to the boiling front during the boiling period; once drift wall temperatures drop below boiling, the boiling front collapses to the drift wall and seepage is possible.

In the NFC model, the evolution of the thermal field through time is calculated using the method developed and validated for use in *In-Drift Natural Convection and Condensation* (SNL 2007 [DIRS 181648], Section 6.3). The method uses a conduction-only analytical solution, implementing the transient solution for continuous point sources in an infinite medium (Carslaw and Jaeger 1959 [DIRS 100968], p. 261) to represent finite line sources. Using the principle of superposition, contributions from all 108 drifts (each as a finite line source) are summed with the initial in situ geotemperature profile, to calculate a thermal profile above each drift location evaluated. The land surface is assumed to be 300 m above the drift center, and is held isothermal using the method of images (i.e., by adding image sources; Carslaw and Jaeger 1959 [DIRS 100968], p. 273). The contribution of the geothermal gradient is based on analysis of borehole temperature data from borehole SD-12. The NFC model assumes a typical repository depth of 300 m; the predicted geothermal gradient ranges from 17°C at the land surface to 23.4°C at the repository level (SNL 2007 [DIRS 177412], Section 6.3.2.4.3). The model implements the same analytical ventilation model for the preclosure ventilation period as *In-Drift Natural Convection and Condensation* (SNL 2007 [DIRS 181648], Section 6.3.5.2.5).

The evolution of the thermal field is modeled at 16 locations in 7 drifts, for three different values of the host-rock thermal conductivity (see SNL 2007 [DIRS 177412], Section 6.3.2.4). Each location is identified by a unique value of a thermal measure, which is the sum of the maximum drift wall temperature, in °C, and the time at which the drift wall drops below boiling, in years. The thermal measure developed for the NFC model (SNL 2007 [DIRS 177412], Section 6.3.2.4.5) is similar to and derived from the waste package selection process used in *Multiscale Thermohydrologic Model* (SNL 2007 [DIRS 181383], Appendix VIII). The NFC model generates a map of WRIP values for each location, for twenty different sets of climate-state-specific percolation fluxes, for 102 points in time, from repository closure to 1 million years after closure.

6.4.3.2 Near-Field Chemistry Model Modifications for Case 1

To represent potential seepage water chemistry for Case 1 a new WRIP map is constructed, implementing changes to the thermal analysis part of the NFC model. Thermal analysis for this purpose is limited to the 16 locations in Drift Choice 5. Drift 5 was chosen because it is a repository-center location, where the temperature effect from higher thermal loading is expected

to be greatest (Figure 6.4.3-1). To do this, the Mathcad file (DTN: SN0703PAEBSPCE.006 [DIRS 181571], folder: \WRIP calculations\Mathcad calculations of WRIP values\thermal-K, 10th percentile, file: *Model for thermal field, 10th percentile, Drift choice 5.xmcd*) that calculates the thermal field through time for the 10th percentile rock thermal conductivity value was modified. The file has an array containing the line load as a function of time, and the new line load was inserted into this array. The Case 1 line load is based on data from Output DTN: MO0705SUPPCALC.000 (folder: \Select Hot and Cold Cases, file: *Hottest and Coolest Discrete Values 1E6 yr (ventilation).xls*) for the hottest 7-point segment in the drift. It includes a preclosure ventilation model assuming 72 years of ventilation. This line load was converted to the format and time steps necessary for use in the NFC model file (Output DTN: MO0707GEORESPO.000, folder: \Calculating the line load, file: *Qload.xls*). The Case 1 average line load is compared to the postclosure reference base case load in Figure 6.4.3-2. The Case 1 line load is shifted by 22 years because of the longer ventilation period, but otherwise does not differ greatly from the postclosure thermal reference case.

The original NFC file is from DTN: SN0703PAEBSPCE.006 [DIRS 181571] (folder: \WRIP calculations\Mathcad calculations of WRIP values\thermal-K, 10th percentile, file: *Model for thermal field, 10th percentile, Drift choice 5.xmcd*). The file modified for use in this report is in Output DTN: MO0707GEORESPO.000 (folder: \WRIP calculations for high line load case, file: *Model for thermal field, 10th percentile, Drift choice 5, hot case.xmcd*). A copy of the embedded spreadsheet containing the model results is saved separately (file: *Drift 5, high line load.xls*).

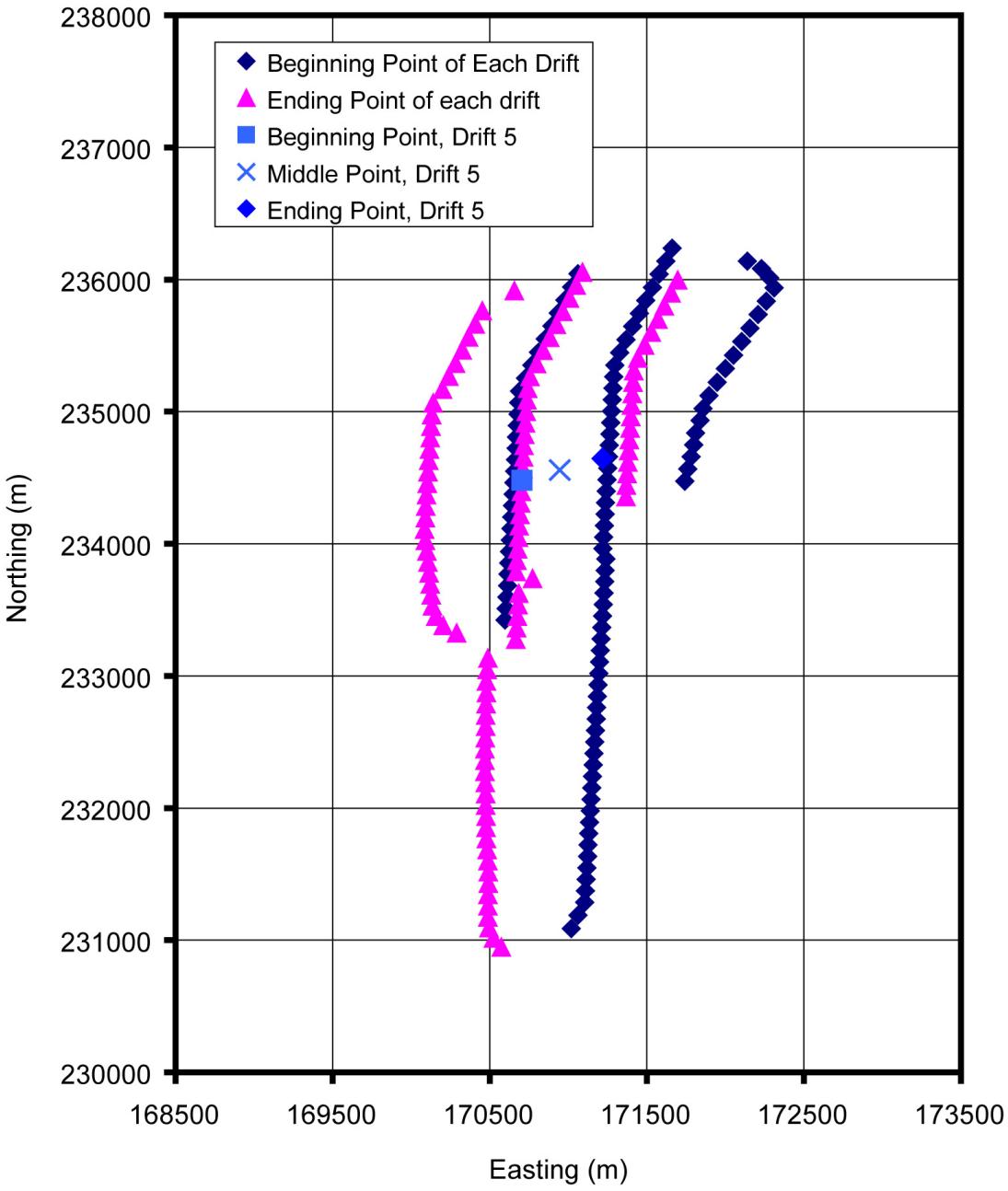

Source: Output DTN: MO0707GEORESPO.000, file: *Repository map for drift 5.xls*.

Figure 6.4.3-1. Repository Layout, Showing the Location of Drift 5

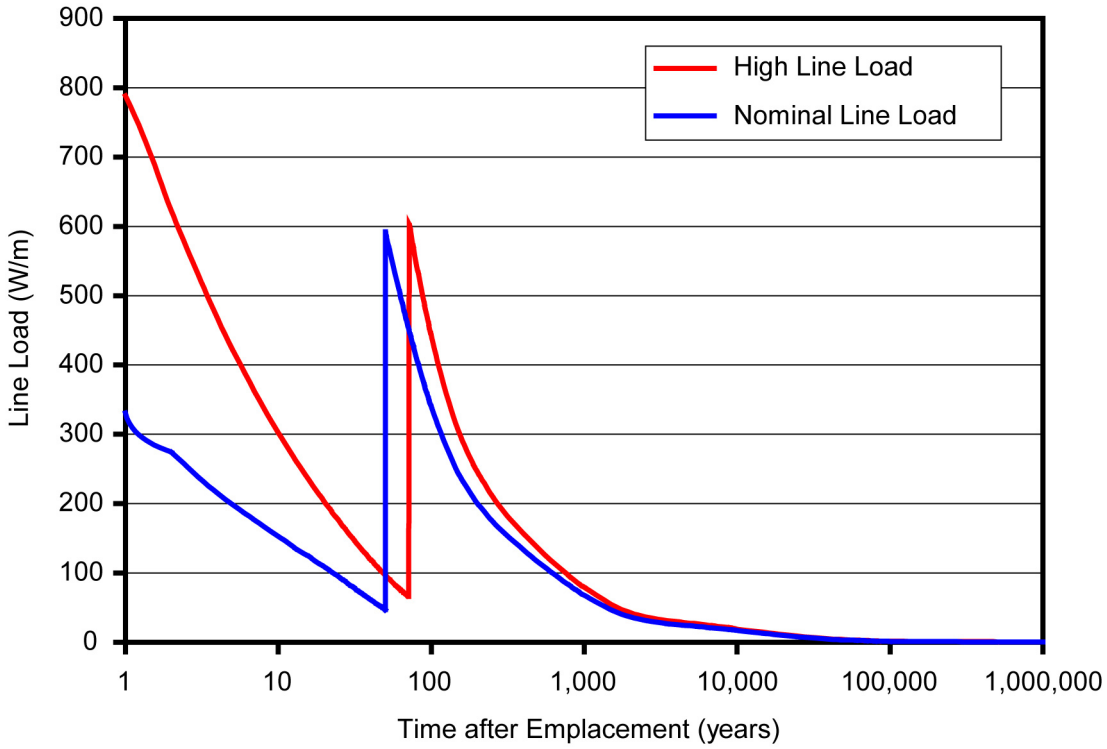

Source: Output DTN: MO0707GEORESPO.000, folder: \Calculating the line load, file: *Qload.xls*.

NOTE: The "High Line Load" is for Case 1 identified in this report, i.e., the 13-package average for the segment encompassing the 7-package hottest segment from Section 6.1.3, which has 72 years of preclosure ventilation. The "Nominal Line Load" is the postclosure reference case discussed in Section 6.1, which has 50 years ventilation.

Figure 6.4.3-2. Comparison of Line Loads Used in the Baseline NFC Simulations for TSPA, and the Higher Line Load Used in This Thermal Envelope Study

Once the evolution of the thermal field was modeled for the waste package locations in Drift 5, a new WRIP map was calculated. The Mathcad file used to calculate the WRIP map for the NFC model was modified slightly to generate a map for only the Drift 5 locations, rather than all seven drifts used in the baseline case. The changes are documented in the file itself, and consist mostly of changing array and index counters so that a WRIP map is only generated for one drift. An additional modification was made to the routine that calculates the boiling duration, to account for the 72-year ventilation period. The original NFC file is from DTN: SN0703PAEBSPCE.006 [DIRS 181571] (folder: \thermal-K 10th percentile, file: *Model for water-rock interactions, 10th percentile.xmcd*). The file modified for use in this analysis is in Output DTN: MO0707GEORESPO.000 (folder: \WRIP calculations for high line load case, file: *Model for water-rock interactions, 10th percentile, thermal env study.xmcd*). A copy of the embedded spreadsheet containing the WRIP map for the Drift 5 locations is saved separately as Output DTN: MO0707GEORESPO.000 (folder: \WRIP calculations for high line load case, file: *WRIP map for Drift 5, high load case.xls*).

Modifications to the files described above are simply changes to the inputs to allow running of a subset of the locations evaluated in the base case used by TSPA. These changes have no effect on the model itself. Also, as will be discussed below, the effect of the Case 1 line load on the

chemistry is relatively minor—the existing EQ3/6 seepage output files for the NFC model easily capture the range of WRIP values observed in these simulations. Hence, the calculations carried out here are within the validation range of the NFC model.

6.4.3.3 Comparison of Case 1 with Base Case Results

In this section, the results of the high line load calculations are compared to the TSPA base case results. The TSPA base case results for the thermal field are from DTN: SN0703PAEBSPCE.006 [DIRS 181571] (folders: \WRIP calculations\Mathcad calculations of WRIP values\thermal-K, 10th percentile, file: *Drift 5.xls*). For convenience, they are included in Output DTN: MO0707GEORESPO.000 (folder: \WRIP values for the nominal case, file: *Drift 5, nominal.xls*). The base case WRIP values for the Drift 5 locations were extracted from DTN: SN0703PAEBSPCE.006 [DIRS 181571] (folders: \WRIP calculations\Mathcad calculations of WRIP values\thermal-K, 10th percentile, file: *Water-rock interactions, 10th percentile.xls*). This file contains the WRIP maps for all seven drifts; for convenience, the data for Drift 5 are included in Output DTN: MO0707GEORESPO.000 (folder: \WRIP values for the nominal case, file: *WRIP map for Drift 5, nominal case.xls*).

The difference in thermal loading produces slightly higher drift wall temperatures through time (Figure 6.4.3-3). Maximum drift wall temperatures at both locations are 12°C to 13°C hotter for Case 1, reaching a maximum of 159.7°C for location 7, relative to 146.9°C for the nominal case at that location. The slight difference between the peak temperatures for location 7, compared with the seven-package 96-2 segment from Table 6.1-2, is attributable to the three-dimensional nature of the NFC thermal analysis compared to the infinite line-source calculations in Section 6.1.4. The Case 1 and base-case drift wall temperatures converge slowly over time, and are less than 1°C different by 50,000 years after closure.

The chemistry of potential seepage is calculated as a function of time since repository closure, for both the base case and Case 1 (Output DTN: MO0707GEORESPO.000, file: *Predicted seepage chemistry.xls*). The calculations are carried out for waste package locations 7 and 15 in Drift 5, for 41 time steps after closure. The WRIP values for each location are taken directly from the base case and Case 1 WRIP maps described in the previous section, for the percolation flux and time step of interest. Percolation flux set-up number 10 from the WRIP map is used, corresponding to the most probable (47.5%) case. The temperature at each time step is taken directly from the base case and Case 1 thermal analysis files described in the previous section. The temperature used was the drift wall temperature or 96°C if the drift wall was at boiling. This is in slight variance with the base case WRIP model for TSPA, which calculates the temperature of the evaporation front from the in-drift partial pressure of water vapor after the boiling period. The temperature calculated from the partial pressure of water vapor may be a few degrees cooler than the drift wall temperature, for a time period after boiling, but converges to the drift wall temperature over time. This small variation is needed for this analysis because, unlike TSPA, this analysis does not include explicit modeling of in-drift humidity. This approximation has no significant effect on the predicted seepage composition, which depends parametrically on WRIP, temperature, and relative humidity.

The WRIP values and the temperature are then used to extract predicted potential seepage water compositions from the NFC model EQ3/6 “seepage” output files for the Group 1 starting water

composition (DTN: SN0701PAEBSPCE.002 [DIRS 179425], folder: \EQ3_6 seepage\Gp1). This was done by extracting the water compositions at the temperature of interest from the output files with the bounding WRIP values (WRIP designations 0, B, C….I, J, L) and interpolating between the compositions using the WRIP values from the base case and Case 1 WRIP maps (see Output DTN: MO0707GEORESPO.000, folder: \WRIP values for the nominal case, file: *WRIP map for Drift 5, nominal case.xls* and folder: \WRIP calculations for the high load case, file: *WRIP map for Drift 5, high load case.xls*). The end results of these calculations are tables of seepage composition as a function of time for each of the two locations and two line loads. These are tabulated in spreadsheet *Predicted seepage chemistry.xls* in Output DTN: MO0707GEORESPO.000.

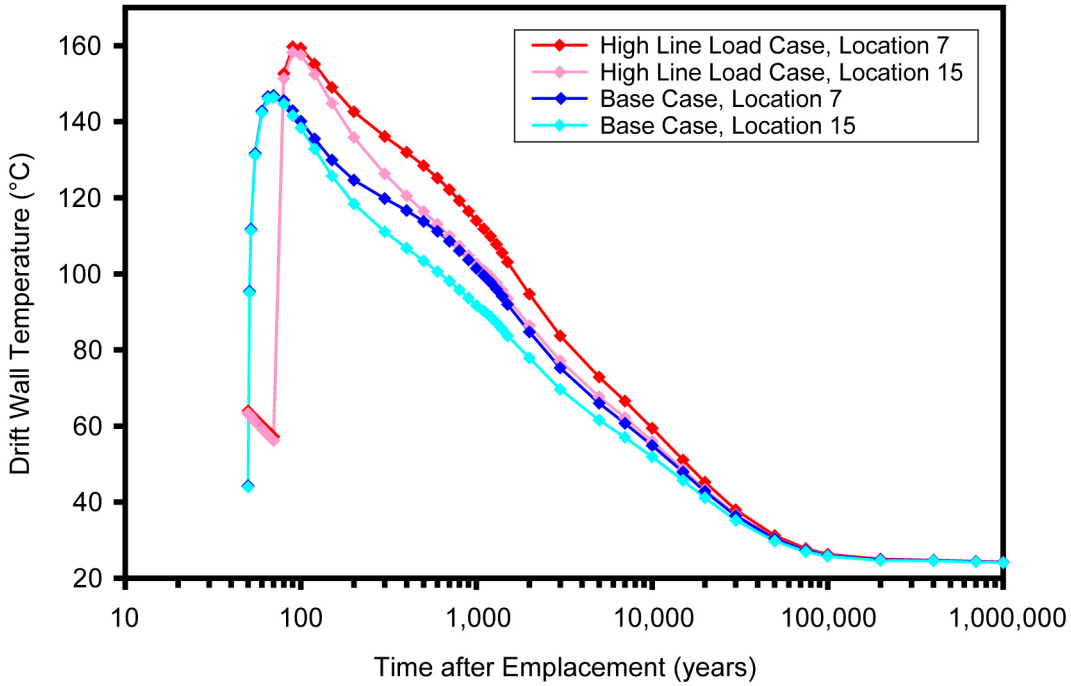

Source: Output DTN: MO0707GEORESPO.000, file: *Drift 5, drift wall temperatures at locs 7 and 15.xls* (see worksheet: "Drift wall temps,1").

NOTE: The "High line load case" is for Case 1 identified in this report, i.e., the 13-package average for the segment encompassing the 7-package hottest segment from Section 6.1.3, which has 72 years of preclosure ventilation. The "Base Case" is the postclosure reference case discussed in Section 6.1, which has 50 years ventilation.

Figure 6.4.3-3. Comparison of Drift Wall Temperatures through Time at Drift 5 Locations 7 and 15, for the TSPA Base Case and the High Line Load Case

6.4.3.4 Discussion

The predicted seepage water compositions are compared to the base case values in Figure 6.4.3-4. Because Cl^- and NO_3^- are conserved in the NFC model, they do not change regardless of the degree of water–rock interaction, so they are not shown in the figure. Similarly, SO_4^{2-} is conserved because water compositions never saturate with respect to sulfate minerals. The degree of water–rock interaction, as typified by the WRIP value, is slightly greater for Case 1 at any given time step, because the feldspar dissolution rate is temperature-dependent. As

discussed in *Engineered Barrier System: Physical and Chemical Environment* (SNL 2007 [DIRS 177412], Section 6.3.2.6) the general effect of this is increased pH, increased concentrations of K and Na in the water, and decreased Ca and Mg concentrations at higher WRIP values (amounts of alkali feldspar dissolved), as celadonite ($KMgAlSi_4O_{10}(OH)_2$) begins to precipitate.

Surprisingly, the pH curves do not vary greatly for the four cases (Figure 6.4.3-4(a)). Two factors influence the pH: temperature and feldspar dissolution. Elevated temperature causes CO_2 degassing and increases the local CO_2 partial pressure, driving the pH down during the boiling period. Temperature-dependent feldspar dissolution consumes H^+ and increases alkalinity, increasing the pH. The pH peaks when the WRIP value peaks, and then decreases slightly. At much longer times, the degree of feldspar dissolution is less, and the temperature effect becomes dominant, resulting in lower pH, eventually returning to the initial value for the pore water as the host rock cools back to ambient. The interaction of these two processes results in a crossover at approximately 3,000 to 5,000 years. Prior to this, the higher WRIP values for Case 1 result in slightly higher pH values relative to the baseline cases; after this time, the effect of the WRIP is less, and the higher temperatures for Case 1 result in lower pH values relative to the baseline cases.

$SiO_2(aq)$ is assumed to be in equilibrium with amorphous silica; hence, its solubility is mostly a function of temperature. The plateau in Figure 6.4.3-4(f) represents the boiling period when the temperature is fixed at 96°C. Because silica solubility also depends on pH, the plateau value increases slightly with time as the pH increases with increasing water–rock interaction.

In summary, the effects from Case 1 thermal loading on the composition of potential seepage water are increased pH, Na, and K and decreased Ca and Mg. These conditions are favorable with respect to localized corrosion of the waste package outer barrier; the incidence of localized corrosion for Alloy 22 is decreased by higher pH and less Cl^- (SNL 2007 [DIRS 178519], Section 8.1). As water–rock interaction increases (e.g., with temperature or thermal loading) the carbonate alkalinity increases, which increases the pH and the total dissolved inorganic carbon (for any particular value of the CO_2 fugacity). Increased alkalinity and pH can enhance the solubilities for certain dissolved radionuclides by carbonate complexation. The result is that thermal loading could slightly increase the mobility of radionuclides in the near-field host rock, but this can occur only after waste packages are breached. By the time when waste package failures become significant, water–rock interaction for potential seepage will have returned to pre-heating ambient conditions, so the effect is likely to be insignificant in TSPA.

The foregoing discussion of seepage water composition does not address evaporative evolution of water on the drip shield, waste package, or in the invert, which may occur when seepage occurs during the thermal period (e.g., within the first 100,000 years). The values of the WRIP parameter calculated for Case 1 are greater than the base case, but within the range of WRIP generated for the TSPA base case. This is because increased water–rock interaction can occur both because of higher temperature and slower water transport in the host rock above the drift. For the lowest values of flux (i.e., slowest transport) seepage is unlikely. Hence, for percolation flux values likely to produce seepage, the water–rock interaction predicted for Case 1 thermal conditions is well within the validated range of the NFC model.

For the coldest thermal loading conditions, depending on the proximity of cold drifts to hotter ones, the extent of water–rock interaction decreases, so the temperature and composition of potential seepage water in the host rock remain close to the starting or ambient values (Section 6.1).

6.4.3.5 Summary

Calculations were carried out using the NFC model with slight modifications to input parameters and the output format, to evaluate the effects of greater thermal loading (Case 1) on the composition of potential seepage water. Comparisons to the TSPA base case indicate that the effects Case 1 thermal loading are minor with respect to potential seepage water chemistry. In general, the effects are to increase the degree of alkali feldspar dissolution by a small amount: the aqueous elemental concentrations change by less than a factor of two in all cases. The resulting effects—increased pH, Na, and K and decreased Ca and Mg—are favorable with respect to localized corrosion of the waste package outer barrier. The incidence of localized corrosion for Alloy 22 is decreased by higher pH and less Cl^- (SNL 2007 [DIRS 178519], Section 8.1). As the WRIP increases, seepage waters that are Ca-rich then become progressively more Na- and K-rich and Ca-poor. The initial compositions for potential seepage waters (i.e., early during the thermal period) evolved into low-pH Ca-NO_3 or Ca-Cl brines, but as calcium is depleted in the water, they cross the calcite chemical divide and instead evolve into neutral or basic Na-K-Cl-NO_3 brines as described in *Engineered Barrier System: Physical and Chemical Environment* (SNL 2007 [DIRS 177412], Section 6.13.3).

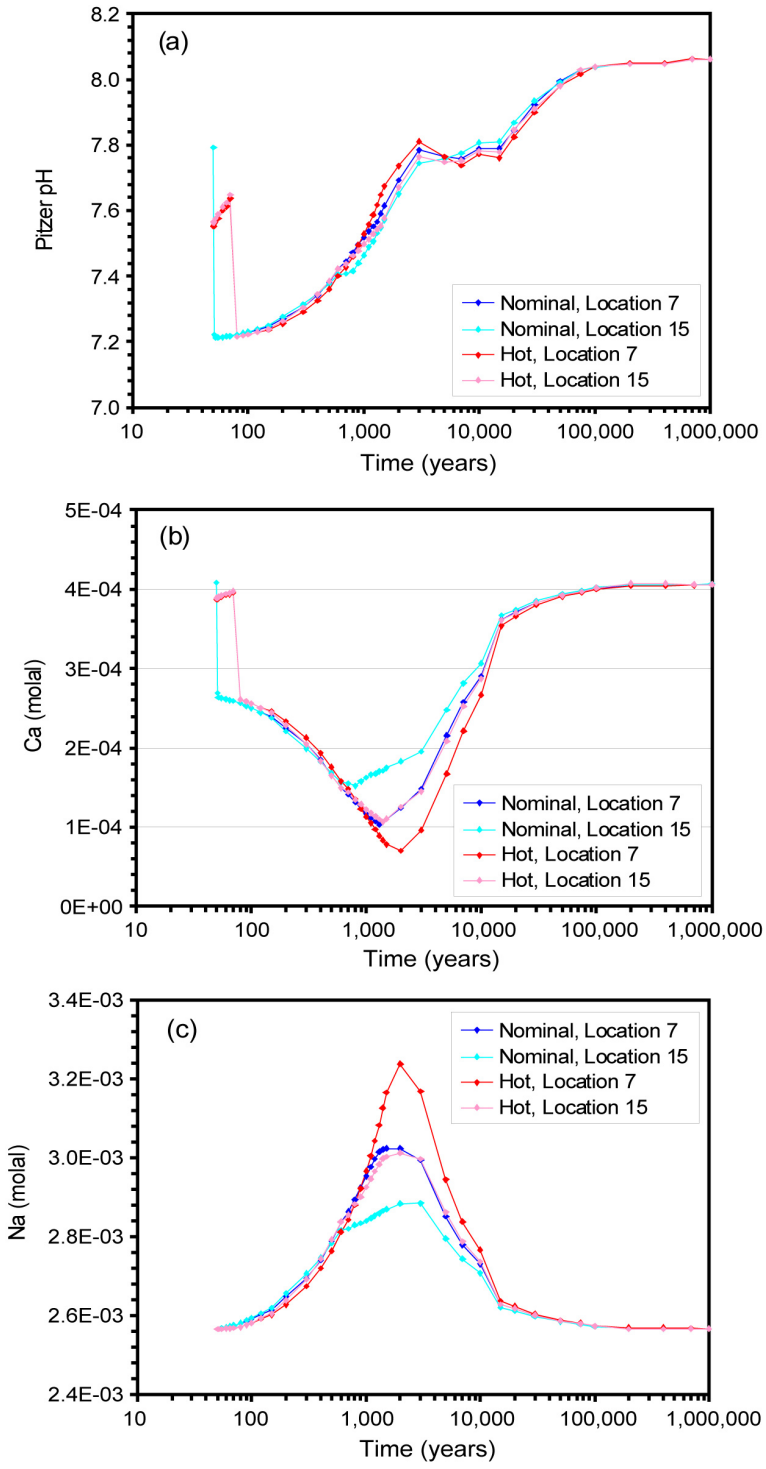

Source: Output DTN: MO0707GEORESPO.000, file: *Predicted seepage chemistry.xls.*

NOTE: X-axis is time after emplacement. The "Hot" case is for Case 1 identified in this report, i.e., the 13-package average for the segment encompassing the 7-package hottest segment from Section 6.1.3, with 72 years of preclosure ventilation. The "Nominal" case is the postclosure reference case discussed in Section 6.1, with 50 years of ventilation.

Figure 6.4.3-4. Comparison of Predicted Seepage Compositions for the Baseline TSPA Case and the High Line Load Case: (a) pH; (b) Ca Concentration; (c) Na Concentration

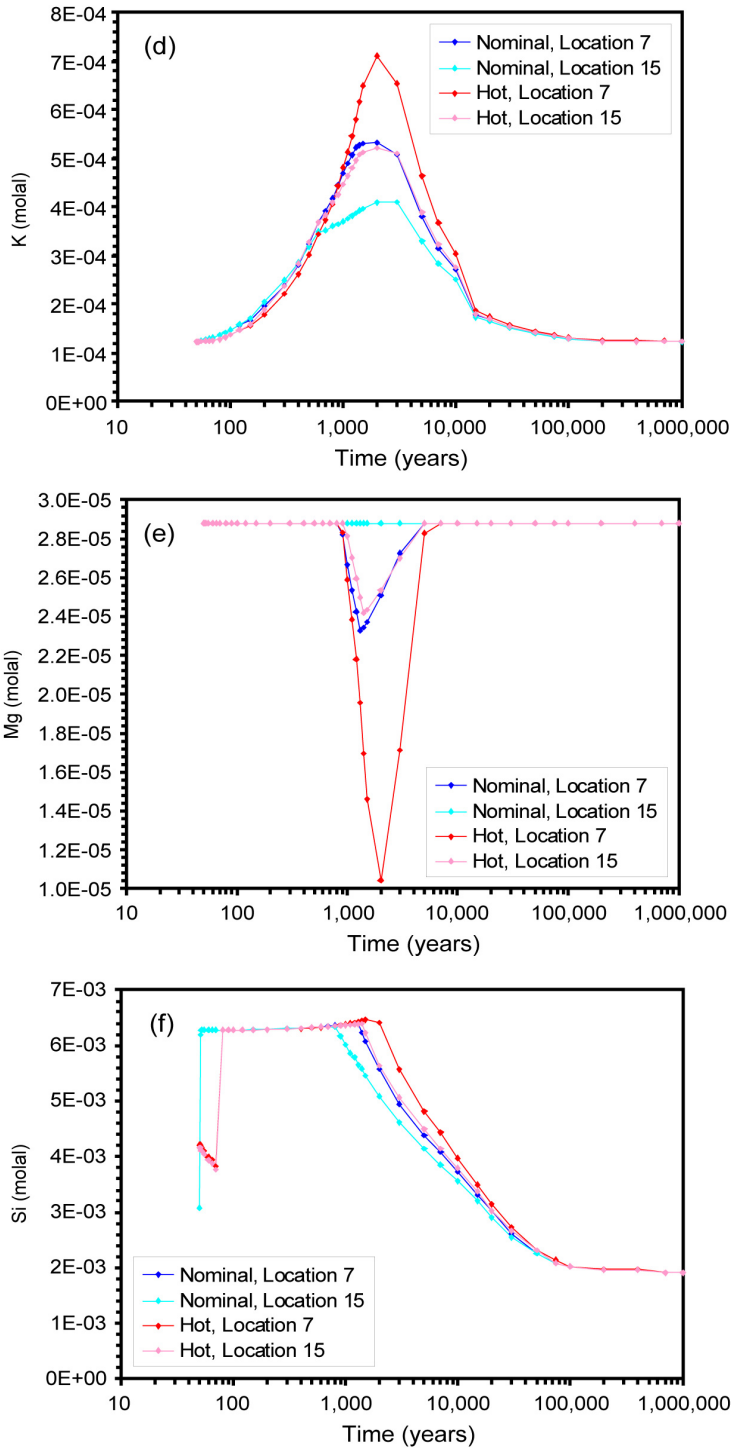

Source: Output DTN: MO0707GEORESPO.000, file: *Predicted seepage chemistry.xls.*

NOTE: X-axis is time after emplacement. The "Hot" case is for Case 1 identified in this report, i.e., the 13-package average for the segment encompassing the 7-package hottest segment from Section 6.1.3, with 72 years of preclosure ventilation. The "Nominal" case is the postclosure reference case discussed in Section 6.1, with 50 years of ventilation.

Figure 6.4.3-4. Comparison of Predicted Seepage Compositions for the Baseline TSPA Case and the High Line Load Case: (d) K Concentration; (e) Mg Concentration; and (f) Si Concentration (Continued)

6.5 FEATURES, EVENTS, AND PROCESSES AFFECTED BY THE RANGE OF THERMAL LOADING

This section evaluates the features, events, and processes (FEPs) that are affected by the range of thermal loading identified in Section 6.1. The affected FEPs are selected from among 374 total, and a rationale is provided as to whether: (1) the screening justification used for excluded FEPs applies to the anticipated range of thermal loading, and (2) the modeling basis used for included FEPs has the capability to represent the range of thermal loadings by representing the appropriate features and processes.

Thermally sensitive included FEPs (Table 6.5-1) are arranged in groups corresponding to categories of processes, showing how thermal effects are included in TSPA. Analyses presented in Section 6.4 and Table 6.5-2 of this report show that the current modeling bases for including FEPs associated with the following processes is valid for the temperature range and thermal duration associated with the anticipated range of thermal loading.

These included FEPs, along with excluded ones that are sensitive, are listed in Table 6.5-2. Backed by Section 6.4 and the supporting references, the analyses in Table 6.5-2 show that there are no significant impacts to included or excluded FEPs from the anticipated range of thermal loading, for intact (uncollapsed) drift conditions.

Of the 374 FEPs (SNL 2007 [DIRS 179476]), only those listed in Table 6.5-2 are potentially affected by the anticipated range of thermal loading. Given the ways that FEPs are defined and organized, some FEPs were not selected as affected because of overlap with other FEPs. All of the FEPs listed in Table 6.5-2 are analyzed in *Features, Events, and Processes for the Total System Performance Assessment* (SNL 2007 [DIRS 179476], indexed by FEP number), which should be the source for the complete screening justifications.

The anticipated range of thermal loading, i.e., emplacement of the ELWS as described in Section 6.1, will cause minor changes in the peak postclosure temperatures for some waste package locations for intact drift conditions, while lowering peak temperatures at other locations (Section 6.4.2.3). At the hotter locations, the duration of the thermal period will increase slightly (compared to the reference case) while the duration will be less at cooler locations. Analyses presented in this report, as discussed in Table 6.5-2, show that these minor changes do not significantly impact the screening justifications for excluded FEPs, or the modeling basis for FEPs that are included in TSPA.

Table 6.5-1. Thermally Sensitive Included FEPs, Arranged by Process Categories

FEP Number	FEP Description
Water–rock geochemical interaction in the host rock	
2.2.08.01.0B	Chemical characteristics of groundwater in the UZ
2.2.08.12.0A	Chemistry of water flowing into the drift
Evaporative concentration of seepage water and condensate in the EBS	
2.1.09.01.0A	Chemical characteristics of water in drifts
2.1.09.01.0B	Chemical characteristics of water in waste package
2.1.11.08.0A	Thermal effects on chemistry and microbial activity in the EBS

Table 6.5-1. Thermally Sensitive Included FEPs, Arranged by Process Categories (Continued)

FEP Number	FEP Description
Degradation of the engineered barrier (i.e., drip shield, waste package, and waste form) including effects from drift collapse	
1.2.03.02.0A	Seismic ground motion damages EBS components
1.2.03.02.0C	Seismic-induced drift collapse damages EBS components
2.1.02.01.0A	DSNF degradation (alteration, dissolution, and radionuclide release)
2.1.02.02.0A	CSNF degradation (alteration, dissolution, and radionuclide release)
2.1.02.03.0A	HLW glass degradation (alteration, dissolution, and radionuclide release)
2.1.03.01.0A	General corrosion of waste packages
2.1.03.03.0A	Localized corrosion of waste packages
Preclosure ventilation efficiency	
1.1.02.02.0A	Preclosure ventilation
Timing of dryout, rewetting, seepage, drift wall condensation, and the onset of environmental conditions that facilitate waste form degradation	
1.2.03.02.0D	Seismic-induced drift collapse alters in-drift thermohydrology
2.1.06.06.0A	Effects of drip shield on flow
2.1.08.01.0A	Water influx at the repository
2.1.08.03.0A	Repository dry-out due to waste heat
2.1.08.04.0A	Condensation forms on roofs of drifts (drift-scale cold traps)
2.1.08.04.0B	Condensation forms at repository edges (repository scale cold traps)
2.1.08.11.0A	Repository resaturation due to waste cooling
2.1.09.01.0A	Chemical characteristics of water in drifts
2.1.09.01.0B	Chemical characteristics of water in waste package
2.1.11.01.0A	Heat generation in EBS
2.1.11.02.0A	Non-uniform heat distribution in EBS
2.1.11.09.0A	Thermal effects on flow in the EBS
2.1.11.09.0C	Thermally driven flow (convection) in drifts
2.2.07.10.0A	Condensation zone forms around drifts
2.2.07.11.0A	Resaturation of geosphere dryout zone
2.2.07.20.0A	Flow diversion around repository drifts
2.2.10.10.0A	Two-phase buoyant flow/heat pipes
2.2.10.12.0A	Geosphere dry-out due to waste heat
Diffusive or advective transport of radionuclides and radionuclide bearing colloids	
2.1.09.08.0A	Diffusion of dissolved radionuclides in EBS
2.1.09.24.0A	Diffusion of colloids in EBS
Changes in waste inventory associated with the anticipated range of thermal loading	
2.1.01.01.0A	Waste inventory
2.1.01.03.0A	Heterogeneity of waste inventory

Note that wide ranges of peak temperature and thermal duration are already incorporated in the TSPA through use of multiscale model results that include variability in host-rock thermal properties, percolation flux, waste package type, and proximity to the repository edge (SNL 2007 [DIRS 181383], Section 6.3[a]). For included FEPs, effects from thermal durations spanning a range from a few hundreds of years for intact-drift, repository-edge thermal conditions, to many

thousands of years for collapsed-drift, repository-center conditions, are already represented in the TSPA modeling basis. For excluded FEPs, the screening justifications address the same range of duration where significant duration effects have been identified (e.g., thermal sensitization).

The potentially important differences in thermal conditions associated with the anticipated range of thermal loading arise in the case of partial or complete drift collapse immediately after repository closure. For such conditions, the peak temperatures for features of the engineered barrier may exceed the temperature ranges used in screening justifications for excluded FEPs, or in the modeling basis for included FEPs. Based on the rationale presented in Table 6.5-2, the following FEPs (SNL 2007 [DIRS 179476]) may be sensitive to peak temperatures greater than the temperatures used in documented screening justifications:

1.2.03.02.0A – Seismic ground motion damages EBS components (included)
1.2.03.02.0B – Seismic-induced rockfall damages EBS components (included)
1.2.03.02.0C – Seismic-induced drift collapse damages EBS components (included)
2.1.07.05.0A – Creep of metallic materials in the waste package (excluded)
2.1.07.05.0B – Creep of metallic materials in the drip shield (excluded)
2.1.11.05.0A – Thermal expansion and stress of in-package EBS components (excluded)
2.1.11.06.0A – Thermal sensitization of waste packages (excluded).

In addition, the following excluded FEPs (SNL 2007 [DIRS 179476]) describe degradation of spent nuclear fuel (SNF) cladding, and are excluded for CSNF (TSPA takes no performance credit for CSNF cladding integrity), but changes in peak waste form temperature and thermal duration may impact disposition of these FEPs for naval SNF:

2.1.02.13.0A – General corrosion of cladding (excluded)
2.1.02.16.0A – Localized (pitting) corrosion of cladding (excluded)
2.1.02.17.0A – Localized (crevice) corrosion of cladding (excluded)
2.1.02.19.0A – Creep rupture of cladding (excluded)
2.1.02.22.0A – Hydride cracking of cladding (excluded)
2.1.02.26.0A – Diffusion controlled cavity growth in cladding (excluded).

Support for excluding the effects from early drift collapse immediately after repository closure (e.g., within 90 years after closure), on the screening or TSPA disposition of the *excluded and included* FEPs listed above, is provided in Section 6.5.1. The low probability of drift collapse during the first 90 years after repository closure, combined with the limited duration of such temperature conditions and the gradational nature of temperature dependence for these FEPs, allows the effects to be excluded because of the low risk associated with seismically induced drift collapse immediately after closure.

Note that the effects associated with the range of thermal loading are limited to the repository near field. FEPs concerning thermally driven processes acting in the far field are not significantly affected by thermal loading from the ELWS, as discussed in Section 6.4 of this report, because the overall global average line load for the ELWS is less than, or closely comparable to the postclosure thermal reference case (Sections 6.1 and 6.4.2).

Table 6.5-2. Evaluation of Sensitivity to the Range of the Thermal Loading, for Thermally Sensitive FEPs

FEP	FEP Name	Status	Groups	Evaluation for Impact of Anticipated Range of Thermal Loading
1.1.02.02.0A	Preclosure ventilation	Included	UZ, EBS	Ventilation heat-removal efficiency is relatively insensitive to, and tends to increase with, higher thermal loading. The modeling basis for TSPA can be readily adapted to any thermal loading arrangement, although the effect on ventilation efficiency from changes in thermal loading has been shown to be small (SNL 2007 [DIRS 179196], Section 6.3).
1.2.03.02.0A	Seismic ground motion damages EBS components	Included	DE, EBS	Analyses were performed using EBS materials properties at 150°C to represent the effects of heating (SNL 2007 [DIRS176828]). Although peak postclosure temperatures will exceed 150°C for some waste packages (SNL 2007 [DIRS 181383]), this is an appropriate simplification because such temperatures will occur only briefly (up to approximately 150 years after closure) for nominal conditions (Sections 6.4.2.3 and 6.4.2.4 of this report). This result holds true for the anticipated range of thermal loading, for which postclosure temperature limits will be met for nominal conditions. For drift collapse, this representation is suitable for use with the range of thermal loading because of the low risk associated with seismically induced drift collapse immediately after repository closure (Section 6.5.1).
1.2.03.02.0B	Seismic-induced rockfall damages EBS components	Excluded	DE, EBS	Analyses were performed using EBS materials properties at 60°C and 150°C (SNL 2007 [DIRS 176828], Section 6.5.6; see also FEP 1.2.03.02.0A). Analyses using properties at 60°C and 150°C are applicable to thermal conditions, because sensitivity studies have demonstrated limited sensitivity of damage simulations to temperature (SNL 2007 [DIRS 176828], Section 8.2). This representation is suitable for use with the range of thermal loading because of the low risk associated with seismically induced drift collapse immediately after repository closure (Section 6.5.1).
1.2.03.02.0C	Seismic-induced drift collapse damages EBS components	Included	DE, EBS	The drip shield has ample strength that will prevent failure from static loading by drift-collapse rubble (SNL 2007 [DIRS 179476]), and damping by rubble prevents excessive displacement that could cause drip shield separation. This representation is suitable for use with the range of thermal loading because of the low risk associated with seismically induced drift collapse immediately after repository closure (Section 6.5.1).
1.2.03.02.0D	Seismic-induced drift collapse alters in-drift thermohydrology	Included	DE, EBS	The anticipated range of thermal loading will impact in-drift temperatures when drift collapse occurs during the thermal period. Dry conditions will pertain after drift collapse, until after near-field temperatures cool to approximately 100°C. Thus, the effects from the range of thermal loading on in-drift thermohydrology are limited to delay, and this FEP can be represented for the anticipated range of thermal loading, using the current modeling basis for TSPA. See other FEPs (e.g., 2.1.11.06.0A and 2.1.11.06.0B) for discussion of the effects from higher temperatures.

Table 6.5-2. Evaluation of Sensitivity to the Range of the Thermal Loading, for Thermally Sensitive FEPs (Continued)

FEP	FEP Name	Status	Groups	Evaluation for Impact of Anticipated Range of Thermal Loading
1.2.03.02.0E	Seismic-induced drift collapse alters in-drift chemistry	Excluded	EBS	Thermal loading affects the EBS temperatures when drift collapse occurs during the thermal period. Water chemistry is potentially important to the repository system only after near-field temperatures return to approximately 100°C, when seepage becomes possible (BSC 2005 [DIRS 172232]). Such conditions are included in TSPA and are within the range of applicability for the near-field chemistry model (SNL 2007 [DIRS 177412]). Thermal loading effects on in-drift chemistry are therefore limited to delay, and slight changes in composition of potential seepage waters, as discussed in Section 6.4.3 of this report. See excluded FEP 2.2.08.04.0A for discussion of related processes affecting seepage composition.
2.1.01.01.0A	Waste inventory	Included	WF	The ELWS described in Section 6.1 has average burnup (waste package or mass weighted) of approx. 47 GWd/ton (Output DTN: MO0705SUPPCALC.000, file: *ELWS Avg. Burnup Calc.xls*), whereas the postclosure reference case corresponds to approximately 38 GWd/ton with an uncertainty multiplier that extends this to a (uniformly sampled) range from 32 to 53 GWd/ton with an average of 43 GWd/ton for CSNF (all values rounded to two significant figures; SNL 2007 [DIRS 180472], Tables 6-5 and 7-2[a]). In addition for TSPA the total inventory includes the contingency area, which amounts to approximately 4% more waste than will actually be emplaced in the repository (SNL 2007 [DIRS 180472], Section 5.14[a]). The effect of burnup associated with the range of thermal loading (and represented by the ELWS) is therefore included within the range of uncertainty used in TSPA.
2.1.01.03.0A	Heterogeneity of waste inventory	Included	WF	An updated inventory for commercial and defense wastes is used in TSPA (SNL 2007 [DIRS 180472]). The ELWS (Section 6.1) differs significantly from that inventory only in respect to the age and burnup for CSNF. Representative decay curves for DHLW waste packages in the ELWS are similar to those used in TSPA, which can be verified by comparing the "WPCodispose" and "WPCodisposeL" decay curves from DTN: MO0707ELWSDNSL.000 [DIRS 183774] (file: *WP_Decay_70K22kw_011707_DS.xls*), with the "5-HLW Short" and "5-HLW Long" decay curves in the LA unit cell from DTN: MO0702PASTREAM.001 [DIRS 179925] (file: *DTN-Inventory-Rev00.xls*). Also see FEP 2.1.01.01.0A.
2.1.02.01.0A	DSNF degradation (alteration, dissolution, and radionuclide release)	Included	WF	In principle, chemical reaction rates and radionuclide solubilities would be increased with increased thermal loading, accelerating degradation processes. However, once the waste package outer corrosion barrier has failed, it is conservatively assumed that the DSNF is directly exposed to the water or air of the repository environment. The model used in TSPA analyses for DSNF degradation (except naval SNF) assumes instantaneous degradation or dissolution of the waste form upon exposure of the waste form to groundwater (BSC 2004 [DIRS 172453], Section 6.2).

Table 6.5-2. Evaluation of Sensitivity to the Range of the Thermal Loading, for Thermally Sensitive FEPs (Continued)

FEP	FEP Name	Status	Groups	Evaluation for Impact of Anticipated Range of Thermal Loading
2.1.02.02.0A	CSNF degradation (alteration, dissolution, and radionuclide release)	Included	WF	The degradation of UO_2 is affected by several environmental parameters, including temperature. Instantaneous release is assumed for any fuel in a waste package that breaches above 100°C (BSC 2004 [DIRS 169987], Section 6.2.2.2). Hence, the effects from the range of thermal loading on CSNF degradation will be limited to the potential for longer duration of CSNF temperatures greater than 100°C (affecting the incidence of instantaneous release), and slower cooling (affecting matrix release rates). Note that no credit for CSNF cladding integrity is taken in TSPA (see FEP 2.1.02.19.0A). The approach implemented in TSPA can therefore represent this FEP for the anticipated range of thermal loading.
2.1.02.03.0A	HLW glass degradation (alteration, dissolution, and radionuclide release)	Included	WF	The glass degradation rate is calculated as a function of pH and temperature. Increased thermal loading would increase the rate of glass degradation (BSC 2004 [DIRS 169988], Section 6.7). The approach implemented in TSPA can therefore represent this FEP for the anticipated range of thermal loading.
2.1.02.06.0A	HLW glass recrystallization	Excluded	WF	Literature studies show that the effect of devitrification on the effective degradation rate for HLW glass is small (SNL 2007 [DIRS 179476]).
2.1.02.13.0A	General corrosion of cladding	Excluded	Cladding	Increased thermal loading will affect cladding corrosion rates. However, no credit for integrity of CSNF cladding is taken in TSPA (SNL 2007 [DIRS 178871]). For naval SNF, the cladding temperature will remain below 350°C for nominal (intact drift) conditions for the reason given in Section 6.1.6. For drift collapse, this representation is suitable for use with the range of thermal loading because of the low risk associated with seismically induced drift collapse immediately after repository closure (Section 6.5.1).
2.1.02.15.0A	Localized (radiolysis enhanced) corrosion of cladding	Excluded	Cladding	Although greater thermal output of SNF will be associated with greater radiation levels that will potentially increase radiolysis, and increased thermal loading would change the half-life of hydrogen peroxide formed by radiolysis and also cladding corrosion rates, no credit is taken in the TSPA for CSNF cladding integrity (SNL 2007 [DIRS 178871]). For naval SNF, the exclusion of this FEP (pertaining to the effects from radiolysis only) is unaffected by the range of thermal loading.
2.1.02.16.0A	Localized (pitting) corrosion of cladding	Excluded	Cladding	Although increased thermal loading would change cladding corrosion rates, no credit is taken in TSPA for CSNF cladding integrity (SNL 2007 [DIRS 178871]). For naval SNF, the treatment of this FEP is unaffected because of the low risk associated with seismically induced drift collapse immediately after repository closure (Section 6.5.1).
2.1.02.17.0A	Localized (crevice) corrosion of cladding	Excluded	Cladding	Although increased thermal loading would change cladding corrosion rates, no barrier credit is given in the TSPA for CSNF cladding (SNL 2007 [DIRS 178871]). For naval SNF, the treatment of this FEP is unaffected because of the low risk associated with seismically induced drift collapse immediately after repository closure (Section 6.5.1).

Table 6.5-2. Evaluation of Sensitivity to the Range of the Thermal Loading, for Thermally Sensitive FEPs (Continued)

FEP	FEP Name	Status	Groups	Evaluation for Impact of Anticipated Range of Thermal Loading
2.1.02.19.0A	Creep rupture of cladding	Excluded	Cladding	Cladding creep is found to be insignificant for postclosure temperatures less than 400°C (BSC 2004 [DIRS 170019]). These temperatures will not be approached in the repository, considering the anticipated range of thermal loading, except in the event of drift collapse during the thermal period, which has low probability (Section 6.5.1). Importantly, no credit for CSNF cladding integrity is taken in TSPA (SNL 2007 [DIRS 178871]), so there can be no risk significance for cladding creep rupture. For naval SNF, the treatment of this FEP is unaffected because of the low risk associated with seismically induced drift collapse immediately after repository closure (Section 6.5.1).
2.1.02.22.0A	Hydride cracking of cladding	Excluded	Cladding	Although hydrides may dissolve in warmer areas of the cladding and migrate to cooler areas, no barrier credit is given in the TSPA for CSNF cladding (SNL 2007 [DIRS 178871]). For naval DSNF, the treatment of this FEP (pertaining to crevice corrosion only) is unaffected by the range of thermal loading. For naval SNF, the treatment of this FEP is unaffected because of the low risk associated with seismically induced drift collapse immediately after repository closure (Section 6.5.1).
2.1.02.26.0A	Diffusion controlled cavity growth in cladding	Excluded	Cladding	Published work predicts that cladding failure by this mechanism will not be significant for postclosure temperatures less than 330°C to 400°C (BSC 2004 [DIRS 170019]). These temperatures will not be approached in the repository, considering the anticipated range of thermal loading, except in the event of drift collapse immediately after closure (Section 6.5.1). Importantly, no credit for CSNF cladding integrity is taken in TSPA (SNL 2007 [DIRS 179476]), so there can be no additional risk significance for cladding creep rupture. For naval SNF, the treatment of this FEP is not impacted because of the low risk associated with seismically induced drift collapse immediately after repository closure (Section 6.5.1). See FEP 2.1.02.19.0A.
2.1.03.01.0A	General corrosion of waste packages	Included	WP	The abstraction used in TSPA to represent temperature-dependent general corrosion of Alloy 22 (SNL 2007 [DIRS 178519], Section 7.2.1) is applicable, and may be highly conservative, over the range of postclosure temperatures associated with the anticipated range of thermal loading (Section 6.1).
2.1.03.01.0B	General corrosion of drip shields	Included	WP	The abstraction used in TSPA to represent general corrosion of titanium alloys used in the drip shield has no temperature dependence (SNL 2007 [DIRS 180778], Sections 6.2.1[a] and 7.2.1[a]) and is applicable over the range of postclosure temperatures associated with the anticipated range of thermal loading.
2.1.03.03.0A	Localized corrosion of waste packages	Included	WP	Localized corrosion of Alloy 22 on contact with seepage is temperature-dependent (SNL 2007 [DIRS 180778]), and the anticipated range of thermal loading will change the duration of elevated temperature conditions (see FEP 1.2.03.02.0E for effects from drift collapse). The consequences from increased duration of thermal conditions can therefore be represented by the corrosion abstraction used for TSPA. The consequences are included in TSPA but may be negligible because: (1) seepage can only occur at lower temperatures (100°C or less; BSC 2005 [DIRS 172232], Section 6.2.4), and (2) seepage is prevented from contacting waste packages by the presence of drip shields.

Table 6.5-2. Evaluation of Sensitivity to the Range of the Thermal Loading, for Thermally Sensitive FEPs (Continued)

FEP	FEP Name	Status	Groups	Evaluation for Impact of Anticipated Range of Thermal Loading
2.1.03.03.0B	Localized corrosion of drip shields	Excluded	WP	The exclusion justification is unaffected by the range of thermal loading, as localized corrosion of the drip shield will not be initiated by the environmental conditions that can occur in the repository (SNL 2007 [DIRS 179476]).
2.1.03.04.0A	Hydride cracking of waste packages	Excluded	WP	Waste package temperatures approaching 400°C could be produced by the anticipated range of thermal loading combined with seismically induced drift collapse immediately after repository closure (Section 6.4.2.5); however, temperature in excess of 500°C is required to initiate hydride cracking of Alloy 22 (SNL 2007 [DIRS 178871]).
2.1.03.04.0B	Hydride cracking of drip shields	Excluded	WP	Drip shield peak temperature approaching 400°C could be produced by the anticipated range of thermal loading combined with seismically-induced drift collapse immediately after repository closure (Section 6.4.2.5); however, such temperatures are insufficient to initiate hydride cracking of Titanium Grade 7. Other environmental conditions in the repository must be met simultaneously with the temperature condition (greater than 80°C), but these other conditions are very unlikely (SNL 2007 [DIRS 178871]).
2.1.06.06.0A	Effects of drip shield on flow	Included	EBS	Flow diversion by the drip shield is unaffected by temperature, once water influx to the repository can occur (see FEP 2.1.08.01.0A). This FEP can therefore be represented for the anticipated range of thermal loading, using the current modeling basis for TSPA.
2.1.06.06.0B	Oxygen embrittlement of drip shields	Excluded	WP	Oxygen embrittlement of titanium depends on diffusion of interstitial oxygen into the metal at temperatures greater than 340°C (SNL 2007 [DIRS 178871]). Although drip shield peak temperature approaching 400°C could be produced by the anticipated range of thermal loading combined with seismically induced drift collapse immediately after repository closure (Section 6.4.2.5), such temperatures are insufficient to significantly change the diffusion coefficient of oxygen. This can be demonstrated using the same approach with an Arrhenius-type equation, to re-calculate the diffusion coefficient of 6×10^{-18} cm^2 /sec at 300°C to a value at 400°C. The result shows negligible increase (SNL 2007 [DIRS 178871]). The thermal peak will be of insufficient duration to cause any oxygen embrittlement, which would require the drip shield to sustain a temperature of 400°C for more than 10^8 years. Regardless, for drift collapse this representation is suitable for use with the range of thermal loading because of the low risk associated with drift collapse near the peak of the thermal period (Section 6.5.1).
2.1.07.05.0A	Creep of metallic materials in the waste package	Excluded	WP	Although waste package peak temperature approaching 400°C could be produced by the anticipated range of thermal loading combined with seismically induced drift collapse immediately after repository closure (Section 6.4.2.5), this will not impact the exclusion justification for creep of the waste package or its internals. As discussed in Section 6.5.1, waste package wall temperature exceeding 300°C will be limited to 90 years or less duration, and has low probability. In addition, no projected temperature approaches the 650°C threshold value identified in the screening justification (BSC 2005 [DIRS 174995]; SNL 2007 [DIRS 179476]).

Table 6.5-2. Evaluation of Sensitivity to the Range of the Thermal Loading, for Thermally Sensitive FEPs (Continued)

FEP	FEP Name	Status	Groups	Evaluation for Impact of Anticipated Range of Thermal Loading
2.1.07.05.0B	Creep of metallic materials in the drip shield	Excluded	WP	Drip shield peak temperature associated with the anticipated range of thermal loading, combined with seismically induced drift collapse immediately after repository closure, could approach 400°C, which could affect creep deformation of the titanium drip shield in response to dead loading from the associated collapse rubble. As such creep occurs, load will be transferred from the drip shield to the rubble (SNL 2007 [DIRS 179476]), mitigating the potential effect on drip shield function. Importantly, the treatment of this FEP is not impacted because of the low risk associated with seismically induced drift collapse immediately after repository closure (Section 6.5.1).
2.1.08.01.0A	Water influx at the repository	Included	UZ	The timing of water influx, as represented by the thermal seepage abstraction (BSC 2005 [DIRS 172232], Section 6.2.4), will change slightly over the range of anticipated thermal loading, but water influx will be otherwise unaffected. This FEP can therefore be represented for the anticipated range of thermal loading using the current modeling basis for TSPA.
2.1.08.03.0A	Repository dry-out due to waste heat	Included	EBS	The extent of rock dryout will increase locally at hotter locations within the repository, and decrease at cooler locations, given the emplacement sequences described in Section 6.1. A limited range of variability on this behavior is included in TSPA (SNL 2007 [DIRS 181383]). Increased dryout will slightly delay the return of humidity or seepage conditions for some waste package locations, based on the similarity of predicted drift wall temperatures with the postclosure reference case (Section 6.4.2.3). This FEP can therefore be represented for the anticipated range of thermal loading using the current modeling basis for TSPA.
2.1.08.04.0A	Condensation forms on roofs of drifts (drift-scale cold traps)	Included	EBS	Drift wall condensation is modeled during Stage 3, which occurs only after all waste package locations have cooled to 96°C or lower (SNL 2007 [DIRS 181648]). The anticipated range of thermal loading may delay Stage 3 for certain drifts. For Stage 2, a reasonable-bound approximation is used that produces condensation only on the coolest waste packages, and the amount is limited by the available percolation flux, and not by thermal loading. Hence, the approach used in TSPA already accommodates the likely effects from the range of thermal loading.
2.1.08.04.0B	Condensation forms at repository edges (repository scale cold traps)	Included	EBS	The range of thermal loading will produce local variation in moisture transport away from the emplacement areas, and toward the repository edges. A broad range of dispersive transport behavior sufficient to represent effects from the range of thermal loading is already included in the existing condensation model and supporting calculations, and in TSPA (SNL 2007 [DIRS 181648]). See FEP 2.1.08.04.0A.
2.1.08.11.0A	Repository resaturation due to waste cooling	Included	EBS	Resaturation will be delayed or accelerated at hotter or cooler locations, respectively, by the range of thermal loading (see Section 6.4.2). The effects for the anticipated range of thermal loading are readily accommodated using the approach incorporated in TSPA.

Table 6.5-2. Evaluation of Sensitivity to the Range of the Thermal Loading, for Thermally Sensitive FEPs (Continued)

FEP	FEP Name	Status	Groups	Evaluation for Impact of Anticipated Range of Thermal Loading
2.1.08.14.0A	Condensation on underside of drip shield	Excluded	EBS	The exclusion justification (SNL 2007 [DIRS 179476]) includes drip shield ventilation effects and evaluation of the likelihood of "high invert" source conditions as developed in *In-Drift Natural Convection and Condensation* (SNL 2007 [DIRS 181648]). These aspects of the exclusion justification do not depend directly on changes in thermal loading.
2.1.09.01.0A	Chemical characteristics of water in drifts	Included	EBS	Effects from thermal loading on the composition of potential seepage water are analyzed in Section 6.4.3. Seepage into drifts is not predicted for drift wall temperature greater than 100°C, which limits the changes in composition caused by changes in thermal loading. In addition, waters that occur as actual seepage in thermal-hydrologic-chemical simulations are dilute (SNL 2007 [DIRS 177413], Section 6.6.3), and are prevented by the drip shield from interacting with the waste, can be represented using the modeling basis already incorporated in TSPA, as discussed in Section 6.4.3. See excluded FEP 2.2.08.04.0A for discussion of related processes affecting seepage composition.
2.1.09.01.0B	Chemical characteristics of water in waste package	Included	WF	The in-package chemistry model (SNL 2007 [DIRS 180506]) accounts for thermal effects and temperature variations when representing the range of uncertainty for in-package chemical conditions. Hence, the effects from the anticipated range of thermal loading can be represented using the approach incorporated in TSPA.
2.1.09.08.0A	Diffusion of dissolved radionuclides in EBS	Included	EBS	Diffusive transport of dissolved radionuclides in the EBS is included in the EBS radionuclide transport abstraction model implemented in TSPA (SNL 2007 [DIRS 177407]). Radionuclide diffusion coefficients are adjusted for the temperature of the EBS domain through which diffusion is occurring. The range of thermal loading may slightly delay diffusive and advective transport, by delaying the return of moisture to the EBS (see FEP 2.1.08.01.0A). Slower cooldown will mean higher temperatures with the potential to slightly increase diffusive transport. These processes are represented for the anticipated range of thermal loading, in the modeling basis used in TSPA.
2.1.09.12.0A	Rind (chemically altered zone) forms in the near-field	Excluded	UZ	The range of thermal loading will affect the extent and duration of the boiling period and dryout, and thus may affect minerals deposited in the near-field host rock during the thermal period. However, the effects on the in-drift environment (see FEP 2.1.09.01.0A) and on radionuclide transport in the UZ (see FEP 2.2.10.06.0A) can be excluded for the anticipated range of thermal loading. See excluded FEP 2.2.08.04.0A for discussion of related processes affecting seepage composition.
2.1.09.24.0A	Diffusion of colloids in EBS	Included	EBS	Diffusion is temperature dependent (see FEP 2.1.09.08.0A). The range of thermal loading may slightly delay diffusive and advective transport, by delaying the return of moisture to the EBS (see FEP 2.1.08.01.0A). Slower cooldown will mean higher temperatures with the potential to slightly increase diffusive transport of colloids (SNL 2007 [DIRS 177407]). These processes are represented for the anticipated range of thermal loading, in the modeling basis used in TSPA.

Table 6.5-2. Evaluation of Sensitivity to the Range of the Thermal Loading, for Thermally Sensitive FEPs (Continued)

FEP	FEP Name	Status	Groups	Evaluation for Impact of Anticipated Range of Thermal Loading
2.1.09.27.0A	Coupled effects on radionuclide transport in the EBS	Excluded	EBS	Coupled effects determined to be insignificant will continue to be, given the moderate increases in temperature and dryout associated with the anticipated range of thermal loading, and the evaluation of coupled process effects on radionuclide sorption (SNL 2007 [DIRS 177396], Appendix I).
2.1.09.28.0A	Localized corrosion on the waste package outer surface due to deliquescence	Excluded	EBS, WP	The range of thermal loading may produce additional, local variability in waste package surface temperature and thermal duration. These effects will change the timing of the onset of deliquescence, and could affect the rates of diffusion and off-gassing that affect the deliquescence environment (SNL 2007 [DIRS 181267]). However, the exclusion justifications are unaffected by the range of thermal loading, including those aspects pertaining to the amount of salt and the resulting brine volume.
2.1.09.28.0B	Localized corrosion on drip shield surfaces due to deliquescence	Excluded	EBS	The exclusion justification (SNL 2007 [DIRS 179476]) is unaffected by the range of thermal loading, as localized corrosion of the drip shield cannot be initiated under the environmental conditions of the repository (see also FEP 2.1.03.03.0B).
2.1.11.01.0A	Heat generation in EBS	Included	EBS	The range of thermal loading will result in local variations in heating, temperatures, and related processes. The consequences of this heat generation are accounted for in the modeling basis of the TSPA. The multiscale model (SNL 2007 [DIRS 181383]) implemented in TSPA already includes broad variability in the duration and magnitude of thermal-hydrologic conditions, and the methodology implemented in TSPA can readily accommodate the anticipated range of thermal loading.
2.1.11.02.0A	Non-uniform heat distribution in EBS	Included	EBS	The 85/4 and 96/2 sequences presented in Section 6.1 are different from the postclosure reference case but respond similarly as discussed in Section 6.4.2. Three-dimensional analysis presented in Section 6.4.2 shows that hydrologic conditions in the vicinity of cooler packages will be controlled by temperature, and not by condensate originating from boiling at adjacent hotter packages. The anticipated range of thermal loading will produce local variability in heating, temperatures, and related processes. The multiscale model implemented in TSPA already includes broad variability in the duration and magnitude of thermal-hydrologic conditions, and the methodology implemented in TSPA can readily accommodate the anticipated range of thermal loading. The condensation model uses a reasonable-bound approach to dispersive transport (SNL 2007 [DIRS 181648]) that spans the range of effects that are likely to occur from convective mixing, given that drift wall condensation behavior is sensitive to dispersivity over a limited range (SNL 2007 [DIRS 181383]). See also FEP 2.1.11.09.0C.
2.1.11.05.0A	Thermal expansion and stress of in-package EBS components	Excluded	Cladding	Although the anticipated range of thermal loading will affect the thermal conditions for in-package components such as cladding and the TAD canister, CSNF cladding is given no barrier credit in the TSPA, and, importantly, the TAD canister is designed to withstand temperatures of 350°C. For drift collapse, this representation is suitable because of the low risk associated with seismically induced drift collapse immediately after repository closure (Section 6.5.1).

Table 6.5-2. Evaluation of Sensitivity to the Range of the Thermal Loading, for Thermally Sensitive FEPs (Continued)

FEP	FEP Name	Status	Groups	Evaluation for Impact of Anticipated Range of Thermal Loading
2.1.11.06.0A	Thermal sensitization of waste packages	Excluded	WP	Through nearly all the regulatory period, waste package temperatures will be less than the conditions identified to ensure phase stability (e.g., 300°C for 500 years; BSC 2004 [DIRS 171924], Section 6.2). For drift collapse this representation is suitable because of the low risk associated with seismically induced drift collapse immediately after repository closure (Section 6.5.1).
2.1.11.06.0B	Thermal sensitization of drip shields	Excluded	WP	The anticipated range of thermal loading will increase peak temperatures for drip shields; however, the temperatures (even for early drift collapse; see FEP 2.1.11.06.0A) will be less than levels of concern for titanium alloys (SNL 2007 [DIRS 179476]).
2.1.11.07.0A	Thermal expansion/stress of in-drift EBS components	Excluded	WP, EBS	Although the anticipated range of thermal loading would change thermally induced stresses of in-drift components, the exclusion justification remains unchanged, based on negligible thermal stress effects (SNL 2007 [DIRS 179476]).
2.1.11.08.0A	Thermal effects on chemistry and microbial activity in the EBS	Included	EBS, WF	Effects from thermal loading on the composition of potential seepage water, and the evaporative evolution of seepage in the drifts, are analyzed in Section 6.4.3. Seepage into drifts is not predicted for drift wall temperature greater than 100°C, which limits the changes in composition caused by changes in thermal loading. The approach used in TSPA has the capability to represent the significant chemical effects from the range of thermal loading, and those effects are likely to be small. Microbial activity is included in TSPA for corrosion of Alloy 22, but is excluded from affecting the EBS environment in other ways because of the lack of nutrients and moisture available (BSC 2004 [DIRS 169991], Section 7.1; SNL 2007 [DIRS 179476]).
2.1.11.09.0A	Thermal effects on flow in the EBS	Included	EBS	Effects from the anticipated range of thermal loading on flow in the EBS will be limited to changes in the timing of the return of moisture after dryout (see Section 6.4.2). These effects are readily accommodated by the modeling basis used in TSPA.
2.1.11.09.0B	Thermally driven flow (convection) in waste packages	Excluded	WF	Spatial variability of environmental conditions within waste packages will be small compared with variability and uncertainty with respect to waste form characteristics (type, age, etc.; SNL 2007 [DIRS 179476]) so the screening justification for this FEP is unchanged by the anticipated range of thermal loading.
2.1.11.09.0C	Thermally driven flow (convection) in drifts	Included	EBS	Thermal loading, and particularly non-uniform thermal loading, produces natural convective circulation that is included in the drift wall condensation model for TSPA. The condensation model uses a reasonable-bound approach to dispersive transport (SNL 2007 [DIRS 181648]) that spans the range of effects that are likely to occur from convective mixing, given that drift wall condensation behavior is sensitive to dispersivity over a limited range (SNL 2007 [DIRS 181383]). This FEP can therefore be represented for the anticipated range of thermal loading using the current modeling basis for TSPA. See also FEP 2.1.11.02.0A.

Table 6.5-2. Evaluation of Sensitivity to the Range of the Thermal Loading, for Thermally Sensitive FEPs (Continued)

FEP	FEP Name	Status	Groups	Evaluation for Impact of Anticipated Range of Thermal Loading
2.1.11.10.0A	Thermal effects on transport in the EBS	Excluded	EBS	Thermally driven indirect coupled processes that could affect transport, and also the effects of temperature on radionuclide sorption, are excluded from TSPA (see FEP 2.1.09.27.0A; SNL 2007 [DIRS 179476]). The range of thermal loading may slightly delay diffusive and advective transport, by delaying the return of moisture to the EBS, as analyzed in Section 6.4.2 of this report (see also FEP 2.1.08.01.0A). See also FEPs 2.1.09.08.0A and 2.1.09.24.0A, respectively, on diffusion of dissolved radionuclides and colloids in the EBS.
2.1.12.06.0A	Gas transport in EBS	Excluded	EBS	The anticipated range of thermal loading would increase the duration of the dryout phase and delay the return of moisture and water vapor into the emplacement drift. In addition, see discussion in FEPs 2.1.11.09.0C and 2.2.10.10.0A, respectively, on thermally driven convection and two-phase flow. The exclusion justification applies directly to conditions associated with the anticipated range of thermal loading.
2.1.13.01.0A	Radiolysis	Excluded	WF, WP EBS	Although the anticipated range of thermal loading will be associated with higher burnup and younger age for CSNF (see FEP 2.1.01.01.0A), and these conditions are associated with higher radiation levels and potentially more radiolysis, the potential consequences of gamma radiolysis depend on the presence of water, which will not be present at the surface of the waste package when radiation levels are sufficient to cause significant radiolysis. The screening justification is therefore unchanged for the anticipated range of thermal loading (SNL 2007 [DIRS 179476]).
2.2.01.02.0A	Thermally induced stress changes in the near field	Excluded	UZ, EBS	Coupled THM effects evaluated for the reference case have negligible impact on heat transfer, and insignificant effects on percolation and seepage (BSC 2004 [DIRS 169864], Section 8.1; SNL 2007 [DIRS 179476]). Extrapolation of the linear-elastic response to increased temperatures from thermal loading would show that changes in host-rock permeability will remain insignificant. Other effects (e.g., sorption, rockfall) are treated in separate FEPs.
2.2.07.10.0A	Condensation zone forms around drifts	Included	UZ	The range of thermal loading may change the duration of boiling and associated condensation within the host rock, as discussed in Section 6.4.2. However, potential impacts on repository performance are limited to changes in timing of the return of water to the EBS (see FEP 2.1.08.01.0A). Potential residual effects on host-rock properties, from thermally driven coupled processes, are addressed separately (see FEP 2.2.08.03.0B). This FEP can therefore be represented for the anticipated range of thermal loading using the current modeling basis for TSPA.
2.2.07.11.0A	Resaturation of geosphere dryout zone	Included	UZ	The extent of dryout and the timing of water influx will be changed slightly by the anticipated range of thermal loading as discussed in Section 6.4.2, but water influx will be otherwise unaffected (see FEP 2.1.08.01.0A). This FEP can therefore be represented for the anticipated range of thermal loading using the current modeling basis for TSPA.

Table 6.5-2. Evaluation of Sensitivity to the Range of the Thermal Loading, for Thermally Sensitive FEPs (Continued)

FEP	FEP Name	Status	Groups	Evaluation for Impact of Anticipated Range of Thermal Loading
2.2.07.20.0A	Flow diversion around repository drifts	Included	UZ	The range of thermal loading will affect the duration and extent of rock dryout around the drifts, but will not change the capillary and vaporization effects that divert water, nor the drift wall temperature criterion that controls thermal seepage in TSPA (BSC 2005 [DIRS 172232]). Hence, the effects from the range of thermal loading are already addressed by the modeling basis included in TSPA.
2.2.08.01.0B	Chemical characteristics of groundwater in the UZ	Included	UZ	Chemical characteristics of potential seepage (as modeled for TSPA) will be changed slightly by the anticipated range of thermal loading, as described in Section 6.4.3. The effects from the range of thermal loading are represented for the anticipated range of thermal loading by the modeling basis used in TSPA. See also FEPs 2.1.09.01.0A and 2.2.08.04.0A for related processes that affect seepage composition.
2.2.08.03.0B	Geochemical interactions and evolution in the UZ	Excluded	UZ	The range of thermal loading will affect the extent and duration of dryout, but will only slightly affect aqueous composition beyond the dryout zone where sub-boiling conditions pertain, as represented by the composition of potential seepage waters described in Section 6.4.3 of this report. The screening justification is therefore unchanged for the anticipated range of thermal loading (SNL 2007 [DIRS 179476]). See FEP 2.2.08.04.0A for related processes that affect seepage composition.
2.2.08.04.0A	Redissolution of precipitates directs more corrosive fluids to waste packages	Excluded	UZ, EBS	Effects from thermal loading on the composition of potential seepage water are analyzed in Section 6.4.3. Waters that occur as actual seepage in thermal-hydrologic-chemical simulations are dilute (SNL 2007 [DIRS 177413], Section 6.6.3), and are prevented by the drip shield from interacting with the waste package or waste forms. Hence, the effects from the range of thermal loading on this FEP are accommodated in TSPA, as discussed in Section 6.4.3, and are not likely to be risk significant (also see FEP 2.1.09.01.0A). The screening justification is therefore unchanged for the anticipated range of thermal loading (SNL 2007 [DIRS 179476]).
2.2.08.12.0A	Chemistry of water flowing into the drift	Included	UZ	Effects from thermal loading on the composition of potential seepage water are analyzed in Section 6.4.3. Seepage into drifts is not predicted for drift wall temperature greater than 100°C, which limits the changes in composition caused by changes in thermal loading. Importantly, waters that occur as actual seepage in thermal-hydrologic-chemical simulations are dilute (SNL 2007 [DIRS 177413], Section 6.6.3), and are prevented by the drip shield from interacting with the waste package or waste forms. Effects from increased temperature on seepage composition include increased pH, increased Na and K, and decreased Ca and Mg. The effects from the range of thermal loading are readily accommodated using the approach included in TSPA. See also FEPs 2.1.09.01.0A and 2.1.11.08.0A.
2.2.10.01.0A	Repository induced thermal effects on flow in the UZ	Excluded	UZ	Far-field and large-scale effects from the anticipated range of thermal loading will be closely comparable to the postclosure reference case, because the overall average thermal loading will be very similar as shown in Section 6.1 of this report. Smaller-scale effects on flow near the drifts are controlled by dryout, and by the mid-pillar peak temperature limit of 96°C as shown in Section 6.2.

Table 6.5-2. Evaluation of Sensitivity to the Range of the Thermal Loading, for Thermally Sensitive FEPs (Continued)

FEP	FEP Name	Status	Groups	Evaluation for Impact of Anticipated Range of Thermal Loading
2.2.10.02.0A	Thermal convection cell develops in SZ	Excluded	SZ	Far-field and large-scale effects from the anticipated range of thermal loading will be or closely comparable to the postclosure reference case, because the overall average thermal loading will be very similar, as shown in Section 6.1 of this report. Therefore, the exclusion justification is directly applicable for the anticipated range of thermal loading.
2.2.10.04.0A	Thermo-mechanical stresses alter characteristics of fractures near repository	Excluded	UZ, SZ	Coupled THM effects evaluated for the reference case have negligible impact on heat transfer, and insignificant effects on percolation (BSC 2004 [DIRS 169864], Section 8.1; SNL 2007 [DIRS 179476]). See FEP 2.2.01.02.0A. Other effects (e.g., sorption, rockfall) are treated in separate FEPs.
2.2.10.04.0B	Thermo-mechanical stresses alter characteristics of faults near repository	Excluded	UZ, SZ	THM effects associated with the range of thermal loading will remain insignificant for faults with greater continuity and permeability, based on the rationale for FEP 2.2.10.04.0A (SNL 2007 [DIRS 179476]).
2.2.10.05.0A	Thermo-mechanical stresses alter characteristics of rocks above and below the repository	Excluded	UZ, SZ	Far-field and large-scale effects from the anticipated range of thermal loading will be closely comparable to the postclosure reference case, because the overall average thermal loading will be very similar, as shown in Section 6.1 of this report. Therefore, the exclusion justification remains unchanged, for the anticipated range of thermal loading.
2.2.10.06.0A	Thermo-chemical alteration in the UZ (solubility, speciation, phase changes, precipitation, dissolution)	Excluded	UZ	The range of thermal loading will change the extent and duration of dryout (Section 6.4.2), but will have only minor effects on the composition of potential seepage water (Section 6.4.3) that are readily accommodated by the approach implemented in TSPA (see FEPs 2.2.08.12.0A and 2.1.09.01.0A). Thermal loading can affect aqueous chemistry only beyond the dryout zone where sub-boiling temperature conditions exist (see FEP 2.2.08.01.0B). Potentially deleterious residual effects from thermal-hydrologic-chemical processes on radionuclide transport have been excluded (SNL 2007 [DIRS 177396], Appendix I; SNL 2007 [DIRS 179476]).
2.2.10.07.0A	Thermo-chemical alteration of the Calico Hills unit	Excluded	UZ	Far-field and large-scale effects from the anticipated range of thermal loading will be closely comparable to the postclosure reference case, because the overall average thermal loading will be very similar as shown in Section 6.1 of this report. Therefore, the exclusion justification remains unchanged for the anticipated range of thermal loading.
2.2.10.08.0A	Thermo-chemical alteration in the SZ (solubility, speciation, phase changes, precipitation/dissolution)	Excluded	SZ	The justification presented for FEP 2.2.10.06.0A that there would be no significant impacts with respect to thermo-chemical alteration in the UZ from the anticipated range of thermal loading also applies to the SZ, which is further distant from the heat sources in the repository. Therefore, the exclusion justification remains unchanged, for the anticipated range of thermal loading.
2.2.10.09.0A	Thermo-chemical alteration of the Topopah Springs basal vitrophyre	Excluded	UZ	Far-field and large-scale effects from the anticipated range of thermal loading will be closely comparable to the postclosure reference case, because the overall average thermal loading will be very similar, as shown in Section 6.1 of this report. Therefore, the exclusion justification remains unchanged, for the anticipated range of thermal loading.

Table 6.5-2. Evaluation of Sensitivity to the Range of the Thermal Loading, for Thermally Sensitive FEPs (Continued)

FEP	FEP Name	Status	Groups	Evaluation for Impact of Anticipated Range of Thermal Loading
2.2.10.10.0A	Two-phase buoyant flow/heat pipes	Included	UZ	The anticipated range of thermal loading may change the boundary conditions for buoyant flow/heat pipe activity in the host rock, but these processes contribute little to thermal-hydrologic response of the host rock, which is dominated by thermal conduction (SNL 2007 [DIRS 181383], Section 6.2.1). Effects from the anticipated range of thermal loading would be limited to possible delay in the shut-down of two-phase circulation (SNL 2007 [DIRS 179476]). This response is included in the thermal-hydrologic modeling basis used in TSPA, which can readily accommodate the range of thermal loading.
2.2.10.11.0A	Natural air flow in the UZ	Excluded	UZ	Far-field and large-scale effects from the anticipated range of thermal loading will be closely comparable to the postclosure reference case, because the overall average thermal loading will be very similar, as shown in Section 6.1 of this report. Therefore, the exclusion justification remains unchanged for the anticipated range of thermal loading.
2.2.10.12.0A	Geosphere dry-out due to waste heat	Included	UZ	The range of thermal loading will change the extent and duration of dryout in the near-field (Section 6.4.2), but thermal-hydrologic processes will be the same as represented for the postclosure reference case, and far-field response will be closely comparable to the postclosure reference case (see FEP 2.2.10.14.0A). Hence, the effects from the range of thermal loading on geosphere dryout are limited to timing of resaturation, and are readily accommodated by the modeling basis for TSPA.
2.2.10.13.0A	Repository-induced thermal effects on flow in the SZ	Excluded	SZ	The justification presented for FEP 2.2.10.01.0A that there will be no significant impacts on flow in the UZ from the anticipated range of thermal loading also applies for the SZ, which is further distant from the heat sources in the repository.
2.2.10.14.0A	Mineralogic dehydration reactions	Excluded	UZ	Far-field and large-scale effects from the anticipated range of thermal loading will be closely comparable to the postclosure reference case, because the overall average thermal loading will be very similar as shown in Section 6.1 of this report.
2.2.11.03.0A	Gas transport in geosphere	Excluded	UZ	Far-field and large-scale effects from the anticipated range of thermal loading will be closely comparable to the postclosure reference case, because the overall average thermal loading will be very similar, as shown in Section 6.1 of this report. Therefore, the exclusion justification remains unchanged, for the anticipated range of thermal loading.

NOTE: Designations for FEP groups are as follows: EBS = Engineered Barrier System; SZ = Saturated Zone; UZ = Unsaturated Zone; WF = Waste Form; WP = Waste Package.

6.5.1 Probability of Drift Collapse Coincident with Peak Thermal Conditions

The probabilistic analysis presented in this section shows that the probability of waste package temperature exceeding 300°C during the first few decades after repository closure is low, and there is low risk associated with seismically induced drift collapse immediately after repository closure. The screening justifications and TSPA dispositions for thermally sensitive FEPs listed in Section 6.5, which typically apply for temperatures up to 300°C, are thereby extended to cover the range of peak temperatures possible due to drift collapse immediately after closure.

This analysis is based on *Seismic Consequence Abstraction* (SNL 2007 [DIRS 176828], Section 6.7.1), which provides an example calculation of the probability of seismically induced drift collapse during an 80-year period immediately after repository closure. Whereas that calculation defined complete drift collapse in terms of a range for the volume of intact rock that collapses (30 to 120 m^3/meter of drift), the analysis presented here uses a range of rubble volume (zero to 83.36 m^3/meter of drift) that represents partial as well as complete collapse. In this way, the important transition at which the drip shield and waste package are barely covered by rubble, with the associated temperature increase, is explicitly represented. This analysis then uses a set of thermal-hydrologic simulations of partial drift collapse to evaluate the probability that seismically induced drift collapse (partial or complete) will cause the temperature of any waste package to exceed 300°C.

Background – The time period when waste package temperatures could exceed 300°C in the event of partial or complete drift collapse extends to approximately 90 years after closure (Figure 6.4.2-28). Note that for the base-case multiscale model feed to TSPA, the maximum temperature for any waste package is below 300°C after 80 years (SNL 2007 [DIRS 176828], Section 6.7). It is appropriate to use characteristics of lithophysal tuff for this analysis, because approximately 85% of the emplacement drifts are in lithophysal tuff (SNL 2007 [DIRS 179466], Table 4-1, Parameter 01-03) and because seismically induced rockfall volume in the lithophysal tuff is shown to be much greater than in nonlithophysal tuff (SNL 2007 [DIRS 176828], Figure 6-57).

To represent thermal-hydrologic effects from drift collapse in TSPA, a set of "delta" functions is provided by the multiscale model, and applied after any seismic event of sufficient intensity occurs in the assessment (SNL 2007 [DIRS 181383], Section 6.3.17[a]). The "delta" functions are developed from the temperatures for drifts that are collapsed immediately at closure, by subtracting the intact-drift (uncollapsed) temperature from the fully collapsed result, for the eight waste package types represented in the multiscale model. Importantly, the "delta" history is added to the intact-drift result starting immediately after occurrence of the seismic event, without any lag period of thermal adjustment (except for the adjustment at closure when collapse is assumed to occur in the "delta" calculation). For consideration of short-term response during the first 90 years after closure, this lag time is potentially significant to the probability of waste package temperature exceeding 300°C; however, it is neglected in this analysis as a conservative simplification, except for the initial adjustment at closure.

Drift collapse is initiated only by seismic events with moderate or high intensity of ground motion. From the bounded hazard and lithophysal rockfall volume curves used in the seismic abstraction (SNL 2007 [DIRS 176828], Figures 6-7 and 6-57), significant partial or complete

drift collapse occurs only for seismic events with peak ground velocity (PGV) of approximately 1 m/sec or greater, and annual probability on the order of 10^{-5} yr^{-1} or less. Only one such event needs to be simulated for evaluating seismically induced drift collapse within a time period of 90 years (or less), because the joint probability for two such events in this time period is insignificant i.e., less than 10^{-4}.

Probabilistic Analysis of Rubble Volume – Consider the incremental probability that the volume of rockfall from a seismic event defined by horizontal peak ground velocity (PGV) centered on a small interval around a value *v* (where *v* is the horizontal peak ground velocity) exceeds a particular volume (defined to represent partial or complete drift collapse). This incremental probability is the product of four factors (SNL 2007 [DIRS 176828], Section 6.7.1.7.3):

1. The probability that a single seismic event occurs during a prescribed time period (e.g., a period of elapsed time starting at closure and extending up to 90 years)

2. The conditional probability that a seismic event with horizontal PGV centered on *v* has nonzero rockfall

3. The conditional probability that the rockfall volume from the event with horizontal PGV centered on *v* equals or exceeds the particular value

4. The conditional probability that a seismic event with horizontal PGV centered on *v* is sampled from the bounded seismic hazard curve (SNL 2007 [DIR 176828], Section 6.4.3).

The probabilities in steps 2 through 4 are conditional because they are based on a single seismic event occurring during the prescribed time period. The exceedance probability is defined in *Seismic Consequence Abstraction* (SNL 2007 [DIRS 176828], Equation 6.7.3).

A scoping calculation was performed to estimate the probability of rockfall volume sufficient to impact waste package temperature. This calculation showed that for a 10-year period after closure, the exceedance probabilities for rubble volumes of 15 and 0.5 m^3/m range from 10^{-4} to 10^{-3}, respectively. For a 90-year period, the exceedance probabilities range from 2×10^{-4} to 8×10^{-3}. These results show that thermal effects from nonzero rockfall cannot be excluded solely on the basis of the initiating event probability.

Extension of Probabilistic Analysis to Waste Package Temperature – The procedure described above is incorporated into a Monte Carlo simulation that generates the exceedance probability for waste package temperature greater than 300°C, as a function of time starting at closure (results shown in Figures 6.5-1 and 6.5-2). The approach describes the exceedance probability for any number of waste packages without considering the actual number of waste packages affected. In the following discussion, a distinction is made between the intact-drift (uncollapsed) waste package temperature for the range of host-rock thermal conductivity values, and the "collapsed" waste package temperature for the range of host-rock and rubble thermal conductivity values. Correlations between the effective thermal conductivity of rubble, and the extent of collapse or the bulking factor are conservatively omitted from this analysis.

The calculation sequence (Table 6.5-3) uses the Poisson distribution to evaluate the frequency of seismic events, and uses the seismic hazard curve to evaluate the horizontal PGV (SNL 2007 [DIRS 176828], Section 6.4). The probability of nonzero rockfall, and the volume of intact rock comprising the rockfall for nonzero events, are based on the Gamma distribution (SNL 2007 [DIRS 176828], Section 6.7.1). The bulking factor (used to convert the rock volume from the seismic consequence abstraction to a rubble volume) is sampled uniformly between limits corresponding to a range of reported rubble characteristics (SNL 2007 [DIRS 176828], Section 6.7.1). Finally, the waste package temperature immediately after the seismic event (applying the "delta" approach) is estimated by interpolating a set of thermal-hydrologic calculations that define the temperature response to degree of partial collapse, host-rock thermal conductivity, and effective thermal conductivity for rubble.

The probability of the waste package temperature exceeding 300°C is presented in Output DTN: MO0709HOTWASTE.000 (file: *Seismic Consequence Analysis (300 C Probability).xmcd*). The calculation is performed in two phases: (1) the first phase estimates the distribution function for the rockfall volume based on the seismic consequence abstraction, and (2) the second phase estimates the temperature of the hottest waste package at a given time based on the rubble volume. A series of Monte Carlo realizations (most of which produce no seismic events in time periods up to 90 years) is performed to estimate the probability of the waste package temperature exceeding 300°C.

The first phase used the method described above to estimate rubble volume (SNL 2007 [DIRS 176828], Section 6.7.1) and is presented in Steps 1 through 6 of Table 6.5-3. User-defined Mathcad functions are developed for estimating (1) the occurrence and intensity of a seismic event; (2) the probability of nonzero rockfall associated with the event; (3) the exceedance probability as a function of the PGV; (4) parameters of the gamma distribution for the cumulative intact rock volume comprising the rockfall; and (5) inversion for the gamma distribution for cumulative intact rock volume comprising the rockfall. These functions are verified against example calculations from *Seismic Consequence Abstraction* (SNL 2007 [DIRS 176828], Section 6.7.1). For example, the relationship of the normalized rockfall volume with PGV is presented in Figure 6-57, and is replicated in the Mathcad file.

The second phase (Steps 7 through 9 of Table 6.5-3) for each realization involves estimating the relationship of the collapsed volume in the drift to the temperature of the hottest waste package. From the thermohydrolgic simulations, the temperature is linearly interpolated from a selected set of interpolation points from a set of six interpolating functions. The six sets of interpolation points represent the rock mass thermal conductivity (low, mean, and high), and two cases of rubble effective thermal conductivity (low and high), for a total of six interpolating functions. The interpolation is performed at the discrete time of each seismic event simulated for a realization (peak temperature occurs immediately), for seismic events out to 90 years from closure. The 10th percentile percolation flux is used for all thermal-hydrologic calculations; greater flux could decrease predicted temperatures but would introduce spatial variability to the analysis. The interpolated values are presented in Output DTN: MO0709HOTWASTE.000 (file: *Interpolation Tables.xls*).

After completion of all realizations, the temperature data are sorted in descending order. The number of realizations exceeding 300°C (or an alternate temperature limit as discussed below) is

tabulated in Output DTN: MO0709HOTWASTE.000 (file: *Worksheet in Seismic Consequence Analysis.xls*) for the base case and for the hottest 3-package and 7-package segments identified in the ELWS emplacement sequences.

Thermal-Hydrologic Analysis – Thermal-hydrologic interpolating functions for temperature of the hottest waste package were developed from the following simulations (Output DTN: MO0709HOTWASTE.000):

- Simulations from the 2-D LDTH submodel (Section 6.4.2.2) of the multiscale model, modified to represent partial collapse using the values shown in Table 6.5-4, and repeated for each combination of P10, P10L, and P10H rock mass thermal conductivity cases with low and high effective rubble thermal conductivity, comprising six sets of simulations in total. These simulations use the 10th percentile percolation flux at the "g_9" location, repeated for intact, partially collapsed, and completely collapsed drifts.

- Simulations from the multiscale model (Section 6.4.2.3) for the hottest waste package in the TSPA base case, using the 10th percentile percolation flux at the "g_9" location, repeated for the P10, P10L, and P10H cases to represent uncertainty in host rock thermal conductivity, in intact drifts. These simulations are based on the unit-cell arrangement from the postclosure thermal reference case, with initial lineal average thermal output of 1.45 kW/m and 50 years of preclosure ventilation. (The P10 and P10L cases define the hottest results for the TSPA base case in Figures 6.4.2-4b, 6.4.2-6b, 6.4.2-10b, and 6.4.2-12b.)

- Simulations from the 3-D TH model described in Section 6.4.2.4, for the 3-package and 7-package hottest segments from the ELWS emplacement sequences, for the P10 and P10L cases, using the 10th percentile percolation flux at the "g_9" location, in intact drifts. Temperature histories for the hottest waste package in each segment, for the P10 and P10L cases, are shown in Figures 6.4.2-4b, 6.4.2-6b, 6.4.2-10b, and 6.4.2-12b.

- Simulations from the 3-D TH model described in Section 6.4.2.5, for the 3-package and 7-package hottest segments from the ELWS emplacement sequences, for the P10 and P10L cases, using the 10th percentile percolation flux at the "g_9" location, for completely collapsed drifts. The temperature histories for hottest waste packages in each segment are plotted in Figure 6.4.2-28.

The LDTH-type simulations (first bullet above) were combined to calculate "delta" histories by subtracting the intact-drift waste package temperature data from the results with partial or complete collapse at repository closure. This was repeated for the six sets of simulations described above, then used to adjust the intact-drift multiscale temperature histories for the hottest waste package (first bullet) to produce six interpolation endpoint functions representing the effects of uncertainty in host rock and rubble thermal conductivity, and the expanded opening profile. The resulting temperature histories, summarized in Output DTN: MO0709HOTWASTE.000 (file: *Worksheet in Seismic Consequence Analysis.xls*), capture the effects from uncertainty in host-rock thermal conductivity, and rubble thermal

conductivity, on temperature of the hottest waste package. Note that this analysis is limited to a 10th percentile percolation flux value, because the approach is reasonably bounding, and use of greater fluxes would have introduced a component of spatial variability to the analysis.

For the 3-package and 7-package segments, the six sets of "delta" histories described above were applied to the hottest waste package temperature histories (third bullet). The resulting six interpolation endpoint functions for each of the 3-package and 7-package segments constitute an estimate of the effects from drift collapse on these waste package sequences. The estimate was checked against explicit simulations for the 3-package and 7-package segments, for the same properties and boundary conditions, and fully collapsed drifts (fourth bullet). The results show that the interpolated relationships are either conservative at early times or are within a few degrees at later times (Output DTN: MO0709HOTWASTE.000, file: *Seismic Consequence Analysis (300 C Probability).xmcd*).

Results – A drift collapse event that occurs within a few years after repository closure is most likely to produce peak waste package temperatures greater than 300°C, whereas events that occur out to 90 years are less likely to do this because the heat output of waste packages decays with time. The results from the probabilistic analysis of the TSPA base case are presented in Figure 6.5-1, which shows that the probability of any waste package exceeding 300°C in response to a single seismic event is of the order of 10^{-4} or less, even at the time of maximum sensitivity at approximately 30 yr after closure. These results were generated from 4×10^6 realizations of the Poisson process for seismic events (Output DTN: MO0709HOTWASTE.000, file: *Seismic Consequence Analysis (300 C Probability).xmcd*).

The results (Figure 6.5-1) are calculated by sampling of the rubble thermal conductivity from a uniform interpolation between the low and high rubble conductivity results discussed above. Uniform interpolation is more realistic than sampling the endpoints of the range discretely, because the low and high rubble thermal conductivity values are reasonable bounds (Section 6.4.2.7). Uniform sampling between the endpoints is appropriate because to a first approximation, the "delta" effect of drift collapse on waste package temperature is inversely proportional to the effective thermal conductivity value used for rubble.

Results for the 3-package and 7-package segments, calculated using uniform interpolation of the low and high rubble conductivity data, are plotted in Figure 6.5-2. These results were also generated from 4×10^6 realizations of the Poisson process for seismic events. The number of seismic events producing rockfall is on the order of several hundred, distributed over 90 years. From repetition of the simulation in Mathcad, as the number of realizations increases the output plotted in Figures 6.5-1 and 6.5-2 becomes more coherent, and a smooth trend emerges with a maximum probability very close to 10^{-4} at approximately 30 years elapsed time.

To determine the range of uncertainty in the results of the Monte Carlo simulations, a two-sided confidence interval was evaluated at 95%, for the 20 trials of 200,000 realizations (4×10^6 total), for the three cases at 30 years after closure, following the method described by Gentle (2003 [DIRS 183701], p. 235). Table 6.5-5 presents the results of the analysis and shows that the half-widths of the confidence intervals on the exceedance probabilities for these cases are approximately 15% of the mean values.

A further sensitivity study was performed to examine the dependence of these results on the temperature threshold selected (i.e., 300°C). A set of Monte Carlo simulations (of 4×10^6 realizations) was resampled for different exceedance temperatures, at 30 years after closure, to show how the maximum probability decreases as the threshold temperature increases (Figure 6.5-3). This calculation shows that a factor of 2 or greater reduction in probability is obtained by increasing the threshold temperature to 320°C.

Summary and Discussion – This supplementary probabilistic analysis has implemented features of the seismic consequence abstraction (SNL 2007 [DIRS 176828], Sections 6.4 and 6.7.1) and the multiscale model (SNL 2007 [DIRS 181383], Section 6.3) to show that there is low probability (on the order of 10^{-4} or smaller) that the temperature of any waste package will exceed 300°C. This estimate takes into account the intensity and frequency of seismic events (which are the only significant cause of drift collapse early in the postclosure period) and uncertainty with respect to thermal conductivity of the host rock and drift-collapse rubble. The probability decreases as the threshold temperature increases, and decreases with time past 30 years after repository closure (Figures 6.5-1 and 6.5-2). The maximum probability is very close to 10^{-4} (subject to the uncertainty of Poisson counting statistics in Monte Carlo simulation). The potential impact to repository performance from excluding waste package and drip shield temperatures greater than 300°C is therefore insignificant. Note also that the thermally sensitive FEPs identified in Section 6.5 are only incrementally sensitive to small differences in temperature, and that the exceedance probability decreases steeply for higher threshold temperatures (Figure 6.5-3).

Excluding peak waste engineered barrier temperatures greater than 300°C is also supported by other information. The multiscale model, and the simulations presented in Section 6.4.2, are based on a porous-medium approach to mass transfer. This approach is suitable for representing heat transfer by conduction, forced convection, and thermal radiation, but not natural convection. Gas-phase natural convection in rubble will decrease the peak waste package temperatures calculated in Section 6.4.2. In addition, temperatures exceeding 300°C are predicted with partial drift collapse when the drip shield is barely covered, and there remains an opening above the rubble. Natural convection operating in this head space, promotes heat transfer away from the engineered barrier.

Finally, the analysis presented here is conservative with respect to the probability that naval SNF waste packages will exceed 300°C, because the heat output of the naval packages does not approach that of the hottest CSNF packages considered. Specifically, the available information on thermal output of naval SNF packages (McKenzie 2001 [DIRS 158051], Table 2) indicates a range of thermal output from 2.20 to 0.38 kW per package, at closure (assume 50 years after emplacement for comparison). By contrast, the output of CSNF waste packages used in the postclosure thermal reference case ranges from 3.116 to 5.306 kW per package at 50 years (DTN: MO0702PASTREAM.001 [DIRS 179925], file: *InitialRadInventories_REV01AD01A_OutputDTN.xl*s, worksheet: "DECAY CURVES"). For the 3-package and 7-package segments of the ELWS 96/2 emplacement sequence (Table 6.1-2), the hottest waste packages have output of up to 8 kW at 50 years after emplacement (Output DTN: MO0705SUPPCALC.000, folder: \Select Hot and Cold Cases, file: *Hottest 3-7 + Coolest WP 96-2 10Jul07.xls*). Accordingly, the peak temperature for naval SNF waste packages will be significantly lower than for CSNF

packages in the ELWS, and the probability that naval packages will exceed 300°C is therefore significantly less than 10^{-4}.

Table 6.5-3. Summary of Calculation Steps in the Monte Carlo Simulation of Waste Package Temperatures for a Nonzero Rockfall Event

Step	Description
1. Select a time for analysis and sample the Poisson Probability Distribution.	The Poisson distribution (SNL 2007 [DIRS 176828], Equation 6.7-3) is sampled for the occurrence of a seismic event.
2. Determine if a seismic event occurred.	Compare the probability to a randomly generated number between zero and one, and determine if a seismic event occurred.
3. In Step 2 if a seismic event occurred, determine the peak ground velocity.	For a seismic event the lambda parameter, defined as the Poisson process rate between 10^{-8} and 4.287×10^{-4}, is sampled uniformly. Enter the seismic hazard curve, and obtain the PGV for the event (SNL 2007 [DIRS 176828], Section 6.7.1.7).
4. Determine the probability of a nonzero rockfall event occurring.	The PGV is used in a relationship that provides the probability of a nonzero event occurring. The relationship shows that if the sampled ground velocity is less than 0.4 m/sec, then no rockfall occurs and the bulk rubble volume for the realization is set to zero. If the sampled PGV is greater than 1 m/sec, then rockfall is very likely.
5. In Step 4 If a nonzero rockfall event occurs then determine the rockfall volume.	For nonzero rockfall, the shape and scale parameters are sampled from the relationships developed for the mean and standard deviation, and the derived relationships for the shape and scale parameters of the gamma distribution (SNL 2007 [DIRS 176828], Figure 6-62). A random number from zero to one is selected, and the inverse gamma distribution relationship is used to determine the volume of intact rock comprising the rockfall.
6. Sample the bulking factor and determine the rubble volume.	Sample the uniform distribution for the bulking factor (SNL 2007 [DIRS 176828], Section 5.3).
7. Sample the intact-drift waste package temperature based on the host-rock thermal conductivity.	Sample the host-rock thermal conductivity for the low, mean, and high cases using the weights determined for rock mass thermal conductivity (SNL 2007 [DIRS 181383], Table 6.3-48).
8. Sample the effective thermal conductivity of the rubble.	Two alternative sampling schemes are used: (1) binary sampling between the high and low rubble thermal conductivity results; and (2) uniform sampling.
9. Interpolate the thermal-hydrologic results to estimate the temperature of the hottest waste package, accounting for partial collapse, host-rock thermal conductivity, and rubble thermal conductivity.	The temperature is obtained by linear interpolation of calculations based on the multiscale model (SNL 2007 [DIRS 181383], Section 6.3), and Section 6.4.2 of this report.

NOTES:

1. PGV = peak ground velocity (horizontal)
2. The process described by this table is repeated many times to develop the distribution function for exceedance probability as a function of time after closure.
3. If the probability of rockfall is zero, then the intact-drift waste package temperature is used.

Table 6.5-4. States of Partial Drift Collapse Analyzed

Percent Collapsed	Nominal Percent	Rubble Volume (m^3/meter of drift)
9	10	1.26
32	32	5.66
50	50	11.28
60	60	15.81
90	90	47.51
100	100	83.36

Source: Output DTN: MO0709HOTWASTE.000.

NOTES: Rubble volume rounded to 2 decimal places.

Analysis uses a bulking factor of 0.2.

Table 6.5-5. Confidence Interval Analysis of Probability for Waste Package Temperature Exceeding 300°C at 30 Years after Closure

Parameter	TSPA Base Case	3-Package Segment	7-Package Segment
Upper Confidence Interval	1.2E-04	6.2E-05	9.3E-05
Mean	1.0E-04	5.4E-05	8.6E-05
Lower Confidence Interval	9.1E-05	4.5E-05	7.9E-05

Source: Output DTN: MO0709HOTWASTE.000.

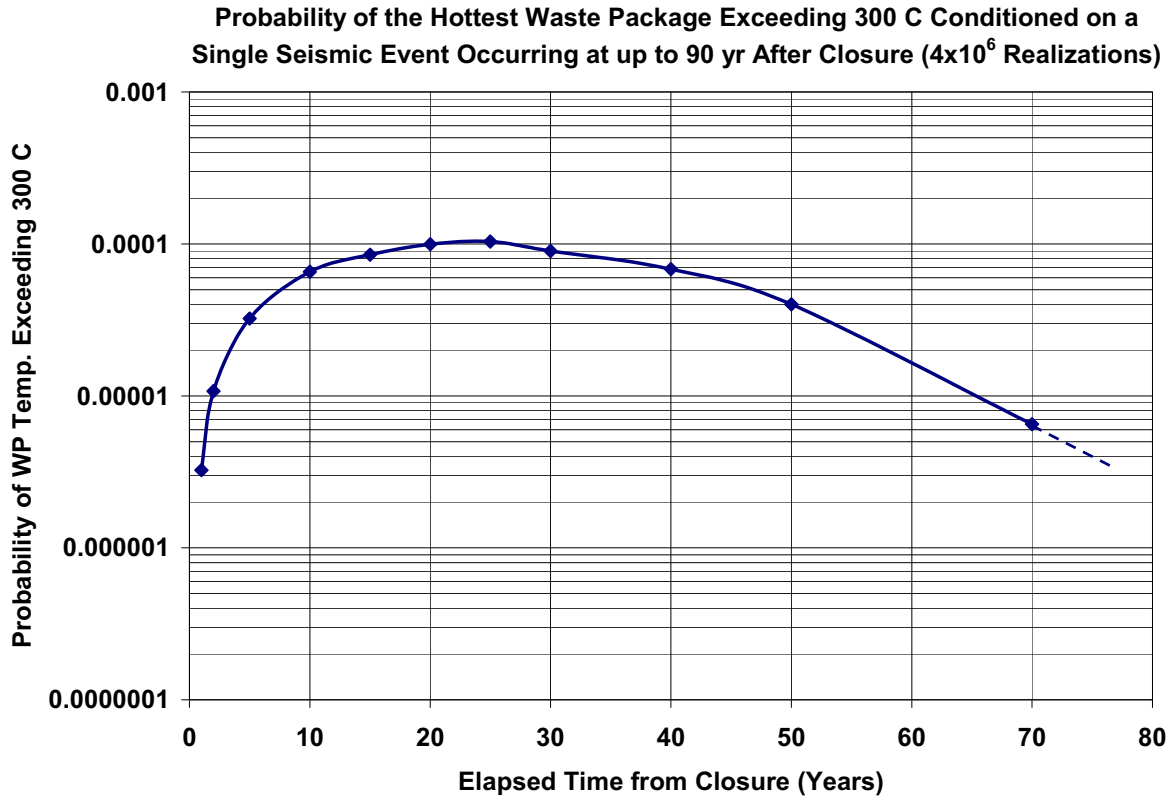

Source: Output DTN: MO0709HOTWASTE.000, file: *Worksheet in Seismic Consequence Analysis.xls*.

Figure 6.5-1. Monte Carlo Distribution for Single-Event Probability That the Hottest Waste Package Exceeds 300°C, for the TSPA Base Case

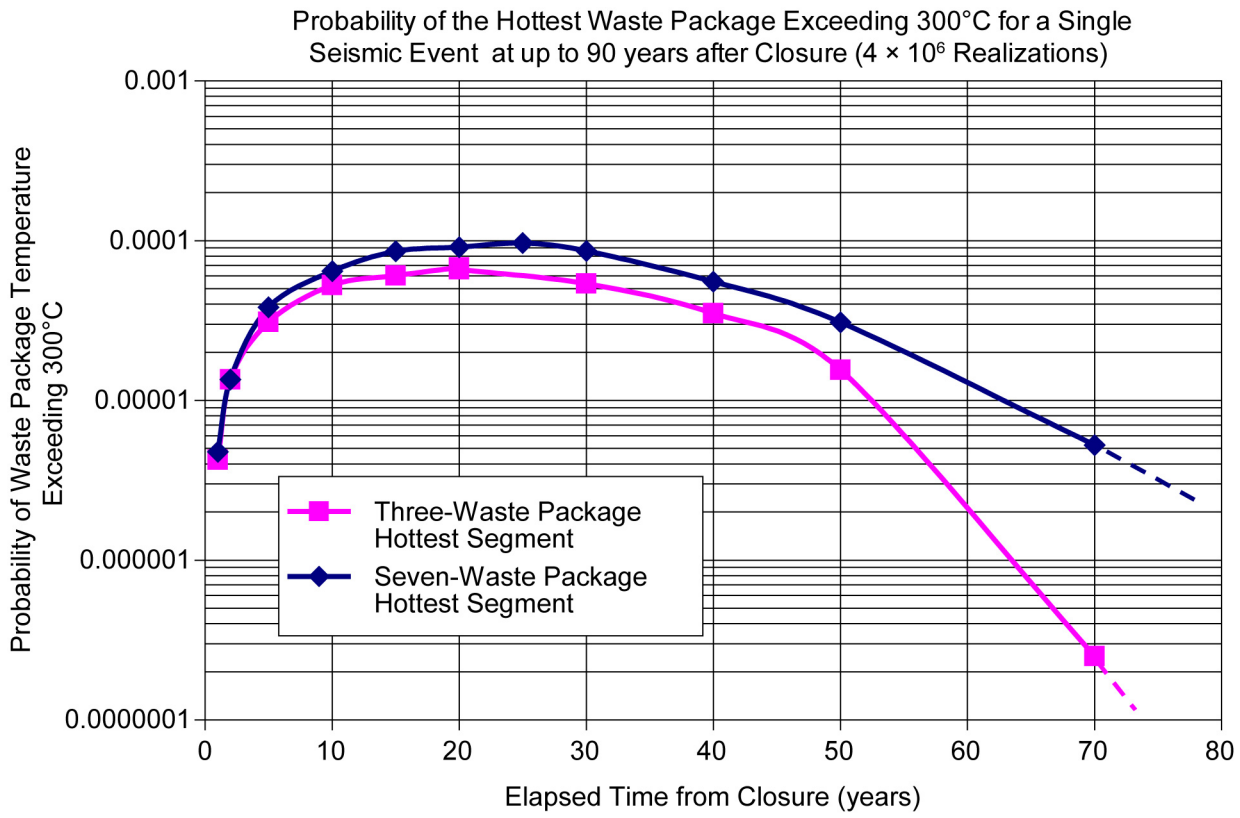

Source: Output DTN: MO0709HOTWASTE.000, file: *Worksheet in Seismic Consequence Analysis.xls*.

Figure 6.5-2. Monte Carlo Distribution for the Single-Event Probability That the Hottest Waste Package Exceeds 300°C, for the 3-Package and 7-Package Hottest Segments

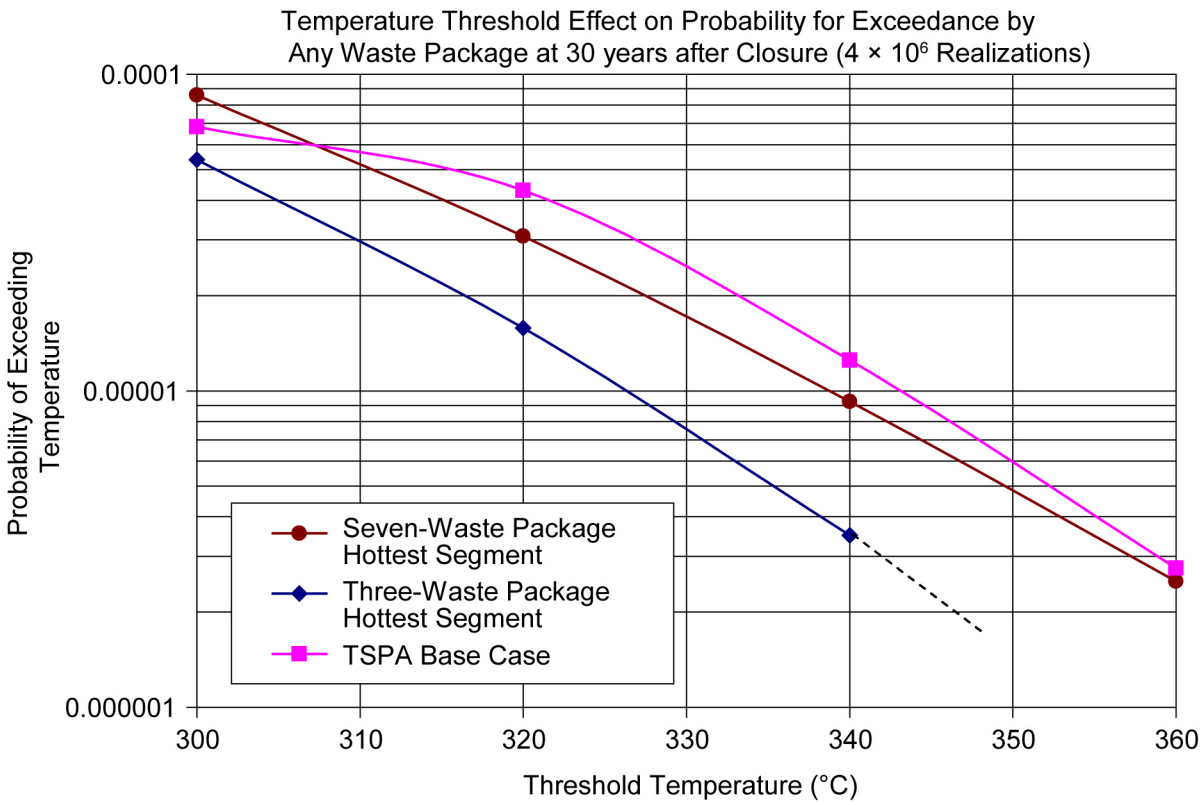

Source: Output DTN: MO0709HOTWASTE.000, file: *Worksheet in Seismic Consequence Analysis.xls*.

Figure 6.5-3. Monte Carlo Distribution for the Probability That the Hottest Waste Package Exceeds a Threshold Temperature, for the TSPA Base Case and the 3-Package and 7-Package Hottest Segments

INTENTIONALLY LEFT BLANK

7. SUMMARY AND CONCLUSIONS

7.1 SUMMARY AND CONCLUSIONS

This analysis has assessed the hydrogeologic, geomechanical, and geochemical responses to the anticipated range of thermal loading, and determined that for nominal conditions (intact, or uncollapsed drifts) there are only minor impacts to the model results used in total system performance assessment (TSPA) for the postclosure reference case; that the TSPA modeling basis is directly applicable; and that screening of features, events, and processes (FEPs) is not affected for these conditions.

For seismically induced drift collapse, a number of FEPs were identified (Section 6.5) that are thermally sensitive, and for which the screening justifications depend on peak temperatures lower than those predicted in Section 6.4.2. However, there is sufficiently low probability that seismically induced drift collapse will occur immediately after repository closure (i.e., within 80 years), combined with uncertainty as to the collapse volume and the thermal conductivity of rubble, that waste package temperature greater than 300°C can be excluded for both the TSPA and the anticipated range of thermal loading (Section 6.5.1).

Notwithstanding the low-probability justification described above, additional measures are available to further limit temperatures, including: increased end-to-end spacing of hotter commercial spent nuclear fuel (CSNF) waste packages, and longer preclosure ventilation (especially for the last CSNF waste packages emplaced). These measures have been previously identified as possible components of the thermal management strategy (SNL 2007 [DIRS 179196], Section 7; DOE 2006 [DIRS 176937], Section 4.6.5). In addition, further investigation of heat transfer in drift-collapse rubble could help to limit temperatures in the Engineered Barrier System (EBS).

The following discussion summarizes the analyses and findings of this report, leading to the conclusions given above:

Identify the Estimated Limiting Waste Stream – The anticipated range of thermal loading is represented using an estimated limiting waste stream (ELWS), consisting of a sequence of waste packages of different types as they are likely to be received at the Yucca Mountain repository. This sequence was developed using output from the total system model (TSM) (SNL 2007 [DIRS 179354], Table 4-4, Parameter 05-03) and qualified as input data for this analysis (Appendix B). The total system model (TSM) is an operational simulation that takes into account such variables as CSNF selection at the nuclear utilities, age and thermal requirements for transport, and throughput of repository facilities. The TSM case adopted as the ELWS constrains the CSNF part of the waste stream as not less than 5 years old (out-of-reactor), not more than 22 kW per canister, and 90% packaged at the nuclear utilities in transportation, aging, and disposal (TAD) canisters.

Importantly, the overall average thermal line load for the ELWS is slightly cooler than the postclosure reference case (Section 6.1), although the preclosure ventilation periods differ in duration, which means that the far-field thermal effects will be closely comparable (Section 6.4.2).

Simulate the Sequence of Waste Packages Emplaced Underground – Emplacement of waste packages underground was simulated by post-processing the ELWS, observing the receipt schedule, and following a set of loading rules:

- Maximum waste package thermal output at emplacement: 18.0 kW
- Maximum 7-package running average of waste package heat output: 2.0 kW/m
- Maximum 7-package running average of the calculated thermal energy density for each waste package, constrained to a value that controls mid-pillar temperature.

The emplacement simulation also honored throughput constraints for repository facilities. Cooler DHLW packages were used to control local thermal loading, and were assumed to be available on demand. Emplacement sequences were constructed by selecting waste packages from surface storage, or selecting DHLW packages, to optimize the mid-pillar loading rule (which was the limiting constraint) while honoring the other rules. This post-processing yielded two emplacement sequences:

- 85/4 Sequence – Optimized to 85°C maximum mid-pillar temperature, requiring repository surface storage capacity corresponding to 4 years of CSNF receipts
- 96/2 Sequence – Optimized to 96°C maximum mid-pillar temperature, requiring repository surface storage capacity corresponding to 2 years of CSNF receipts.

These emplacement sequences were also qualified as input data for this analysis (Appendix B). Whereas these sequences were developed using thermal measures based on the mean thermal conductivity for the lithophysal host rock, sensitivity analyses (Section 6.2) were performed to show that there is margin in the analysis, which compensates for the known uncertainty and variability in host-rock thermal conductivity. The margin comes from repository drift-end and edge-drift cooling effects, stratigraphic variation of rock properties, and the influence of hydrology on mid-pillar temperatures.

Select Local Hottest Segments for Near-Field Sensitivity Analyses – The 85/4 and 96/2 emplacement sequences were searched to find the hottest and coolest segments of 13 waste packages, and the locations of maximum heterogeneity (or difference in thermal output between adjacent packages). A drift wall thermal energy density criterion was used to quantify waste package heat output in a manner suited for selecting the hottest segments. A side-calculation supported the use of drift wall temperature to identify the hottest segments, by showing that peak drift wall temperature correlates with highest temperatures for several meters into the surrounding rock (Section 6.1).

Hottest segments were selected on the basis of the hottest 7-point running average, and the hottest 3-point running average, of the drift wall thermal energy density (Table 6.1-2). Both segments were found in the 96/2 emplacement sequence, and both were emplaced near the end of the 50-year operational period. The 7-point segment represents the most likely hottest local-average thermal loading condition. It consists of 13 different waste packages but can also be represented by an average line-load, due to axial heat sharing by thermal radiation within the

drift. Finite-element calculations were performed (Section 6.3) explicitly simulating the 7-point and 3-point segments, to confirm the extent of postclosure axial heat sharing. By comparison, the 3-point segment contains the hottest overall waste package (flanked by cooler packages), and produces thermal effects that are more three-dimensional and cannot be reasonably represented by an average line load. These hottest segments are used to assess the responses of the geomechanical, hydrogeologic, and geochemical systems.

Peak Drift Wall Temperature Analysis Summary – This analysis shows that the anticipated range of thermal loading will meet the postclosure 200°C limit, even using the 10th percentile thermal conductivity for the lower lithophysal (Tptpll) host rock unit. The first scenario considered in Section 6.3 is a repeat of the original base case from *Repository Twelve Waste Package Segment Thermal Calculation* (BSC 2006 [DIRS 179686]) substituting the lower, 10th percentile value for thermal conductivity. The second scenario is the same case, with further substitution of new functions describing the heat capacity effect from host-rock dewatering (Appendix C). Both of these scenarios produced peak postclosure drift wall temperatures significantly less than 200°C.

Scenarios 3 and 4 presented in Section 6.3 implement the 3-package and 7-package hottest segments identified in the 96/2 ELWS emplacement sequence (Section 6.1). In other respects, the simulations are the same as the second scenario discussed above. These results also show that peak postclosure drift wall temperatures will be significantly less than 200°C, particularly if cooler DHLW waste packages are used to comply with the "loading rules" identified in Section 6.1.3. The ANSYS simulations in Section 6.3 demonstrate the importance of axial heat sharing among waste packages, which spreads heat by thermal radiation over distances of approximately three waste packages, in intact (uncollapsed) drifts.

Geomechanical Impact Evaluation Summary – Thermal-mechanical analyses were performed using a distinct element (UDEC) approach documented in *Drift Degradation Analysis* (BSC 2004 [DIRS 166107]). This modeling approach has been used to assess the impacts of seismic ground motion, and variability in rock quality on rockfall and drift collapse, for use in TSPA abstractions (SNL 2007 [DIRS 176828]). The principal focus of this analysis was to determine if higher rock temperatures possible with the range of thermal loading, represented by average line loads from the selected 7-point (Case 1) and 3-point (Case 2) hottest segments, would significantly change the likelihood of drift collapse or the amount of rockfall. The results (Section 6.4.1) show that the strength-to-stiffness ratios for the host rock units are large enough that higher temperatures will not significantly increase the amount of rockfall, even considering the lowest quality of lithophysal rock (Category 1). Complete drift collapse was not predicted as a consequence of thermal loading. Seismic ground motion would therefore remain the principal cause of drift collapse, possibly augmented by time-dependent degradation of rock strength properties (SNL 2007 [DIRS 179476], FEP 1.2.03.02.0C).

Hydrogeologic Impact Evaluation Summary – A series of two-dimensional (2-D) and three-dimensional (3-D) thermal-hydrologic analyses was performed (Section 6.4.2) using the NUFT simulator, implementing modeling approaches used in *Multiscale Thermohydrologic Model* (SNL 2007 [DIRS 181383]). Both the 7-point (Case 1) and 3-point (Case 2) segments were simulated in 3-D, using various combinations of rock properties and percolation flux boundary conditions. The resulting postclosure peak temperatures (i.e., waste package, drift

wall, and mid-pillar) were in compliance with previously established limits (DOE 2006 [DIRS 176937], Section 4.6.5). Examination of package-to-package variability showed that rewetting behavior is temperature controlled rather than driven by liquid flux generated as condensate around hotter packages. Thermal-hydrologic processes occurred coherently among the different waste package types, with, at most, moderate differences in the timing of cooling and rewetting. Using a 2-D modeling approach, far-field thermal-hydrologic effects were examined for the average line load for the postclosure reference case, and for the average line load corresponding to the ELWS. Far-field effects are very similar, which is expected from the similarity of the line loads, and the tendency for far-field conditions to respond to average thermal loading. Finally, the 3-D simulations were repeated in a configuration representing completed drift-collapse, using bounding values for rubble thermal conductivity, host rock thermal conductivity, and percolation flux. The resulting waste package temperature histories show that temperatures approaching 400°C could be reached for a few waste packages, for these worst-case conditions (Figure 6.4.2-29).

The multiscale modeling approach used to generate Figure 6.4.2-29 is the same as previous versions of this model (SNL 2007 [DIRS 181383]) except that a new method is used to estimate effective thermal conductivity of rubble, giving a broader range of uncertainty and higher peak waste package temperatures (SNL 2007 [DIRS 181383], Appendix XI[a]).

Geochemical Impact Evaluation Summary – The near-field chemistry (NFC) model (SNL 2007 [DIRS 177412]) was used to evaluate potential changes in composition of seepage water that could result from the anticipated range of thermal loading. This model is validated for this use in TSPA, and includes the effects from variability and uncertainty in host-rock thermal properties, percolation flux, repository edge-cooling effects, in situ geochemical properties, and kinetics of water–rock interaction (Section 6.4.3). A representative average line load was extracted from the 7-point (Case 1) segment and used as input to the NFC model. The resulting seepage compositions exhibit slightly more water–rock interaction, and thus higher pH, and less Ca and Mg compared to Na and K. These aspects are generally favorable to corrosion resistance of Alloy 22. The model results used in this analysis are within the range of uncertainty that is incorporated in the NFC model abstraction used in TSPA.

FEP Impact Evaluation Summary – An evaluation of FEPs was conducted by the authors of this study and the FEP team to identify and analyze those that are thermally sensitive (Section 6.5). Of approximately 374 FEPs overall, 79 were evaluated to determine whether: (1) the screening justification used for inclusion/exclusion applies to the anticipated range of thermal loading, and (2) the modeling basis used for included FEPs in TSPA has the capability to represent the range of thermal loading. The results showed that for nominal conditions (intact, or uncollapsed drifts) all the FEP screening justifications could be applied, and that the TSPA modeling basis is adequate.

For collapsed-drift conditions, the following FEPs (Section 6.5) are thermally sensitive, and the screening justifications depend on peak waste package temperatures lower than the extreme temperatures predicted for the anticipated range of thermal loading (Section 6.4.2):

1.2.03.02.0A – Seismic ground motion damages EBS components (included)
1.2.03.02.0B – Seismic-induced rockfall damages EBS components (included)

1.2.03.02.0C – Seismic-induced drift collapse damages EBS components (included)
2.1.07.05.0A – Creep of metallic materials in the waste package (excluded)
2.1.07.05.0B – Creep of metallic materials in the drip shield (excluded)
2.1.11.05.0A – Thermal expansion and stress of in-package EBS components (excluded)
2.1.11.06.0A – Thermal sensitization of waste packages (excluded).

In addition, the following excluded FEPs (SNL 2007 [DIRS 179476]) describe degradation of SNF cladding, and are excluded for CSNF (TSPA takes no performance credit for CSNF cladding integrity), but changes in peak waste form temperature and thermal duration may impact disposition of these FEPs for naval SNF:

2.1.02.13.0A – General corrosion of cladding (excluded)
2.1.02.16.0A – Localized (pitting) corrosion of cladding (excluded)
2.1.02.17.0A – Localized (crevice) corrosion of cladding (excluded)
2.1.02.19.0A – Creep rupture of cladding (excluded)
2.1.02.22.0A – Hydride cracking of cladding (excluded)
2.1.02.26.0A – Diffusion controlled cavity growth in cladding (excluded).

Characteristics of naval SNF and its inclusion in repository performance assessment are beyond the scope of this report. However, all of the FEPs listed above, including aspects pertaining to naval SNF, have already been screened for peak waste temperatures up to 300°C (SNL 2007 [DIRS 179476]). The additional screening justification provided in Section 6.5.1 of this report shows that there is low probability of waste package temperatures exceeding 300°C due to seismically induced drift collapse immediately after closure.

Excluding peak temperatures greater than 300°C, due to drift collapse immediately after repository closure, is supported by additional information. The multiscale model, and the simulations presented in Section 6.4.2, are based on a porous-medium modeling approach that does not include heat transfer by gas-phase natural convection in rubble. Also, the peak temperature calculations in Section 6.4.2 generally use bounding values for waste package heat output, rubble thermal conductivity, host rock thermal conductivity, and percolation flux. The 3-point segment (Case 2) includes the hottest waste package in the ELWS. Thus, the actual number of waste packages for which temperature could exceed 300°C following a seismic event with low probability is small.

Conclusions – This analysis has assessed the hydrogeologic, geomechanical, and geochemical responses to the anticipated range of thermal loading and has determined that, for nominal conditions (intact, or uncollapsed drifts), the TSPA modeling basis is directly applicable, and that FEP screening is unaffected.

For seismically induced drift collapse, a number of FEPs are identified which are thermally sensitive and for which the screening justifications depend on peak waste package temperatures being lower than those predicted for the anticipated range of thermal loading. An additional probabilistic analysis in this report (Section 6.5.1), shows that there is low probability that the peak temperature of any waste package will exceed 300°C, so there is low risk associated with seismically induced drift collapse immediately after repository closure. Additional measures are available during repository emplacement and operations to further limit temperatures, including

increased end-to-end spacing of hotter CSNF waste packages, and extended duration of preclosure ventilation (especially for the last CSNF waste packages emplaced).

7.2 YUCCA MOUNTAIN REVIEW PLAN CRITERIA

This section summarizes the contributions made by this analysis report toward satisfaction of listed criteria from *Yucca Mountain Review Plan, Final Report* (YMRP) (NRC 2003 [DIRS 163274]). The information is organized by YMRP section. The YMRP criteria and sub-criteria are given verbatim, followed by discussion.

Criteria or sub-criteria from the YMRP (NRC 2003 [DIRS 163274], Section 2.2.3.3) that are not presented here are beyond the scope of this report, or are duplicated (e.g., data qualification, which is addressed only once in the discussion below). This is the case for Acceptance Criterion 4 and sub-criteria from Acceptance Criteria 1, 2, and 3 from Section 2.2.1.3.3.3, which were called out in the technical work plan (TWP) (BSC 2006 [DIRS 179791], Section 3). Criteria for degradation of engineered barriers, and mechanical disruption of engineered barriers, were added to this section in consideration of the conclusions reached in the FEP analysis of Section 6.5 and represent a deviation from the TWP (BSC 2006 [DIRS 179791], Section 3.3), as noted in Section 1.

Degradation of Engineered Barriers (NRC 2003 [DIRS 163274], Section 2.2.1.3.2.3)—from 10 CFR 63.114(a), (b), (e), (f):

Acceptance Criterion 1 – System Description and Model Integration Are Adequate

(1) The total system performance assessment adequately incorporates important design features, physical phenomena, and couplings, and uses consistent and appropriate assumptions throughout the degradation of engineered barriers abstraction process.

This analysis evaluates the effects from the anticipated range of thermal loading (a possible design feature) on the physical phenomena and couplings that affect engineered barrier degradation in the TSPA. For example, higher temperature can affect thermal sensitization of Alloy 22 (Section 6.5).

(2) Assessment abstraction of the degradation of engineered barriers uses assumptions, technical bases, data, and models that are appropriate and consistent with other related U.S. Department of Energy abstractions. For example, the assumptions used for degradation of engineered barriers should be consistent with the abstractions of the quantity and chemistry of water contacting waste packages and waste forms (Section 2.2.1.3.3); climate and infiltration (Section 2.2.1.3.5); and mechanical disruption of waste packages (Section 2.2.1.3.2). The descriptions and technical bases provide transparent and traceable support for the abstraction of the degradation of engineered barriers.

The geomechanical, hydrogeologic, and geochemical analyses provided in this report (Section 6.4) are developed using consistent assumptions about the range of thermal loading, drift collapse, and other processes that are important to assessing degradation of engineered

barriers. The results of the analyses in Section 6.4 are then evaluated with respect to the included and excluded FEPs that control engineered barrier degradation in Section 6.5.

(3) The descriptions of engineered barriers, design features, degradation processes, physical phenomena, and couplings that may affect the degradation of the engineered barriers are adequate. For example, materials and methods used to construct the engineered barriers are included, and degradation processes, such as uniform corrosion, pitting corrosion, crevice corrosion, stress corrosion cracking, intergranular corrosion, microbially influenced corrosion, dry-air oxidation, hydrogen embrittlement, and the effects of wet and dry cycles, material aging and phase stability, welding, and initial defects on the degradation modes for the engineered barriers are considered.

The effects from the anticipated range of thermal loading on the features and processes that potentially control waste package and drip shield performance are considered in the FEP analysis of Section 6.5.

(4) Boundary and initial conditions used in the total system performance assessment abstractions are propagated consistently throughout the abstraction approaches. For example, the conditions and assumptions used in the degradation of engineered barriers abstraction are consistent with those used to model the quantity and chemistry of water contacting waste packages and waste forms (Section 2.2.1.3.3); climate and infiltration (Section 2.2.1.3.5); and mechanical disruption of waste packages (Section 2.2.1.3.2).

The thermal boundary condition associated with the anticipated range of thermal loading is developed in this report (Section 6.1) and consistently used to evaluate the potential for geomechanical, hydrogeologic, and geochemical effects that could influence degradation of engineered barriers (Section 6.4).

(5) Sufficient technical bases for the inclusion of features, events, and processes related to degradation of engineered barriers in the total system performance assessment abstractions are provided.

The FEP analysis in Section 6.5 includes an evaluation of whether the TSPA modeling basis can accommodate the cooler and hotter temperatures associated with the anticipated range of thermal loading.

(7) Guidance in NUREG–1297 and NUREG–1298 (Altman et al. 1988 [DIRS 103597]; Altman et al. 1988 [DIRS 103750]), or other acceptable approaches, is followed.

Qualified data are used in this analysis, principally by incorporating the same data used for the TSPA modeling basis. The total system model input is qualified in Appendix B.

Mechanical Disruption of Engineered Barriers (NRC 2003 [DIRS 163274], Section 2.2.1.3.2.3)—from 10 CFR 63.114(a), (b), (e), (f):

Acceptance Criterion 1 – System Description and Model Integration Are Adequate

(1) Total system performance assessment adequately incorporates important design features, physical phenomena, and couplings, and uses consistent and appropriate assumptions throughout the mechanical disruption of engineered barrier abstraction process.

The thermal effects from drift collapse, combined with the anticipated range of thermal loading, are an important topic of this analysis. The geomechanical analysis (Section 6.4.1) shows that drift collapse during the thermal period is a seismically induced process (and not strictly thermomechanical). Predictions of waste package temperature under drift-collapse rubble (Section 6.4.2) are consistent with the modeling basis used for TSPA. Probabilistic analysis of drift collapse and the consequent changes in engineered barrier temperature (Section 6.5.1), are consistent with the seismic consequence abstraction.

(2) The description of geological and engineering aspects of design features, physical phenomena, and couplings, that may affect mechanical disruption of engineered barriers, is adequate. For example, the description may include materials used in the construction of engineered barrier components, environmental effects (e.g., temperature, water chemistry, humidity, radiation, etc.) on these materials, and mechanical-failure processes and concomitant failure criteria used to assess the performance capabilities of these materials. Conditions and assumptions in the abstraction of mechanical disruption of engineered barriers are readily identified and consistent with the body of data presented in the description.

The temperature increase caused by drift collapse during the thermal period, with the anticipated range of thermal loading, is a key result of this analysis (Section 6.4.2). The rubble properties used for this purpose are based on geological characteristics of the lithophysal host rock, and include an appropriate range of uncertainty on the size of voids in the rubble.

(4) Boundary and initial conditions used in the total system performance assessment abstraction of mechanical disruption of engineered barriers are propagated throughout its abstraction approaches.

The potential effects of elevated temperature on mechanical disruption, for example the rate of creep in the drip shield loaded by rubble, are addressed in the FEP analysis (Section 6.5).

(5) Sufficient data and technical bases to assess the degree to which features, events, and processes have been included in this abstraction are provided.

This analysis develops temperature boundary conditions associated with the anticipated range of thermal loading, which are used to evaluate whether the TSPA modeling basis and its included and excluded FEPs can accommodate the range (Section 6.5).

Quantity and Chemistry of Water Contacting Waste Packages and Waste Forms (NRC 2003 [DIRS 163274], Section 2.2.1.3.3.3)—from 10 CFR 63.114(a), (b), (e), (f):

Acceptance Criterion 1 – System Description and Model Integration Are Adequate:

(1) Total system performance assessment adequately incorporates important design features, physical phenomena, and couplings, and uses consistent and appropriate assumptions throughout the quantity and chemistry of water contacting engineered barriers and waste forms abstraction process.

This analysis addresses the anticipated range of design thermal loading (Section 6). This includes review of features, events, and processes (FEPs; Section 6.5) to identify the various physical processes and couplings, represented by FEPs, that could be affected by thermal loading with consequent impact on the quantity and chemistry of water contacting waste packages and waste forms. For the FEPs identified as thermally sensitive, the review addresses the applicability of each FEP screening justification to the range of thermal loading, and whether included FEPs can be appropriately represented by the TSPA modeling basis.

(2) The abstraction of the quantity and chemistry of water contacting engineered barriers and waste forms uses assumptions, technical bases, data, and models, that are appropriate and consistent with other related U.S. Department of Energy abstractions. appropriate and consistent with other related U.S. Department of Energy abstractions. For example, the assumptions used for the quantity and chemistry of water contacting engineered barriers and waste forms are consistent with the abstractions of "Degradation of Engineered Barriers" (Section 2.2.1.3.2.3); "Mechanical Disruption of Engineered Barriers (Section 2.2.1.3.2); "Radionuclide Release Rates and Solubility Limits" (Section 2.2.1.3.4); "Climate and Infiltration" (Section 2.2.1.3.5); and "Flow Paths in the Unsaturated Zone" (Section 2.2.1.3.6). The descriptions and technical bases provide transparent and traceable support for the abstraction of quantity and chemistry of water contacting engineered barriers and waste forms.

The geomechanical, geochemical, and hydrogeologic analyses presented in this report (Section 6.4) are based directly on the relevant abstractions used in TSPA.

(3) Important design features, such as waste package design and material selection, backfill, drip shield, ground support, thermal loading strategy, and degradation processes, are adequate to determine the initial and boundary conditions for calculations of the quantity and chemistry of water contacting engineered barriers and waste forms.

The purpose of this analysis is to evaluate whether the thermal loading strategy, the TSPA modeling basis, and FEP screening justifications are adequate to determine the system response including quantity and chemistry of water contacting engineered barriers and waste forms.

(4) Spatial and temporal abstractions appropriately address physical couplings (thermal-hydrologic-mechanical-chemical). For example, the U.S. Department of Energy evaluates the potential for focusing of water flow into drifts, caused by coupled thermal-hydrologic mechanical-chemical processes.

The significance of physical couplings is included in the FEP evaluation (Section 6.5).

(5) Sufficient technical bases and justification are provided for total system performance assessment assumptions and approximations for modeling coupled thermal-hydrologic-mechanical-chemical effects on seepage and flow, the waste package chemical environment, and the chemical environment for radionuclide release. The effects of distribution of flow on the amount of water contacting the engineered barriers and waste forms are consistently addressed, in all relevant abstractions.

The technical bases for TSPA treatment of coupled processes, waste package chemical environment, and the chemical environment for radionuclide release have been established by other studies (see SNL 2007 [DIRS 179476]; SNL 2007 [DIRS 181383]; SNL 2007 [DIRS 181648]; SNL 2007 [DIRS 177412]; SNL 2007 [DIRS 177407]; SNL 2007 [DIRS 176828]). The applicability of the approaches used in those studies to the range of thermal loading is addressed in the analysis of FEP screening in Section 6.5 of this report. This analysis treats the distribution of flow in ways that are consistent with the basis reports cited above.

(6) The expected ranges of environmental conditions within the waste package emplacement drifts, inside the breached waste packages, and contacting the waste forms and their evolution with time are identified. These ranges may be developed to include: (i) the effects of the drip shield and backfill on the quantity and chemistry of water (e.g., the potential for condensate formation and dripping from the underside of the shield); (ii) conditions that promote corrosion of engineered barriers and degradation of waste forms; (iii) irregular wet and dry cycles; (iv) gamma-radiolysis; and (v) size and distribution of penetrations of engineered barriers.

The effects from the range of thermal loading on environmental conditions are identified and evaluated in Sections 6.4 and 6.5 of this report.

(7) The model abstraction for quantity and chemistry of water contacting engineered barriers and waste forms is consistent with the detailed information on engineered barrier design and other engineered features. For example, consistency is demonstrated for: (i) dimensionality of the abstractions; (ii) various design features and site characteristics; and (iii) alternative conceptual approaches. Analyses are adequate to demonstrate that no deleterious effects are caused by design or site features that the U.S. Department of Energy does not take into account in this abstraction.

Current design information, including a projection of the range of thermal loading (Section 6.1), is used in this report (Sections 6.2 through 6.5). Exceptions to this statement are minor differences in EBS configuration (e.g., invert height as applied in Sections 6.2 and 6.4.2), which are justified in the basis documents for TSPA as having negligible impact, and carried forward into this report.

(8) Adequate technical bases are provided, including activities such as independent modeling, laboratory or field data, or sensitivity studies, for inclusion of any thermal-hydrologic-mechanical-chemical couplings and features, events, and processes.

This report relies on the TSPA basis reports cited above, particularly the FEP screening analysis (SNL 2007 [DIRS 179476]), to establish the inclusion or exclusion of coupled processes and FEPs.

(10) Likely modes for container corrosion (Section 2.2.1.3.3.3 of the Yucca Mountain Review Plan) are identified and considered in determining the quantity and chemistry of water entering the engineered barriers and contacting waste forms. For example, the model abstractions consistently address the role of parameters, such as pH, carbonate concentration, and the effect of corrosion on the quantity and chemistry of water contacting engineered barriers and waste forms.

The effect from the range of thermal loading on the composition of potential seepage water is described in Section 6.4.3. The screening basis for other modes of container corrosion is addressed in Section 6.5.

(12) Guidance in NUREG–1297 and NUREG–1298 (Altman et al. 1988 [DIRS 103597]; Altman et al. 1988 [DIRS 103750]), or other acceptable approaches, is followed.

The data qualification process that is based on NUREG-1298 (Altman et al. 1988 [DIRS 103750]) is applied for qualification of key data in Appendices A and B of this report.

Acceptance Criterion 2 – Data Are Sufficient for Model Justification:

(2) Sufficient data were collected on the characteristics of the natural system and engineered materials to establish initial and boundary conditions for conceptual models of thermal-hydrological-mechanical-chemical coupled processes, that affect seepage and flow and the engineered barrier chemical environment.

The technical bases for treatment of coupled processes that affect seepage, flow, and the EBS chemical environment are established by other studies as discussed above. This report contributes by showing how the natural and engineered systems will respond to the anticipated range of thermal loading.

Acceptance Criterion 3 – Data Uncertainty Is Characterized and Propagated through the Model Abstraction:

(1) Models use parameter values, assumed ranges, probability distributions, and bounding assumptions that are technically defensible, reasonably account for uncertainties and variabilities, and do not result in an under-representation of the risk estimate.

The attributes of models and analyses applied in this report are established by other reports as discussed above. The analyses in this report (Sections 6.4 and 6.5) specifically consider the applicability of those models and analyses to evaluating responses to the anticipated range of thermal loading.

(3) Input values used in TSPA are consistent with the boundary conditions and assumptions associated with the design concepts for the Yucca Mountain site. Reasonable or conservative ranges of parameters or functional relations are established.

One of the purposes of this analysis is to determine through review of FEPs (Section 6.5) whether the TSPA modeling basis as documented in model reports cited in Section 6.4 is applicable to thermal conditions associated with the anticipated range of thermal loading. In addition, this analysis uses a realization of the likely waste stream, and relies on the application of "loading rules," to describe how that waste stream would likely be emplaced in the repository (Section 6.1). The emplaced sequence represents thermal loading aspects of the repository design, and the "loading rules" are based on reasonable or conservative treatment of parameters.

7.3 OUTPUT DATA

The DTNs listed in Table 7-1 were developed for this analysis, are supported by this report, and are intended to be technical product output.

Table 7-1. Output DTNs

DTN	Section(s)	Description
MO0705SUPPCALC.000	Sections 6.1 and 6.2	Thermal analysis used in (1) the emplacement sequence analysis (2) identification of hottest local conditions in the repository and (3) demonstration of thermal margin from edge- and end-loading
MO0707THERMHYD.000	Section 6.2	Thermal-hydrologic analysis used in demonstration of thermal margin
MO0707THERMRES.000	Section 6.4.1	Geomechanical analysis used to analyze response to the range of thermal loading
MO0707TH2D3DDC.000	Section 6.4.2	Thermal-hydrologic analysis used to analyze hydrogeologic response to the range of thermal loading
MO0707GEORESPO.000	Section 6.4.3	Geochemical analysis used to analyze response to the range of thermal loading
MO0709REVTHERM.000	Appendix C	Revised thermal properties – heat capacity
MO0707HOTWASTE.000	Section 6.5.1	Probabilistic analysis of hottest waste package temperature for drift collapse
MO0709THERMAL1.000	Section 6.3	Thermal drift analysis – Scenario 1
MO0709THERMAL2.000	Section 6.3	Thermal drift analysis – Scenario 2
MO0709THERMAL3.000	Section 6.3	Thermal drift analysis – Scenario 3
MO0709THERMAL4.000	Section 6.3	Thermal drift analysis – Scenario 4
MO0711SENSTEST.000	Section 6.3.2.5	Sensitivity Analysis for TPTPV3 Unit heat capacity values

8. INPUTS AND REFERENCES

8.1 DOCUMENTS CITED

103597 Altman, W.D.; Donnelly, J.P.; and Kennedy, J.E. 1988. *Peer Review for High-Level Nuclear Waste Repositories: Generic Technical Position.* NUREG-1297. Washington, D.C.: U.S. Nuclear Regulatory Commission. TIC: 200651.

103750 Altman, W.D.; Donnelly, J.P.; and Kennedy, J.E. 1988. *Qualification of Existing Data for High-Level Nuclear Waste Repositories: Generic Technical Position.* NUREG-1298. Washington, D.C.: U.S. Nuclear Regulatory Commission. TIC: 200652.

100653 Brodsky, N.S.; Riggins, M.; Connolly, J.; and Ricci, P. 1997. *Thermal Expansion, Thermal Conductivity, and Heat Capacity Measurements for Boreholes UE25 NRG-4, UE25 NRG-5, USW NRG-6, and USW NRG-7/7A.* SAND95-1955. Albuquerque, New Mexico: Sandia National Laboratories. ACC: MOL.19980311.0316.

171924 BSC (Bechtel SAIC Company) 2004. *Aging and Phase Stability of Waste Package Outer Barrier.* ANL-EBS-MD-000002 REV 02. Las Vegas, Nevada: Bechtel SAIC Company. ACC: DOC.20041005.0003.

170019 BSC 2004. *Clad Degradation – FEPs Screening Arguments.* ANL-WIS-MD-000008 REV 02. Las Vegas, Nevada: Bechtel SAIC Company. ACC: DOC.20041020.0014; DOC.20060213.0007.

169987 BSC 2004. *CSNF Waste Form Degradation: Summary Abstraction.* ANL-EBS-MD-000015 REV 02. Las Vegas, Nevada: Bechtel SAIC Company. ACC: DOC.20040908.0001; DOC.20050620.0004.

169988 BSC 2004. *Defense HLW Glass Degradation Model.* ANL-EBS-MD-000016 REV 02. Las Vegas, Nevada: Bechtel SAIC Company. ACC: DOC.20041020.0015; DOC.20050922.0002.

166107 BSC 2004. *Drift Degradation Analysis.* ANL-EBS-MD-000027 REV 03. Las Vegas, Nevada: Bechtel SAIC Company. ACC: DOC.20040915.0010; DOC.20050419.0001; DOC.20051130.0002; DOC.20060731.0005.

169864 BSC 2004. *Drift Scale THM Model.* MDL-NBS-HS-000017 REV 01. Las Vegas, Nevada: Bechtel SAIC Company. ACC: DOC.20041012.0001; DOC.20060103.0002.

172453 BSC 2004. *DSNF and Other Waste Form Degradation Abstraction.* ANL-WIS-MD-000004 REV 04. Las Vegas, Nevada: Bechtel SAIC Company. ACC: DOC.20041201.0007.

169991 BSC 2004. *Evaluation of Potential Impacts of Microbial Activity on Drift Chemistry.* ANL-EBS-MD-000038 REV 01. Las Vegas, Nevada: Bechtel SAIC Company. ACC: DOC.20041118.0005; DOC.20050505.0001; DOC.20050609.0001.

170029 BSC 2004. *Geologic Framework Model (GFM2000).* MDL-NBS-GS-000002 REV 02. Las Vegas, Nevada: Bechtel SAIC Company. ACC: DOC.20040827.0008.

170003 BSC 2004. *Heat Capacity Analysis Report.* ANL-NBS-GS-000013 REV 01. Las Vegas, Nevada: Bechtel SAIC Company. ACC: DOC.20041101.0003.

169854 BSC 2004. *Thermal Conductivity of the Potential Repository Horizon.* MDL-NBS-GS-000005 REV 01. Las Vegas, Nevada: Bechtel SAIC Company. ACC: DOC.20040928.0006.

169862 BSC 2004. *Ventilation Model and Analysis Report.* ANL-EBS-MD-000030 REV 04. Las Vegas, Nevada: Bechtel SAIC Company. ACC: DOC.20041025.0002.

166941 BSC 2004. *Waste Form, Heat Output, and Waste Package Spacing for an Idealized Drift Segment.* 000-00C-WIS0-00500-000-00A. Las Vegas, Nevada: Bechtel SAIC Company. ACC: ENG.20040121.0007; ENG.20050817.0031; ENG.20051019.0002.

172232 BSC 2005. *Drift-Scale Coupled Processes (DST and TH Seepage) Models.* MDL-NBS-HS-000015 REV 02. Las Vegas, Nevada: Bechtel SAIC Company. ACC: DOC.20050114.0004; DOC.20051115.0002.

174101 BSC 2005. *Mountain-Scale Coupled Processes (TH/THC/THM) Models.* MDL-NBS-HS-000007 REV 03. Las Vegas, Nevada: Bechtel SAIC Company. ACC: DOC.20050825.0007.

175539 BSC 2005. *Q-List.* 000-30R-MGR0-00500-000-003. Las Vegas, Nevada: Bechtel SAIC Company. ACC: ENG.20050929.0008.

174995 BSC 2005. *Screening of Features, Events, and Processes in Drip Shield and Waste Package Degradation.* ANL-EBS-PA-000002 REV 05. Las Vegas, Nevada: Bechtel SAIC Company. ACC: DOC.20050817.0003; DOC.20050826.0002; DOC.20050929.0007.

177636 BSC 2006. *Basis of Design for the TAD Canister-Based Repository Design Concept.* 000-3DR-MGR0-00300-000-000. Las Vegas, Nevada: Bechtel SAIC Company. ACC: ENG.20061023.0002; ENG.20061121.0005; ENG.20061116.0005; ENG.20061204.0002; ENG.20061218.0003; ENG.20061218.0004; ENG.20070220.0010; ENG.20070220.0011; ENG.20070220.0012; ENG.20070314.0009; ENG.20070412.0002; ENG.20070222.0007; ENG.20070222.0008; ENG.20070221.0010; ENG.20070222.0009; ENG.20070308.0029; ENG.20070501.0009; ENG.20070507.0028; ENG.20070608.0019.

178308 BSC 2006. *Project Design Criteria Document.* 000-3DR-MGR0-00100-000-006. Las Vegas, Nevada: Bechtel SAIC Company. ACC: ENG.20061201.0005; ENG.20070111.0025; ENG.20070111.0026; ENG.20070111.0027; ENG.20070111.0028; ENG.20070112.0001; ENG.20070201.0021; ENG.20070222.0011; ENG.20070222.0012; ENG.20070226.0030; ENG.20070308.0028; ENG.20070412.0001; ENG.20070501.0008; ENG.20070510.0002; ENG.20070516.0030; ENG.20070518.0006; ENG.20070621.0002; ENG.20070627.0009.

179686 BSC 2006. *Repository Twelve Waste Package Segment Thermal Calculation.* 800-00C-WIS0-00100-000-00B. Las Vegas, Nevada: Bechtel SAIC Company. ACC: ENG.20061116.0001.

179791 BSC 2006. *Technical Work Plan for Postclosure Thermal Envelope Study.* TWP-MGR-PA-000041 REV 00. Las Vegas, Nevada: Bechtel SAIC Company. ACC: DOC.20061010.0002.

184615 BSC 2006. *TSM GROA Basis and Check.* 000-00C-G000-01100-000-00A. Las Vegas, NV: Bechtel SAIC Company. ACC: ENG.20060912.0003.

179640 BSC 2007. *Underground Layout Configuration for LA.* 800-KMC-SS00-00200-000-00B. Las Vegas, Nevada: Bechtel SAIC Company. ACC: ENG.20070727.0004.

183627 BSC 2008. *Postclosure Modeling and Analyses Design Parameters.* TDR-MGR-MD-000037 REV 02. Las Vegas, Nevada: Bechtel SAIC Company. ACC: ENG.20080108.0002.

100968 Carslaw, H.S. and Jaeger, J.C. 1959. *Conduction of Heat in Solids.* 2nd Edition. Oxford, Great Britain: Oxford University Press. TIC: 206085.

183072 Cooper, H.W. and Simmons, G. 1977. "The Effect of Cracks on the Thermal Expansion of Rocks." *Earth and Planetary Science Letters, 36,* 404-412. Amsterdam, The Netherlands: Elsevier. TIC: 259789.

100439 de Marsily, G. 1986. *Quantitative Hydrogeology: Groundwater Hydrology for Engineers.* San Diego, California: Academic Press. TIC: 208450.

176937 DOE (U.S. Department of Energy) 2006. *Yucca Mountain Project Conceptual Design Report.* TDR-MGR-MD-000014, Rev. 05. Las Vegas, Nevada: U.S. Department of Energy, Office of Repository Development. ACC: ENG.20060505.0003.

182051 DOE 2007. *Quality Assurance Requirements and Description.* DOE/RW-0333P, Rev. 19. Washington, D. C.: U.S. Department of Energy, Office of Civilian Radioactive Waste Management. ACC: DOC.20070717.0006.

181403 DOE 2007. *Transportation, Aging and Disposal Canister System Performance Specification.* WMO-TADCS-000001, Rev. 0. Washington, D.C.: U.S. Department of Energy, Office of Civilian Radioactive Waste Management. ACC: DOC.20070614.0007.

183701 Gentle, J.E. 2003. *Random Number Generation and Monte Carlo Methods.* 2nd Edition. New York, New York: Springer-Verlag. TIC: 259875.

150043 Hardin, E.L. and Chesnut, D.A. 1997. *Synthesis Report on Thermally Driven Coupled Processes.* UCRL-ID-128495. Livermore, California: Lawrence Livermore National Laboratory. TIC: 234838.

163337 Incropera, F.P. and DeWitt, D.P. 2002. *Fundamentals of Heat and Mass Transfer.* 5th Edition. New York, New York: John Wiley & Sons. TIC: 254280.

108184 Incropera, F.P. and DeWitt, D.P. 1996. *Fundamentals of Heat and Mass Transfer.* 4th Edition. New York, New York: John Wiley & Sons. TIC: 243950.

158051 McKenzie, J.M. 2001. Thermal Data for Naval Nuclear Propulsion Program Spent Nuclear Fuel Canister. Letter from J.M. McKenzie (Department of the Navy) to S.P. Mellington (DOE/YMSCO), August 29, 2001, Ser 08U/01-13933, with enclosure. ACC: MOL.20011029.0285.

100690 Nimick, F.B. and Connolly, J.R. 1991. *Calculation of Heat Capacities for Tuffaceous Units from the Unsaturated Zone at Yucca Mountain, Nevada.* SAND88-3050. Albuquerque, New Mexico: Sandia National Laboratories. ACC: NNA.19910308.0017.

163274 NRC (U.S. Nuclear Regulatory Commission) 2003. *Yucca Mountain Review Plan, Final Report.* NUREG-1804, Rev. 2. Washington, D.C.: U.S. Nuclear Regulatory Commission, Office of Nuclear Material Safety and Safeguards. TIC: 254568.

125806 Perry, R.H.; Green, D.W.; and Maloney, J.O., eds. 1984. *Perry's Chemical Engineers' Handbook.* 6th Edition. New York, New York: McGraw-Hill. TIC: 246473.

181244 SNL (Sandia National Laboratories) 2007. *Abstraction of Drift Seepage.* MDL-NBS-HS-000019 REV 01 ADD 01. Las Vegas, Nevada: Sandia National Laboratories. ACC: DOC.20070807.0001.

181267 SNL 2007. *Analysis of Dust Deliquescence for FEP Screening.* ANL-EBS-MD-000074 REV 01 AD 01. Las Vegas, Nevada: Sandia National Laboratories. ACC: DOC.20070911.0004; DOC.20070824.0001.

179545 SNL 2007. *Calibrated Unsaturated Zone Properties.* ANL-NBS-HS-000058 REV 00. Las Vegas, Nevada: Sandia National Laboratories. ACC: DOC.20070530.0013.

177404 SNL 2007. *Drift-Scale THC Seepage Model.* MDL-NBS-HS-000001 REV 05. Las Vegas, Nevada: Sandia National Laboratories. ACC: DOC.20071010.0004.

177407 SNL 2007. *EBS Radionuclide Transport Abstraction.* ANL-WIS-PA-000001 REV 03. Las Vegas, Nevada: Sandia National Laboratories. ACC: DOC.20071004.0001.

177412 SNL 2007. *Engineered Barrier System: Physical and Chemical Environment.* ANL-EBS-MD-000033 REV 06. Las Vegas, Nevada: Sandia National Laboratories. ACC: DOC.20070907.0003.

179476 SNL 2007. *Features, Events, and Processes for the Total System Performance Assessment.* ANL-WIS-MD-000026 REV 00. Las Vegas, Nevada: Sandia National Laboratories.

180778 SNL 2007. *General Corrosion and Localized Corrosion of the Drip Shield.* ANL-EBS-MD-000004 REV 02 ADD 01. Las Vegas, Nevada: Sandia National Laboratories. ACC: DOC.20060427.0002; DOC.20070807.0004; DOC.20071003.0019.

178519 SNL 2007. *General Corrosion and Localized Corrosion of Waste Package Outer Barrier.* ANL-EBS-MD-000003 REV 03. Las Vegas, Nevada: Sandia National Laboratories. ACC: DOC.20070730.0003; DOC.20070807.0007.

181648 SNL 2007. *In-Drift Natural Convection and Condensation.* MDL-EBS-MD-000001 REV 00 AD 01. Las Vegas, Nevada: Sandia National Laboratories. ACC: DOC.20050330.0001; DOC.20051122.0005; DOC.20070907.0004.

180506 SNL 2007. *In-Package Chemistry Abstraction.* ANL-EBS-MD-000037 REV 04 ADD 01. Las Vegas, Nevada: Sandia National Laboratories. ACC: DOC.20070816.0004.

180472 SNL 2007. *Initial Radionuclides Inventories.* ANL-WIS-MD-000020 REV 01 ADD 01. Las Vegas, Nevada: Sandia National Laboratories. ACC: DOC.20050927.0005; DOC.20070801.0001.

181383 SNL 2007. *Multiscale Thermohydrologic Model.* ANL-EBS-MD-000049 REV 03 ADD 01. Las Vegas, Nevada: Sandia National Laboratories. ACC: DOC.20070831.0003.

177396 SNL 2007. *Radionuclide Transport Models Under Ambient Conditions.* MDL-NBS-HS-000008 REV 02 ADD 01. Las Vegas, Nevada: Sandia National Laboratories. ACC: DOC.20050823.0003; DOC.20070718.0003.

176828 SNL 2007. *Seismic Consequence Abstraction.* MDL-WIS-PA-000003 REV 03. Las Vegas, Nevada: Sandia National Laboratories. ACC: DOC.20070928.0011.

177413 SNL 2007. *THC Sensitivity Study of Heterogeneous Permeability and Capillarity Effects.* ANL-NBS-HS-000047 REV 01. Las Vegas, Nevada: Sandia National Laboratories. ACC: DOC.20070807.0006.

179196 SNL 2007. *Thermal Management Flexibility Analysis.* ANL-EBS-MD-000075 REV 01. Las Vegas, Nevada: Sandia National Laboratories. ACC: DOC.20070207.0001.

177414 SNL 2007. *Thermal Testing Measurements Report.* TDR-MGR-HS-000002 REV 01. Las Vegas, Nevada: Sandia National Laboratories. ACC: DOC.20070307.0010.

179567 SNL 2007. *Total System Performance Assessment Data Input Package for Requirements Analysis for DOE SNF/HLW and Naval SNF Waste Package Physical Attributes Basis for Performance Assessment.* TDR-TDIP-ES-000009 REV 00. Las Vegas, Nevada: Sandia National Laboratories. ACC: DOC.20070921.0009.

179354 SNL 2007. *Total System Performance Assessment Data Input Package for Requirements Analysis for Engineered Barrier System In-Drift Configuration.* TDR-TDIP-ES-000010 REV 00. Las Vegas, Nevada: Sandia National Laboratories. ACC: DOC.20070921.0008.

179466 SNL 2007. *Total System Performance Assessment Data Input Package for Requirements Analysis for Subsurface Facilities.* TDR-TDIP-PA-000001 REV 00. Las Vegas, Nevada: Sandia National Laboratories. ACC: DOC.20070921.0007.

179394 SNL 2007. *Total System Performance Assessment Data Input Package for Requirements Analysis for Transportation Aging and Disposal Canister and Related Waste Package Physical Attributes Basis for Performance Assessment.* TDR-TDIP-ES-000006 REV 00. Las Vegas, Nevada: Sandia National Laboratories. ACC: DOC.20070918.0005.

178871 SNL 2007. *Total System Performance Assessment Model/Analysis for the License Application.* MDL-WIS-PA-000005 REV 00. Las Vegas, Nevada: Sandia National Laboratories.

159516 Williams, N.H. 2001. "Contract #: DE-AC08-01NV12101 - Drift Scale Test (DST) White Paper: Scaling Along the Roof of the Heated Drift." Letter from N.H. Williams (BSC) to S.P. Mellington (DOE/YMSCO), May 15, 2001, PROJ.05/01.033, with enclosure. ACC: MOL.20010622.0252.

8.2 CODES, STANDARDS, REGULATIONS, AND PROCEDURES

IM-PRO-003, Rev. 3, ICN 0. *Software Management*. Washington, D.C.: U.S. Department of Energy, Office of Civilian Radioactive Waste Management. ACC: DOC.20070918.0001.

SCI-PRO-001, Rev. 5, ICN 0. *Qualification of Unqualified Data*. Washington, D.C.: U.S. Department of Energy, Office of Civilian Radioactive Waste Management. ACC: DOC.20071106.0020.

SCI-PRO-005, Rev. 6, ICN 0. *Scientific Analyses and Calculations.* Washington, D.C.: U.S. Department of Energy, Office of Civilian Radioactive Waste Management. ACC: DOC.20071026.0002.

8.3 SOURCE DATA, LISTED BY DATA TRACKING NUMBER

165790 LL030808623122.036. Input and Output Files for NUFT MSTHM Sub-Models Supporting LA Multi-Scale Analyses. Submittal date: 09/11/2003.

180553 LL0702PA013MST.068. Input and Output Files for the SMT, SDT and DDT Submodels and MSTHAC Extract Output Files Used in ANL-EBS-MD-000049 Multiscale Thermohydrologic Model. Submittal date: 04/27/2007.

179591 LL0702PA014MST.069. Input and Output Files for the LDTH Submodels and MSTHAC Extract Output Files Used in ANL-EBS-MD-000049 Multiscale Thermohydrologic Model for the Mean Host-Rock Thermal Conductivity, 10-Percentile Percolation Flux Case. Submittal date: 02/23/2007.

179594 LL0702PA020MST.075. Input and Output Files for the LDTH Submodels and MSTHAC Extract Output Files Used in ANL-EBS-MD-000049 Multiscale Thermohydrologic Model for the Mean Host-Rock Thermal Conductivity, 90-Percentile Percolation Flux Case. Submittal date: 02/14/2007.

179595 LL0702PA022MST.077. Input and Output Files for the LDTH Submodels and MSTHAC Extract Output Files Used in ANL-EBS-MD-000049 Multiscale Thermohydrologic Model for the Low Host-Rock Thermal Conductivity, 10-Percentile Percolation Flux Case. Submittal date: 02/14/2007.

179590 LL0702PA027MST.082. Output for ANL-EBS-MD-000049 Multiscale Thermohydrologic Model for the Mean Host-Rock Thermal Conductivity, 10-Percentile Percolation Flux, Collapsed-Drift, High and Low Rubble Thermal Conductivity Cases. Submittal date: 02/15/2007.

179981 LL0703PA026MST.013. Weighting Factors for Low (10-Percentile), Mean, and High (90-Percentile) Host-Rock Thermal Conductivity Cases for ANL-EBS-MD-000049 Multiscale Thermohydrologic Model. Submittal date: 03/28/2007.

182706 LL0705PA032MST.028. Model-Confidence Building and Sensitivity Studies for ANL-EBS-MD-000049 Multiscale Thermohydrologic Model (MSTHM). Submittal date: 08/23/2007.

182332 LL0705PA038MST.030. Model Preparation and Analysis Files for ANL-EBS-MD-000049 Multiscale Thermohydrologic Model (MSTHM). Submittal date: 07/17/2007.

180552 MO0612MEANTHER.000. Mean Thermal Conductivity of Yucca Mountain Repository Units. Submittal date: 04/27/2007.

179343 MO0702PAGLOBAL.000. Global 10th and 90th Percentile Mean Thermal Conductivity of Yucca Mountain Repository Units. Submittal date: 02/22/2007.

179925 MO0702PASTREAM.001. Waste Stream Composition and Thermal Decay Histories for LA. Submittal date: 02/15/2007.

181570 MO0705WASTELIM.000. Estimated Limiting Waste Stream Design Information. Submittal date: 06/12/2007.

181613 MO0706SPAFEPLA.001. FY 2007 LA FEP List and Screening. Submittal date: 06/20/2007.

183774 MO0707ELWSDNSL.000. Estimated Limiting Waste Stream Design Information-Including Waste Package Counts, Temperatures and Powers. Submittal date: 10/16/2007.

162401 SN0303T0503102.008. Revised Thermal Conductivity of the Non-Repository Layers of Yucca Mountain. Submittal date: 03/19/2003.

164196 SN0307T0510902.003. Updated Heat Capacity of Yucca Mountain Stratigraphic Units. Submittal date: 07/15/2003.

169129 SN0404T0503102.011. Thermal Conductivity of the Potential Repository Horizon Rev 3. Submittal date: 04/27/2004.

179425 SN0701PAEBSPCE.002. PCE TDIP PCO2 and Total Carbon Lookup Tables. Submittal date: 01/30/2007.

181571 SN0703PAEBSPCE.006. Physical and Chemical Environment (PCE) TDIP Water-Rock Interaction Parameter Table and Salt Separation Tables with Supporting Files. Submittal date: 06/27/2007.

8.4 OUTPUT DATA, LISTED BY DATA TRACKING NUMBER

MO0705SUPPCALC.000. Supporting Calculations for Postclosure Thermal Envelope Study. Submittal date: 01/10/2008.

MO0707THERMHYD.000. Thermal-Hydrologic Margin Analysis. Submittal date: 07/18/2007.

MO0707THERMRES.000. Thermomechanical Response to Range of Design Thermal Loadings. Submittal date: 07/18/2007.

MO0707TH2D3DDC.000. 2-D AND 3-D Thermal-Hydrologic Analysis. Submittal date: 08/15/2007.

MO0707GEORESPO.000. Geochemical Response Analysis. Submittal date: 07/18/2007.

MO0709REVTHERM.000. Revised Thermal Properties - Heat Capacity. Submittal date: 09/04/2007.

MO0709HOTWASTE.000. Probabilistic Analysis of Hottest Waste Package Temperature for Drift Collapse Immediately after Repository Closure. Submittal date: 09/19/2007.

MO0709THERMAL1.000. Thermal Drift Analysis for Yucca Mountain – Scenario 1. Submittal date: 09/04/2007.

MO0709THERMAL2.000. Thermal Drift Analysis for Yucca Mountain – Scenario 2. Submittal date: 09/04/2007.

MO0709THERMAL3.000. Thermal Drift Analysis for Yucca Mountain – Scenario 3. Submittal date: 09/04/2007.

MO0709THERMAL4.000. Thermal Drift Analysis for Yucca Mountain – Scenario 4. Submittal date: 09/04/2007.

MO0711SENSTEST.000. Sensitivity Analysis for Tptpv3 Unit Heat Capacity Values. Submittal date: 11/15/2007.

8.5 SOFTWARE CODES

170070 ANSYS V. 8.0. 2004. HP-UX 11.0, HP-UX 11.22, SunOS 5.8. STN: 10364-8.0-00.

162228 EQ3/6 V. 8.0. 2003. WINDOWS 2000, WIN NT 4.0, WIN 98, WIN 95. STN: 10813-8.0-00.

173680 GetEQData V. 1.0.1. 2002. WINDOWS 2000. STN: 10809-1.0.1-00.

155201 MVIEW V. 2.20. 2000. HPUX, SOLARIS, IRIX6.3, IRIX6.4, IRIX6.5, DIGITAL UNIX. STN: 10072-2.20-00.

157280 NUFT V. 3.0s. 2002. Sun O.S. 5.6 & 5.7. STN: 10088-3.0s-01.

180382 NUFT V. 4.0. 2007. SUN O.S. 5.8, AIX 5.2, AIX 5.3, CHAOS 3.1. STN: 11228-4.0-00.

164273 RADPRO V. 4.0. 2002. SUN O.S. 5.8. STN: 10204-4.0-00.

172322 UDEC V. 3.14. 2004. WINDOWS 2000. STN: 10173-3.14-00.

148638 XTOOL V. 10.1. 2000. Sun O.S. 5.6.1. STN: 10208-10.1-00.

APPENDIX A

PLAN FOR QUALIFICATION OF ELWS AND EMPLACEMENT SEQUENCES

INTENTIONALLY LEFT BLANK

Data Qualification Plan

Complete only applicable items.

QA: QA
Page 1 of 2

Section I. Organizational Information

Qualification Title

Qualification of Total System Model output that provides the arrival and emplacement sequencing of waste packages (WPs)

Requesting Organization

Near Field Environment

Section II. Process Planning Requirements

1. List of Unqualified Data to be Evaluated

DTN MO0707ELWSDNSL.000.
This DTN contains three files that are the information being qualified. This information was developed by the BSC Waste Management Integration organization, using the Total System Model (TSM) unqualified software, and is documented in 000-00C-G000-01100-000-00A (TSM GROA Basis and Check) and 000-00R-G000-00600-000-000 (Engineering Study, Total System Model Analysis for Repository Postclosure Thermal Envelope Study, Phase 1); both TSM reports are QA: N/A.
The files are the following:

File 1: AvailShip_CD-1_YFF5_22kW_Rev 2-DS.xls contains the list of CSNF canisters shipped to YM by date and content (assembly count and characteristics). The overall file is used as context in this data qualification, and qualification of the overall file is limited to that use.

File 2: WP_Decay_70K22kw_011707-DS.xls contains a list of WPs with emplacement dates, content, type, and thermal decay curve. This list of packages constitutes the Estimated Limiting Waste Stream (ELWS), but does not indicate how they would be emplaced in the repository. The data contained in this file are qualified by this data qualification, for use to represent the ELWS.

File 3: WP_Emplaced_ELWS_011707_23C_050107-DS.xls contains emplacement results for two emplacement operational rules (85/4 and 96/2). The sorted list contains only the identification number, type, length, year created, and spent fuel type column from File 2. In addition, this file contains the calculated results used in simulating emplacement (the 7-WP average of mid-pillar peak temperature index, emplacement year, WP thermal output at emplacement, and 7-WP lineal average thermal output at emplacement). The latter two are calculated from the decay curves in File 2.

Each of these three files is based on the similarly named file in unqualified DTN MO0705WASTELIM.000 (without the "-DS" characters just before the file extension; "DS indicates down-select"). The qualified DTN (developed by executing this plan) includes less information than the unqualified DTN and also clearly labels what information is being passed into these TSM files from the TPO output DTN from ANL-NBS-HS-000057 R0 (Postclosure Analysis for the Range of Design Thermal Loadings), which is the AMR that is the home for this data qualification.

2. Type of Data Qualification Method(s) [Including rationale for selection of method(s) (Attachment 3) and qualification attributes (Attachment 4)]

Method 5, Technical Assessment will be used to qualify the data.
The other methods are not used for the following reasons:

Method 1, Equivalent QA Program, cannot be used because the data originated from non-Q work funded by OCRWM.

Method 2, Corroborating Data, cannot be used because no corroborating data are available.

Method 3, Confirmatory Testing, cannot be used because the data are not physical test data, but rather are combinations of waste characterization data that are used to assemble two waste package emplacement realizations.

Method 4, Peer Review, is not selected because Method 5 is appropriate, and because novel practices have not been utilized to generate these data.

Method 5 (Technical Assessment), the remaining method, is appropriate because the data collection procedures are not subject to the QARD, and because the documentation of the data was not subject to the QARD.

The attributes to be addressed in performing this data qualification include (but are not limited to):

- The technical adequacy of equipment and procedures used to collect and analyze the data;
- The extent to which the data demonstrate the properties of interest (e.g., physical, chemical, geologic, mechanical);
- Extent and reliability of the documentation associated with the data;
- The importance of the data to showing that the proposed U.S. Department of Energy repository design meets the performance objectives of the QA program that supports the YMP License Application process or post closure science.

SCI-PRO-001.1-R1

Data Qualification Plan

Complete only applicable items.

QA: QA
Page 2 of 2

3. Data Qualification Team and Additional Support Staff Required

Chairperson: Ernest Hardin
Member: James Blink
Additional Support: Robert Zimmerman will perform checking of the data qualification aspect of ANL-NBS-HS-000057 R0 (Postclosure Analysis for the Range of Design Thermal Loadings), which is the AMR that includes this Data Qualification activity.

4. Data Evaluation Criteria

1. The total WP count, MTHM, and thermal power of the WP ensemble (in Files 2 and 3) will be compared to the totals from the Initial Radionuclide Inventories AMR (ANL-WIS-MD-000020 Rev 01 Addendum 01) and associated TPO DTN (MO0702PASTREAM.001). This source uses limited input from the TSM, and is QA.
2. The total WP count, MTHM, and thermal power of the WP ensemble will be compared to the totals from 000-00C-WIS0-00500-000-00A (Waste Form, Heat Output, and Waste Package Spacing for an Idealized Drift Segment). This source is independent of the TSM and is QA.
3. The total WP count, MTHM, and thermal power of the WP ensemble (in Files 2 and 3) will be compared to the totals from the CSNF assemblies in File 1.

Comparisons 1, 2, and 3 will be deemed acceptable if the totals are consistent within 10%.

5. Identification of Procedures Used

SCI-PRO-001 Rev 5 is the governing procedure for this work.

6. Plan coordinated with the following known organizations providing input to or using the results of the data qualification

BSC Waste Management Integration (Scott Gillespie). This organization provided the TSM output files (Files 1-3 in the unqualified DTN cited in Block 1 above.) It should be noted that the files interweave with the TPO output DTN from ANL-NBS-HS-000057 R0 (Postclosure Analysis for the Range of Design Thermal Loadings), which is the AMR that is the home for this data qualification. The data flow is as follows:

1. TSM assembles waste packages from shipping casks of CSNF assemblies with known thermal properties and MTU content. The cask/assembly information is in File 1 (Block 1 above). The resulting waste package sequence (including thermal decay history) is in File 2 (Block 1 above). The TSM case is based on Youngest Fuel First (YFF) with no waste younger than 5 yr, and with a 22 kW thermal limit for shipping casks.
2. The decay history information for each waste package in File 2 (Block 1 above) is used in an analysis documented in ANL-NBS-HS-000057. This analysis calculates mid-pillar temperature for each TSM waste package assuming that the entire repository is filled with clones of that single TSM waste package. The result is documented in a DTN that is TPO of the AMR; however, the result is also indicated in File 2 (Block 1 above), because that result is input to the next stage of TSM calculations described below. File 2 (Block 1 above) describes the sequence of waste packages that come to the repository site (for the waste acceptance realization documented in File 1), but does not indicate whether these waste packages are immediately emplaced or if they go to surface storage.
3. The mid-pillar temperatures (from the AMR TPO DTN, and repeated in File 2 of Block 1 above) and the WP decay curves (from File 2 of Block 1 above) are input to another TSM routine that computes the waste emplacement sequence. Each year's set of new waste packages (from File 2 of Block 1 above) is combined with the waste packages previously placed into surface storage. The TSM routine determines the optimal sequence of waste packages subject to three constraints: No waste package above 18 kW at emplacement, no 7-WP segment average to exceed 2.0 kW/m at emplacement, and each 7-WP segment to have a mid-pillar temperature average that is as close to the target as possible, without exceeding the target. Two Target Cases were run: Targets of 96 and 85°C. The result of this step is File 3 of Block 1 above, which also includes the mid-pillar temperature values from the AMR TPO DTN.

Section III. Approval

Qualification Chairperson Printed Name	Qualification Chairperson Signature	Date
Ernest Hardin	Ernest Hardin	12/6/07
Responsible Manager Printed Name	**Responsible Manager Signature**	**Date**
Geoffrey A. Freeze	Geoff Freeze	12/6/07

SCI-PRO-001.1-R1

APPENDIX B

QUALIFICATION OF ELWS AND EMPLACEMENT SEQUENCES

INTENTIONALLY LEFT BLANK

QUALIFICATION OF TOTAL SYSTEM MODEL (TSM) INPUT FROM DTN: MO0707ELWSDNSL.000 [DIRS 183774]

This appendix qualifies the total system model (TSM) input (located in DTN: MO0707ELWSDNSL.000 [DIRS 183774]) to this report; the Data Qualification Plan (DQP) is located in Appendix A. These data are being qualified in accordance with the procedures SCI-PRO-005 and SCI-PRO-001.

The DTN contains three files, referred to as Files 1, 2, and 3 in this appendix:

- File 1: *AvailShip_CD-1_YFF5_22kW_Rev 2-DS.xls* contains the list of CSNF canisters shipped to Yucca Mountain by date and content (assembly count and characteristics). The overall file is used as context in this data qualification, and qualification of the overall file is limited to that use.

- File 2: *WP_Decay_70K22kw_011707_DS.xls* contains a list of waste packages with emplacement dates, content, type, and thermal decay curve. This list of packages constitutes the estimated limiting waste stream (ELWS), but does not indicate how they would be emplaced in the repository. The data contained in this file are qualified by this data qualification, for use to represent the ELWS.

- File 3: *WP_Emplaced_ELWS_011707_23C_050107_DS.xls* contains emplacement results for two emplacement operational rules (85/4 and 96/2, as described in Section 6.1.3). The sorted list contains only the identification number, type, length, year created, and spent fuel type column from File 2. In addition, this file contains the calculated results used in simulating emplacement (the 7-package average of mid-pillar peak temperature index, emplacement year, waste package thermal output at emplacement, and 7-package lineal average thermal output at emplacement). The latter two are calculated from the decay curves in File 2.

B.1 CRITERIA 1 AND 2 FOR QUALIFICATION OF DTN: MO0707ELWSDNSL.000 [DIRS 183774]

The first acceptance criterion of the DQP is the following:

- The total package count, metric tons of heavy metal (MTHM), and thermal power of the waste package ensemble (DTN: MO0707ELWSDNSL.000 [DIRS 183774], files: *WP_Decay_70K22kw_011707_DS.xls* [File 2] and *WP_Emplaced_ELWS_011707_23C_050107_DS.xls* [File 3]) will be compared to the totals from the DTN: MO0702PASTREAM.001 [DIRS 179925], which is output from *Initial Radionuclide Inventories* (SNL 2007 [DIRS 180472]). This source uses limited input from the TSM, and is qualified.

The second acceptance criterion of the DQP is the following:

- The total waste package count, MTHM, and thermal power of the waste package ensemble will be compared to the totals from *Waste Form, Heat Output, and Waste Package Spacing*

for an Idealized Drift Segment (BSC 2004 [DIRS 166941]). This source is independent of the TSM and is qualified.

The DQP states that these criteria will be met "if the totals are consistent within 10%."

DTN: MO0707ELWSDNSL.000 [DIRS 183774] (file: *WP_Decay_70K22kw_011707_DS.xls* [File 2]) contains a list of waste packages with emplacement dates, content, type, and thermal decay curve. The characters "_DS" in its name indicate that it is a down-selected portion from similarly named file *WP_Decay_70K22kw_011707.xls*, which is part of an unqualified DTN (DTN: MO0705WASTELIM.000 [DIRS 181570]) that was provided by the TSM organization. The list of packages in File 2 constitutes the ELWS, but does not indicate how they would be emplaced in the repository. The data contained in this file are qualified by this data qualification, for use to represent the ELWS.

DTN: MO0707ELWSDNSL.000 [DIRS 183774] (file: *WP_Emplaced_ELWS_011707_23C_050107_DS.xls* [File 3]), contains the emplacement results for two emplacement operational rules (85/4 and 96/2). The characters "_DS" in its name indicate that it is a down-selected portion from similarly named file *WP_Decay_70K22kw_011707.xls*, which is part of an unqualified DTN (DTN: MO0705WASTELIM.000 [DIRS 181570]) that was provided by the TSM organization. The sorted lists in File 3 contain only the identification number, type, length, year created, and spent fuel type column from File 2 discussed above. In addition, File 3 contains the calculated results used in simulating emplacement: the 7-package average of mid-pillar peak temperature index, emplacement year, waste package thermal output at emplacement, and 7-package lineal average thermal output at emplacement. The latter two are calculated from the decay curves in File 2.

To evaluate compliance with the acceptance criteria, a new file was created from the existing File 2. The new file, named *WP_Decay_70K22kw_011707_DS-DQ.xls* (called "File DS-DQ" below) is included in the DTN being qualified: MO0707ELWSDNSL.000 [DIRS 183774]. File DS-DQ includes the following modifications:

- In Sheet "WP_Decay," a column was inserted (becoming Column "H") entitled "P at Receipt, W." The value for each row is calculated as the maximum value of the row entries in columns I through DE, which are entitled "Y1", "Y2", … "Y110", where Y1 is the first year after the repository opens. For each row (which represents one waste package), these cells are zero before emplacement, and are the power at each indicated time after emplacement. Thus, the formula results in the power at emplacement, because waste package power decays in the years after emplacement.

- Sheet "DataQual" is inserted. This sheet begins by copying into columns A–F the chronologically sorted rows from Sheet "WP_Decay" (columns A, B, F, H, C, and E, respectively). These columns are pasted as values and then copied to columns H–M (as values). These latter columns are formatted and sorted as noted in rows 1 and 2 of those columns. The result is a grouping of the waste packages by waste package and waste types. The grouping is annotated in columns N–O.

- In columns Q–U of Sheet "DataQual," the count, length, MTHM, and power of waste packages / waste forms of each type are extracted from the grouped sets of information.

- In columns W–X of Sheet "DataQual," the same information from DTN: MO0702PASTREAM.001 [DIRS 179925] (called the "IRI DTN" below) is shown. It should be noted that 12 PWR assembly packages from that DTN were converted to 21 PWR assembly packages (by multiplying the count by 12/21 and rounding), to allow direct comparison.

  Similarly, in columns Z–AA of Sheet "DataQual," the same information from *TSM GROA Basis and Check* (BSC 2006 [DIRS 184615]) (called the "Design Calc" below) is shown. It should be noted that 12 PWR and 24 BWR assembly packages from that DTN were converted to 21 PWR and 44 BWR assembly packages, respectively (by multiplying the count by 12/21 and 24/44, respectively, and rounding), to allow direct comparison. It should also be noted that the Design Calc is based on waste package designs and a waste stream that were developed several years ago.

- Columns AC–AD of Sheet "DataQual" show ratios between values from File DS-DQ divided by the values from the two qualified sources.

Although the acceptance criteria are applied for the repository ensemble, examination of the waste package/waste type information can add confidence or identify limitations that should be placed on the TSM data.

The waste package count for waste package/waste types and the ensemble of waste packages are shown in Table B-1, using the information from File DS-DQ, the IRI DTN, and the Design Calc.

The total waste package count of 10,394 in File DS-DQ is smaller than the two qualified sources; however, it is within the 10% criteria (within 6% of both sources). Therefore, the total waste package count in the DTN being qualified is acceptable for the intended use.

Although not required by the DQP, the waste package count consistency among the three sources was also examined. The CSNF waste package count for File DS-DQ is within 1% of the two qualified sources. The codisposal (CDSP) waste package count, however, is more than 20% less than the two qualified sources (20% less than the IRI DTN, which is the most recent estimate, and 23% less than the Design Calc). For naval SNF, the IRI-DTN matches the most recent qualified source, and the older qualified source was correct at the time, before the Navy reconfigured its waste packages to use more waste packages for the same MTHM of waste.

Based on the comparisons between the three sources, it is concluded that the file DS-DQ does not include enough CDSP waste packages. Because the CDSP waste packages have lower thermal power output than CSNF waste packages, the shortage of CDSP waste packages in File DS-DQ (DTN: MO0707ELWSDNSL.000 [DIRS 183774]) will result in slightly higher peak temperatures, which is conservative from the perspective of meeting upper bound thermal limits.

The PWR/BWR waste package ratios are consistent among the three sources (1.54, 1.54, and 1.56 for File DS-DQ, IRI DTN, and Design Calc, respectively).

Table B-1. Comparison of Waste Package Count from the Three Sources

	File DS-DQ	IRI DTN (note 1)	Design Calc (note 2)
Ensemble	10,394	11,091	11,076
PWR-TAD (note 3)	4,383	4,402	4,394
21P-Long-TAD	96	95	93
BWR-TAD (note 3)	2,902	2,915	2,831
44B (converted from 24B)	0	0	46
Total Medium TAD CSNF Waste Packages	7,381	7,412	7,364
Naval-Long	310	310	156
Naval-Short	90	90	144
Total Naval SNF Waste Packages	400	400	300
CDSP-Long (note 3)	982	1,862	2,116
CDSP-Short (note 3)	1,427	1,207	1,147
CDSP-MCO (note 3)	204	210	210
Total CDSP Waste Packages	2,613	3,279	3,412

NOTES:

(1) The IRI DTN values were for the nominal 70,000 MTHM inventory; the DTN also includes values for the somewhat larger inventory used in the TSPA, which fills the entire design footprint. The 166 12P-Long-TAD waste package count in the IRI DTN was converted to a 95 21P-Long-TAD waste package count for the purpose of comparing the three data sources.

(2) The Design Calc values of 163 12P-Long-TAD waste packages and 84 24-BWR waste packages were converted to 93 21P-Long-TAD waste packages and 46 44-BWR waste packages, respectively, for the purpose of comparing the three data sources.

(3) The File DS-DQ information for PWR-TAD waste packages and PWR-Bare waste packages were combined, as was the information for BWR-TAD waste packages and BWR-Bare waste packages. Similarly, the CDSP waste packages were grouped into three groups (long, short, and MCO), and the AP and CR criticality control types of 21P waste packages were grouped, in the Design Calc information.

The waste package lengths for waste package/waste types are shown in Table B-2, using the information from File DS-DQ, the IRI DTN, and the Design Calc.

The lengths of the File DS-DQ waste packages are all either shorter or the same as the same waste package types in the IRI DTN. The average waste package length (including the 10-cm gap between waste packages) is 5.562 m per waste package for File DS-DQ, less than 1% shorter than the 5.614 m per waste package for the IRI DTN. Shorter lengths will result in slightly higher peak temperatures, which is conservative from the perspective of meeting upper bound thermal limits. Therefore, the waste package lengths in the DTN being qualified are acceptable for the intended use.

The lengths of the Design Calc are considered to be less accurate than the more recent IRI DTN, because the design has evolved to longer lengths after the Design Calc was approved, e.g., TAD

canisters are now within CSNF waste packages and shield plugs are now within CDSP waste packages; both increased the waste package length.

Table B-2. Comparison of Waste Package Length (m, not including waste package-to-waste package gap) from the Three Sources

	File DS-DQ	IRI DTN	Design Calc
PWR-TAD	5.8500	5.8501	5.165
21P-Long-TAD	5.8500	6.4343	5.651
BWR-TAD	5.8500	5.8501	5.165
44B (converted from 24B)	5.8500	5.8501	5.105
Naval-Long	5.8500	5.8501	6.065
Naval-Short	5.2100	5.2151	5.430
CDSP-Long	5.2200	5.2880	5.217
CDSP-Short	3.5900	3.6814	3.590
CDSP-MCO	5.2200	5.2786	5.217

The waste package powers for waste package/waste types are shown in Table B-3, using the information from File DS-DQ, the IRI DTN, and the Design Calc. The categories of PWR TADs in File DS-DQ and the Design Calc are included along with their weighted averages.

Table B-3. Comparison of Waste Package power (kW) from the Three Sources

	File DS-DQ (inventory)	IRI DTN (unit cell)	Design Calc (inventory)
PWR-TAD	8.1 (bare fuel-shipped) 16.6 (TAD-shipped) 15.2 (weighted average)	12.17 (average waste package)	11.53 (absorber plate) 3.11 (control rod) 11.35 (weighted average)
21P-Long-TAD	17.0	N/A	9.55 (12 SNF assemblies)
BWR-TAD	13.0	7.70	7.38
44B (converted from 24B)	N/A	N/A	0.521
Naval-Long	3.0	N/A	3.98
Naval-Short	3.0	N/A	3.98
CDSP-Long	0.41	0.41	0.367
CDSP-Short	2.9	3.62	2.98
CDSP-MCO	1.7	N/A	1.66

To compare the powers on an ensemble basis, the linear power for each source was calculated from the information in Tables B-1, B-2, and B-3. The linear power of File DS-DQ waste packages is 1.940 kW/m, higher than the IRI DTN value of 1.450 kW/m. The higher value is expected because this report is based on evaluating the thermally limiting waste stream. It should be noted that File DS-DQ uses an inventory average while the IRI DTN powers are based on a representative repeating unit cell that has been increased from its (Design Calc) basis of

1.359 kW/m. The Design Calc average value of 1.358 kW/m on an inventory basis was also increased in its unit cell (in the Design Calc report) to be 1.450 kW/m, to match the values specified for thermal calculations supporting the TSPA base case. The kW/m of File DS-DQ is somewhat higher than it would have been if that file had included more CDSP waste packages; this is conservative from the perspective of meeting upper bound thermal limits. Therefore, the waste package powers in the DTN being qualified are acceptable for the intended use.

The waste package MTHM (or MTU) quantities for waste packages/waste types are shown in Table B-4, using the information from File DS-DQ and the IRI DTN. The Design Calc does not include MTHM information.

Table B-4. Comparison of MTHM per Waste Package from Two Sources

	File DS-DQ	IRI DTN
PWR-TAD	6.510 (bare fuel-shipped) 9.091 (TAD-shipped) 8.671 (weighted average)	9.087
21P-Long-TAD	11.163 (21 assembly)	5.193 (12 assembly) 9.087 (21 assembly)
BWR-TAD	7.040 (bare fuel-shipped) 7.744 (TAD-shipped) 7.702 (weighted average)	7.617
Naval-Long	0.006	0.163
Naval-Short	0.007	0.163
CDSP-Long	2.502	3.059 (average)
CDSP-Short	2.501	
CDSP-MCO	1.005	

The overall radioactive waste (based on weighting by waste package type) of File DS-DQ waste packages is 6.510 MTHM per waste package, similar to the 6.539 MTHM per waste package from the qualified IRI DTN. The File DS-DQ values for naval SNF are clearly too small, but that will not affect thermal calculations which are based on the powers in Table B-3. The CDSP waste package MTHM content of File DS-DQ is somewhat lower than the qualified IRI DTN, but that will not affect thermal calculations which are based on the powers in Table B-3. Therefore, the waste package MTHM content in the DTN being qualified is acceptable for the intended use.

File DS-DQ also shows, in Columns AF and AG, the waste package count, total emplaced waste package length, and total emplaced power, all taken from File 3, from the two emplacement scenario sheets: "96C 2 Year 18Kw" and "85C 4 Year 18Kw". Visual comparison shows that the values for waste package count (10,394) and total emplaced length (56,775 m) exactly match that in File DS-DQ (from File 2). The total emplaced power is reasonable:

- File 2, which has total power at receipt, has 112.182 MW.
- File 3, Sheet "96C 2 Year 18Kw," has 98.48 MW, which is less than the receipt value because of decay during processing and surface storage at the repository.
- File 3, Sheet "85C 4 Year 18Kw," has 91.483 MW, which is less than the receipt value and the two-year storage value, because of decay during the additional (up to four years) of surface storage at the repository.

Therefore, the waste package count, waste package length, and waste package power information in File 3 of the DTN being qualified are acceptable for the intended use.

B.2 CRITERION 3 FOR QUALIFICATION OF DTN: MO0707ELWSDNSL.000 [DIRS 183774]

The third acceptance criterion of the DQP is the following:

- The total waste package count, MTHM, and thermal power of the waste package ensemble (in Files 2 and 3) will be compared to the totals from the CSNF assemblies in File 1.

The DQP states that this criterion will be met "if the totals are consistent within 10%."

File 1 has CSNF waste, only. The waste is packaged into shipping casks, which have different capacities than waste packages, for non-TAD waste. The count of casks is 9,452, which is somewhat above the CSNF waste package count of 7,381 from the File 2. The total number of CSNF assemblies in File 1 is 221,631, which is 116 assemblies less than File 2 value of 221,747 assemblies, assuming the waste packages are full in File 2. The two values are within 10% of each other; therefore, the information in File 1 of the DTN being qualified is adequate for the intended use.

A further look was taken at the CSNF assembly count in Files 1 and 2. File 1 has 221,631 assemblies available to ship, and the pre-downselect non-Q version of File 2 has 221,560 assemblies received (which is 71 assemblies not converted to waste packages). The capacity of the CSNF waste packages is 221,747 assemblies, which is 116 more than the assemblies available to ship and 187 more than the quantity in the waste packages included in the downselect DTN being qualified. Inspection of the pre-downselect non-Q version of File 2 shows that the 187 empty slots are all in WPMPC waste packages, i.e., are intentionally shown as only partly-filled in the TSM output. This is documented in the DTN being qualified (File 2, sheet: "Assembly Count"). It is probably due to the TSM software shipping a partly filled TAD as the last shipment from a plant, rather than consolidating the assemblies from two plants into a single TAD either at one of the plants or at the repository.

File 1 has average heat per assembly for each cask and assembly quantity for each cask. The product of these two attributes of each cask, summed over the casks, is 103.341 MW, which is 2.725 MW less than the 106.066 MW CSNF power in File 2. The two values are within 10% of each other; therefore, the information in File 1 of the DTN being qualified is adequate for the intended use.

File 1 has a total of 62,999 MTHM of CSNF, which is 1,572 MTHM more than the value of 61,427 MTHM in File 2. The two values are within 10% of each other; therefore, the information in File 1 of the DTN being qualified is adequate for the intended use.

In summary, File 1 ships 1,572 MTHM more than is included in the receipt calculation of File 2. The CSNF assembly count of File 1 (available to ship) is 116 less than the full capacity of the waste packages in File 2, and the power available to ship is 2.725 MW less than the power stated in File 2.

APPENDIX C

CALCULATION OF EFFECTIVE HEAT CAPACITY

INTENTIONALLY LEFT BLANK

C.1 OVERVIEW

This appendix summarizes the development of effective heat capacity functions for the repository host rock units, for use in finite element (ANSYS) simulations of in-drift and drift wall temperature histories during the preclosure and early postclosure periods (Section 6.3). These heat capacity functions include a nonlinear, temperature-dependent response that accounts for the latent heat that is dispersed during heating and dewatering of the near-field host rock. The Mathcad and Excel files generated are available in Output DTN: MO0709REVTHERM.000.

C.2 CALCULATION OF EFFECTIVE HEAT CAPACITY

Derivation of these functions follows the same approach used in *Heat Capacity Analysis Report* (BSC 2004 [DIRS 170003], Section 6.7), but with the following differences:

- Credit is taken for latent heat that is dispersed by evaporation of all the matrix pore water present in situ, instead of the average of pore water present during the transitional dewatering period. The previous work (BSC 2004 [DIRS 170003], Section 6.7) used an average transitional liquid saturation instead of the in situ saturation available initially, thus reducing the dewatering effect by approximately half.

- Functions are derived only for the four host rock units (Tptpul, Tptpmn, Tptpll, and Tptpln) because these are the only units that reach temperatures high enough to undergo dewatering, especially during the early postclosure period for which ANSYS finite element analyses are applied (Section 6.3).

- Matrix porosity values for the Tptpmn unit are applied also to the Tptpln; similarly, matrix porosity for the Tptpll is applied also to the Tptpul. This simplification follows the approach used in the multiscale model (SNL 2007 [DIRS 181383]), and is based on the lithologic and hydrologic similarities between the lithophysal units, and between nonlithophysal units. Note that distinct mean values for lithophysal porosity for all units were used (from DTN: SN0404T0503102.011 [DIRS 169129]; also presented in BSC 2004 [DIRS 169854], Table 6-6).

- In situ matrix saturation of 90.5%, based on an assumption justified in *Thermal Management Flexibility Analysis* (SNL 2007 [DIRS 179196], Section 5.3), is used for all host rock units (note that this value was later rounded down to 2 significant figures for heat capacitance derivation).

Like the earlier work, the heat capacity functions use transitions from 94°C to 95°C, and from 114°C to 115°C, to represent the onset and the end of dewatering, respectively. Between 95°C and 114°C the dewatering effect on apparent heat storage is applied uniformly as a function of temperature.

Use of the in situ matrix saturation value of 90.5% to represent water content at elevated temperature (e.g., at 94°C when dewatering begins in the approximation used in Appendix C), slightly underestimates the mass of water present per unit volume of bulk rock, due to thermal expansion. The effect is a few percent of the total amount of water present, which can be

confirmed by evaluating the thermal expansion of water (expansion of the matrix porosity is negligible). For a temperature range of ambient (23°C; SNL 2007 [DIRS 179196], Section 5.5) to 94°C, a mid-point temperature of 62°C is chosen (also used in Section 6.1; see Table 4.1-4). The bulk thermal expansion coefficient for water at this temperature is 5.355×10^{-4} K^{-1} (Incropera and DeWitt 1996 [DIRS 108184], Table A.6). Multiplying the temperature change by the expansion coefficient, the bulk expansion is estimated to be 3.8%.

The calculation is presented in four files for the four host repository horizon units (Output DTN: MO0709REVTHERM.000):

- *Effective Specific Heat Capacity Function Tptpll 05Sep07.xmcd* for the Tptpll unit
- *Effective Specific Heat Capacity Function Tptpul 05Sep07.xmcd* for the Tptpul unit
- *Effective Specific Heat Capacity Function Tptpmm 05Sep07.xmcd* for the Tptpmn unit
- *Effective Specific Heat Capacity Function Tptpln 27Nov07.xmcd* for the Tptpln unit.

Each file starts with a verification of the volumetric heat capacity function that accounts for the matrix porosity, the lithophysal porosity, and the degree of saturation, as developed in *Ventilation Model and Analysis Report* (BSC 2004 [DIRS 169862], Appendix II; see also BSC 2004 [DIRS 170003], Equation 6-9).

$$C_{rock} = \frac{S\frac{\phi_m}{1-\phi_m}C_{vw} + \rho_g C_p}{1 + \frac{\phi_m}{1-\phi_m} + \frac{\phi_l}{1-\phi_l}\left(1 + \frac{\phi_m}{1-\phi_m}\right)} \qquad \text{(Eq. C-1)}$$

where

C_{rock} = volumetric heat capacitance of the rock mass (J/m^3-K).
S = matrix liquid saturation.
ϕ_m = matrix porosity.
ϕ_l = lithophysal porosity.
ρ_g = grain density (2,549.9 kg/m^3).
C_p = gravimetric grain heat capacity of the solids (930 J/kg-K).

Values for these properties, for each host rock unit, are input to the respective Mathcad files, and volumetric heat capacitance is calculated for wet and dry conditions:

- Wet conditions: S = 90.5%; bulk heat capacitance = $C_{p,wet}$; and bulk density = $\rho_{b,wet}$
- Dry conditions: S = 0; bulk heat capacitance = $C_{p,dry}$; and bulk density = $\rho_{b,dry}$.

The sources for matrix porosity, lithophysal porosity, grain heat capacity, grain density, and matrix liquid saturation are discussed in Section 4.1.4.4.

The latent heat of vaporization for water is determined from:

$$H = S\,\phi_m\,\rho_w\,H_v \qquad \text{(Eq. C-2)}$$

where

H = heat of vaporization expressed volumetrically (J/m ^{3}).

ρ_w = density of water; 957.85 kg/m^3 at 96°C (Incropera and DeWitt 1996 [DIRS 108184], Table A.6).

H_v = enthalpy of vaporization; 2.265 $\times 10^6$ J/kg (Incropera and DeWitt 1996 [DIRS 108184], Table A.6).

The heat of vaporization is distributed over a temperature range from 94°C to 115°C, first ramping linearly from 94°C to a plateau that starts at 95°C, then uniformly from 95°C to 114°C, then ramping back to the dry rock heat capacitance at 115°C. These temperature limits were selected in *Heat Capacity Analysis Report* (BSC 2004 [DIRS 170003], Section 6.7) based on threshold dewatering behavior observed in the heated rock around the Drift Scale Test.

The functional form of the heat capacitance function is integrated from 94°C to 115°C, subtracting off the contributions from solid rock and liquid water. The result is set equal to the total heat of vaporization from Equation C-2, to solve for the plateau value, H_3:

$$\left\{ \begin{array}{r} 0.5\left(H_3 - C_{p,wet}\right)(95-94) + \left(H_3 - \dfrac{C_{p,dry} + C_{p,wet}}{2}\right)(114-95) + \\ 0.5\left(H_3 - C_{p,dry}\right)(115-114) \end{array} \right\} \frac{\rho_{b,wet} + \rho_{b,dry}}{2} = H \qquad \text{(Eq. C-3)}$$

The step function approach is the same as that used previously (BSC 2004 [DIRS 170003], Section 6.7) except for the differences listed above. Each of the four files listed above solves for the value of the latent heat plateau (H_3) by manual iteration. The ramped step function starts at 94°C, ramps up to the plateau value at 95°C, ramps down at 114°C, and represents completely dry conditions above 115°C. The value of the area under the plateau minus the specific heat of the dry rock equals the latent heat of evaporated water. The result for the Tptpll unit is shown in Figure C-1. The results of the calculations for all units are presented in Output DTN: MO0709REVTHERM.000, file: *Summary of Thermal Properties.xls*.

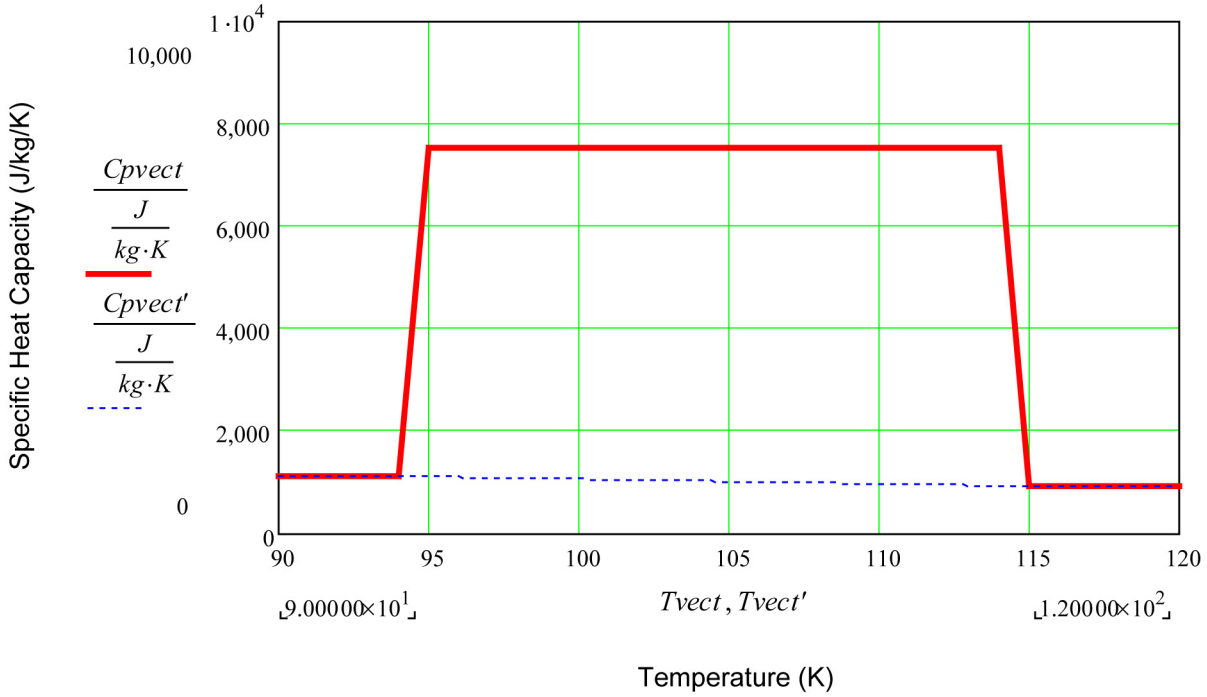

Source: Output DTN: MO0709REVTHERM.000, file: *Effective Specific Heat Capacity Function Tptpll 05Sep07.xmcd*.

Figure C-1. Nonlinear Specific Heat Capacity as a Function of Temperature Developed for the Tptpll Host Rock

This is an approximate derivation intended for use with thermal calculations using software (e.g., ANSYS) that can accommodate nonlinear temperature-dependent rock properties, but does not implement full thermal-hydrologic processes. Accordingly, it is appropriate to use these approximate functions only to represent the heat-up phase of repository thermal evolution. Beyond a few tens or hundreds of years after closure, hydrologic processes not represented here have a significant effect on repository thermal conditions.